Dissertation
zur Erlangung des akademischen Grades
Doktor der Naturwissenschaften (Dr. rer. nat.)

Flavorful New Physics Models in the Light of the B Decay Anomalies

Dennis Loose

geboren in Dortmund

Lehrstuhl für Theoretische Physik IV
Fakultät Physik
Technische Universität Dortmund
August 2021

Gutachter der Dissertation:
Prof. Dr. Gudrun Hiller und Prof. Dr. Heinrich Päs

Vorsitzender des Promotionsausschusses:
Prof. Dr. Mirko Cinchetti

Datum der mündlichen Prüfung:
12. Oktober 2021

Contents

Abstract

Current experimental data on the flavor observables R_K and R_{K^*} shows evidence for a violation of lepton universality – an essential feature of the Standard Model of particle physics. Together with several deviations seen in other $b \to s\mu^+\mu^-$ observables as well as R_D and R_{D^*}, these results constitute the so-called B decay anomalies. In this thesis we investigate new physics models that provide potential solutions to these anomalies and put a special emphasis on their flavor structure. To this end, we consider an $A_4 \times U_{\rm FN}(1)$-based flavor symmetry, which addresses the SM flavor puzzle, and study patterns that it imposes on the couplings of leptoquark models. We find that flavorful leptoquarks provide good explanations of $R_{K^{(*)}}$, while constraints from rare kaon decays and charged lepton flavor violating processes are too strong to allow to accommodate the deviations in $R_{D^{(*)}}$. As another consequence of the imposed flavor structure, flavorful leptoquarks are light enough to be produced at current and future hadron colliders. We compute estimates for the production cross sections of the S_3, V_1 and V_3 leptoquarks in different flavor scenarios, focusing on single production, which is sensitive to the leptoquark coupling and its flavor structure. We find that future hadron colliders with higher center of mass energies are needed to cover the full parameter space and determine leptoquark mass bound for benchmark scenarios.

Kurzfassung

Aktuelle experimentelle Daten zu den Flavor Observablen R_K and R_{K^*} zeigen Evidenz für eine Verletzung der Leptonuniversalität – einem wesentlichen Bestandteil des Standardmodells der Teilchenphysik. Zusammen mit mehreren Abweichungen in anderen $b \to s\mu^+\mu^-$ Observablen, ebenso wie R_D und R_{D^*}, bilden diese Ergebnisse die sogenannten B-Anomalien. In dieser Dissertation untersuchen wir neue Physik Modelle die mögliche Lösungen zu diesen Anomalien bereitstellen, und legen dabei besonderen Fokus auf deren Flavorstruktur. Zu diesem Zweck betrachten wir eine $A_4 \times U_{\mathrm{FN}}(1)$-basierte Flavorsymmetrie, welche das SM Flavor Puzzle angeht, und untersuchen Strukturen die sie den Kopplungen von Leptoquarkmodellen auferlegt. Wir stellen fest, dass Flavor-behaftete Leptoquarks gute Erklärungen der $R_{K^{(*)}}$ Anomalien liefern, während Einschränkungen von seltenen Kaon Zerfällen und Leptonflavor-verletzenden Prozessen zu stark sind um die Abweichungen in $R_{D^{(*)}}$ erklären zu können. Als weitere Konsequenz der auferlegten Flavorstruktur sind Flavor-behaftete Leptoquarks leicht genug um an gegenwärtigen und zukünftigen Hadronenbeschleunigern produziert werden zu können. Wir berechnen Abschätzungen für die Produktionsquerschnitte der S_3, V_1 and V_3 Leptoquarks in verschiedenen Flavorszenarien mit Fokus auf der Einzelproduktion, welche sensitiv auf die Leptoquarkkopplungen und deren Flavorstruktur ist. Wir stellen fest, dass Hadronenbeschleuniger mit höherer Schwerpunktsenergie als gegenwärtig verfügbar nötig sind um den vollständigen Parameterraum abzudecken, und bestimmen Schranken an die Leptoquarkmassen für Benchmarkszenarien.

Publications

This thesis is based on the following publications:

- G. Hiller, D. Loose, and K. Schönwald. "Leptoquark Flavor Patterns & B Decay Anomalies". In: *JHEP* 12 (2016), p. 027. DOI: 10.1007/JHEP12(2016)027. arXiv: 1609.08895 [hep-ph]
- G. Hiller, D. Loose, and I. Nišandžić. "Flavorful leptoquarks at hadron colliders". In: *Phys. Rev.* D97.7 (2018), p. 075004. DOI: 10.1103/PhysRevD.97.075004. arXiv: 1801.09399 [hep-ph]
- G. Hiller, D. Loose, and I. Nišandžić. "Flavorful leptoquarks at the LHC and beyond: spin 1". In: *JHEP* 06 (2021), p. 080. DOI: 10.1007/JHEP06(2021)080. arXiv: 2103.12724 [hep-ph]

Acknowledgements

First of all, I'd like to thank my advisor Gudrun Hiller for giving me the opportunity to learn more about the fundamentals of nature in an environment filled with amazing people. This doesn't only include the local groups of T III and T IV, but also the numerous people I've met during many trips to conferences, schools and workshops throughout Europe. I'd also like to thank her for her seemingly endless enthusiasm for physics, which provided the spark for all of the research projects I've been involved in. Then, I'd like to thank Heinrich Päs for accepting the role as second advisor, writing helpful recommendation letters, and joining many entertaining coffee room discussion on physics and beyond.

I couldn't have written this thesis without the help of my collaborators Kay and Ivan who have contributed a lot to our projects – thank you!

Very special thanks to Maggi for luring me into her ~~Kochstudio~~ office when I was still a master student, teaching me very useful practical IT skills, and for being the best office mate one could wish for; to Clara for repeatedly explaining to me how to count parameters in the flavor sector, having beers in very memorable places with me and for being wonderful; to Peter for all the endless climbing sessions, coffee room and ~~film~~ media room discussions and for being a beacon of joy; to Mathias for taking me on exciting adventures such as skydiving and hiking through heavy thunderstorms in the slovenian alps; to Fagner for all the discussions about films, life, plans and the lack thereof on our long walks home; to Erik and Ivan for having a great taste in music and attending some fantastic concerts with me; to Dominik and Philipp for being great neighbors and always letting me interrupt their very important work to discuss even more important issues; to Andrey and Marcel for all the post-climbing beers; to Tim and Stefan for taking over the admin duties and for bringing a lot of kindness to the group; to Cornelis, and Sebastian for always wanting to play cards instead of solving exercise sheets and to Manni for trying to make us get at least *some* work done before playing cards all day; and to my parents for fostering my passion for science from very early on and for always supporting me.

Chapter 1.

Introduction

The field of elementary particle physics has emerged from the pursuit to answer the most profound questions about nature: what are the fundamental building blocks of matter and how do they interact? Over the past centuries, the scientific method, driven by the interplay between theory and experiment, has led to remarkable progress in this pursuit, simplifying and unifying the mathematical descriptions of natural phenomena. Most recently, the discovery of the Higgs boson by the ATLAS [4] and CMS [5] experiments at the Large Hadron Collider (LHC) in 2012 has completed the Standard Model (SM) of particle physics, which provides the most precise and well-tested description of nature at fundamental scales to date. Besides the fact that the SM does not incorporate gravity, it suffers from further shortcomings: it explains neither the observed neutrino mass differences nor the origin of the baryon asymmetry and contains no potential dark matter candidates. Furthermore, the flavor sector of the SM, which encompasses most of its free parameters, exhibits a non-trivial structure, for which there is no explanation.

Due to the absence of direct experimental evidence for physics beyond the Standard Model (BSM), which is required to overcome the deficiencies of the SM, investigating precision observables that allow to probe key features of the SM has become more and more important. Currently, several measurements of flavor observables in the rare flavor-changing neutral current (FCNC) transitions $b \to s\ell^+\ell^-$ as well as in the flavor-changing charged current (FCCC) processes $b \to c\ell\bar{\nu}$ challenge the SM's built-in feature of lepton flavor universality (LFU) [6–12]. Additionally, there is a long-standing discrepancy between the very precisely known SM prediction and the experimentally determined value of the anomalous magnetic moment (AMM) of the muon [13]. Recently, an improved calculation of the fine structure constant has lead to a tension in the electron's AMM as well [14].

In this thesis, we focus on the deviations measured in the ratios of branching fractions $R_{K^{(*)}} \simeq \frac{\mathcal{B}(\bar{B}\to\bar{K}^{(*)}\mu^+\mu^-)}{\mathcal{B}(\bar{B}\to\bar{K}e^+e^-)}$ and $R_{D^{(*)}} \simeq \frac{\mathcal{B}(\bar{B}\to\bar{D}^{(*)}\tau\bar{\nu})}{\mathcal{B}(\bar{B}\to\bar{D}\ell\bar{\nu})}$ in the $b \to s\ell^+\ell^-$ and $b \to c\ell\bar{\nu}$ sectors, respectively. After laying out the foundations of flavor physics in the SM in Chapter 2, we review the current experimental and theoretical status of the previously mentioned

sectors in Chapter 3. To this end, we introduce the model-independent framework of effective field theories (EFTs), which will enable us to identify and classify possible BSM scenarios in a data-driven manner. We then consider concrete new physics (NP) models adressing the B anomalies and the flavor puzzles in chapters 4 and 5, respectively. In Chapter 6 we employ a flavor model to derive patterns for the couplings of leptoquark models that can potentially explain the $R_{K^{(*)}}$ and $R_{D^{(*)}}$ anomalies. These patterns allow us to use experimental bounds from related flavor sectors to constrain the leptoquark couplings, resulting in a predictive NP scenario with a rich phenomenology. Since the masses of flavorful leptoquarks required to account for the B anomalies are in the TeV region, they can potentially be produced at current or future hadron colliders. Chapter 7 is dedicated to the study of possible collider signals. We examine how collider searches can reveal information about the flavor structure of the leptoquark couplings by considering different flavor scenarios and determining their characteristic signatures. We conclude in Chapter 8.

Chapter 2.

Flavor Physics in the Standard Model

To begin, we provide a brief overview of the SM of particle physics with a focus on its flavor sector following standard literature [15–18]. After outlining the mathematical structure of the model and providing a summary of the particles and interactions it describes in the unbroken phase, we explore the breaking of electroweak (EW) symmetry and the consequences this has for the particles and interactions. This naturally leads us to the concept of *flavor*, which we review in the context of the available experimental data. Finally, we discuss the puzzles that emerge and how accidental symmetries of the SM can help to construct models BSM that seek to resolve them.

2.1. Field Content and Gauge Symmetries

The SM of particle physics is a mathematical framework, which describes all known fundamental particles and all their known interactions with the exception of gravity. It is constructed as a gauge quantum field theory (QFT) with the local gauge group

$$SU(3)_{\mathrm{C}} \times SU(2)_{\mathrm{L}} \times U(1)_Y \,, \tag{2.1}$$

where the first factor belongs to Quantum Chromodynamics (QCD), the theory of the strong interaction, while the remaining part is associated with the EW sector and is spontaneously broken by the Higgs mechanism to yield the $U(1)_{\mathrm{em}}$ gauge symmetry of Quantum Electrodynamics (QED).

The matter content of the SM comprises two classes of fermions: the color-charged up- and down-type quarks, respectively denoted u and d, and the color-neutral leptons, which can be divided into the electrically neutral neutrinos ν and the electrically charged leptons e. Furthermore, there are three copies, called *generations*, of all of those fermions, so that in total there are six *flavors* of each quarks and leptons. Before further exploring the flavor sector in the next section, we first need to review the gauge group representations

Field	$SU(3)_\mathrm{C}$	$SU(2)_\mathrm{L}$	$U(1)_Y$
Q	**3**	**2**	$1/6$
U	**3**	**1**	$2/3$
D	**3**	**1**	$-1/3$
L	**1**	**2**	$-1/2$
E	**1**	**1**	-1
H	**1**	**2**	$1/2$

Table 2.1.: Standard Model fields and their gauge group representations.

of the matter fields and discuss the resulting Lagrangian. On that account, we define the chiral fields[1]

$$Q \equiv \begin{pmatrix} u_\mathrm{L} \\ d_\mathrm{L} \end{pmatrix},\ U \equiv u_\mathrm{R},\ D \equiv d_\mathrm{R},\ L \equiv \begin{pmatrix} \nu_\mathrm{L} \\ e_\mathrm{L} \end{pmatrix},\ E \equiv e_\mathrm{R}, \tag{2.2}$$

which transform under the SM gauge group (2.1) according to Table 2.1. Here, the column vectors denote $SU(2)_\mathrm{L}$ doublets, while the $SU(3)_\mathrm{C}$ and generation structure are left implicit. The complex scalar Higgs field H is needed to generate fermion mass terms, which would otherwise be forbidden by gauge invariance.

Consequently, the most general renormalizable and gauge invariant Lagrangian that can be constructed from these fields contains the kinetic terms

$$\mathcal{L}_\mathrm{kin} = \sum_{\substack{\psi\in\{Q,U,D,\\ L,E\}}} \bar{\psi} i \not{D} \psi - \frac{1}{4}\left(G^A_{\mu\nu}G_A^{\mu\nu} + W^a_{\mu\nu}W_a^{\mu\nu} + B_{\mu\nu}B^{\mu\nu}\right) \tag{2.3}$$

of the fermions ψ and of the gauge bosons G, W and B of QCD and the EW sector, respectively, which appear in the form of their associated field strength tensors, which have the form

$$\mathcal{F}^i_{\mu\nu} \equiv \partial_\mu \mathcal{A}^i_\nu - \partial_\nu \mathcal{A}^i_\mu + \kappa f^{ijk} \mathcal{A}^j_\mu \mathcal{A}^k_\nu \tag{2.4}$$

for a given gauge group with coupling κ, gauge boson $\mathcal{A}$ and structure constants f^{ijk} of the associated Lie algebra. The interactions between fermions and gauge bosons arise from the gauge covariant derivative

$$D_\mu \equiv \partial_\mu - i g_\mathrm{s} t_A G^A_\mu - i g T_a W^a_\mu - i g' Y B_\mu\,, \tag{2.5}$$

with the generators t_A, T_a, and Y and the gauge couplings g_s, g, and g' of $SU(3)_\mathrm{C}$, $SU(2)_\mathrm{L}$, and $U(1)_Y$, respectively.

[1] See Appendix A for mathematical notation and conventions.

All remaining terms [2] in the SM Lagrangian include the Higgs field H, which is responsible for spontaneously breaking the EW gauge symmetry and shaping the flavor sector, as we will see in the next section.

2.2. Electroweak Symmetry Breaking

The part of the Lagrangian involving only H reads

$$\mathcal{L}_{\text{Higgs}} = (D_\mu H)^\dagger (D^\mu H) - V(H)\,, \tag{2.6}$$

with the scalar potential

$$V(H) = -\mu^2 H^\dagger H + \lambda \left(H^\dagger H\right)^2\,, \tag{2.7}$$

where the parameters μ^2 and λ are real and positive, so that H acquires a non-zero vacuum expectation value (vev) that can be chosen as

$$\langle H \rangle = \frac{1}{\sqrt{2}} \begin{pmatrix} 0 \\ v \end{pmatrix}\,, \tag{2.8}$$

with $v = \sqrt{\frac{\mu^2}{\lambda}}$. This choice of $\langle H \rangle$ spontaneously breaks the EW symmetry to the local gauge group $U(1)_{\text{em}}$, which is generated by the electric charge $Q \equiv T_3 + Y$. The massless gauge boson associated with this symmetry is the photon.

According to Goldstone's theorem [19] a new scalar degree of freedom appears for each broken generator of a spontaneously broken continuous global symmetry. In the case of a broken gauge symmetry, however, the new degrees of freedom can be absorbed into additional polarizations of the associated gauge bosons, rendering them massive. Diagonalizing the mass terms that arise from the kinetic term in (2.6) after H is replaced by its vev (2.8) yields the spectrum of massive gauge bosons after symmetry breaking. The electrically charged gauge bosons

$$W^\pm \equiv \frac{1}{\sqrt{2}}(W^1 \mp i W^2) \tag{2.9}$$

have mass $m_W = gv/2$. Besides the massless photon A, there is another electrically neutral, but massive, gauge boson Z. These two fields are defined as

$$\begin{pmatrix} Z \\ A \end{pmatrix} \equiv \begin{pmatrix} \cos\theta_{\text{W}} & -\sin\theta_{\text{W}} \\ \sin\theta_{\text{W}} & \cos\theta_{\text{W}} \end{pmatrix} \begin{pmatrix} W^3 \\ B \end{pmatrix}\,, \tag{2.10}$$

[2] We tacitly assume that the theory has been quantized and renormalized; hence we omit the gauge-fixing and ghost parts of the Lagrangian.

where the Weinberg angle θ_{W} is defined by

$$\sin\theta_{\mathrm{W}} = \frac{g'}{\sqrt{g^2+g'^2}}\,. \tag{2.11}$$

The mass of the Z boson is then $m_Z = m_W/\cos\theta_{\mathrm{W}}$.

The interactions of the fermions with the EW gauge bosons after symmetry breaking follow from the EW part of the gauge covariant derivative (2.5), which now reads

$$D_\mu^{\mathrm{EW}} = \partial_\mu - i\frac{g}{\sqrt{2}}\left(T^+W_\mu^+ + T^-W_\mu^-\right) - ie\left(\cot\theta_{\mathrm{W}}T^3 - \tan\theta_{\mathrm{W}}Y\right)Z_\mu - ieQA_\mu\,, \tag{2.12}$$

where $T^\pm = T^1 \pm iT^2$ and $e = g\sin\theta_{\mathrm{W}}$. To further inspect these interactions, we first need to discuss masses and mixing of the fermions.

2.3. Fermion Masses and Mixing

With the Higgs field H (and its $SU(2)_{\mathrm{L}}$ conjugate $\tilde{H} \equiv i\sigma_2 H^*$) at hand it is possible to include the Yukawa interaction terms

$$-\mathcal{L}_{\mathrm{Yukawa}} = \bar{Q}_i H Y_D^{ij} D_j + \bar{Q}_i \tilde{H} Y_U^{ij} U_j + \bar{L}_i H Y_E^{ij} E_j + \mathrm{h.c.}\,, \tag{2.13}$$

which yield Dirac masses $M_\psi^{ij} = \frac{v}{\sqrt{2}}Y_\psi^{ij}$ for the fermions $\psi = u, d, e$ once H acquires its vev. Here, we explicitly include generation indices $i, j = 1, 2, 3$ to emphasize the flavor structure of the Yukawa couplings Y_ψ^{ij}. Using chiral, unitary field transformations in flavor space

$$\psi_{\mathrm{L,R}}^i \to U_{\psi_{\mathrm{L,R}}}^{ij}\psi_{\mathrm{L,R}}^j, \tag{2.14}$$

the mass matrices can be diagonalized. These transformations manifest themselves in the charged currents mediated by the $W^\pm$ bosons. Defining the Cabbibo–Kobayashi–Maskawa (CKM) matrix

$$V_{\mathrm{CKM}} \equiv U_{u_{\mathrm{L}}}^\dagger U_{d_{\mathrm{L}}}\,, \tag{2.15}$$

and using (2.12), the charged-current interactions of the quarks in the mass eigenbasis read

$$\mathcal{L}_{\mathrm{kin}} \supset \frac{g}{\sqrt{2}}\left(\bar{u}_{\mathrm{L}}^i\gamma^\mu V_{ij} d_{\mathrm{L}}^j W_\mu^+ + \bar{d}_{\mathrm{L}}^i\gamma^\mu V_{ij}^\dagger u_{\mathrm{L}}^j W_\mu^-\right)\,, \tag{2.16}$$

where the indices i, j now iterate over the mass eigenstates *up* (u), *charm* (c), and *top* (t) and *down* (d), *strange* (s), and *bottom* (b) of the up- and down-type quarks, respectively. Therefore, off-diagonal entries in V_{CKM} lead to FCCCs in the quark sector. The neutral currents, however, are not affected by the flavor rotations of the fermions, because the couplings to the photon and the Z boson are *flavor universal*. Hence, *there are no tree-level FCNCs in the SM*. Furthermore, loop contributions as exemplarily depicted in Figure 2.1 are suppressed due to the Glashow–Iliopoulos–Maiani (GIM) mechanism, which is based on the destructive interference between diagrams with quarks from different

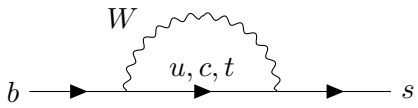

Figure 2.1.: Loop-level Feynman diagram that induces the FCNCs $b \to s$ in the SM.

generations propagating in the loop. If all quark mass differences were zero, summing over all quark generations would lead to an exact cancellation due to the unitarity of the CKM matrix. In reality the quark masses are strongly hierarchical so that only partial cancellations occur and a small contribution to down-type FCNCs, dominated by the top quark, remains [20, 21].

In the absence of neutrino masses there is no mixing in the lepton sector. We will come back to the more general case after reviewing some fundamental experimental results of the SM flavor parameters.

Since the Yukawa couplings are free parameters of the SM, there is no reason to expect any distinct structure. Nevertheless, the experimentally determined values of the quark masses [22]

$$\begin{array}{lcll} m_u \simeq 2.2\,\text{MeV} & < & m_d \simeq 4.7\,\text{MeV} & \ll \quad m_s \simeq 95\,\text{MeV} \\ & < & \Lambda_{\text{QCD}} \simeq \mathcal{O}(100)\,\text{MeV} & \ll \\ m_c \simeq 1.3\,\text{GeV} & < & m_b \simeq 4.2\,\text{GeV} & \ll \quad m_t \simeq 173\,\text{GeV} \simeq \frac{v}{\sqrt{2}} \end{array} \tag{2.17}$$

exhibit a strong hierarchy, where only the top quark mass is of the order of the EW scale, while all others are much smaller. Here Λ_{QCD} denotes the QCD confinement scale. A similar hierarchical structure is observed in quark mixing. With the sines $s_{ij} \equiv \sin\vartheta_{ij}$ of the three mixing angles ϑ_{ij}, as defined in (A.9), the observed hierarchy is [23]

$$s_{13} \ll s_{23} \ll s_{12} \ll 1\,. \tag{2.18}$$

This means the CKM matrix is equal to the unit matrix up to corrections of the order of the Wolfenstein parameter

$$\lambda \equiv s_{12} = 0.224\,53 \pm 0.000\,44\,. \tag{2.19}$$

More precisely, the CKM matrix can be parametrized as

$$V_{\text{CKM}} = \begin{pmatrix} 1 - \frac{\lambda^2}{2} & \lambda & A\lambda^3(\bar{\rho} - i\bar{\eta}) \\ -\lambda & 1 - \frac{\lambda^2}{2} & A\lambda^2 \\ A\lambda^3(1 - \bar{\rho} - i\bar{\eta}) & -A\lambda^2 & 1 \end{pmatrix} + \mathcal{O}\left(\lambda^4\right), \tag{2.20}$$

where the three parameters

$$A = 0.836 \pm 0.015, \quad \bar{\rho} = 0.122^{+0.018}_{-0.017}, \quad \bar{\eta} = 0.355^{+0.012}_{-0.011} \tag{2.21}$$

are introduced to accommodate for the two remaining mixing angles and the complex phase.

The fact that the SM flavor parameters are small and hierarchical without any apparent reason poses the *SM flavor puzzle* [24].

While the masses of the charged leptons follow a resembling pattern

$$m_e \simeq 0.51\,\text{MeV} \lll m_\mu \simeq 106\,\text{MeV} \ll m_\tau \simeq 1.8\,\text{GeV}\,, \tag{2.22}$$

the neutrino sector looks very different. The experimental data on neutrino oscillations shows that two of the three mixing angles (see (A.9)) of the Pontecorvo–Maki–Nakagawa–Sakata (PMNS) matrix

$$U_{\text{PMNS}} \equiv U_{e_\text{L}}^\dagger U_{\nu_\text{L}} \tag{2.23}$$

are of order one, while the third one is comparably small [23]:

$$\theta_{23} \simeq \frac{\pi}{4}, \quad \theta_{12} \simeq \frac{\pi}{5.4}, \quad \theta_{13} \simeq \frac{\pi}{20}\,. \tag{2.24}$$

Even though it is now excluded by experimental data the so-called tribimaximal (TBM) mixing pattern [25]

$$U_{\text{PMNS}}^{\text{TBM}} = \begin{pmatrix} \sqrt{\frac{2}{3}} & \frac{1}{\sqrt{3}} & 0 \\ -\frac{1}{\sqrt{6}} & \frac{1}{\sqrt{3}} & -\frac{1}{\sqrt{2}} \\ -\frac{1}{\sqrt{6}} & \frac{1}{\sqrt{3}} & \frac{1}{\sqrt{2}} \end{pmatrix} \tag{2.25}$$

provides a good leading order approximation for the PMNS matrix and hence serves as a useful starting point for flavor model building in the lepton sector.

Furthermore, the observation of non-trivial mixing in the lepton sector implies non-vanishing neutrino masses. From neutrino oscillation data the two mass squared differences have been determined to be of the orders $10^{-5}\,\text{eV}^2$ and $10^{-3}\,\text{eV}^2$, while cosmological data imposes an upper bound of about $0.5\,\text{eV}$ on the absolute neutrino mass scale [22]. This scale is so small that, due to the GIM mechanism, neutrino contributions to FCNCs in the charged lepton sector are negligibly small so that there is virtually no charged lepton flavor violation (cLFV) in the SM.

Since neutrino masses are absent in the SM, the observation of neutrino oscillations already require physics beyond the SM. Extending the SM field content by the gauge singlet fermion $N \equiv \nu_\text{R}$ allows to include the terms

$$-\mathcal{L}_{\text{Neutrino}} = \bar{L}_i \tilde{H} Y_N^{ij} N_j + \frac{1}{2} \bar{N}_i^c M_\text{M}^{ij} N_j + \text{h.c.} \tag{2.26}$$

that give rise to neutrino masses and thus permit non-trivial mixing. Besides the usual Yukawa interaction that yields a Dirac mass matrix $M_\text{D} \equiv \frac{v}{\sqrt{2}} Y_N$, there is a Majorana mass term involving the Majorana mass matrix M_M. If the Dirac masses are much smaller than the Majorana masses, the heavy mass eigenstates remain at the scale

of M_{M}, while the light mass eigenstates are of the order $M_{\mathrm{D}}^T M_{\mathrm{M}}^{-1} M_{\mathrm{D}}$. This so-called *seesaw-mechanism* [26] provides a specific UV completion of the dimension-5 effective operator

$$\mathcal{O}_\nu^{ij} = \left(\bar{L}^i \tilde{H}\right)\left(\tilde{H} L^j\right)^\dagger , \tag{2.27}$$

also known as the Weinberg operator.

We will often make use of such effective operators in order to parametrize NP and its underlying flavor structure in a model-independent manner. The details of this EFT approach will be discussed in the next chapter. In this thesis, we focus on NP at the TeV scale, which is becoming more and more accessible at current collider experiments. However, we would expect this NP to have a generic flavor structure that would lead to easily detectable signals in FCNC observables. The absence of such signals presents the *BSM flavor puzzle* [24].

2.4. Symmetries of the Flavor Sector

The gauge part of the SM Lagrangian exhibits the large accidental flavor symmetry

$$U(3)_Q \times U(3)_U \times U(3)_D \times U(3)_L \times U(3)_E \tag{2.28}$$

which reflects the freedom to rotate the five fermion fields Q, U, D, L, E in flavor space. In the presence of the Yukawa interactions this symmetry is broken down to

$$U(1)_B \times U(1)_{L_e} \times U(1)_{L_\mu} \times U(1)_{L_\tau} \tag{2.29}$$

corresponding to the global symmetries associated with the conservation of baryon number and the individual lepton numbers of each generation. Since there are 41 broken generators this means that of the 54 real parameters present in the three Yukawa matrices $Y_{U,D,E}$ only 13 are physical. These are the six quark masses, three mixing angles and one CP phase of the quark sector and the three charged lepton masses.

It should be noted that if non-perturbative QCD effects are taken into account the axial vector symmetry $U(1)_A$ of the quark sector is anomalous so that there is one more physical parameter in the SM, namely the strong CP phase θ_{QCD}. Experimentally there is no evidence for CP violation in QCD so that θ_{QCD} must be very small – this poses the *strong CP problem*.

A way to approach the BSM flavor puzzle is to assume that the SM Yukawa interactions are the only terms that break the flavor symmetry (2.28). This idea is formalized in the framework of minimal flavor violation (MFV) [27–29] in which the SM Yukawas are promoted to spurion fields that transform as bifundamentals under the SM flavor symmetry group, rendering the Yukawa interactions formally invariant under that symmetry. In this framework the flavor structure of any NP interactions can then be expressed

in terms of the Yukawa spurions by requiring that new terms in the Lagrangian also formally respect the flavor symmetry.

In order to solve the SM flavor puzzle in this symmetry-based manner the flavor symmetry, or a subgroup thereof, has to be broken by some mechanism that gives rise to the Yukawa couplings. This needs to happen in such a way that the structure of the resulting matrices yields the observed pattern of masses and mixing of the fermions. We will further discuss this approach in Chapter 5.

Chapter 3.

Model-Independent Study of Flavor Observables

Experimentally, the flavor structure of the quark sector is accessible through the study of flavor-changing processes, which, due to the confinement of QCD, necessarily involve hadronic bound states. Thus, we focus on EW decays of hadronic states that are stable with respect to the flavor-universal QCD interactions. However, bound states that can decay through QCD may still occur as intermediate resonances in decay spectra of heavier states.

Since the flavor dynamics, which is governed by the weak interaction, can be handled in perturbation theory, it is essential to disentangle it from the confining dynamics that stems from the non-perturbative regime of QCD. The fact that this is at all possible, relies on *factorization* theorems that allow us to separate contributions that arise from physics at different scales.

3.1. Effective Field Theory Approach

EFTs allow us to separate short-distance and long-distance effects in a systematic manner, thereby providing the foundation for a model-independent parametrization of NP contributions from high scales.

The foundation of this factorization approach is provided by the Appelquist–Carrazone decoupling theorem [31], which states that at low energies contributions from heavy states are suppressed by their mass scale. Processes that only involve initial and final states with energies that are small compared to a particular scale Λ can therefore be described by an effective Hamiltonian of the form

$$\mathcal{H}_{\text{eff}} = \sum_i \frac{C_i}{\Lambda^{d-4}} \mathcal{O}_i^{(d)} + \text{h.c.}\,, \tag{3.1}$$

where all short-distance contributions from scales higher than Λ are included in the *Wilson coefficients* C_i and the long-distance contributions from scales lower than Λ are contained in the matrix elements of the local operators $\mathcal{O}_i^{(d)}$ of mass dimension $d > 4$.

As the top quark is so heavy that it decays before it can form any hadronic states, the heaviest hadrons are the ones involving b quarks and hence they are much lighter than the EW gauge bosons. The EFT that describes weak interactions at hadronic scales can thus be obtained from the SM by removing the heavy degrees of freedom, such as the top quark, the W and Z bosons, and the Higgs, from the theory.

The standard example for a hadronic process mediated by the weak interaction is nuclear β decay. Figure 3.1 shows at constituent level the leading order Feynman diagrams for this process in the full EW theory (left) and in the EFT obtained in the limit of small momenta (right). In this limit, the matrix element calculated in the full theory (in unitary gauge) reads

$$\left(\frac{ig}{\sqrt{2}}\right)^2 V_{ud}\,(\bar{u}_\mathrm{L}\gamma^\mu d_\mathrm{L})\,\frac{-\eta_{\mu\nu}+\frac{q_\mu q_\nu}{m_W^2}}{q^2-m_W^2}\,(\bar{e}_\mathrm{L}\gamma^\nu \nu_{e\mathrm{L}}) \;\xrightarrow{q\ll m_W}\; -\frac{4G_\mathrm{F}}{\sqrt{2}}V_{ud}\,(\bar{u}_\mathrm{L}\gamma^\mu d_\mathrm{L})\,(\bar{e}_\mathrm{L}\gamma_\mu \nu_{e\mathrm{L}})\;, \tag{3.2}$$

where $G_\mathrm{F} \equiv \frac{\sqrt{2}}{8}\frac{g^2}{m_W^2}$ is the Fermi constant. Hence, in order that the EFT described by the weak Hamiltonian [32]

$$\mathcal{H}_\mathrm{eff}^{d\to ue\bar{\nu}_e} = -\frac{4G_\mathrm{F}}{\sqrt{2}}V_{ud}\,C\,(\bar{u}_\mathrm{L}\gamma^\mu d_\mathrm{L})\,(\bar{e}_\mathrm{L}\gamma_\mu \nu_{e\mathrm{L}}) + \mathrm{h.c.} \tag{3.3}$$

yield the same result as the full theory, the Wilson coefficient C must be taken to be one. This procedure is called *matching* and can be used to obtain the Wilson coefficients of a low energy EFT from the ultraviolet (UV) theory in a "top-down" manner.

This approach is formally described by the Operator Product Expansion (OPE), which allows us to express products of charged current operators as a series of local operators [32].

Of course, the UV theory does not need to be the SM, but can be any BSM model. Since EFTs provide the foundation for all calculations of flavor processes they serve as an interface between the construction of BSM models and their flavor phenomenology – after matching a specific model onto the EFT, predictions for flavor observables can be calculated. But this also means that EFTs enable the study of flavor observables independent of the underlying UV model if all effective operators that are compatible with the existing symmetries are included and their Wilson coefficients are treated as free parameters. In contrast to the aforementioned method, this "bottom-up" approach allows for a data-driven analysis in which experimental data on flavor observables is used to constrain the Wilson coefficients of the EFT. By this means, hints for NP in

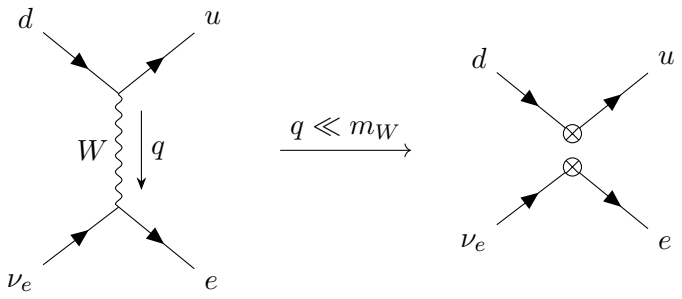

Figure 3.1.: Feynman diagrams for nuclear β decay at parton level in the EW theory (left) and in Fermi's theory (right) – an EFT valid at scales below m_W where the heavy degrees of freedom are integrated out [32].

experimental data can be used to identify the responsible operators and thereby guide the construction of BSM models.

So far we have not taken into account any QCD corrections. However, they turn out to be essential, because in the calculation of hadronic decay rates the renormalization scale is typically chosen to be of the order of the mass of the decaying hadron, while the Wilson coefficients are determined at the matching scale $\Lambda \sim m_W$. Therefore, radiative QCD corrections can give large logarithmic contributions of order $\alpha_\mathrm{s} \ln \frac{\Lambda}{\mu_\mathrm{H}}$, where μ_H is the hadronic scale. These large logarithms can be resummed to all orders in α_s by means of the renormalization group (RG) [30]. By introducing a renormalization scale $\mu \leq \Lambda$ in the effective Hamiltonian

$$\mathcal{H}_\mathrm{eff} = \sum_i \frac{C_i(\mu)}{\Lambda^{d-4}} \mathcal{O}_i^{(d)}(\mu) + \mathrm{h.c.}\,, \tag{3.4}$$

we can shift long-distance contributions to the hadronic matrix elements, while the short-distance contributions remain in the Wilson coefficients. The renormalization group equations (RGEs) that govern the scale dependence of the Wilson coefficients are obtained from the requirement that physical observables be independent of the scale parameter μ and read

$$\frac{\mathrm{d}\vec{C}(\mu)}{\mathrm{d}\ln\mu} - \vec{C}(\mu)\gamma^T(\mu) = 0\,, \tag{3.5}$$

where γ is the anomalous dimension matrix. As the relevant radiative corrections stem from QCD only, the scale dependence can be completely expressed in terms of the running of the strong coupling constant α_s. This allows us to solve the RGEs (3.5), yielding at leading order

$$\vec{C}(\mu) = \vec{C}(\Lambda) \exp\left(\frac{\gamma_0^T}{2\beta_0^{(n_\mathrm{f})}} \ln\frac{\alpha_\mathrm{s}(\Lambda)}{\alpha_\mathrm{s}(\mu)}\right)\,, \tag{3.6}$$

where $\beta_0^{(n_\mathrm{f})} = 11 - \frac{2}{3}n_\mathrm{f}$ is the leading order contribution to the beta function of α_s for n_f fermions. In this approximation the RGE evolution resums the leading logarithms of the form $\left(\alpha_\mathrm{s} \ln\frac{\Lambda}{\mu}\right)^n$ to all orders, leaving corrections of order $\alpha_\mathrm{s}^n \left(\ln\frac{\Lambda}{\mu}\right)^{n-1}$.

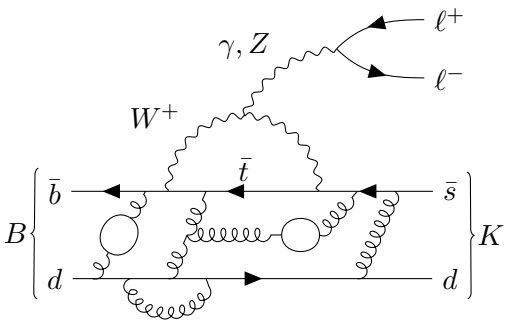

Figure 3.2.: Electroweak penguin diagram contributing to the semileptonic decay $B \to K\ell^+\ell^-$. Hadronic effects are schematically included in terms of gluon and quark loops between the hadronic states.

3.2. Parametrization of Long-Distance QCD Contributions to Hadronic Processes

We will now turn to the matrix elements of the local operators and discuss how the long-distance QCD effects can be parametrized in terms of non-perturbative quantities as well as how these quantities can be determined.

As a trivial consequence of the OPE, leptonic parts of the matrix elements can be factorized out and calculated perturbatively. Therefore, (semi-)leptonic decays of hadrons provide the simplest observables for the study of quark flavor transitions, while simultaneously adding a potential link to lepton flavor. As an example, we show in Figure 3.2 a Feynman diagram contributing to the rare semileptonic B decay $B \to K\ell^+\ell^-$, explicitly including gluon and quark loops to schematically illustrate the non-perturbative QCD contributions to the hadronic part of the process.

As matrix elements of quark current operators involving hadronic states generally cannot be calculated perturbatively, one is led to exploit the knowledge of the Lorentz structure of these matrix elements to parametrize them in the most general way.

In the case of only one hadronic state (as e.g. in a purely leptonic decay of a meson), all non-vanishing matrix elements of hadronic operators are proportional to the *decay constant*. For instance, the decay constant f_P of a pseudoscalar meson P is defined by

$$\langle 0|j_5^\mu|P(p)\rangle \equiv -ip^\mu f_P\,, \tag{3.7}$$

where p^μ is the meson's 4-momentum and j_5^μ is the axial vector quark current operator that annihilates $|P(p)\rangle$.

Hadronic matrix elements involving two or more hadrons can be expressed as linear combinations of the involved kinematic variables and so-called *form factors*, which can depend on Lorentz invariant kinematic quantities. In the case of a transition $P_1 \to P_2$ between

two pseudoscalar mesons that is induced at the quark level by the transition $q_1 \to q_2$, the matrix element of the vector quark current operator $j^\mu \equiv \bar{q}_2 \gamma^\mu q_1$ can be parametrized by two independent form factors $F_0(q^2)$ and $F_1(q^2)$ (in some conventions called $f_0(q^2)$ and $f_+(q^2)$, respectively), which are defined by [34]

$$\langle P_2(p_2)|j^\mu|P_1(p_1)\rangle \equiv \left((p_1+p_2)^\mu - \frac{m_1^2-m_2^2}{q^2}q^\mu\right)F_1(q^2) + \frac{m_1^2-m_2^2}{q^2}q^\mu F_0(q^2)\,, \quad (3.8)$$

where $q^\mu \equiv (p_1-p_2)^\mu$ is the hadronic momentum transfer and $F_0(0) = F_1(0)$. Furthermore, the tensor form factor $F_\mathrm{T}(q^2)$ is defined by

$$\langle P_2(p_2)|t^{\mu\nu}|P_1(p_1)\rangle \equiv -i(p_1^\mu p_2^\nu - p_1^\nu p_2^\mu)\frac{2F_\mathrm{T}(q^2)}{m_1+m_2}\,, \quad (3.9)$$

where $t^{\mu\nu} \equiv \bar{q}_2\sigma^{\mu\nu}q_1$. Matrix elements of (pseudo)scalar, pseudotensor and axial vector operators can be expressed in terms of (3.8) and (3.9) by exploiting the quarks' equations of motion.

In the following chapters we will also study processes in which the initial pseudoscalar meson decays into a vector meson. With the polarization vector ε^μ of the vector meson V there are more options to decompose the hadronic matrix elements, resulting in a larger number of independent form factors than before. For the vector and axial vector currents, the definitions read [34, 35]

$$\langle V(p_2,\varepsilon)|j^\mu|P(p_1)\rangle \equiv -i\epsilon^{\mu\nu\rho\sigma}\varepsilon^*_\nu p_{1\rho}p_{2\sigma}\frac{2V(q^2)}{m_P+m_V} \quad (3.10)$$

$$\begin{aligned}\langle V(p_2,\varepsilon)|j_5^\mu|P(p_1)\rangle \equiv{}& \varepsilon^{*\mu}(m_P+m_V)A_1(q^2) - (p_1+p_2)^\mu(\varepsilon^*\cdot q)\frac{A_2(q^2)}{m_P+m_V}\\ &- q^\mu(\varepsilon^*\cdot q)\frac{2m_V}{q^2}\Big(A_3(q^2)-A_0(q^2)\Big)\end{aligned} \quad (3.11)$$

where $A_3(q^2) \equiv \frac{m_P+m_V}{2m_V}A_1(q^2) - \frac{m_P-m_V}{2m_V}A_2(q^2)$ and $A_3(0) = A_0(0)$. The tensor form factors are defined by

$$\begin{aligned}\langle V(p_2,\varepsilon)|t^{\mu\nu}|P(p_1)\rangle \equiv \epsilon^{\mu\nu\rho\sigma}\Bigg[&-\varepsilon^*_\rho(p_1+p_2)^\sigma T_1(q^2)\\ &+\varepsilon^*_\rho q_\sigma\frac{m_P^2-m_V^2}{q^2}\Big(T_1(q^2)-T_2(q^2)\Big)\\ &+2\frac{(\varepsilon^*\cdot q)}{q^2}p_{1\rho}p_{2\sigma}\left(T_1(q^2)-T_2(q^2)-\frac{q^2}{m_P^2-m_V^2}T_3(q^2)\right)\Bigg]\,,\end{aligned} \quad (3.12)$$

where $T_1(0) = T_2(0)$. As in the previous case, all other matrix elements can be expressed in terms of the ones considered here.

Due to their non-perturbative nature these quantities are very difficult to calculate. Even though there are a number of very successful methods to determine them, form

factors and decay constants are still the major source of uncertainty in the prediction of flavor observables. On account of their universality among processes that only differ in their non-hadronic parts, a viable method of their determination is the extraction from experiment.

We briefly introduce theoretical frameworks that allow to either simplify form factor parametrizations, thereby reducing the number of parameters that have to be extracted from experimental data, or to even calculate form factors.

Heavy Quark Effective Theory (HQET) For hadrons composed of a single heavy quark ($m_Q \gg \Lambda_{\text{QCD}}$, $Q = b, c$) and one or more light quarks the short-distance effects from the heavy quark scale can be systematically separated from the long-distance effects that occur at the QCD confinement scale Λ_{QCD}. The resulting EFT, namely HQET, allows to establish form factor relations [36] that are particularly useful for $\bar{B} \to D$ and $\bar{B} \to D^*$ transitions. See e.g. [37, 38] for in-depth discussions.

Lattice Quantum Chromodynamics (LQCD) A direct approach towards the calculation of non-perturbative hadronic matrix elements is taken by LQCD [39] where space-time is discretized, resulting in a finite QFT. Due to large discretization uncertainties at low q^2 LQCD form factors only provide useful information at high q^2.

Light Cone Sum Rules (LCSR) In the kinematic region of low hadronic recoil, i.e. high q^2, LCSR provide a complementary theoretical method of calculating form factors. This method is based on a light-cone expansion of the correlator of the time-ordered product of two local quark current operators, which are evaluated between the on-shell final state hadron and the vacuum [40].

In order to minimize the influence of the large uncertainties stemming from long-distance QCD contributions, it is beneficial to construct observables in which substantial parts of the hadronic uncertainties cancel (often referred to as "clean" observables). A prominent example for an observable of this kind is

$$R_K \simeq \frac{\mathcal{B}(\bar{B} \to \bar{K}\mu^+\mu^-)}{\mathcal{B}(\bar{B} \to \bar{K}e^+e^-)} \,, \tag{3.13}$$

i.e. the ratio of branching ratios of the rare semileptonic decays $\bar{B} \to \bar{K}\ell^+\ell^-$ in which the numerator and denominator only differ by the flavor of the leptons in the final state. The SM predicts this ratio to be unity owing to the lepton-universal nature of the couplings of the Z boson and the photon and the fact that the mass difference between the muon and the electron is negligibly small compared to the masses of the Kaon and the B meson. As the hadronic parts of the branching ratios can be factorized from the leptonic part, the respective hadronic uncertainties largely cancel in the ratio (3.13).

We will discuss this particular observable and similar ones in much more detail in the following sections.

3.3. The FCCC Processes $b \to c\ell\bar{\nu}$

The first set of observables we introduce are based on the FCCC transitions $b \to c\ell\bar{\nu}$, which can be regarded as the heavy-flavor equivalent of the quark transitions underlying nuclear β decay in the SM. After introducing the effective operators that govern this class of processes and reviewing the hadronic processes $\bar{B} \to D^{(*)}\ell\bar{\nu}$ in a model-independent manner, we will take a closer look at several NP-sensitive observables and report on the current experimental status as well as recent developments.

3.3.1. Hadronic Observables in the Effective Theory

Analogous to the weak Hamiltonian (3.3), the effective Hamiltonian describing $b \to c\ell\bar{\nu}$ transitions can be expressed as

$$\mathcal{H}_{\text{eff}}^{b\to c\ell\bar{\nu}} = \frac{4G_{\text{F}}}{\sqrt{2}} V_{cb} \left(\delta_{\ell\nu} \mathcal{O}_{\text{V}_1}^{\ell\nu} + \sum_i C_i^{\ell\nu} \mathcal{O}_i^{\ell\nu} \right) + \text{h.c.}\,, \tag{3.14}$$

where δ denotes the Kronecker symbol and the effective dimension-six operators are given as

$$\begin{aligned} \mathcal{O}_{\text{V}_{1(2)}}^{\ell\nu} &= \left[\bar{c}_{\text{L(R)}}\gamma^\mu b_{\text{L(R)}}\right]\left[\bar{\ell}_{\text{L}}\gamma_\mu \nu_{\text{L}}\right]\,, \\ \mathcal{O}_{\text{S}_{1(2)}}^{\ell\nu} &= \left[\bar{c}_{\text{L(R)}} b_{\text{R(L)}}\right]\left[\bar{\ell}_{\text{R}}\nu_{\text{L}}\right]\,, \\ \mathcal{O}_{\text{T}}^{\ell\nu} &= \left[\bar{c}_{\text{R}}\sigma^{\mu\nu} b_{\text{L}}\right]\left[\bar{\ell}_{\text{R}}\sigma_{\mu\nu}\nu_{\text{L}}\right]\,. \end{aligned} \tag{3.15}$$

We use a notation where $\ell \in \{e, \mu, \tau\}$ and $\nu \in \{\nu_e, \nu_\mu, \nu_\tau\}$ are used as placeholders for fields of a specific flavor and also as flavor indices of the operators and Wilson coefficients. In the SM only the operator $\mathcal{O}_{\text{V}_1}$ receives a non-negligible contribution, which is explicitly included in the definition of the effective Hamiltonian so that the $C_i^{\ell\nu}$ contain only the NP contributions.

Since the chiral vector quark currents of $\mathcal{O}_{\text{V}_{1(2)}}$ are conserved in the limit of massless quarks, the respective anomalous dimensions vanish [30]. The anomalous dimension matrix of the remaining operators is diagonal, which, in the leading logarithmic approximation, results in

$$C_i(\mu_b) = \left(\frac{\alpha_{\text{s}}(m_t)}{\alpha_{\text{s}}(\mu_b)}\right)^{\frac{\gamma_i}{2\beta_0^{(5)}}} \left(\frac{\alpha_{\text{s}}(\Lambda)}{\alpha_{\text{s}}(m_t)}\right)^{\frac{\gamma_i}{2\beta_0^{(6)}}} C_i(\Lambda)\,, \tag{3.16}$$

where $i \in \{\text{S}_1, \text{S}_2, \text{T}\}$ and the respective anomalous dimensions are $\gamma_{\text{S}_{1,2}} = -8$ and $\gamma_{\text{T}} = \frac{8}{3}$ [41].

The simplest hadronic processes based on the $b \to c\ell\bar{\nu}$ transition are the semileptonic decays $\bar{B} \to D\ell\bar{\nu}$ and $\bar{B} \to D^*\ell\bar{\nu}$ (unless the charges of the hadronic states are explicitly specified, we average over different isospin modes). Both of these decays have and continue to play an important role in flavor physics by providing a way to determine

the CKM element V_{cb} and by presenting us with a variety of observables that are highly sensitive to NP contributions. Within the EFT described above the differential branching fractions $\bar{B} \to D^{(*)}\ell\bar{\nu}$ can be written as

$$\begin{aligned}\frac{\mathrm{d}\mathcal{B}(\bar{B}\to D\ell\bar{\nu})}{\mathrm{d}q^2} &= \frac{\mathrm{d}\mathcal{B}^{\mathrm{SM}}(\bar{B}\to D\ell\bar{\nu})}{\mathrm{d}q^2}\Big|\delta_{\ell\nu}+C^{\ell\nu}_{\mathrm{V}_1}+C^{\ell\nu}_{\mathrm{V}_2}\Big|^2 + A_{\mathrm{S}}(q^2)\Big|C^{\ell\nu}_{\mathrm{S}_1}+C^{\ell\nu}_{\mathrm{S}_2}\Big|^2 \\ &\quad + A_{\mathrm{T}}(q^2)\Big|C^{\ell\nu}_{\mathrm{T}}\Big|^2 + A_{\mathrm{VS}}(q^2)\,\mathrm{Re}\left[(\delta_{\ell\nu}+C^{\ell\nu}_{\mathrm{V}_1}+C^{\ell\nu}_{\mathrm{V}_2})(C^{\ell\nu}_{\mathrm{S}_1}+C^{\ell\nu}_{\mathrm{S}_2})^*\right] \\ &\quad + A_{\mathrm{VT}}(q^2)\,\mathrm{Re}\left[(\delta_{\ell\nu}+C^{\ell\nu}_{\mathrm{V}_1}+C^{\ell\nu}_{\mathrm{V}_2})C^{\ell\nu *}_{\mathrm{T}}\right],\end{aligned} \tag{3.17}$$

and

$$\begin{aligned}\frac{\mathrm{d}\mathcal{B}(\bar{B}\to D^*\ell\bar{\nu})}{\mathrm{d}q^2} &= \frac{\mathrm{d}\mathcal{B}^{\mathrm{SM}}(\bar{B}\to D^*\ell\bar{\nu})}{\mathrm{d}q^2}\left[\Big|\delta_{\ell\nu}+C^{\ell\nu}_{\mathrm{V}_1}\Big|^2+\Big|C^{\ell\nu}_{\mathrm{V}_2}\Big|^2\right] \\ &\quad + B_{\mathrm{V}_1\mathrm{V}_2}(q^2)\,\mathrm{Re}\left[(\delta_{\ell\nu}+C^{\ell\nu}_{\mathrm{V}_1})C^{\ell\nu *}_{\mathrm{V}_2}\right] + B_{\mathrm{S}}(q^2)\Big|C^{\ell\nu}_{\mathrm{S}_1}-C^{\ell\nu}_{\mathrm{S}_2}\Big|^2 \\ &\quad + B_{\mathrm{T}}(q^2)\Big|C^{\ell\nu}_{\mathrm{T}}\Big|^2 + B_{\mathrm{VS}}(q^2)\,\mathrm{Re}\left[(\delta_{\ell\nu}+C^{\ell\nu}_{\mathrm{V}_1}-C^{\ell\nu}_{\mathrm{V}_2})(C^{\ell\nu}_{\mathrm{S}_1}-C^{\ell\nu}_{\mathrm{S}_2})^*\right] \\ &\quad + B_{\mathrm{V}_1\mathrm{T}}(q^2)\,\mathrm{Re}\left[(\delta_{\ell\nu}+C^{\ell\nu}_{\mathrm{V}_1})C^{\ell\nu *}_{\mathrm{T}}\right] + B_{\mathrm{V}_2\mathrm{T}}(q^2)\,\mathrm{Re}\left[C^{\ell\nu}_{\mathrm{V}_2}C^{\ell\nu *}_{\mathrm{T}}\right],\end{aligned} \tag{3.18}$$

where the square of the hadronic momentum transfer q^2 corresponds to the dilepton invariant mass squared and is bounded by $m_\ell^2 \le q^2 \le (m_B - m_{D^{(*)}})^2$. The SM contribution to $\bar{B}\to D\ell\bar{\nu}$ is given by

$$\frac{\mathrm{d}\mathcal{B}^{\mathrm{SM}}(\bar{B}\to D\ell\bar{\nu}_\ell)}{\mathrm{d}q^2} = N(q^2)\left[\left(1+\frac{m_\ell^2}{2q^2}\right)H^{s2}_{V,0}(q^2)+\frac{3}{2}\frac{m_\ell^2}{q^2}H^{s2}_{V,t}(q^2)\right] \tag{3.19}$$

with the normalization factor

$$N(q^2) \equiv \tau_B \frac{G_{\mathrm{F}}^2|V_{cb}|^2}{192\pi^3 m_B^3} q^2\sqrt{\lambda_{D^{(*)}}(q^2)}\left(1-\frac{m_\ell^2}{q^2}\right)^2, \tag{3.20}$$

where $\lambda_{D^{(*)}}(q^2) \equiv \lambda(q^2, m_B, m_{D^{(*)}})$ denotes the Källén function given in Appendix A and τ_B is the lifetime of the B meson. For $\bar{B}\to D^*\ell\bar{\nu}$ the SM contribution reads

$$\begin{aligned}\frac{\mathrm{d}\mathcal{B}^{\mathrm{SM}}(\bar{B}\to D^*\ell\bar{\nu}_\ell)}{\mathrm{d}q^2} &= N(q^2)\Bigg[\left(1+\frac{m_\ell^2}{2q^2}\right)\left(H^2_{V,+}(q^2)+H^2_{V,-}(q^2)+H^2_{V,0}(q^2)\right) \\ &\quad + \frac{3}{2}\frac{m_\ell^2}{q^2}H^2_{V,t}(q^2)\Bigg].\end{aligned} \tag{3.21}$$

Explicit expressions for the non-perturbative quantities $A_i(q^2)$ and $B_i(q^2)$ in terms of the hadronic matrix elements $H_i(q^2)$ are given in Appendix C. We suppress indices that denote their dependence on the lepton and its polarization for the sake of legibility. For the evaluation of the hadronic matrix elements we employ the HQET and lattice form factors

provided in [35, 42, 43]. As the shapes of the q^2 distributions can potentially be affected by NP contributions to operators other than $\mathcal{O}_{\mathrm{V}_1}$, their knowledge is very useful in the search for NP and provides a way of distinguishing between different scenarios. In Figure 3.3 we show the SM predictions for the differential branching ratios along with experimental results to be discussed in the following section.

3.3.2. NP-Sensitive Observables and Experimental Status

While the data on the decay distributions in the case with light leptons in the final state is generally consistent with the theory predictions at the one sigma level, the *BABAR* results for the tauonic modes show a slight excess. This excess can also be seen in the data on the integrated branching ratios listed in Table 3.1. However, due to the large uncertainties on both the theoretical and experimental side of these observables the statistical significance of these deviations is rather small.

In order to reduce the impact of theoretical uncertainties, we consider the ratios

$$R_{D^{(*)}} \equiv \frac{\mathcal{B}(\bar{B} \to D^{(*)}\tau\bar{\nu}_\tau)}{\mathcal{B}(\bar{B} \to D^{(*)}l\bar{\nu}_l)}\,, \tag{3.22}$$

where l denotes the average over the light lepton flavors e and μ. The numerator suffers from phase space suppression caused by the large mass of the τ lepton, leading to SM predictions smaller than one and also leaving small residual form factor uncertainties. Numerical results are provided in Table 3.1 together with all the available experimental data. It can be seen that each individual experimental result exceeds the SM prediction and that the effects in R_D and R_{D^*} are of similar size. With the averages provided by the Heavy Flavor Averaging Group (HFLAV) in summer 2018 [12], taking into account the correlations between R_D and R_{D^*} obtained in the measurements performed by *BABAR* in 2013 and by Belle in 2015, this results in a deviation from the SM value of about $3.8\,\sigma$. Including the most recent values measured by Belle in 2019 reduces the significance of the excess to about $3.1\,\sigma$ [47], as can be seen in Figure 3.4, which shows the updated HFLAV average and the experimental data. Even though this might indicate that the excess be a statistical fluke rather than a sign of NP, it still provides valuable information for the construction of models in flavor physics beyond the SM. As we will see in more detail later on, there are reasons to expect potential NP contributions to $R_{D^{(*)}}$ to be smaller than the current data suggests. In any case, this issue is expected to be clarified by the forthcoming results of Belle II, which have projected relative uncertainties of $\pm 7\,\%$ ($\pm 3\,\%$) for R_D and $\pm 4\,\%$ ($\pm 2\,\%$) for R_{D^*}, respectively, for an integrated luminosity of $5\,\mathrm{ab}^{-1}$ ($50\,\mathrm{ab}^{-1}$) anticipated by the end of 2020 (2024) [48].

A straightforward explanation of the excess can be realized by a contribution to the SM-like operator $\mathcal{O}^\tau_{V_1}$. To linear order in the NP contribution (3.17) and (3.18) yield

$$\hat{R}_{D^{(*)}} - 1 \simeq 2\,\mathrm{Re}\,C^\tau_{\mathrm{V}_1}\,, \tag{3.23}$$

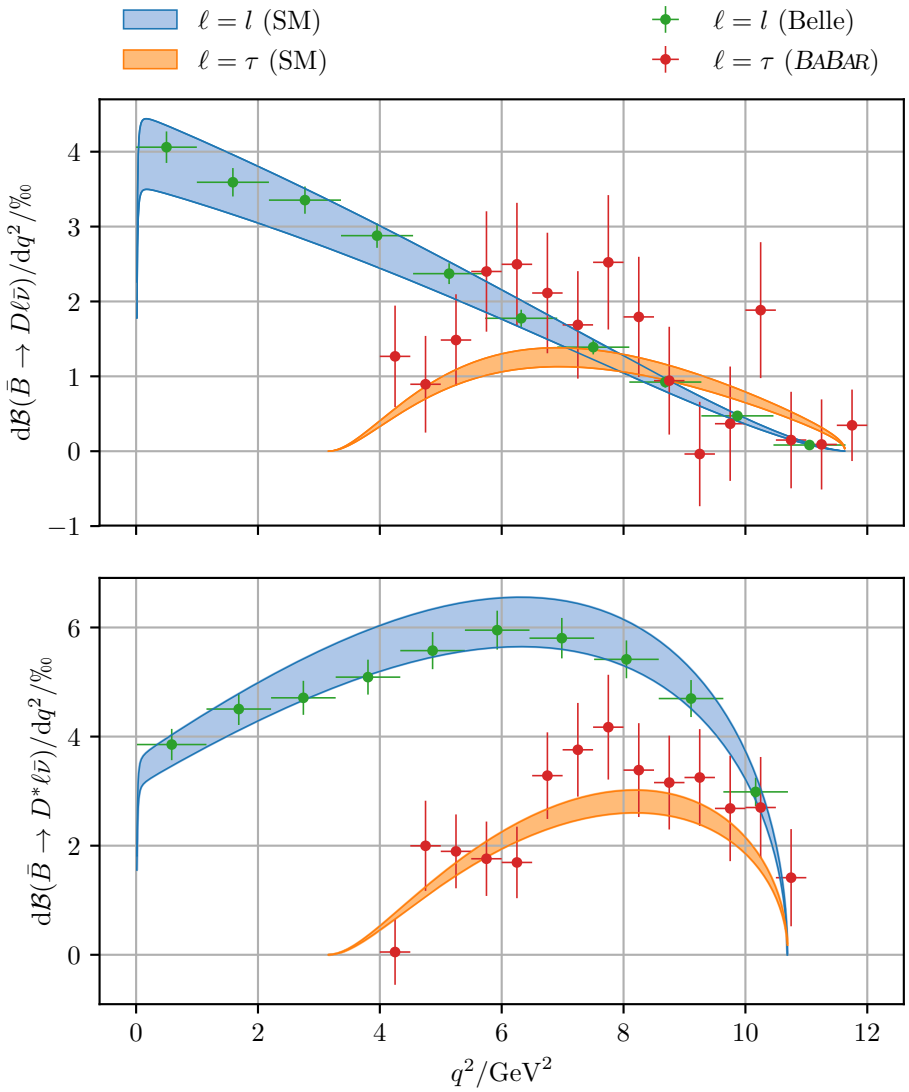

Figure 3.3.: SM predictions and experimental data for the differential branching fractions $\mathrm{d}\mathcal{B}(\bar{B} \to D\ell\nu)/\mathrm{d}q^2$ (top) and $\mathrm{d}\mathcal{B}(\bar{B} \to D^*\ell\bar{\nu})/\mathrm{d}q^2$ (bottom). We use the lepton flavor "l" to indicate taking the average over the light leptons e and μ. The bands mark the one sigma uncertainty ranges, which are driven by the uncertainties of the form factors (see Appendix C for details). The data points for $\bar{B} \to D^{(*)}\tau\bar{\nu}$ are taken from the BABAR collaboration [44]. For the decays with light leptons in the final state we show experimental results provided by the Belle collaboration [45, 46]. Note that the Belle data in the bottom plot (and also our respective SM prediction) relates to the mode $\bar{B}^0 \to D^{*+}l\bar{\nu}$, while in all other cases isospin averaged modes are concerned.

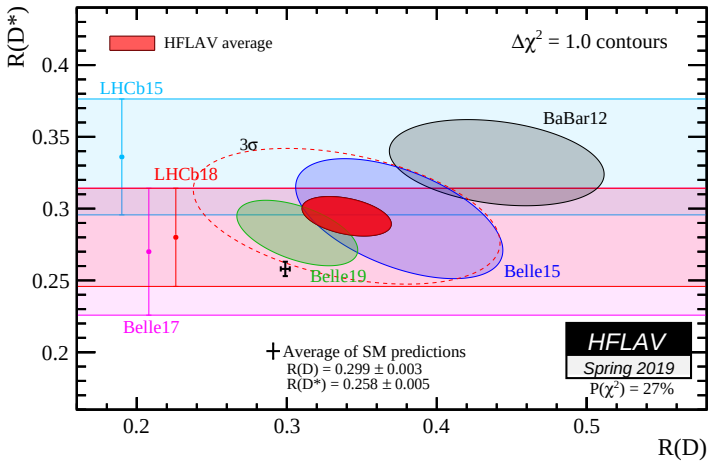

Figure 3.4.: Overview of the available experimental data in the R_D–R_{D^*} plane provided by the HFLAV collaboration in spring 2019 [12].

where we define $\hat{R}_{D^{(*)}} \equiv R_{D^{(*)}}/R^{\text{SM}}_{D^{(*)}}$. Consequently, as the experimental data exceeds the SM prediction by about twenty percent, the required NP contribution is of the order of ten percent. For a generic heavy particle with $\mathcal{O}(1)$ couplings that induces $\mathcal{O}^{\tau}_{V_1}$ at tree-level this implies a mass scale of about 1 TeV. If the couplings are smaller, as typically predicted by flavor models, the mass of the new particle needs to be much lower, which can cause large effects in other low-energy flavor observables. We will also consider contributions to other operators within concrete NP scenarios as a resolution to these tensions later on.

A similar excess in the related observable $R_{J/\psi} \equiv \mathcal{B}(B_c^+ \to J/\psi\tau^+\nu_\tau)/\mathcal{B}(B_c^+ \to J/\psi\mu^+\nu_\mu)$ has been reported by LHCb in 2018 [49]. Adding statistical and systematic uncertainties in quadrature they find $R^{\text{LHCb}}_{J/\psi} = 0.71 \pm 0.25$ – a two sigma excess over the SM predictions, which, depending on the form factors used, range from 0.25 to 0.28 [50–60]. However, such a large central value cannot even be explained by NP contributions [47].

The last NP-sensitive observable we consider is the polarization

$$P_\tau(D^{(*)}) \equiv \frac{\mathcal{B}^+(D^{(*)}) - \mathcal{B}^-(D^{(*)})}{\mathcal{B}^+(D^{(*)}) + \mathcal{B}^-(D^{(*)})} \tag{3.24}$$

of the τ lepton in the rest frame of the decaying $\bar{B}$ meson in $\bar{B} \to D^{(*)}\tau\bar{\nu}_\tau$. Here, $\mathcal{B}^\pm(D^{(*)})$ is a short form for the branching ratio $\mathcal{B}(\bar{B} \to D^{(*)}\tau\bar{\nu}_\tau)$ with a lepton helicity of $\pm 1/2$. As can be seen in Table 3.1 the only available result thus far is Belle's measurement $P^{\text{Belle}}_\tau(D^*) = -0.38 \pm 0.54$, which is compatible with the SM prediction but has a fairly large uncertainty. However, the results are soon expected to become considerably more precise owing to the much higher instantaneous luminosity at the

SuperKEKB collider - the upgrade to KEKB which began operations recently. The projected absolute uncertainty is ± 0.20 (± 0.07) for an integrated luminosity of $5\,\text{ab}^{-1}$ ($50\,\text{ab}^{-1}$) [48].

Further progress in the search for possible NP effects in $b \to c\ell\bar{\nu}$ transitions can be made by investigating angular observables of $\bar{B} \to D^{(*)}\ell\bar{\nu}$ decays. Although this is very challenging as the neutrino in the final state cannot be completely reconstructed in experimental analyses, with the increasing experimental sensitivity and the development of new reconstruction methods angular analyses of these decays might become feasible in the future [61].

Observable	SM Prediction	Exp. Results	Reference	
$\mathcal{B}(\bar{B} \to Dl\bar{\nu}) \times 10^2$	2.30 ± 0.20	2.28 ± 0.10	*BABAR* '07	[62]
		2.31 ± 0.11	Belle '15	[45]
$\mathcal{B}(\bar{B} \to D^* l\bar{\nu}) \times 10^2$	5.58 ± 0.31	5.64 ± 0.22	*BABAR* '07	[62]
$\mathcal{B}(\bar{B}^0 \to D^{*+} l\bar{\nu}) \times 10^2$	5.31 ± 0.37	4.95 ± 0.25	Belle '17	[46]
$\mathcal{B}(\bar{B} \to D\tau\bar{\nu}) \times 10^2$	0.68 ± 0.07	1.02 ± 0.17	*BABAR* '12	[44, 63]
$\mathcal{B}(\bar{B} \to D^*\tau\bar{\nu}) \times 10^2$	1.4 ± 0.1	1.76 ± 0.17	*BABAR* '12	[44, 63]
R_D	0.300 ± 0.008	0.440 ± 0.072	*BABAR* '12	[44, 63]
		0.375 ± 0.069	Belle '15	[64]
		0.307 ± 0.040	Belle '19	[65]
		0.346 ± 0.031	average	
R_{D^*}	0.252 ± 0.003	0.332 ± 0.030	*BABAR* '12	[44, 63]
		0.293 ± 0.041	Belle '15	[64]
		0.336 ± 0.040	LHCb '15	[66]
		0.302 ± 0.032	Belle '16	[67]
		0.270 ± 0.044	Belle '17	[68]
		0.291 ± 0.035	LHCb '18	[69]
		0.283 ± 0.023	Belle '19	[65]
		0.300 ± 0.012	average	
$P_\tau(D)$	0.330 ± 0.023			
$P_\tau(D^*)$	-0.497 ± 0.011	-0.38 ± 0.54	Belle '17	[68]

Table 3.1.: SM predictions and experimental results for key observables in $b \to c\ell\bar{\nu}$ transitions. Statistical and systematic uncertainties are added in quadrature. The averages provided for the experimental values of $R_{D^{(*)}}$ are error weighted arithmetic means. For the LHCb results on R_{D^*} the light lepton flavor refers only to muons. Our predictions are in good agreement with the results available in the literature [43, 70–76].

3.4. The FCNC Processes $b \to s\ell^+\ell^-$

We will now turn to the much rarer transitions $b \to s\ell^+\ell^-$. As FCNCs they only occur at loop level in the SM while also suffering from GIM suppression and are thus much more sensitive to tree-level NP contributions. They are also more accessible at hadron colliders than the previously discussed processes, since typically all decay products can be fully reconstructed in experimental analyses. Thus, a substantial amount of precision data is already available and a lot more is expected to be produced by future experiments.

3.4.1. Hadronic Observables in the Effective Theory

The effective Hamiltonian for this class of processes can be written as

$$\mathcal{H}_{\text{eff}}^{b\to s\ell^+\ell'^-} = -\frac{4G_{\text{F}}}{\sqrt{2}} V_{tb}V_{ts}^* \frac{\alpha_{\text{e}}}{4\pi} \sum_i C_i \mathcal{O}_i + \text{h.c.} \tag{3.25}$$

Our main focus lies on the semileptonic operators

$$\begin{aligned} \mathcal{O}_9^{(\prime)\ell\ell'} &= \left[\bar{s}\gamma_\mu P_{\text{L(R)}} b\right]\left[\bar{\ell}\gamma^\mu \ell'\right] , & \mathcal{O}_{10}^{(\prime)\ell\ell'} &= \left[\bar{s}\gamma_\mu P_{\text{L(R)}} b\right]\left[\bar{\ell}\gamma^\mu\gamma_5 \ell'\right] , \\ \mathcal{O}_{\text{S}}^{(\prime)\ell\ell'} &= \left[\bar{s} P_{\text{R(L)}} b\right]\left[\bar{\ell}\ell'\right] , & \mathcal{O}_{\text{P}}^{(\prime)\ell\ell'} &= \left[\bar{s} P_{\text{R(L)}} b\right]\left[\bar{\ell}\gamma_5 \ell'\right] . \end{aligned} \tag{3.26}$$

Although lepton flavor is conserved in the SM the flavors ℓ and ℓ' can differ in the general case and we will see later on that experimental data on lepton flavor violating processes imposes strong constraints on flavorful NP models. The dominant SM contribution arises from electroweak penguin diagrams, as previously shown in Figure 3.2, resulting in $C_9^{\text{SM}}(m_b) \simeq -C_{10}^{\text{SM}}(m_b) \simeq 4.2$, universally for all leptons [77]. Contributions to (pseudo)scalar and primed operators, in which the chirality of the quark current is flipped, are negligible in the SM but can become sizable in NP scenarios. For the sake of simplicity we disregard tensor operators, which are induced neither in the SM nor in any of the NP models considered later on. Beyond that, there are the quark operators $\mathcal{O}_1$–$\mathcal{O}_6$ as well as the photon dipole operator $\mathcal{O}_7$, each of which receive a non-negligible SM contribution. But since the coupling of these operators to leptonic currents is induced by QED, their contributions – including potential NP effects – are necessarily lepton-universal, making them less interesting for flavorful model building beyond the SM. For a comprehensive study of this EFT we refer to [78].

Like before, we focus on the simplest hadronic processes which in this case are the semileptonic decays $\bar{B} \to \bar{K}\ell^+\ell^-$ and $\bar{B} \to \bar{K}^*\ell^+\ell^-$. We will take a more detailed look at the angular distribution of the former decay mode as it is sufficiently simple and serves as an example that highlights the beneficial properties of angular observables.

Following [79], the matrix element for $\bar{B} \to \bar{K}\ell^+\ell^-$ can be expressed as

$$\begin{aligned}\mathcal{M} = i\frac{G_\mathrm{F}\alpha_\mathrm{e}}{\sqrt{2}\pi}V_{tb}V_{ts}^*\Big(&F_\mathrm{V}(q^2)\,p_B^\mu\left[\bar{\ell}\gamma_\mu\ell\right] + F_\mathrm{A}(q^2)\,p_B^\mu\left[\bar{\ell}\gamma_\mu\gamma_5\ell\right] \\ &+ F_\mathrm{S}(q^2)\left[\bar{\ell}\ell\right] + F_\mathrm{P}(q^2)\left[\bar{\ell}\gamma_5\ell\right]\Big),\end{aligned} \tag{3.27}$$

where the functions $F_i(q^2)$ read

$$\begin{aligned}F_\mathrm{A}(q^2) &\equiv f_+(q^2)C_{10}\,,\\ F_\mathrm{V}(q^2) &\equiv f_+(q^2)C_9^\mathrm{eff}(q^2) + 2C_7^\mathrm{eff}m_b\frac{f_\mathrm{T}(q^2)}{m_B+m_K}\,,\\ F_\mathrm{P}(q^2) &\equiv \frac{1}{2}\frac{m_B^2-m_K^2}{m_b-m_s}f_0(q^2)C_\mathrm{P}^\ell \\ &\quad + f_+(q^2)m_\ell C_{10}^\ell\left[\frac{m_B^2-m_K^2}{q^2}\left(\frac{f_0(q^2)}{f_+(q^2)}-1\right)-1\right],\\ F_\mathrm{S}(q^2) &\equiv \frac{1}{2}\frac{m_B^2-m_K^2}{m_b-m_s}f_0(q^2)C_\mathrm{S}^\ell\,.\end{aligned} \tag{3.28}$$

Effects of chirality-flipped operators can be included by replacing $C_i \to C_i + C_i'$, where $i \in \{7, 9, 10, \mathrm{S}, \mathrm{P}\}$. Note that this means that all observables in $\bar{B} \to \bar{K}\ell^+\ell^-$ are only sensitive to vectorial quark currents. The parametrizations we use for the form factors $f_0(q^2)$, $f_+(q^2)$ and $f_\mathrm{T}(q^2)$ are given in [80]. Contributions from the quark operators $\mathcal{O}_1$–$\mathcal{O}_6$ are absorbed into the effective coefficients $C_7^\mathrm{eff} \simeq -0.3$ and $C_9^\mathrm{eff}(q^2) = C_9 + Y(q^2)$. Further details and the loop function $Y(q^2)$ and can be found in [77].

The double-differential partial decay width can be written as

$$\frac{\mathrm{d}^2\Gamma(\bar{B}\to\bar{K}\ell^+\ell^-)}{\mathrm{d}q^2\,\mathrm{d}\cos\theta} = a_\ell(q^2) + b_\ell(q^2)\cos\theta + c_\ell(q^2)\cos^2\theta\,, \tag{3.29}$$

where $4m_\ell^2 \le q^2 \le (m_B - m_K)^2$ and θ denotes the angle between the momenta of the kaon and the lepton in the rest frame of the decaying B meson and the angular coefficient functions are given as [81]

$$\begin{aligned}\frac{a_\ell(q^2)}{\Gamma_0\sqrt{\lambda_K}\beta_\ell} &\equiv q^2\left(\beta_\ell^2|F_\mathrm{S}|^2 + |F_\mathrm{P}|^2\right) + \frac{\lambda_K}{4}\left(|F_\mathrm{A}|^2 + |F_\mathrm{V}|^2\right)\\ &\quad + 2m_\ell(m_B^2 - m_K^2 + q^2)\,\mathrm{Re}(F_\mathrm{P}F_\mathrm{A}^*) + 4m_\ell^2 m_B^2|F_\mathrm{A}|^2,\\ \frac{b_\ell(q^2)}{\Gamma_0\sqrt{\lambda_K}\beta_\ell} &\equiv 2m_\ell\sqrt{\lambda_K}\beta_\ell\,\mathrm{Re}(F_\mathrm{S}F_\mathrm{V}^*)\,,\\ \frac{c_\ell(q^2)}{\Gamma_0\sqrt{\lambda_K}\beta_\ell} &\equiv -\frac{\lambda_K}{4}\left(|F_\mathrm{A}|^2 + |F_\mathrm{V}|^2\right).\end{aligned} \tag{3.30}$$

For the sake of legibility, we suppress the q^2 dependences of the involved functions and employ the short forms

$$\Gamma_0 \equiv \frac{G_\mathrm{F}^2\alpha_\mathrm{e}^2|V_{tb}V_{ts}^*|^2}{2^9\pi^5 m_B^3}, \quad \beta_\ell(q^2) \equiv \sqrt{1-4\frac{m_\ell^2}{q^2}}, \quad \lambda_{K^{(*)}}(q^2) \equiv \lambda(q^2, m_B, m_{K^{(*)}})\,. \tag{3.31}$$

The fully integrated decay width

$$\Gamma_{K\ell} \equiv \Gamma(\bar{B} \to \bar{K}\ell^+\ell^-) = 2\int_{q^2_{\min}}^{q^2_{\max}} \mathrm{d}q^2 \left(a_\ell(q^2) + \frac{1}{3}c_\ell(q^2)\right) \tag{3.32}$$

only depends on $a_\ell(q^2)$ and $c_\ell(q^2)$ and is dominated by (axial)vector contributions. The coefficient function $b_\ell(q^2)$ of the $\cos\theta$ term in the angular distribution is related to the dilepton forward–backward asymmetry

$$A^\ell_{\mathrm{FB}} \equiv \frac{1}{\Gamma_{K\ell}} \int_{q^2_{\min}}^{q^2_{\max}} \mathrm{d}q^2 \; b_\ell(q^2)\,, \tag{3.33}$$

which vanishes in the SM, thus making it sensitive to scalar NP contributions. However, the strong suppression by the lepton mass prevents the asymmetry from becoming large enough to be detected in current experiments.

It can be seen from (3.30) that in the SM $a_\ell(q^2) = -c_\ell(q^2)$ holds up to corrections that are also suppressed by the lepton mass. As the purely (pseudo)scalar contributions to $a_\ell(q^2)$ do not suffer from such a suppression, the observable

$$F^\ell_{\mathrm{H}} \equiv \frac{2}{\Gamma_{K\ell}} \int_{q^2_{\min}}^{q^2_{\max}} \mathrm{d}q^2 \left(a_\ell(q^2) + c_\ell(q^2)\right)\,, \tag{3.34}$$

in which the SM part largely cancels, is highly sensitive to these contributions. Both A^ℓ_{FB} and F^ℓ_{H} are normalized to the total decay width in order to reduce form factor uncertainties. Neglecting corrections from higher-dimensional operators and QED these two quantities completely determine the normalized angular distribution [81]

$$\frac{1}{\Gamma_{K\ell}}\frac{\mathrm{d}\Gamma_{K\ell}}{\mathrm{d}\cos\theta} = \frac{3}{4}(1 - F^\ell_{\mathrm{H}})(1 - \cos^2\theta) + \frac{1}{2}F^\ell_{\mathrm{H}} + A^\ell_{\mathrm{FB}}\cos\theta. \tag{3.35}$$

Since the $\bar{K}^*$ vector meson in the final state of $\bar{B} \to \bar{K}^*\ell^+\ell^-$ further decays into $\bar{K}\pi$ via the strong interaction, the final state reconstructed in experiments actually consists of four bodies, providing access to an angular distribution with a much larger set of observables. However, in this thesis we will mainly make use of the q^2 distribution, which, following [82], can be expressed as

$$\frac{\mathrm{d}\Gamma(\bar{B} \to \bar{K}^*\ell^+\ell^-)}{\mathrm{d}q^2} = 2J_{1\mathrm{s}}(q^2) + J_{1\mathrm{c}}(q^2) - \frac{2}{3}J_{2\mathrm{s}}(q^2) - \frac{1}{3}J_{2\mathrm{c}}(q^2)\,, \tag{3.36}$$

where the required subset of angular coefficient functions is given by

$$\begin{aligned}
\frac{4}{3}J_{1\mathrm{s}} &= \frac{2+\beta_\ell^2}{4}\left[\left|A^{\mathrm{L}}_\perp\right|^2 + \left|A^{\mathrm{L}}_\parallel\right|^2 + (\mathrm{L}\to\mathrm{R})\right] + \frac{4m_\ell^2}{q^2}\,\mathrm{Re}\left(A^{\mathrm{L}}_\perp A^{\mathrm{R}*}_\perp + A^{\mathrm{L}}_\parallel A^{\mathrm{R}*}_\parallel\right),\\
\frac{4}{3}J_{1\mathrm{c}} &= \left|A^{\mathrm{L}}_0\right|^2 + \left|A^{\mathrm{R}}_0\right|^2 + \frac{4m_\ell^2}{q^2}\left[|A_{\mathrm{t}}|^2 + 2\,\mathrm{Re}\left(A^{\mathrm{L}}_0 A^{\mathrm{R}*}_0\right)\right] + \beta_\ell^2|A_{\mathrm{S}}|^2,\\
\frac{4}{3}J_{2\mathrm{s}} &= \frac{\beta_\ell^2}{4}\left[\left|A^{\mathrm{L}}_\perp\right|^2 + \left|A^{\mathrm{L}}_\parallel\right|^2 + (\mathrm{L}\to\mathrm{R})\right],\\
\frac{4}{3}J_{2\mathrm{c}} &= -\beta_\ell^2\left[\left|A^{\mathrm{L}}_0\right|^2 + \left|A^{\mathrm{R}}_0\right|^2\right].
\end{aligned} \tag{3.37}$$

Later on we will briefly discuss additional observables, which are related to the eight remaining angular coefficient functions $\{J_3, J_4, J_5, J_{6s}, J_{6c}, J_7, J_8, J_9\}$ that appear in the full angular distribution. The transversity amplitudes from (3.37) read

$$\begin{aligned}
A_\perp^{\mathrm{L,R}} &= \sqrt{2}N\sqrt{\lambda_{K^*}}\left[\left(C_9^{\mathrm{eff}} \mp C_{10}\right)\frac{V}{m_B + m_{K^*}} + \frac{2m_b}{q^2}C_7^{\mathrm{eff}}T_1\right], \\
A_\parallel^{\mathrm{L,R}} &= -\sqrt{2}N\left(m_B^2 - m_{K^*}^2\right)\left[\left(C_9^{\mathrm{eff}} \mp C_{10}\right)\frac{A_1}{m_B - m_{K^*}} + \frac{2m_b}{q^2}C_7^{\mathrm{eff}}T_2\right], \\
A_0^{\mathrm{L,R}} &= -\frac{N}{2m_{K^*}\sqrt{q^2}} \\
&\quad \times \left\{\left(C_9^{\mathrm{eff}} \mp C_{10}\right)\left[\left(m_B^2 - m_{K^*}^2 - q^2\right)(m_B + m_{K^*})A_1 - \frac{\lambda_{K^*}}{m_B + m_{K^*}}A_2\right]\right. \\
&\quad \left. + 2m_b C_7^{\mathrm{eff}}\left[\left(m_B^2 + 3m_{K^*}^2 - q^2\right)T_2 - \frac{\lambda_{K^*}}{m_B^2 - m_{K^*}^2}T_3\right]\right\}, \\
A_{\mathrm{t}} &= N\frac{\sqrt{\lambda_{K^*}}}{\sqrt{q^2}}\left[2C_{10} + \frac{q^2}{m_\ell}\frac{C_{\mathrm{P}}^\ell}{m_b + m_s}\right]A_0, \\
A_{\mathrm{S}} &= -2N\sqrt{\lambda_{K^*}}\frac{C_{\mathrm{S}}^\ell}{m_b + m_s}A_0\,,
\end{aligned} \tag{3.38}$$

where we employ the normalization factor

$$N(q^2) \equiv G_{\mathrm{F}}\alpha_{\mathrm{e}}V_{tb}V_{ts}^*\sqrt{\frac{q^2\beta_\ell\sqrt{\lambda_{K^*}}}{3\cdot 2^{10}\pi^5 m_B^3}}\,, \tag{3.39}$$

and, as before, suppress the q^2 dependences to avoid clutter. We employ the form factors from [83]. Contributions from chirality-flipped operators can be accounted for by replacing all Wilson coefficients $C_i \to C_i - C_i'$ in all the transversity amplitudes except for $A_\perp^{\mathrm{L,R}}$ where they need to be replaced by the orthogonal combination $C_i + C_i'$ that already appeared in $\bar{B} \to \bar{K}\ell^+\ell^-$. Therefore, $\bar{B} \to \bar{K}^*\ell^+\ell^-$ offers observables that are complementary to those in $\bar{B} \to \bar{K}\ell^+\ell^-$ with respect to the Lorentz structure of the quark current.

In Figure 3.5 the general form of the $\bar{B} \to \bar{K}^*\ell^+\ell^-$ dilepton invariant mass squared spectrum is sketched. For $\bar{B} \to \bar{K}\ell^+\ell^-$ the photon pole is not present while the rest of the spectrum looks similar. The kinematic regions where $6\,\mathrm{GeV}^2 \leq q^2 \leq 15\,\mathrm{GeV}^2$ contain the narrow charmonium resonances $J/\psi(1S)$ and $\psi(2S)$ with masses of about 3.1 GeV and 3.7 GeV, respectively. These resonances are usually vetoed in experimental analyses and the spectrum is divided into a low q^2 region and a high q^2 that begin below and above the previously mentioned bounds, respectively. The low q^2 region is generally further confined to the interval[1] $1\,\mathrm{GeV}^2 \leq q^2 \leq 6\,\mathrm{GeV}^2$ in order to exclude the photon pole [85]. Theoretical uncertainties in both the low and high q^2 regions can be kept under control by employing the appropriate tools discussed earlier. They are expected to

[1] in some experimental results a lower cut of $1.1\,\mathrm{GeV}^2$ is used

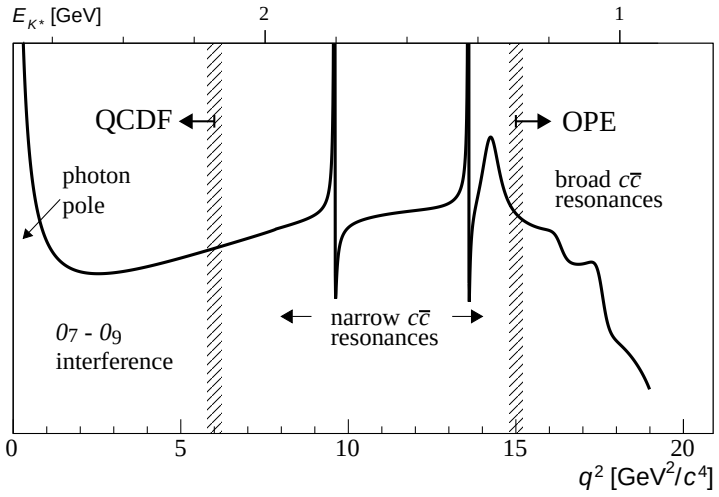

Figure 3.5.: Schematic illustration of the $\bar{B} \to \bar{K}^* \ell^+ \ell^-$ dilepton invariant mass squared spectrum. While the region where $6\,\text{GeV}^2 \leq q^2 \leq 15\,\text{GeV}^2$ is dominated by narrow charmonium resonances that give rise to non-perturbative QCD contributions, perturbative methods can be employed above and below this region. Figure taken from [84].

be of the order of 10 % [48]. It is therefore customary to integrate observables only over these subregions of the spectrum.

3.4.2. NP-Sensitive Observables and Experimental Status

Experimental data on the differential decay widths of $B^+ \to K^{(*)+}\mu^+\mu^-$ is shown in the upper row of Figure 3.6 together with the respective theory predictions. In both cases small deficits with respect to the SM values can be seen in the bins of the low q^2 regions. This is consistent with the data on the alternative isospin modes $B^0 \to K^{(*)0}\mu^+\mu^-$ [86, 87]. The largest discrepancy appears in the bin $1\,\text{GeV}^2 \leq q^2 \leq 6\,\text{GeV}^2$ of the decay mode $B_s^0 \to \phi\mu^+\mu^-$ where the tension amounts to more than three standard deviations. This can be seen in the lower row of Figure 3.6 where we show the latest LHCb results for the q^2 spectra of the decays $B_s^0 \to \phi\mu^+\mu^-$ and also the baryonic mode $\Lambda_b^0 \to \Lambda\mu^+\mu^-$ which exhibits this deviation as well. Of course, due to the sizable form factor uncertainties in the respective SM predictions none of these individual discrepancies are statistically significant on their own – it is the seeming emergence of a consistent pattern that has provoked the community's curiosity within the past few years. Even though upcoming data by LHCb and Belle II will substantially increase the experimental precision, the large form factor uncertainties make it impossible to find NP in these observables.

As mentioned in the previous section, a large set of observables is provided by the

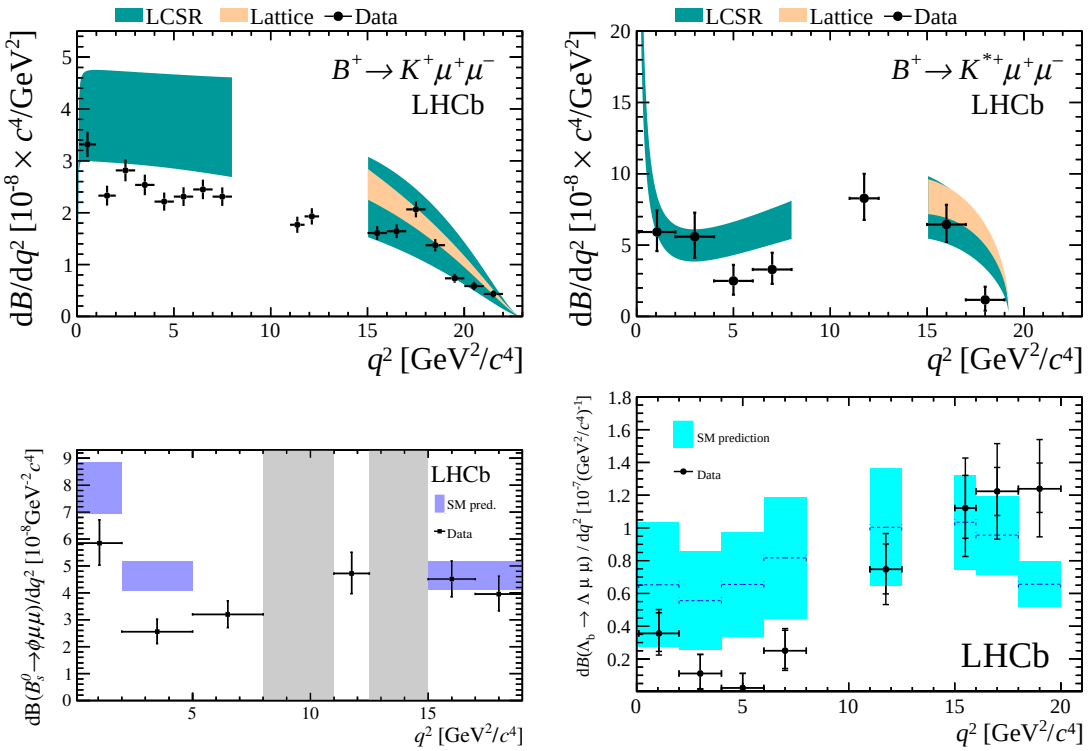

Figure 3.6.: Top row: LHCb data on the differential branching fractions of $B^+ \to K^+\mu^+\mu^-$ (left) and $B \to K^{*+}\mu^+\mu^-$ (right) [87]. The colored bands indicate the SM predictions and their form factor uncertainties based on LCSR and lattice QCD calculations. Bottom row: LHCb data on the differential branching fractions of $B_s^0 \to \phi\mu^+\mu^-$ (left) [88] and the baryonic decay mode $\Lambda_b^0 \to \Lambda\mu^+\mu^-$ (right) [89] together with binned SM predictions provided by [40, 90] and [91], respectively.

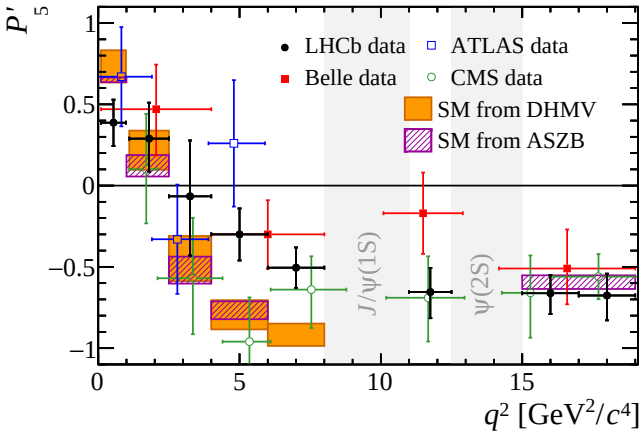

Figure 3.7.: Experimental data on the clean observable P_5' derived from the $\bar{B} \to \bar{K}^* \mu^+ \mu^-$ angular distribution measured by LHCb [98], Belle [99], ATLAS [100] and CMS [101]. Note that the Belle results also include data from the electronic mode. The boxes show SM predictions by DHMV [102] and ASZB [40, 90]. Figure taken from [103].

angular coefficients J_i of the decay $\bar{B} \to \bar{K}^*(\to \bar{K}\pi)\mu^+\mu^-$. This set can be used to construct clean observables that do not suffer from large theory uncertainties and are hence highly sensitive to NP contributions. In the past, the normalized CP-averaged angular coefficients $S_i \simeq (J_i + \bar{J}_i)/(\Gamma_{K^*\mu} + \bar{\Gamma}_{K^*\mu})$, where the bar indicates the CP-conjugate, have been considered as a starting point for experimental analyses [92]. Even though experimental and theoretical uncertainties are reduced in these ratios, they are still sensitive to the choice of form factors and their parametrizations. Anticipating precision data from LHCb and other experiments, the construction of clean observables from the angular distribution of $\bar{B} \to \bar{K}^* \mu^+ \mu^-$ has been tackled in a systematic manner over the past years [93–97]. As a result of this endeavor, a set of six clean observables, namely $P_{1,2,3}$ and $P'_{4,5,6}$, has emerged. Following [97], these quantities can be related to the S_i as

$$P_{1,2,3} \simeq \frac{S_{3,6,9}}{F_\mathrm{T}}, \quad P'_{4,5,6} \simeq \frac{S_{4,5,7}}{\sqrt{F_\mathrm{T} F_\mathrm{L}}}, \tag{3.40}$$

where $F_{\mathrm{T(L)}}$ is the transverse (longitudinal) polarization fraction of $\bar{K}^*$ mesons. The $P_i^{(\prime)}$ are theoretically clean in the sense that all form factor uncertainties cancel at leading order. Together with their experimental accessibility, this makes them play a major role in finding deviations from the SM and constraining NP models.

Current data on these clean observables shows a tension of about $3.4\,\sigma$ compared with SM expectation [98]. Most prominently, the largest local discrepancy is observed by LHCb in the two low q^2 bins $4\,\mathrm{GeV}^2 \leq q^2 \leq 6\,\mathrm{GeV}^2$ and $6\,\mathrm{GeV}^2 \leq q^2 \leq 8\,\mathrm{GeV}^2$ of the observable P_5' where the tensions amount to 2.8 and $3.0\,\sigma$, respectively, as can be seen in Figure 3.7 where we show the currently available experimental results for P_5' including SM predictions. While the ATLAS data is compatible with the LHCb result but has much larger uncertainties, the CMS result is more precise but compatible with both the

LHCb result and the SM prediction. The Belle result is the first one to also include the electronic mode $\bar{B} \to \bar{K}^* e^+ e^-$ and shows a $2.5\,\sigma$ tension with respect to the SM prediction in the bin $4\,\text{GeV}^2 \leq q^2 \leq 8\,\text{GeV}^2$ that includes both of the bins in which LHCb reports the largest discrepancy. Although the tension slightly increases to $2.6\,\sigma$ in case the muonic mode alone is considered, the individual measurements are compatible between different lepton flavors. Future measurements by Belle II will lower the experimental uncertainties in P_5' for both the muonic and electronic mode by about a factor of three (ten) given an integrated luminosity of $5\,\text{ab}^{-1}$ ($50\,\text{ab}^{-1}$) [48]. More such flavor-specific analyses are required to check whether these discrepancies are exclusive to muons and hence require lepton non-universal NP or whether they occur universally. In the latter case they could possibly be attributed to underestimated long-distance QCD effects stemming from charm loop contributions [104–106]. Since the motivation of this thesis is rooted in the flavor puzzles that are present in and beyond the SM we concentrate on the former case and, abiding by the lepton-specific nature of the experimental results, focus on flavorful NP scenarios.

Crucial tests of the SM's built-in feature of LFU are provided by the ratios

$$R_{K^{(*)}}\big|_{[q_1^2,q_2^2]} \equiv \frac{\displaystyle\int_{q_1^2}^{q_2^2} \mathrm{d}q^2\, \frac{\mathrm{d}\Gamma(\bar{B} \to \bar{K}^{(*)}\mu^+\mu^-)}{\mathrm{d}q^2}}{\displaystyle\int_{q_1^2}^{q_2^2} \mathrm{d}q^2\, \frac{\mathrm{d}\Gamma(\bar{B} \to \bar{K}^{(*)}e^+e^-)}{\mathrm{d}q^2}}\,, \tag{3.41}$$

which play a central role in this thesis. Unlike in the case of $R_{D^{(*)}}$, phase space effects due to the mass difference of the final state leptons can be neglected in the ratios considered here so that they are expected to be unity in the SM. This also implies a larger cancellation of form factor uncertainties, leaving behind only tiny QCD corrections of the order m_μ^2/m_B^2 [81, 107]. In fact, the dominant theoretical uncertainties of the ratios (3.41) stem from QED and amount to about 1 % [108]. Thus, the observables $R_{K^{(*)}} - 1$ are considered to be clean null-tests of the SM as any significant deviation from zero would be a clear sign of lepton flavor universality violation (LFUV).

The measurement that provides a main motivation for this thesis is the result

$$R_K^{\text{LHCb '14}}\Big|_{[1,6]} = 0.745^{+0.090}_{-0.074}\,(\text{stat}) \pm 0.036\,(\text{syst}) \tag{3.42}$$

obtained by the LHCb collaboration in 2014 using Run 1 data corresponding to an integrated luminosity of $3.0\,\text{fb}^{-1}$ at center of mass energies of 7 and 8 TeV [6]. It shows a deficit of $2.6\,\sigma$ compared with the SM prediction, which persists in the most recent update of this measurement published in 2019 [7]. Furthermore, using only the Run 1 dataset, in 2017 LHCb has reported similar deficits in $R_{K^*}|_{[1.1,6]}$ and $R_{K^*}|_{[0.045,1.1]}$ which correspond to tensions of $2.5\,\sigma$ and $2.3\,\sigma$, respectively. Note that the SM prediction for the very low q^2 region $4m_\mu^2 \leq q^2 \leq 1.1\,\text{GeV}^2$ is slightly smaller than unity, because the electronic mode receives a stronger enhancement from the photon pole than the muonic

Observable	SM Prediction	Exp. Results	Reference	
$R_K\|_{[1,6]}$	1.00 ± 0.01	0.752 ± 0.090	LHCb '14	[6]
$R_K\|_{[1.1,6]}$	1.00 ± 0.01	0.847 ± 0.042	LHCb '21	[8]
$R_{K^*}\|_{[0.045,1.1]}$	0.906 ± 0.028	0.68 ± 0.10	LHCb '17	[109]
		0.57 ± 0.31	Belle '19	[110]
$R_{K^*}\|_{[1.1,6]}$	1.00 ± 0.01	0.71 ± 0.10	LHCb '17	[109]
		1.04 ± 0.39	Belle '19	[110]

Table 3.2.: Experimental results for R_K and R_{K^*} in the low and very low q^2 bins with symmetrized uncertainties. See [108] for more details on the SM predictions.

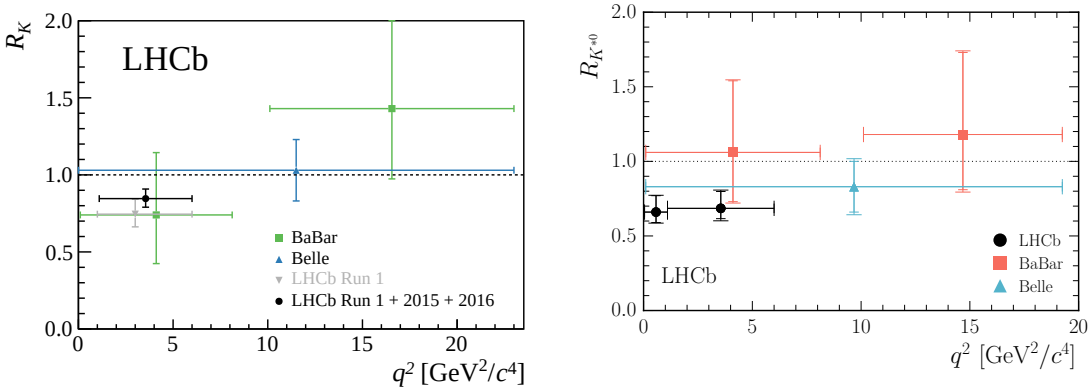

Figure 3.8.: Available experimental results for R_K (left) and R_{K^*} (right). LHCb [7, 109], *BABAR* [111], Belle [112]

mode near its kinematic endpoint. The available experimental results for $R_{K^{(*)}}$ are shown in Figure 3.8 where we also include older results by *BABAR* (2012) and Belle (2009) that are compatible with both the SM prediction and the LHCb results due to their much larger uncertainties. Numerical results for the low and very low q^2 bins are compiled in Table 3.2 along with the respective SM predictions. Additionally, the latest update of Belle's results for R_{K^*} published in 2019 is included.

3.4.3. Global Fits and NP Scenarios

With the vast amount of available data it becomes difficult to see whether the pattern of discrepancies observed in the measurements of branching fractions that we discussed in the beginning is compatible with the discrepancies seen in the clean angular observables and $R_{K^{(*)}}$. For this reason, several groups [9–11] have specialized in performing global fits of the Wilson coefficients to the experimental data. The main result of these fits is

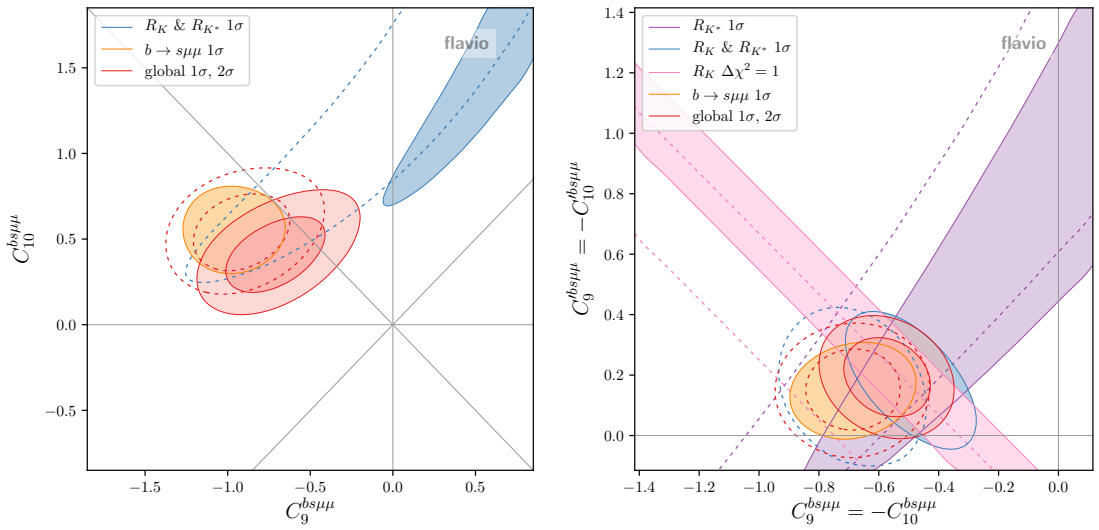

Figure 3.9.: Likelihood contours of the individual $R_{K^{(*)}}$ and $b \to s\mu^+\mu^-$ constraints, as well as the global fit in the plane of $C_9^{\mu\text{NP}}$ and $C_{10}^{\mu\text{NP}}$ (left), and $C_9^{\mu\text{NP}} = -C_{10}^{\mu\text{NP}}$ and $C_9^{\prime\mu\text{NP}} = -C_{10}^{\prime\mu\text{NP}}$ (right). The dashed contours indicate the constraints and fit results excluding the 2019 Moriond data. Figures taken from [11].

quite remarkable: a single NP contribution

$$C_9^{\mu\text{NP}} = -C_{10}^{\mu\text{NP}} \simeq -0.5 \tag{3.43}$$

suffices to consistently explain all of the anomalies that are currently seen in $b \to s\ell^+\ell^-$ transitions. This simple scenario is found to improve the fit to the experimental data by at least five standard deviations in comparison with the SM and is hence widely considered as a benchmark point to resolve the $b \to s\ell^+\ell^-$ anomalies. On the left side of Figure 3.9 we show the most recent global fit results in the plane spanned by $C_9^{\mu\text{NP}}$ and $C_{10}^{\mu\text{NP}}$ and a breakdown of the fit into the experimental data on the branching fractions and angular observables in $b \to s\mu^+\mu^-$ decays alone on the one hand and R_K and R_{K^*} on the other hand. While it can be seen that the $1\,\sigma$ contours derived from the individual datasets have slightly drifted apart with the 2019 update of the LHCb data, the pull with respect to the SM still exceeds five standard deviations. Nevertheless, this shows that more cross-checks are required to verify that these deviations share a common origin.

For instance, as we have discussed earlier, $\bar{B} \to \bar{K}\ell^+\ell^-$ and $\bar{B} \to \bar{K}^*\ell^+\ell^-$ provide complementary sensitivity to the chirality of the quark current. Accordingly, this is also true for R_K and R_{K^*}, as can be seen in the following simplified expressions that result from an expansion in the dominant NP contributions [113]:

$$\begin{aligned} R_K &= 1 + \Delta_+ + \Sigma_+ \,, \\ R_{K^*} &= 1 + \Delta_+ + \Sigma_+ + p\,(\Sigma_- - \Sigma_+ + \Delta_- - \Delta_+) \,, \end{aligned} \tag{3.44}$$

with

$$\begin{aligned} \Delta_\pm &= 2\,\mathrm{Re}\left(\frac{C_{\mathrm{LL}}^{\mu\mathrm{NP}} \pm C_{\mathrm{RL}}^{\mu}}{C_{\mathrm{LL}}^{\mathrm{SM}}} - (\mu \to e)\right), \\ \Sigma_\pm &= \frac{\left|C_{\mathrm{LL}}^{\mu\mathrm{NP}} \pm C_{\mathrm{RL}}^{\mu}\right|^2 + \left|C_{\mathrm{LR}}^{\mu} \pm C_{\mathrm{RR}}^{\mu}\right|^2}{\left|C_{\mathrm{LL}}^{\mathrm{SM}}\right|^2} - (\mu \to e), \end{aligned} \tag{3.45}$$

where we write the Wilson coefficients in the basis

$$\begin{aligned} C_{\mathrm{LL}} &= C_9 - C_{10}, \quad C_{\mathrm{LR}} = C_9 + C_{10}, \\ C_{\mathrm{RL}} &= C_9' - C_{10}', \quad C_{\mathrm{RR}} = C_9' + C_{10}' \end{aligned} \tag{3.46}$$

that reflects the chirality of both the quark and the lepton current in the first and second index, respectively. The polarization fraction p is close to unity in the low q^2 region [114]. Hence, any difference between R_K and R_{K^*} would be an indicator of NP contributions to right-handed quark currents i.e. primed operators. This complementary sensitivity can be seen on the right side of Figure 3.9 where the global fit results are displayed in the plane spanned by $C_9^{\mu\mathrm{NP}} = -C_{10}^{\mu\mathrm{NP}}$ and $C_9^{\prime\mu\mathrm{NP}} = -C_{10}^{\prime\mu\mathrm{NP}}$ and the $R_{K^{(*)}}$ contour is further decomposed into those derived from R_K and R_{K^*} individually. Here, the impact of the 2019 data is very small and does not change the fact that primed operators are currently not needed for a joint explanation of all $b \to s\ell^+\ell^-$ anomalies.

Furthermore, as there is presently only very limited data available on $b \to se^+e^-$ the anomalies observed in $b \to s\mu^+\mu^-$ do not necessarily require lepton-specific NP and can hence also be explained by a lepton-universal NP contribution $C_9^{\mathrm{NP}} = -C_{10}^{\mathrm{NP}} \simeq -0.5$ which does not affect $R_{K^{(*)}}$. More generally, the observed deficits in R_K and R_{K^*} can not only be caused by a suppression of the muonic mode but also by an enhancement of the electronic mode or a combination of those cases. Analyses dedicated to $b \to se^+e^-$ are therefore needed to examine these possibilities. For instance, if the electronic mode is enhanced due to (pseudo)scalar NP contributions to $C_{\mathrm{S,P}}^{(\prime)e}$ causing a deficit in R_K, this will also lead to a non-vanishing flat term F_{H}^e in the $\bar{B} \to \bar{K}e^+e^-$ angular distribution, as the two quantities are in this scenario related by

$$R_K = 1 - F_{\mathrm{H}}^e \tag{3.47}$$

if lepton masses are neglected [81]. Note that in this scenario cancellations between primed and unprimed operators are necessary in order to evade bounds from $B_s \to e^+e^-$.

In the following, we will focus on the benchmark scenario (3.43) and treat any additional contributions from flavor models as predictions or, if necessary, as constraints. While disfavored by global fits, we will also explore explanations of R_K involving right-handed quark currents.

3.5. Constraints on NP Contributions from Flavor Processes

While we are mainly interested in finding deviations from the predictions of the SM, there is an abundance of experimental data that is in agreement with these predictions and needs to be taken into account. This means NP models which are meant to explain the previously discussed discrepancies must not make predictions that disagree with existing data. As we have seen, within the framework of EFTs this condition directly translates into bounds on the Wilson coefficients. Focusing on resolving the $b \to s\ell^+\ell^-$ anomalies, we will discuss further $b \to s$ transitions such as $b \to s\nu\bar{\nu}$ and $\bar{B}_s$–B_s mixing that strongly constrain NP contributions to that sector.

So far, we have always studied a single class of low-energy transitions at a time. However, as soon as specific NP models from higher energy scales are considered, contributions to several different classes of processes might be induced simultaneously. In the context of flavor models even more relations between various classes of flavor transitions arise, further increasing the amount of constraints that need to be satisfied. In this section we will therefore also discuss constraints emerging from flavor transitions different from those in which the anomalies are seen. This includes decays in the charm and kaon sector as well as lepton flavor violating processes.

3.5.1. Further $b \to s$ Transitions

In order to obtain the desired benchmark scenario (3.43) in which the quark and lepton current are both left-handed, NP contributions to operators involving the quark and lepton doublets are required above the electroweak scale. At low energies this can potentially induce the transitions $b \to s\nu\bar{\nu}$, which can be described by the previously discussed effective Hamiltonian (3.25) provided that the set of effective operators is amended by

$$\mathcal{O}^{\nu\nu'}_{\mathrm{L(R)}} = \left[\bar{s}\gamma_\mu P_{\mathrm{L(R)}} b\right] \left[\bar{\nu}\gamma^\mu P_{\mathrm{L}} \nu'\right] \,. \tag{3.48}$$

In the SM the dominant contributions arise from Z penguins and W boxes resulting in

$$C^{\mathrm{SM}}_{\mathrm{L}} = -\frac{2X_t}{\sin^2\theta_{\mathrm{W}}} \simeq -13 \tag{3.49}$$

while $C^{\mathrm{SM}}_{\mathrm{R}}$ is negligible [115]. Details about the evaluation of the loop function X_t can be found in [116] and references therein. The most stringent constraint on NP contributions are imposed by the upper limit

$$\mathcal{B}(B \to K\nu\bar{\nu}) < 1.7 \times 10^{-5} \tag{3.50}$$

at 90 % confidence level obtained by *BABAR* in 2013 [117]. This amounts to a maximum enhancement over the SM prediction by a factor of 4.3 [115], yielding

$$\sqrt{\sum_{\nu}\left|C_{\mathrm{L}}^{\mathrm{SM}}+C_{\mathrm{L}}^{\mathrm{NP}\nu\nu}+C_{\mathrm{R}}^{\nu\nu}\right|^2+\sum_{\nu\neq\nu'}\left|C_{\mathrm{L}}^{\nu\nu'}+C_{\mathrm{R}}^{\nu\nu'}\right|^2}\leq\left|C_{\mathrm{L}}^{\mathrm{SM}}\right|\sqrt{4.3\cdot 3}\simeq 47\,. \tag{3.51}$$

In the case of a single real flavor-diagonal coupling $C_{\mathrm{L}}^{\mathrm{NP}\nu\nu}$ involving left-handed quarks this bound simplifies to

$$-30\leq C_{\mathrm{L}}^{\mathrm{NP}\nu\nu}\leq 56\,. \tag{3.52}$$

New results from the Belle II experiment, which are anticipated within the next few years and can potentially reach SM-level sensitivity, are expected to further tighten this constraint.

3.5.2. B_s–$\bar{B}_s$ Mixing

So far we have only considered FCNC processes in which the flavor quantum number changes by one unit. Another important class of FCNCs consists of $\Delta F = 2$ transitions that induce neutral meson oscillations and thus lead to mixing between neutral mesons and their antiparticles. The study of meson mixing in the kaon sector has played a crucial role in the construction of the SM, as it provided the first evidence for indirect CP violation [118] and led to the prediction of the charm quark mass before its discovery [119]. In the B sector B_d–$\bar{B}_d$ mixing has provided first hints towards a large top quark mass. Here we focus on B_s–$\bar{B}_s$ mixing, as current experimental data imposes strong bounds on models that address the $b\to s\ell^+\ell^-$ anomalies.

The time evolution of the meson and antimeson states is governed by the Schrödinger equation

$$i\frac{\mathrm{d}}{\mathrm{d}t}\begin{pmatrix}|B_s(t)\rangle\\|\bar{B}_s(t)\rangle\end{pmatrix}=\left(M^s-\frac{i}{2}\Gamma^s\right)\begin{pmatrix}|B_s(t)\rangle\\|\bar{B}_s(t)\rangle\end{pmatrix}\,, \tag{3.53}$$

where M^s and Γ^s are the hermitian mass and decay matrices, respectively. Diagonalizing the mass matrix results in two mass eigenstates with masses $m_{B_s}^{\mathrm{light}}$ and $m_{B_s}^{\mathrm{heavy}}$. Their mass difference corresponds to the frequency of the meson oscillation and thus provides an excellent experimental observable. It can be expressed in terms of the off-diagonal matrix element as

$$\Delta m_{B_s}=2|M_{12}^s|=\left|\frac{\langle B_s|\mathcal{H}_{\mathrm{eff}}^{|\Delta B|=2}|\bar{B}_s\rangle}{m_{B_s}}\right|, \tag{3.54}$$

where m_{B_s} denotes the average of $m_{B_s}^{\mathrm{light}}$ and $m_{B_s}^{\mathrm{heavy}}$.

The effective Hamiltonian describing B_s–$\bar{B}_s$ mixing can be expressed as [120]

$$\mathcal{H}_{\mathrm{eff}}^{|\Delta B|=2}=(V_{tb}V_{ts}^*)^2\,C_1Q_1+\mathrm{h.c.}\,, \tag{3.55}$$

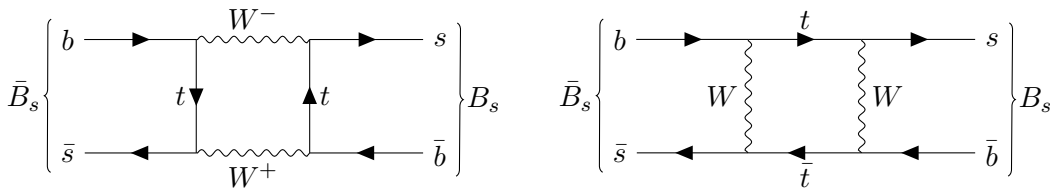

Figure 3.10.: Dominant SM contributions to the B_s–$\bar{B}_s$ mixing amplitude.

where the only necessary effective operator reads

$$Q_1 = [\bar{s}_\mathrm{L}\gamma_\mu b_\mathrm{L}]\,[\bar{s}_\mathrm{L}\gamma_\mu b_\mathrm{L}]\ . \tag{3.56}$$

Within the SM the dominant contribution stems from box diagrams with W bosons and top quarks propagating in the loop, as depicted in Figure 3.10. Evaluating these diagrams gives

$$C_1^\mathrm{SM} = \frac{G_\mathrm{F}^2}{4\pi^2} m_W^2 \hat{\eta}_{B_s} S_0\left(\frac{m_t^2}{m_W^2}\right), \tag{3.57}$$

where S_0 is an Inami–Lim function and $\hat{\eta}_{B_s}$ parametrizes perturbative 2-loop QCD corrections. For details we refer to [120] and references therein. Parametrizing the hadronic matrix element as

$$\langle B_s|Q_1|\bar{B}_s\rangle = \frac{2}{3} m_{B_s}^2 f_{B_s}^2 B_{B_s}\,, \tag{3.58}$$

with the decay constant f_{B_S} and the bag parameter B_{B_s}, the SM prediction for the mass difference reads

$$\Delta m_{B_s}^\mathrm{SM} = \left|\frac{G_\mathrm{F}^2}{6\pi^2}\left(V_{tb}V_{ts}^*\right)^2 m_W^2 S_0\left(\frac{m_t^2}{m_W^2}\right) B_{B_s} f_{B_s}^2 m_{B_s}\hat{\eta}_{B_s}\right|. \tag{3.59}$$

Currently the precision of the SM value is strongly limited by the large hadronic uncertainties of the bag parameter and the decay constant which are obtained from lattice calculations and sum rules. The weighted average of the most recent results is [121]

$$\Delta m_{B_s}^\mathrm{SM} = (18.15 \pm 0.95)\,\mathrm{ps}^{-1} = (1.025 \pm 0.055)\Delta m_{B_s}^\mathrm{exp}\,, \tag{3.60}$$

where uncertainties are symmetrized and the average of experimental results provided by HFLAV [12] reads

$$\Delta m_{B_s}^\mathrm{exp} = (17.749 \pm 0.020)\,\mathrm{ps}^{-1}\,. \tag{3.61}$$

3.5.3. Lepton Flavor Violation, Kaon and Charm Decays

Lastly, we consider constraints that can arise indirectly through an imposed flavor structure.

cLFV Processes As soon as a link between two or more lepton generations is established, strong bounds from experimental limits on cLFV transitions arise, because their signatures are very clean and have virtually no SM background. In the context of the $b \to s\ell^+\ell^-$ anomalies the relevant processes are

- $\mu^- \to e^-\gamma$,
- $\mu^- N \to e^- N$,
- $\mu^- \to e^- e^+ e^-$.

In the following we apply the bounds derived in [122]. For more details we refer to [123]. The current constraints are expected to be improved by at least two orders of magnitude with upcoming data from the Mu2e [124], COMET [125] and MEG [126] experiments.

Kaon Decays If NP couplings to the first two quark generations are induced by a hierarchical flavor structure, contributions to leptonic and semileptonic kaon decays can approach current experimental limits [127]. From a flavor perspective cLFV kaon decays are particularly interesting. Relevant processes which impose the strongest bounds include

- $K_L \to \mu^+\mu^-$,
- $K_L \to e^-\mu^+$,
- $K \to \pi\nu\bar{\nu}$.

We make use of the constraints on the Wilson coefficients of four-quark operators discussed in [127–129].

Charm Decays In the charm sector the corresponding decay channels

- $D \to \mu^+\mu^-$,
- $D \to e^-\mu^+$,
- $D \to \pi\nu\bar{\nu}$

are relevant in the context of flavorful NP models related to the B anomalies. However, the situation on both the experimental and the theoretical side is very different for rare charm decays. The branching ratios of these processes are particularly small and dominated by resonances which complicate the search for NP signals. Since the mass of the charm quark is neither very large, as it is the case for the bottom quark, nor small, as the strange quark, theoretical methods used in the B and kaon sectors can only be applied to a limited extent so that theoretical uncertainties are large. Consequently, rare charm decays provide only weak constraints on NP models [122].

Chapter 4.

Specific Models for the Resolution of the B Anomalies

In this chapter we will review classes of models which can potentially induce the desired NP contribution to $\mathcal{O}^{\mu}_{\mathrm{LL}} \equiv \left(\mathcal{O}^{\mu}_{9} - \mathcal{O}^{\mu}_{10}\right)/2$ that resolves the $b \to s\ell^+\ell^-$ anomalies. This means, we will leave the completely model-independent EFT approach behind and will instead study specific particles that contribute to $\mathcal{O}_{\mathrm{LL}}$ when they are integrated out, while still remaining agnostic about the detailed UV completion. At tree-level, only the three options shown in Figure 4.1 are possible: scalar leptoquarks, vector leptoquarks and also neutral vector currents (Z' models). Even though $\mathcal{O}_{\mathrm{LL}}$ consists of (axial)vector currents, it can still receive contributions from scalar leptoquarks due to the Fierz transformations that are necessarily involved when the effective interactions invovling lepton-quark currents are matched onto the basis (3.26). This has the additional effect that leptoquarks can potentially induce $b \to c\ell\bar{\nu}$ transitions as well and hence might provide a joint explanation of the B anomalies.

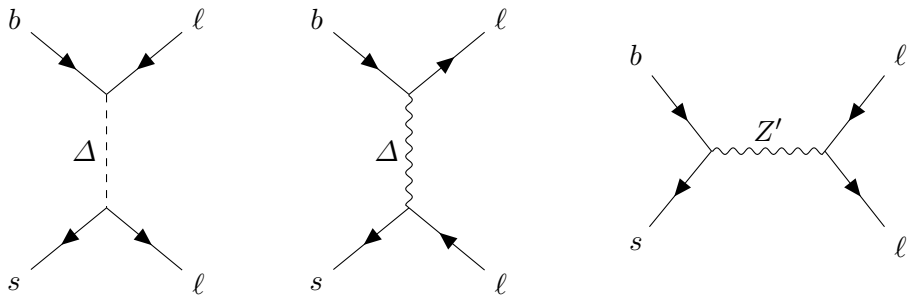

Figure 4.1.: Tree-level Feynman diagrams of possible NP contributions that allow to resolve the $b \to s\ell^+\ell^-$ anomalies. We use Δ to generically denote a leptoquark.

4.1. Leptoquarks

In the SM, the quark sector and the lepton sector are completely independent from each other. The only thing relating them is the peculiar fact that their contributions to gauge anomalies cancel exactly within each generation. As this does not necessarily need to be the case in models beyond the SM, many of them are expected to include new particles, called leptoquarks, that mediate interactions between quarks and leptons [128, 130]. Among those models are Grand Unified Theories (GUTs) [131, 132], supersymmetric models with R-parity violation [133] and also those in which leptoquarks appear as bound states resulting from new confining dynamics [134].

Leptoquarks can be scalars or vectors with interactions that schematically have the form

$$\mathcal{L} \supset Y_{AB} A B \Delta + \text{h.c.}\,, \tag{4.1}$$

where $A \in \{Q, \bar{Q}, U, \bar{U}, D, \bar{D}\}$ denotes an (anti)quark field and $B \in \{L, E\}$ denotes a lepton field. The couplings Y_{AB} are 3×3 matrices in flavor space, where the rows and columns correspond to different quark and lepton generations, respectively. Furthermore, some leptoquarks can have interactions that violate lepton and baryon number and thus potentially give rise to proton decay [135]. However, focusing on low-energy flavor phenomenology, we only consider leptoquark interactions that conserve both lepton and baryon number and thus do not endanger the proton lifetime.

In total there are twelve possible coupling matrices that can appear in the interactions of the ten leptoquark models with distinct SM gauge group representations. Table 4.1 shows which coupling matrix is present in a particular leptoquark model and whether it induces tree-level FCNCs in the up and down type sectors. The detailed interactions and SM representations of the individual models are listed in Tables 4.2, 4.3. In these tables we also present all the effective vertices obtained by integrating out the respective leptoquark and subsequently Fierz transforming the resulting current-current interactions.

Regarding the $b \to s\ell^+\ell^-$ anomalies, of course, only those models are relevant in which FCNCs in the down type sector are induced. However, some of the models contribute only

AB	QL	$\bar{Q}L$	UL	$\bar{U}L$	DL	$\bar{D}L$	QE	$\bar{Q}E$	UE	$\bar{U}E$	DE	$\bar{D}E$
model	$S_{1,3}$	$V_{1,3}$	$\tilde{V}_2$	S_2	V_2	$\tilde{S}_2$	V_2	S_2	S_1	$\tilde{V}_1$	$\tilde{S}_1$	V_1
d FCNCs	✓	✓	–	–	✓	✓	✓	✓	–	–	✓	✓
u FCNCs	✓	✓	✓	✓	–	–	✓	✓	✓	✓	–	–

Table 4.1.: Baryon and lepton number conserving leptoquark couplings Y_{AB} as they appear in the different models. A check mark indicates tree-level contributions to up and down type FCNCs.

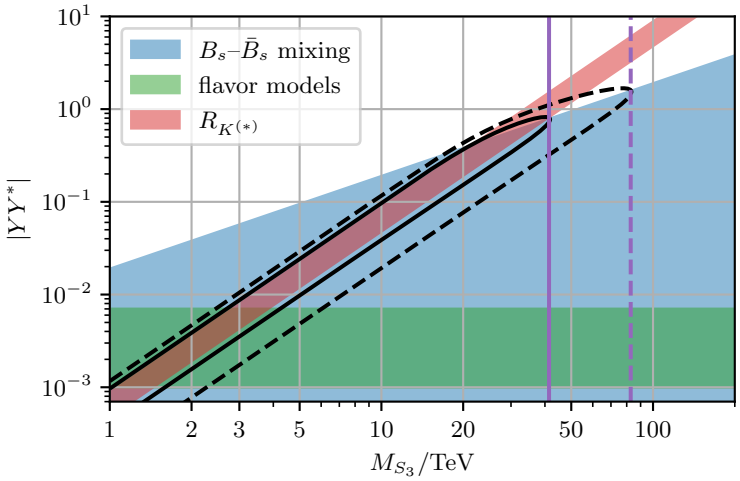

Figure 4.2.: Experimental constraints from B_s–$\bar{B}_s$ mixing (blue) and $R_{K^{(*)}}$ (red) in the YY^*–M plane for the S_3 leptoquark. The solid and dashed black lines indicates the resulting one and two sigma contours, respectively. The corresponding upper bounds on the leptoquark mass are shown in purple. Typical sizes for the couplings in flavor models are depicted in green.

to right handed lepton currents or $b \to s\nu\bar{\nu}$, leaving just $V_{1,2,3}$, S_3 and $\tilde{S}_2$ as potential candidates, where $V_{1,3}$ as well as S_3 contribute to $\mathcal{O}_{\text{LL}}$ while V_2 and $\tilde{S}_2$ contribute to $\mathcal{O}_{\text{RL}}$. The leptoquarks contributing to right-handed quark currents are disfavored by current data as they predict $R_K \neq R_{K^*}$. All of these models have been extensively studied within various scenarios in recent literature [114, 136–140]. The strongest constraint that applies to leptoquark models in the context of $b \to s\ell^+\ell^-$ transitions is due to the mass difference in B_s–$\bar{B}_s$ mixing as discussed in Section 3.5.2. Following [113] the leptoquark contribution to the $\Delta B = 2$ effective operator (3.56) stemming from box diagrams reads

$$C_1^{\text{LQ}} = \frac{p_{\text{LQ}}\,(YY^*)^2}{32\pi^2 (V_{tb}V_{ts}^*)^2 M^2}\,, \quad \text{where } p_{\text{LQ}} = 5, 4, 20 \text{ for } S_3, V_1, V_3\,. \tag{4.2}$$

Since this contribution scales as $\frac{(YY^*)^2}{M^2}$ while effects in semileptonic decays are proportional to $\frac{YY^*}{M^2}$ the experimental data on B_s–$\bar{B}_s$ mixing imposes an upper limit on the mass of leptoquarks that can explain the observed deviation in $R_{K^{(*)}}$. In Figure 4.2 we show the one sigma regions of to the bounds from Δm_{B_s} and $R_{K^{(*)}}$ in blue and red, respectively, for the S_3 leptoquark together with the resulting one and two sigma contours from which we infer the upper leptoquark mass bound. At one (two) sigma we find

$$M/\text{TeV} \lesssim 41\ (83)\,, 46\ (92)\,, 21\ (41) \text{ for } S_3, V_1, V_3\,. \tag{4.3}$$

The leptoquarks $S_{1,2,3,}$ and $V_{1,2,3}$ are all capable of giving rise to the charged currents

$b \to c\ell\bar{\nu}$. As the hints for NP in this sector are far less established than in $b \to s\ell^+\ell^-$ and there is no preferred direction in the space of BSM Wilson coefficients, we will later on explore multiple scenarios that have been previously studied in the literature [35, 141].

Instead of just focusing on one individual anomaly it is of course tempting to study models that can resolve multiple anomalies at once. Such combined scenarios have also received a lot of attention from the community. While most of them focus on $R_{K^{(*)}}$ and $R_{D^{(*)}}$ [142–150] there are also models which address additional problems such as the deviation seen in the anomalous magnetic moment of the muon or the lack of neutrino masses in the SM [151–154]. The consensus of those works is that a combined single leptoquark explanation of the B decay anomalies is only possible with V_1 – all other remaining models either induce opposing effects in $R_{K^{(*)}}$ and $R_{D^{(*)}}$ or are excluded by other flavor observables [149].

We provide tables summarizing the tree-level leptoquark contributions to the Wilson coefficients for the transitions $b \to s\ell^+\ell^-$, $b \to s\nu\bar{\nu}$, $b \to c\ell\bar{\nu}$ as well as the charm FCNCs $c \to u\ell^+\ell^-$ and $c \to u\nu\bar{\nu}$, obtained from comparing the effective vertices listed in Tables 4.2, 4.3 with the respective operator bases, in Appendix D. Contributions to these different sectors arise from different sectors of the coupling matrix Y, as schematically shown here:

$$Y = \begin{pmatrix} Y^{11} & Y^{12} & Y^{13} \\ Y^{21} & Y^{22} & Y^{23} \\ Y^{31} & Y^{32} & Y^{33} \end{pmatrix}$$

Charm FCNCs, Kaon decays, ... ; $R_{D^{(*)}}$; $R_{K^{(*)}}$

Although there is some overlap between these regions of the coupling matrix it can be possible to tune the entries in such a way that constraints from the charm and kaon sectors or cLFV decays can be avoided while at the same time accounting for the B anomalies. In the literature discussed above the flavor structure is typically either tuned to match the experimental data directly, assumed to follow simple structures like such ones that are dominated by third generation couplings with others induced by mixing, or obtained from variants of MFV. Here, we aim to establish more rigid structures within these coupling matrices by imposing flavor symmetries which are also capable of describing the observed pattern of masses and mixing of the SM fermions.

In order to study the hadron collider phenomenology of leptoquarks we also need to consider their gluon interactions. As gauge interactions they arise from the kinetic terms, which read

$$\mathcal{L}_{\text{kin}} = (D_\mu \Delta)^\dagger \, D^\mu \Delta \,, \tag{4.4}$$

Interaction Lagrangian	SM Rep.	Effective Vertices
$\left(Y_{QL}\bar{Q}^c_{\mathrm{L}} i\sigma_2 L_{\mathrm{L}} + Y_{UE}\bar{u}^c_{\mathrm{R}} e_{\mathrm{R}}\right) S_1$	$(\bar{\mathbf{3}}, \mathbf{1}, 1/3)$	$\frac{Y^{ij}_{QL}\left(Y^{mn}_{QL}\right)^*}{2M^2}(\bar{u}_{\mathrm{L}m}\gamma_\mu u_{\mathrm{L}i})(\bar{\ell}_{\mathrm{L}n}\gamma^\mu \ell_{\mathrm{L}j})$ $-\frac{Y^{ij}_{QL}\left(Y^{mn}_{QL}\right)^*}{2M^2}(\bar{u}_{\mathrm{L}m}\gamma_\mu d_{\mathrm{L}i})(\bar{\ell}_{\mathrm{L}n}\gamma^\mu \nu_{\mathrm{L}j})$ $\frac{Y^{ij}_{QL}\left(Y^{mn}_{QL}\right)^*}{2M^2}(\bar{d}_{\mathrm{L}m}\gamma_\mu d_{\mathrm{L}i})(\bar{\nu}_{\mathrm{L}n}\gamma^\mu \nu_{\mathrm{L}j})$ $\frac{Y^{ij}_{UE}(Y^{mn}_{UE})^*}{2M^2}(\bar{u}_{\mathrm{R}m}\gamma_\mu u_{\mathrm{R}i})(\bar{\ell}_{\mathrm{R}n}\gamma^\mu \ell_{\mathrm{R}j})$ $-\frac{Y^{ij}_{QL}(Y^{mn}_{UE})^*}{2M^2}(\bar{u}_{\mathrm{R}m}u_{\mathrm{L}i})(\bar{\ell}_{\mathrm{R}n}\ell_{\mathrm{L}j})$ $\frac{Y^{ij}_{QL}(Y^{mn}_{UE})^*}{8M^2}(\bar{u}_{\mathrm{R}m}\sigma_{\mu\nu}u_{\mathrm{L}i})(\bar{\ell}_{\mathrm{R}n}\sigma^{\mu\nu}\ell_{\mathrm{L}j})$ $\frac{Y^{ij}_{QL}(Y^{mn}_{UE})^*}{2M^2}(\bar{u}_{\mathrm{R}m}d_{\mathrm{L}i})(\bar{\ell}_{\mathrm{R}n}\nu_{\mathrm{L}j})$ $-\frac{Y^{ij}_{QL}(Y^{mn}_{UE})^*}{8M^2}(\bar{u}_{\mathrm{R}m}\sigma_{\mu\nu}d_{\mathrm{L}i})(\bar{\ell}_{\mathrm{R}n}\sigma^{\mu\nu}\nu_{\mathrm{L}j})$
$Y_{DE}\bar{d}^c_{\mathrm{R}} e_{\mathrm{R}}\tilde{S}_1$	$(\bar{\mathbf{3}}, \mathbf{1}, 4/3)$	$\frac{Y^{ij}_{DE}(Y^{mn}_{DE})^*}{2M^2}(\bar{d}_{\mathrm{R}m}\gamma_\mu d_{\mathrm{R}i})(\bar{e}_{\mathrm{R}n}\gamma^\mu e_{\mathrm{R}j})$
$\left(Y_{\bar{U}L}\bar{u}_{\mathrm{R}} L_{\mathrm{L}} + Y_{\bar{Q}E}\bar{Q}_{\mathrm{L}} i\sigma_2 e_{\mathrm{R}}\right) S_2$	$(\mathbf{3}, \mathbf{2}, 7/6)$	$-\frac{Y^{ij}_{\bar{U}L}\left(Y^{mn}_{\bar{U}L}\right)^*}{2M^2}(\bar{u}_{\mathrm{R}i}\gamma_\mu u_{\mathrm{R}m})(\bar{\nu}_{\mathrm{L}n}\gamma^\mu \nu_{\mathrm{L}j})$ $-\frac{Y^{ij}_{\bar{U}L}\left(Y^{mn}_{\bar{U}L}\right)^*}{2M^2}(\bar{u}_{\mathrm{R}i}\gamma_\mu u_{\mathrm{R}m})(\bar{\ell}_{\mathrm{L}n}\gamma^\mu \ell_{\mathrm{L}j})$ $-\frac{Y^{ij}_{\bar{Q}E}\left(Y^{mn}_{\bar{Q}E}\right)^*}{2M^2}(\bar{u}_{\mathrm{L}i}\gamma_\mu u_{\mathrm{L}m})(\bar{\ell}_{\mathrm{R}n}\gamma^\mu \ell_{\mathrm{R}j})$ $-\frac{Y^{ij}_{\bar{Q}E}\left(Y^{mn}_{\bar{Q}E}\right)^*}{2M^2}(\bar{d}_{\mathrm{L}i}\gamma_\mu d_{\mathrm{L}m})(\bar{\ell}_{\mathrm{R}n}\gamma^\mu \ell_{\mathrm{R}j})$ $\frac{Y^{ij}_{\bar{U}L}\left(Y^{mn}_{\bar{Q}E}\right)^*}{2M^2}(\bar{u}_{\mathrm{R}i}d_{\mathrm{L}m})(\bar{\ell}_{\mathrm{R}n}\nu_{\mathrm{L}j})$ $\frac{Y^{ij}_{\bar{U}L}\left(Y^{mn}_{\bar{Q}E}\right)^*}{8M^2}(\bar{u}_{\mathrm{R}i}\sigma_{\mu\nu}d_{\mathrm{L}m})(\bar{\ell}_{\mathrm{R}n}\sigma^{\mu\nu}\nu_{\mathrm{L}j})$ $-\frac{Y^{ij}_{\bar{U}L}\left(Y^{mn}_{\bar{Q}E}\right)^*}{2M^2}(\bar{u}_{\mathrm{R}i}u_{\mathrm{L}m})(\bar{\ell}_{\mathrm{R}n}\ell_{\mathrm{L}j})$ $-\frac{Y^{ij}_{\bar{U}L}\left(Y^{mn}_{\bar{Q}E}\right)^*}{8M^2}(\bar{u}_{\mathrm{R}i}\sigma_{\mu\nu}u_{\mathrm{L}m})(\bar{\ell}_{\mathrm{R}n}\sigma^{\mu\nu}\ell_{\mathrm{L}j})$
$Y_{\bar{D}L}\bar{d}_{\mathrm{R}} L_{\mathrm{L}}\tilde{S}_2$	$(\mathbf{3}, \mathbf{2}, 1/6)$	$-\frac{Y^{ij}_{\bar{D}L}\left(Y^{mn}_{\bar{D}L}\right)^*}{2M^2}(\bar{d}_{\mathrm{R}i}\gamma_\mu d_{\mathrm{R}m})(\bar{\nu}_{\mathrm{L}n}\gamma^\mu \nu_{\mathrm{L}j})$ $-\frac{Y^{ij}_{\bar{D}L}\left(Y^{mn}_{\bar{D}L}\right)^*}{2M^2}(\bar{d}_{\mathrm{R}i}\gamma_\mu d_{\mathrm{R}m})(\bar{\ell}_{\mathrm{L}n}\gamma^\mu \ell_{\mathrm{L}j})$
$Y_{QL}\bar{Q}^c_{\mathrm{L}} i\sigma_2\vec{\sigma} L_{\mathrm{L}}\vec{S}_3$	$(\bar{\mathbf{3}}, \mathbf{3}, 1/3)$	$\frac{Y^{ij}_{QL}\left(Y^{mn}_{QL}\right)^*}{M^2}(\bar{u}_{\mathrm{L}m}\gamma_\mu u_{\mathrm{L}i})(\bar{\nu}_{\mathrm{L}n}\gamma^\mu \nu_{\mathrm{L}j})$ $\frac{Y^{ij}_{QL}\left(Y^{mn}_{QL}\right)^*}{M^2}(\bar{d}_{\mathrm{L}m}\gamma_\mu d_{\mathrm{L}i})(\bar{\ell}_{\mathrm{L}n}\gamma^\mu \ell_{\mathrm{L}j})$ $\frac{Y^{ij}_{QL}\left(Y^{mn}_{QL}\right)^*}{2M^2}(\bar{u}_{\mathrm{L}m}\gamma_\mu u_{\mathrm{L}i})(\bar{\ell}_{\mathrm{L}n}\gamma^\mu \ell_{\mathrm{L}j})$ $\frac{Y^{ij}_{QL}\left(Y^{mn}_{QL}\right)^*}{2M^2}(\bar{u}_{\mathrm{L}m}\gamma_\mu d_{\mathrm{L}i})(\bar{\ell}_{\mathrm{L}n}\gamma^\mu \nu_{\mathrm{L}j})$ $\frac{Y^{ij}_{QL}\left(Y^{mn}_{QL}\right)^*}{2M^2}(\bar{d}_{\mathrm{L}m}\gamma_\mu d_{\mathrm{L}i})(\bar{\nu}_{\mathrm{L}n}\gamma^\mu \nu_{\mathrm{L}j})$

Table 4.2.: Interaction Lagrangians and tree-level effective vertices of scalar leptoquark models with given SM gauge group representation.

Interaction Lagrangian	SM Rep.	Effective Vertices
$\left(Y_{\bar{Q}L}\bar{Q}_{\rm L}\gamma_\mu L_{\rm L} + Y_{\bar{D}E}\bar{d}_{\rm R}\gamma_\mu e_{\rm R}\right) V_1^\mu$	$(\mathbf{3},\mathbf{1},2/3)$	$-\frac{Y^{ij}_{\bar{Q}L}\left(Y^{mn}_{\bar{Q}L}\right)^*}{M^2}(\bar{u}_{{\rm L}i}\gamma_\mu u_{{\rm L}m})(\bar{\nu}_{{\rm L}n}\gamma^\mu \nu_{{\rm L}j})$ $-\frac{Y^{ij}_{\bar{Q}L}\left(Y^{mn}_{\bar{Q}L}\right)^*}{M^2}(\bar{u}_{{\rm L}i}\gamma_\mu d_{{\rm L}m})(\bar{\ell}_{{\rm L}n}\gamma^\mu \nu_{{\rm L}j})$ $-\frac{Y^{ij}_{\bar{Q}L}\left(Y^{mn}_{\bar{Q}L}\right)^*}{M^2}(\bar{d}_{{\rm L}i}\gamma_\mu d_{{\rm L}m})(\bar{\ell}_{{\rm L}n}\gamma^\mu \ell_{{\rm L}j})$ $-\frac{Y^{ij}_{\bar{D}E}\left(Y^{mn}_{\bar{D}E}\right)^*}{M^2}(\bar{d}_{{\rm R}i}\gamma_\mu d_{{\rm R}m})(\bar{\ell}_{{\rm R}n}\gamma^\mu \ell_{{\rm R}j})$ $\frac{2Y^{ij}_{\bar{Q}L}\left(Y^{mn}_{\bar{D}E}\right)^*}{M^2}(\bar{u}_{{\rm L}i}d_{{\rm R}m})(\bar{\ell}_{{\rm R}n}\nu_{{\rm L}j})$ $\frac{2Y^{ij}_{\bar{Q}L}\left(Y^{mn}_{\bar{D}E}\right)^*}{M^2}(\bar{d}_{{\rm L}i}d_{{\rm R}m})(\bar{\ell}_{{\rm R}n}\ell_{{\rm L}j})$
$Y_{\bar{U}E}\bar{u}_{\rm R}\gamma_\mu e_{\rm R}\tilde{V}_1^\mu$	$(\mathbf{3},\mathbf{1},5/3)$	$-\frac{Y^{ij}_{\bar{U}E}\left(Y^{mn}_{\bar{U}E}\right)^*}{M^2}(\bar{u}_{{\rm R}i}\gamma_\mu u_{{\rm R}m})(\bar{\ell}_{{\rm R}n}\gamma^\mu \ell_{{\rm R}j})$
$\left(Y_{DL}\bar{d}^c_{\rm R}\gamma_\mu L_{\rm L} + Y_{QE}\bar{Q}^c_{\rm L}\gamma_\mu e_{\rm R}\right) i\sigma_2 V_2^\mu$	$(\bar{\mathbf{3}},\mathbf{2},5/6)$	$\frac{Y^{ij}_{DL}(Y^{mn}_{DL})^*}{M^2}(\bar{d}_{{\rm R}m}\gamma_\mu d_{{\rm R}i})(\bar{\nu}_{{\rm L}n}\gamma^\mu \nu_{{\rm L}j})$ $\frac{Y^{ij}_{DL}(Y^{mn}_{DL})^*}{M^2}(\bar{d}_{{\rm R}m}\gamma_\mu d_{{\rm R}i})(\bar{\ell}_{{\rm L}n}\gamma^\mu \ell_{{\rm L}j})$ $\frac{Y^{ij}_{QE}\left(Y^{mn}_{QE}\right)^*}{M^2}(\bar{u}_{{\rm L}m}\gamma_\mu u_{{\rm L}i})(\bar{\ell}_{{\rm R}n}\gamma^\mu \ell_{{\rm R}j})$ $\frac{Y^{ij}_{QE}\left(Y^{mn}_{QE}\right)^*}{M^2}(\bar{d}_{{\rm L}m}\gamma_\mu d_{{\rm L}i})(\bar{\ell}_{{\rm R}n}\gamma^\mu \ell_{{\rm R}j})$ $\frac{2Y^{ij}_{DL}\left(Y^{mn}_{QE}\right)^*}{M^2}(\bar{u}_{{\rm L}m}d_{{\rm R}i})(\bar{\ell}_{{\rm R}n}\nu_{{\rm L}j})$ $\frac{2Y^{ij}_{DL}\left(Y^{mn}_{QE}\right)^*}{M^2}(\bar{d}_{{\rm L}m}d_{{\rm R}i})(\bar{\ell}_{{\rm R}n}\ell_{{\rm L}j})$
$Y_{UL}\bar{u}^c_{\rm R}\gamma_\mu L_L\tilde{V}_2^\mu$	$(\bar{\mathbf{3}},\mathbf{2},-1/6)$	$\frac{Y^{ij}_{UL}(Y^{mn}_{UL})^*}{M^2}(\bar{u}_{{\rm R}m}\gamma_\mu u_{{\rm R}i})(\bar{\nu}_{{\rm L}n}\gamma^\mu \nu_{{\rm L}j})$ $\frac{Y^{ij}_{UL}(Y^{mn}_{UL})^*}{M^2}(\bar{u}_{{\rm R}m}\gamma_\mu u_{{\rm R}i})(\bar{\ell}_{{\rm L}n}\gamma^\mu \ell_{{\rm L}j})$
$Y_{\bar{Q}L}\bar{Q}_{\rm L}\gamma_\mu\vec{\sigma}L_{\rm L}\vec{V}_3^\mu$	$(\mathbf{3},\mathbf{3},2/3)$	$-\frac{2Y^{ij}_{\bar{Q}L}\left(Y^{mn}_{\bar{Q}L}\right)^*}{M^2}(\bar{u}_{{\rm L}i}\gamma_\mu u_{{\rm L}m})(\bar{\ell}_{{\rm L}n}\gamma^\mu \ell_{{\rm L}j})$ $-\frac{2Y^{ij}_{\bar{Q}L}\left(Y^{mn}_{\bar{Q}L}\right)^*}{M^2}(\bar{d}_{{\rm L}i}\gamma_\mu d_{{\rm L}m})(\bar{\nu}_{{\rm L}n}\gamma^\mu \nu_{{\rm L}j})$ $-\frac{Y^{ij}_{\bar{Q}L}\left(Y^{mn}_{\bar{Q}L}\right)^*}{M^2}(\bar{u}_{{\rm L}i}\gamma_\mu u_{{\rm L}m})(\bar{\nu}_{{\rm L}n}\gamma^\mu \nu_{{\rm L}j})$ $\frac{Y^{ij}_{\bar{Q}L}\left(Y^{mn}_{\bar{Q}L}\right)^*}{M^2}(\bar{u}_{{\rm L}i}\gamma_\mu d_{{\rm L}m})(\bar{\ell}_{{\rm L}n}\gamma^\mu \nu_{{\rm L}j})$ $-\frac{Y^{ij}_{\bar{Q}L}\left(Y^{mn}_{\bar{Q}L}\right)^*}{M^2}(\bar{d}_{{\rm L}i}\gamma_\mu d_{{\rm L}m})(\bar{\ell}_{{\rm L}n}\gamma^\mu \ell_{{\rm L}j})$

Table 4.3.: Same as Table 4.2 but for vector leptoquark models.

in the case of scalar leptoquarks and

$$\mathcal{L}_{\text{kin}} = -\left((D_\mu \Delta_\nu)^\dagger D^\mu \Delta^\nu - (D_\nu \Delta_\mu)^\dagger D^\mu \Delta^\nu \right) \tag{4.5}$$

for vector leptoquarks. In the latter case, an additional gauge invariant coupling to the gluon field strength tensor appears, which is given by

$$\mathcal{L} \supset -i g_{\text{s}} \kappa \Delta^{\dagger\mu} t^A \Delta^\nu G^A_{\mu\nu} \,, \tag{4.6}$$

where κ is a dimensionless parameter.

4.2. Z' Models

New electrically neutral and colorless vector bosons arise as gauge bosons in models with an additional $U(1)'$ symmetry, including all GUTs based on gauge groups larger than $SU(5)$ [155]. Once the new symmetry is broken the Z' boson acquires a mass $M_{Z'}$ related to the breaking scale. Generically, the Z' interactions with the SM fermions in the mass basis can be expressed as

$$\mathcal{L}_{Z'} = \sum_f \left[\bar{f}_{\text{L}} \gamma^\mu g_{\text{L}} f_{\text{L}} + \bar{f}_{\text{R}} \gamma^\mu g_{\text{R}} f_{\text{R}} \right] Z'_\mu \,, \tag{4.7}$$

where the couplings $g^f_{\text{L,R}}$ are 3×3 matrices in flavor space. The values of these couplings depend on the new gauge coupling as well as the charges of the SM fermions under the $U(1)'$. Fermion mixing allows to obtain contributions to off-diagonal entries that give rise to tree-level FCNCs if the fermion charges under the new symmetry are non-universal among different generations.

Within a general Z' model an explanation of the anomalies in $R_{K^{(*)}}$ is readily obtained by integrating out the Z' at tree-level, which results in

$$C_9^{Z'} = -C_{10}^{Z'} = -\frac{\pi}{\sqrt{2}\alpha_{\text{e}} G_{\text{F}} V_{tb} V_{ts}^*} \frac{g_{\text{L}}^{bs} g_{\text{L}}^{\mu\mu}}{M_{Z'}^2} \,. \tag{4.8}$$

This minimal scenario as well as variations in which the lepton current is vectorial, resulting in a contribution only to C_9, have been the subject of many recent studies [156–163] which consider a variety of different UV completions. A strong, model-independent, constraint on the g_{L}^{bs} coupling arises from B_s–$\bar{B}_s$ mixing to which Z' bosons contribute at tree-level. The respective Wilson coefficient reads [121]

$$C_1^{Z'} = \frac{1}{2(V_{tb} V_{ts}^*)^2} \frac{\left(g_{\text{L}}^{bs}\right)^2}{M_{Z'}^2} \,. \tag{4.9}$$

Hence, a large muon coupling $g_{\text{L}}^{\mu\mu}$ is needed to successfully explain the data on $R_{K^{(*)}}$. Similar to the case of leptoquarks, B_s–$\bar{B}_s$ mixing imposes a model-independent upper

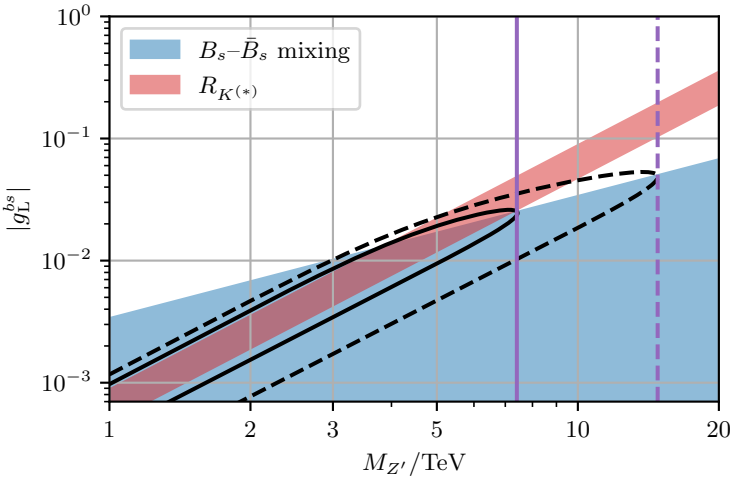

Figure 4.3.: One sigma constraints from B_s–$\bar{B}_s$ mixing (blue) and $R_{K^{(*)}}$ (red) in the plane spanned by the Z' mass $M_{Z'}$ and the off-diagonal coupling g_{L}^{bs}, assuming $g_{\mathrm{L}}^{\mu\mu} = 1$. The solid and dashed purple lines indicate the model-independent bounds imposed on $M_{Z'}$ at one and two sigma, respectively, resulting from the corresponding black contours.

bound on the masses of Z' bosons that can account for the deviation in $R_{K^{(*)}}$. This can be seen in Figure 4.3, where we show the mixing constraint on g_{L}^{bs} in blue and the one sigma range that allows for an explanation of $R_{K^{(*)}}$, assuming $g_{\mathrm{L}}^{\mu\mu} = 1$. From the resulting one and two sigma contours shown as solid and dashed black lines, respectively, we obtain

$$M_{Z'}/\mathrm{TeV} \lesssim 7\ (15)\,. \tag{4.10}$$

While typical explanations of the $b \to s\ell^+\ell^-$ anomalies employ heavy fields that can be integrated out and yield q^2-independent contributions to the Wilson coefficients of the EFT, the parameter space of models with light new degrees of freedom is not yet fully exhausted by experimental data. As the deviation seen in $R_{K^{(*)}}$ is located in the low-q^2 interval between $1\,\mathrm{GeV}^2$ and $6\,\mathrm{GeV}^2$, a viable explanation can be obtained by means of a light Z' with a mass of $M_{Z'}/\mathrm{GeV} \simeq \sqrt{6} \simeq 2.5$ that causes a negative interference in this region. This idea is studied in [164, 165] in the context of the deviation measured in the muon anomalous magnetic moment. The effect of the light Z' boson on $b \to s\ell^+\ell^-$ observables can be written as a q^2-dependent conribution to the Wilson coefficients C_9 and C_{10} as

$$C_{9,10}^{\text{light } Z'}(q^2) = \frac{g_{\mathrm{L}}^{bs} g_{\mathrm{V,A}}^{\mu\mu}/N}{q^2 - M_{Z'}^2 + iM_{Z'}\Gamma_{Z'}}\,, \tag{4.11}$$

where $g_{\mathrm{V,A}} = g_{\mathrm{L}} \pm g_{\mathrm{R}}$ and $N = G_{\mathrm{F}} V_{tb} V_{ts}^* \alpha_{\mathrm{e}}/\sqrt{2}\pi$. The decay width $\Gamma_{Z'}$ is assumed to be dominated by the decay to a light SM singlet fermion and to be moderately narrow – $\Gamma_{Z'}/M_{Z'} \simeq 20\,\%$. We are able to reproduce the benchmark scenario from [164] using

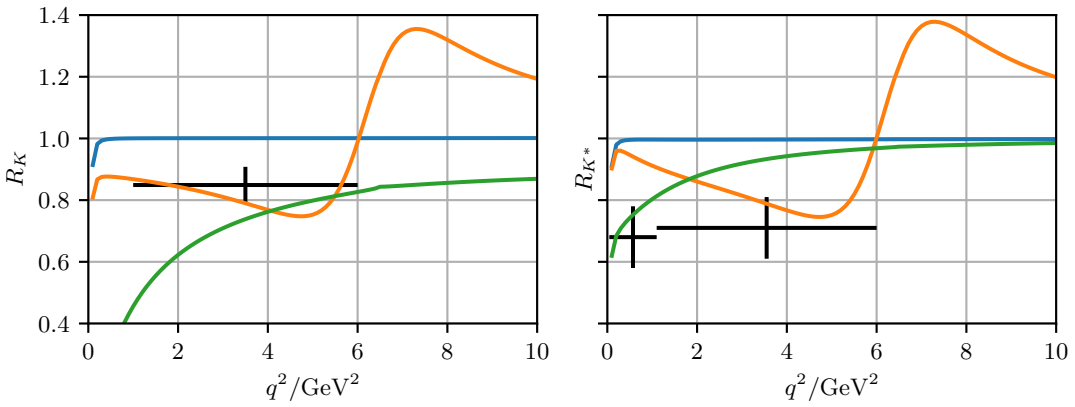

Figure 4.4.: q^2-dependent results for R_K and R_{K^*} in the light Z' scenario from [164] (orange), in the light scalar scenario from [166] (green), and in the SM (blue). Experimental data on $R_{K^{(*)}}$ from the LHCb collaboration is shown in black.

the values $g_{\mathrm{V}}^{\mu\mu} = 0.1$ and $g_{\mathrm{A}}^{\mu\mu} = -0.044$ for the muon couplings, and $g_{\mathrm{L}}^{bs} = 1.75 \times 10^{-8}$, which saturates the limit imposed by $B \to K\nu\bar{\nu}$. In Figure 4.4 we show R_K and R_{K^*} as functions of q^2 in the NP scenario from [164] (orange) and in the SM (blue) together with the most recent LHCb data (black). It can be seen that the light Z' with $M_{Z'} = 2.5\,\mathrm{GeV}$ and large muon couplings interferes with the SM contribution in such a way that the LHCb data on R_K and R_{K^*} can be accommodated in the regions $1\,\mathrm{GeV} < q^2 < 6\,\mathrm{GeV}$ and $1.1\,\mathrm{GeV} < q^2 < 6\,\mathrm{GeV}$, respectively. However, the tension in the very low q^2 region for R_{K^*} remains.

A different approach is taken by [166] where light scalar and vector bosons in the $\mathcal{O}(10)\,\mathrm{MeV}$ range are considered. In particular, a simple scenario involving a light scalar of mass $M_S = 25\,\mathrm{MeV}$ with the fermion interactions

$$\mathcal{L}_S = \left[\bar{s}_{\mathrm{R}} g_S^{bs} b_{\mathrm{L}} + \bar{s}_{\mathrm{L}} g_S^{bs} b_{\mathrm{R}} + \bar{e} g_S^{ee} e\right] S \tag{4.12}$$

provides a good fit to the $R_{K^{(*)}}$ in all q^2 regions. Note that for scalar mediators only couplings to electrons can help to explain $R_{K^{(*)}}$ since there is no interference with the SM contribution, making it impossible to suppress $B \to K^{(*)}\mu^+\mu^-$. However, the enhancement of $\mathcal{B}(B \to K^{(*)}e^+e^-)$ in this simple scenario is in conflict with measurements by BABAR [167] and Belle [112, 168], which can be resolved with q^2-dependent couplings. We are able to reproduce this scenario with the parameters provided in [166] and show the q^2-dependent results for R_K and R_{K^*} in comparison with the previously discussed light Z' scenario from [164] and the SM expectation in Figure 4.4.

Chapter 5.

Approaches to the Flavor Puzzles

Before discussing concrete models that seek to solve the flavor puzzles in and beyond the SM let us briefly highlight the special role that is played by flavor in general by comparing the structure of the SM's flavor and gauge sectors. Since the latter is described by the kinetic terms of the Lagrangian alone, it is completely determined by the matter fields and their transformation properties under the gauge group. As we have seen before, this means that the only free parameters of this sector are the three gauge couplings. However, according to the parameter counting performed in Section 2.4 there are 13 parameters in the Yukawa sector alone. Taking into account the two parameters associated with electroweak symmetry breaking and the strong CP phase, this means that 16 out of the total 19 free parameters of the SM belong to its flavor sector. This uneven distribution of parameters between the two sectors reflects the fact that the flavor sector is much more complex and exhibits a smaller degree of symmetry than the gauge sector.

Any effort towards solving the flavor puzzles must reduce the number of flavor parameters and consequently entail a larger degree of symmetry of the flavor sector at some higher scale. Hence, the canonical starting point for any symmetry-based flavor model is a subgroup of the SM's flavor symmetry group (2.28) in the absence of Yukawa couplings. In the following, we first discuss one of the the simplest options – a $U(1)$ symmetry. Models based on this subgroup have proven to be successful in answering the central question of the flavor puzzles as to why the parameters of the flavor sectors are so small and hierarchical, while those in the gauge sector are all approximately of $\mathcal{O}(1)$. At this point it is important to remark that we generally do not expect flavor models to make precise predictions for the parameters, but rather to provide a qualitative understanding of the hierarchies in terms of power counting in a small expansion parameter. Afterwards, we consider a more complex model based on the non-abelian discrete group A_4, which naturally gives rise to tribimaximal mixing in the lepton sector, thus providing are more quantitative explanation of the non-hierarchical neutrino mixing pattern.

5.1. The Froggatt–Nielsen Mechanism

From the masses of the quarks and charged leptons given in (2.17) and (2.22), respectively, we can see that the mass ratios follow the approximate pattern

$$\begin{aligned} m_u &: m_c : m_t \simeq \lambda^8 : \lambda^4 : 1\,, \\ m_d &: m_s : m_b \simeq \lambda^4 : \lambda^2 : 1\,, \\ m_e &: m_\mu : m_\tau \simeq \lambda^4 : \lambda^2 : 1\,, \end{aligned} \tag{5.1}$$

where λ is the Wolfenstein parameter. This hierarchy can be explained by the Froggatt–Nielsen (FN) mechanism [169], which is based on a global $U(1)$ symmetry under which the SM fermion generations transform distinctively. A new gauge singlet scalar field θ, dubbed "flavon", is introduced that spontaneously breaks the symmetry by acquiring a vev. Furthermore, we assume a UV cutoff scale Λ beyond current experimental reach, as we follow an EFT approach in which we remain agnostic about the details of the UV completion. The cutoff scale and the flavon vev are chosen in such a way that they provide a small expansion parameter

$$\epsilon \equiv \frac{\langle\theta\rangle}{\Lambda} \simeq \lambda\,, \tag{5.2}$$

which is assumed to be of the order of the Wolfenstein parameter.

In order to generate hierarchical SM fermion Yukawa couplings, the fermions are assigned $U(1)_{\mathrm{FN}}$ charges q in such a way that a certain number of insertions of the flavon field θ, carrying $U(1)_{\mathrm{FN}}$ charge -1, is required to form Yukawa interactions that are invariant under the FN symmetry. Consequently, the Yukawa interaction terms can be written in terms of effective operators as

$$-\mathcal{L}_{\mathrm{Yukawa}} = \sum_\psi \underbrace{Y'_{\psi,ij}\left(\frac{\theta}{\Lambda}\right)^{q(\bar{\psi}^i_L)+q(\psi^j_R)}}_{Y_{\psi,ij}} H\bar{\psi}^i_L\psi^j_R + \mathrm{h.c.}\,, \tag{5.3}$$

where, after breaking the $U(1)_{\mathrm{FN}}$ symmetry, the Yukawa couplings are given by

$$Y_{\psi,ij} = Y'_{\psi,ij}\ \epsilon^{q(\bar{\psi}^i_L)+q(\psi^j_R)} \sim \epsilon^{q(\bar{\psi}^i_L)+q(\psi^j_R)} \tag{5.4}$$

and the coefficients $Y'_{\psi,ij}$ are of $\mathcal{O}(1)$. We use the symbol "$\sim$" for relations that hold in terms of power counting in ϵ up to unknown factors of $\mathcal{O}(1)$. Note that this means we allow for small deviations in power counting relations for quantities that can contain sums or products of multiple $\mathcal{O}(1)$ factors.

UV completions of this effective model require new heavy fermions, called FN fields or, more generally, "messengers", at the mass scale Λ which mediate the interactions between the SM fermions and the flavon field, as shown in the exemplary diagram depicted in Figure 5.1. However, Λ is typically so large that effects stemming from the

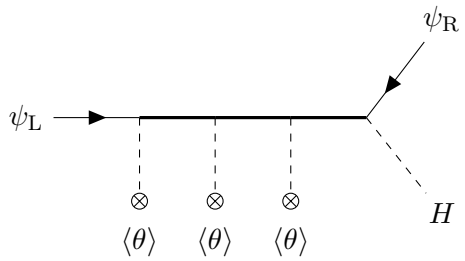

Figure 5.1.: Schematic Feynman diagram of a UV completion of the effective interaction in (5.3). Thick black lines denote heavy FN fermions. The crosses denote vev insertions of the flavon field. In this example three insertions are necessary to obtain a $U(1)_{\mathrm{FN}}$-invariant amplitude.

messenger fields are too small to be detected with current experimental sensitivities.

Perturbatively diagonalizing the Yukawa matrices (5.4) in powers of ϵ yields the mass hierarchies

$$\frac{m_i}{m_j} \sim \epsilon^{q(\bar{\psi}^i_{\mathrm{L}})-q(\bar{\psi}^j_{\mathrm{L}})+q(\psi^i_{\mathrm{R}})-q(\psi^j_{\mathrm{R}})}\,. \tag{5.5}$$

The resulting unitary rotation matrices, defined in (2.14), follow the hierarchical structure

$$U^{ij} \sim \epsilon^{\left|q(\psi^i_{\mathrm{L}})-q(\psi^j_{\mathrm{L}})\right|}\,. \tag{5.6}$$

Therefore, the quark and lepton mixing matrices V_{CKM} and U_{PMNS}, respectively, derived from (5.6) adhere to this pattern as well, since they are products of two unitary rotation matrices.

In the quark sector, where the mixing angles are small, this mechanism provides a good explanation of the current experimental data. The charge assignments [170]

$$q(\bar{Q}) = q(U) = (4,2,0)\,, \quad q(D) = (3,2,2)\,, \tag{5.7}$$

yield the desired quark mass hierarchies from (5.1) and correctly reproduce the quark mixing matrix. Furthermore, the charged lepton mass hierarchies can be modeled by assigning charges only to the lepton singlets, i.e.

$$q(E) = (4,2,0)\,, \quad q(L) = 0\,. \tag{5.8}$$

If right-handed neutrinos are included to generate neutrino masses through the seesaw-mechanism, FN models can explain mixing in the lepton sector as well. However, as can be seen in the detailed analysis provided in [170], some fine-tuning of the unknown $\mathcal{O}(1)$ coefficients is necessary.

The main limitation of the FN approach is the lack of quantitative predictions for sets of non-hierarchical quantities such as the neutrino mixing angles, of which only one is

small while the other two are large and of similar size. More suitable descriptions of large mixing angles can be achieved within models based on discrete non-abelian symmetries such as A_4, which we discuss in the following section.

5.2. Lepton Flavor from Discrete Symmetries

The TBM mixing pattern (2.25) hints at a flavor symmetry group based on rotations by discrete angles. A particularly well-suited discrete group is A_4 - the alternating group of degree four, which describes the symmetry of a regular tetrahedron. It is the smallest discrete group that contains three distinct irreducible singlet representations $\mathbf{1}$, $\mathbf{1}'$ and $\mathbf{1}''$, as well as an irreducible triplet representation $\mathbf{3}$ – perfectly suitable to harbor three generations of leptons.

While the singlet representations follow the trivial multiplication rules of the Z_3 subgroup, the triplet obeys

$$\mathbf{3} \otimes \mathbf{3} = \mathbf{1} \oplus \mathbf{1}' \oplus \mathbf{1}'' \oplus \mathbf{3} \oplus \mathbf{3}\,. \tag{5.9}$$

Explicitly, denoting two triplets as $a = (a_1, a_2, a_3)$ and $b = (b_1, b_2, b_3)$, their products resulting in singlets read

$$\begin{aligned} [ab] &= a_1 b_1 + a_2 b_3 + a_3 b_2\,, \\ [ab]' &= a_1 b_2 + a_2 b_1 + a_3 b_3\,, \\ [ab]'' &= a_1 b_3 + a_2 b_2 + a_3 b_1\,. \end{aligned} \tag{5.10}$$

The resulting triplets can be symmetric or antisymmetric and are given by

$$[ab]_s = \frac{1}{3}\begin{pmatrix} 2a_1 b_1 - a_2 b_3 - a_3 b_2 \\ 2a_3 b_3 - a_1 b_2 - a_2 b_1 \\ 2a_2 b_2 - a_3 b_1 - a_1 b_3 \end{pmatrix}\,, \quad [ab]_a = \frac{1}{2}\begin{pmatrix} a_2 b_3 - a_3 b_2 \\ a_1 b_2 - a_2 b_1 \\ a_3 b_1 - a_1 b_3 \end{pmatrix}\,. \tag{5.11}$$

The earliest application of this symmetry to lepton flavor models dates back to 2001 [171]. Since then many more variants have been constructed and constantly adapted to new experimental developments.

In this thesis, we focus on the Altarelli–Feruglio (AF) models introduced in [172–174], which give rise to the TBM mixing pattern and have been subsequently modified [175] to account for a non-zero reactor angle θ_{13}. These models are based on the flavor symmetry group

$$A_4 \times Z_3 \times U(1)_{\mathrm{FN}}\,, \tag{5.12}$$

where the additional Z_3 is used to separate the neutrino and charged lepton sectors, and the $U(1)_{\mathrm{FN}}$ corresponds to the FN symmetry discussed before, which induces hierarchical masses for the charged leptons. This symmetry is spontaneously broken by several scalar flavon fields that each acquire a vev.

	L	ν_{R}	e_{R}	μ_{R}	τ_{R}	ϕ_ℓ	ϕ_ν	ξ	ξ'	θ
A_4	**3**	**3**	**1**	**1′**	**1″**	**3**	**3**	**1**	**1′**	**1**
Z_3	1	1	1	1	1	0	2	2	2	0
$U(1)_{\mathrm{FN}}$	0	0	4	2	0	0	0	0	0	-1

Table 5.1.: Charge and representation assignments of the lepton and flavon fields with respect to the $A_4 \times Z_3 \times U(1)_{\mathrm{FN}}$ symmetry.

Here we consider the modified model [175], which contains the same number of flavons as the original AF model, namely two triplet flavons, ϕ_ℓ and ϕ_ν, and two singlet flavons ξ and ξ', where the only difference is that the ξ' flavon transforms as a non-trivial singlet $\mathbf{1'}$ under A_4 instead of as a trivial singlet. The vevs of the flavons read

$$\frac{\langle\phi_\ell\rangle}{\Lambda} = c_\ell(1,0,0)\,, \quad \frac{\langle\phi_\nu\rangle}{\Lambda} = c_\nu(1,1,1)\,, \quad \frac{\langle\xi^{(\prime)}\rangle}{\Lambda} = \kappa^{(\prime)}\,, \tag{5.13}$$

where, as before, Λ corresponds to a UV cutoff associated with the flavor dynamics. The expansion parameters[1] $c_{\ell,\nu}, \kappa^{(\prime)}$ are generally model-dependent with typical values of the order of the Wolfenstein parameter. Note that the triplet flavons acquire vevs in the particular directions $(1,0,0)$ and $(1,1,1)$, which break down A_4 to subgroups isomorphic to Z_3 and Z_2, respectively. As detailed in [174], these subgroups describe the low-energy symmetries that shape the charged lepton and neutrino sectors, respectively.

With the transformation properties of the lepton and flavon fields under the flavor symmetry group (5.12) provided in Table 5.1 the charged lepton mass matrix resulting from

$$-\mathcal{L}_\ell = \frac{y_e}{\Lambda^5}\theta^4[\phi_\ell\bar{L}]e_{\mathrm{R}}H + \frac{y_\mu}{\Lambda^3}\theta^2[\phi_\ell\bar{L}]''\mu_{\mathrm{R}}H + \frac{y_\tau}{\Lambda}[\phi_\ell\bar{L}]'\tau_{\mathrm{R}}H + \mathrm{h.c.} \tag{5.14}$$

is diagonal due to the coupling to the vev of ϕ_ℓ in the $(1,0,0)$ direction, which selects the relevant component of the lepton doublet by means of the triplet multiplication rules from (5.11). As discussed in the previous chapter, the charged lepton mass hierarchies are explained by the additional FN suppression. The neutrino sector is described by

$$-\mathcal{L}_\nu = y[\bar{L}\nu_{\mathrm{R}}]\tilde{H} + x_A\xi[\bar{\nu}_{\mathrm{R}}\nu^c_{\mathrm{R}}] + x'_A\xi'[\bar{\nu}_{\mathrm{R}}\nu^c_{\mathrm{R}}]'' + x_B[\phi_\nu\bar{\nu}_{\mathrm{R}}\nu^c_{\mathrm{R}}] + \mathrm{h.c.}\,. \tag{5.15}$$

Note that the products that result in trivial A_4 singlets give rise to contributions to the Dirac and Majorana mass matrices that are symmetric under the exchange of the second and third lepton generation. Thus, in the resulting mixing matrix θ_{23} is maximal. In fact, in the limit $\langle\xi'\rangle \to 0$ (5.15) yields exactly the TBM mixing pattern from (2.25). The contribution of the ξ' flavon then enables a non-zero value for θ_{13}.

[1] In the following we refer to the expansion parameters $\epsilon, c_{\ell,\nu}, \kappa^{(\prime)}$ as "vevs".

Chapter 6.

Leptoquarks in the Context of Flavor Models

We will now use the flavor models discussed in the previous chapter to impose constraints on the couplings of leptoquark models. First, we derive and classify the resulting flavor patterns and compute corrections that arise from flavor rotations and higher order flavon contributions. We then consider modifications of the patterns that can be engineered with dedicated charge assignments, and explore their phenomenology with a focus on the B anomalies. We use experimental data on rare kaon decays and μ-e conversion to constrain our patterns and work out predictions for charm decays.

The results of this chapter are based on the findings of [1].

6.1. Flavor Structure Imposed by the AF $\times$ FN Model

Based on the AF $\times$ FN model introduced in Section 5.2 we derive possible textures for the leptoquark couplings Y_{AB} listed in Table 4.1. We generally assume that leptoquarks transform under singlet representations of A_4. The possibility of three generations of leptoquarks residing in the A_4 triplet representation is considered in [176]. We begin under the assumption that quarks transform as trivial A_4 singlets and study possible generalizations later on.

6.1.1. Quarks in the Trivial A_4 Singlet Representation

In the case where all quarks transform as trivial singlets under A_4 and are equally charged under Z_3, we only need to distinguish between couplings to lepton singlets Y_{AE} and to lepton doublets Y_{AL}. The resulting patterns are then determined by the leptoquark representation under $A_4 \times Z_3$. The choice of the leptoquark's A_4 representation determines

to which lepton generation(s) it can couple, while its Z_3 charge selects the flavon field mediating the interaction.

For the couplings to lepton doublets the leading order contributions arise from the A_4 triplet flavons ϕ_ℓ and ϕ_ν, which lead to patterns that isolate a single lepton generation or couple equally to all generations, respectively. Interactions involving lepton singlets can be rendered Z_3-invariant by an appropriate choice of the leptoquark's Z_3 charge without the need of any flavon insertion. This leads to lepton flavor isolating patterns in which, in contrast to the case of lepton doublets, the isolated column is not suppressed by a flavon vev but by a power of ϵ due to the lepton singlet FN charges. If neither the quark nor the leptoquark carry a Z_3 charge an insertion of one of the flavons ξ or ξ' is required. As these share the same Z_3 charge but transform under different singlet representations of A_4 the resulting pattern isolates two lepton generations. A democratic pattern is obtained for $[\Delta]_{Z_3} = 1$ where two flavon insertions of $\xi^{(\prime)}$ are needed. Similarly, a second democratic pattern with two flavon insertions arises for the lepton doublets as well. Note that the democratic patterns do not induce LFUV.

In order to summarize these patterns we introduce the lepton flavor isolation textures

$$k_e = \begin{pmatrix} * & 0 & 0 \\ * & 0 & 0 \\ * & 0 & 0 \end{pmatrix}, \quad k_\mu = \begin{pmatrix} 0 & * & 0 \\ 0 & * & 0 \\ 0 & * & 0 \end{pmatrix}, \quad k_\tau = \begin{pmatrix} 0 & 0 & * \\ 0 & 0 & * \\ 0 & 0 & * \end{pmatrix}, \tag{6.1}$$

in which the "$*$" denote non-zero entries whose parametric flavor dependence is governed by the FN symmetry. We present the resulting patterns in Table 6.1 as linear combinations of those matrices. As an example, consider the pattern named "$R_{e\mu}$", which is obtained for couplings to lepton singlets if the leptoquark resides in the $\mathbf{1}''$ representation of A_4 and the Z_3 charges are chosen such that $[A\Delta B]_{Z_3} = 1$. The structure imposed by the discrete symmetries is then given by the linear combination $\kappa' k_e + \kappa k_\mu$, which is further amended by powers of ϵ stemming from the FN symmetry and hence depends on the quark field involved in the interaction. For instance, in the case of $A = U$ or $A = \bar{U}$ the full patterns read

$$R_{e\mu}(UE) = \begin{pmatrix} \kappa'\epsilon^8 & \kappa\epsilon^6 & 0 \\ \kappa'\epsilon^6 & \kappa\epsilon^4 & 0 \\ \kappa'\epsilon^4 & \kappa\epsilon^2 & 0 \end{pmatrix}, \quad R_{e\mu}(\bar{U}E) = \begin{pmatrix} \kappa'\epsilon^0 & \kappa\epsilon^2 & 0 \\ \kappa'\epsilon^2 & \kappa\epsilon^0 & 0 \\ \kappa'\epsilon^4 & \kappa\epsilon^2 & 0 \end{pmatrix}. \tag{6.2}$$

Note that the interference of the FN charges of the quarks and leptons permits cancellations so that couplings to the lighter quark generations can be enhanced over those to heavier generations.

Just like their leptonic counterparts, the quark doublets and singlets must carry equal Z_3 charges to make sure the SM Yukawa interactions remain invariant. Consequently, for the

	k_e	k_μ	k_τ	$[\Delta]_{A_4}$	$[A\Delta B]_{Z_3}$	name
	c_ℓ	0	0	$\mathbf{1}$		L_e
	0	c_ℓ	0	$\mathbf{1}''$	0	L_μ
Y_{AL}	0	0	c_ℓ	$\mathbf{1}'$		L_τ
	c_ν	c_ν	c_ν	$\mathbf{1}^{(\text{any})}$	1	L_d
	$c_\nu\kappa$	$c_\nu\kappa$	$c_\nu\kappa$	$\mathbf{1}^{(\text{any})}$	2	$L_{d'}$
	1	0	0	$\mathbf{1}$		R_e
	0	1	0	$\mathbf{1}''$	0	R_μ
	0	0	1	$\mathbf{1}'$		R_τ
Y_{AE}	κ	0	κ'	$\mathbf{1}$		$R_{e\tau}$
	κ'	κ	0	$\mathbf{1}''$	1	$R_{e\mu}$
	0	κ'	κ	$\mathbf{1}'$		$R_{\mu\tau}$
	κ^2	κ'^2	$\kappa\kappa'$	$\mathbf{1}^{(\text{any})}$	2	R_d

Table 6.1.: Patterns for the lepton-quark coupling matrices of interactions involving lepton doublets (upper part) and lepton singlets (lower part) generated by the $A_4 \times Z_3$ symmetry.

leptoquarks S_1, S_2, V_1 and V_2, for which couplings to lepton doublets and singlets are simultaneously present, the respective patterns are related through

$$\begin{aligned} [QL\Delta]_{Z_3} &= [UE\Delta]_{Z_3}\,, \qquad [\bar{U}L\Delta]_{Z_3} = [\bar{Q}E\Delta]_{Z_3}\,, \\ [\bar{Q}L\Delta]_{Z_3} &= [\bar{D}E\Delta]_{Z_3}\,, \qquad [DL\Delta]_{Z_3} = [QE\Delta]_{Z_3}\,. \end{aligned} \tag{6.3}$$

If the Z_3 charges are chosen such that $A\Delta B$ is Z_3-invariant the patterns L_ℓ and R_ℓ are induced for the couplings to lepton doublets and singlets, respectively, where the joint lepton flavor ℓ is determined by the A_4 representation of the leptoquark. In this case there is a hierarchy between the couplings to lepton doublets, which are suppressed by c_ℓ, and the couplings to lepton singlets The latter require no flavon insertion so that they remain of order one. For $[A\Delta B]_{Z_3} = 1$ the coupling to lepton doublets follows the democratic pattern L_d, while the lepton singlet coupling adheres to one of the $R_{\ell\ell'}$ patterns that isolates two lepton families depending on the choice of $[\Delta]_{A_4}$. Unless there is a large hierarchy $c_\nu \ll \kappa, \kappa'$ suppressing the democratic pattern, the phenomenology is dominated by strong bounds from cLFV decays. In the remaining case, where $[A\Delta B]_{Z_3} = 2$, the subleading democratic patterns with two flavon insertions are induced for both couplings.

The vev suppression of the lepton doublet couplings is not exclusive to the $A_4 \times Z_3$ model studied here, but appears generically in flavor models in which the lepton doublet

transforms under a triplet representation of the non-abelian group in order to generate the observed mixing in the lepton sector. As a possibility to circumvent this suppression due to the insertion of a triplet flavon one could let the leptoquark transform as a triplet. However, this leads again to democratic patterns that are not phenomenologically viable.

6.1.2. Corrections to the Flavor Patterns

Since the patterns derived above apply to the leptoquark couplings in the flavor basis, we need to consider the modifications that arise from rotations to the mass basis. As discussed in Section 2.3, these rotations correspond to the unitary transformations (2.14) of the fermion fields. Consequently, the leptoquark couplings transform as

$$Y_{AB} \to U_A^T Y_{AB} U_B \,, \quad Y_{\bar{A}B} \to U_A^\dagger Y_{\bar{A}B} U_B \,, \tag{6.4}$$

so that combinations of unitary matrices other than the CKM and PMNS matrices defined in (2.15) and (2.23), respectively, can become physical. Note that the rotations of the quark sector only mix the rows of the leptoquark couplings, while the lepton flavor rotations only affect the columns. The FN symmetry dictates the parametric dependence of the quark rotation matrices to be

$$\begin{aligned} (U_{u_\mathrm{L}})_{ij} \sim (U_{d_\mathrm{L}})_{ij} &\sim \epsilon^{|q(Q_i)-q(Q_j)|} \,, \\ (U_{u_\mathrm{R}})_{ij} &\sim \epsilon^{|q(U_i)-q(U_j)|} \,, \\ (U_{d_\mathrm{R}})_{ij} &\sim \epsilon^{|q(D_i)-q(D_j)|} \,. \end{aligned} \tag{6.5}$$

As a result, the mixing of the rows parametrically preserves the hierarchical suppression by powers of ϵ unless the quarks transform non-trivially under A_4 – an option that leads to more complicated patterns to be discussed in Section 6.1.3.

Observables that can be accessed in collider experiments are insensitive to neutrino flavors, so that the neutrino rotation matrix U_{ν_L} has no phenomenological significance. Beyond that, no mixing among charged leptons arises at leading order in the AF $\times$ FN model. If we consider higher order flavon insertions the charged lepton Yukawa matrix receives corrections of the order of the product of two vevs, which we parametrize as

$$\delta \sim \max\left(\frac{c_\nu^3}{c_\ell}, \frac{c_\nu \kappa^2}{c_\ell}, \frac{c_\nu \kappa \kappa'}{c_\ell}, \frac{c_\nu \kappa'^2}{c_\ell}\right) . \tag{6.6}$$

At this order we find

$$Y_\ell \sim c_\ell \left[\begin{pmatrix} \epsilon^4 & 0 & 0 \\ 0 & \epsilon^2 & 0 \\ 0 & 0 & 1 \end{pmatrix} + \delta \begin{pmatrix} \epsilon^4 & \epsilon^2 & 1 \\ \epsilon^4 & \epsilon^2 & 1 \\ \epsilon^4 & \epsilon^2 & 1 \end{pmatrix} \right] \sim c_\ell \begin{pmatrix} \epsilon^4 & \delta\epsilon^2 & \delta \\ \delta\epsilon^4 & \epsilon^2 & \delta \\ \delta\epsilon^4 & \delta\epsilon^2 & 1 \end{pmatrix} , \tag{6.7}$$

which, using perturbative diagonalization [177], yields the rotation matrices

$$U_L \sim \begin{pmatrix} 1 & \delta & \delta \\ \delta & 1 & \delta \\ \delta & \delta & 1 \end{pmatrix}, \quad U_E \sim \begin{pmatrix} 1 & \delta\epsilon^2 & \delta\epsilon^4 \\ \delta\epsilon^2 & 1 & \delta\epsilon^2 \\ \delta\epsilon^4 & \delta\epsilon^2 & 1 \end{pmatrix}. \tag{6.8}$$

For the lepton flavor isolation patterns L_ℓ this means that entries which are forbidden at leading order receive corrections of order δ relative to their suppression due to the vev of the triplet flavon ϕ_ℓ. Because the lepton flavor rotations only mix the columns of the leptoquark couplings and in the case of lepton doublets do not contain any powers of ϵ, the FN hierarchy from the isolated column is preserved. As an explicit example, consider the L_τ patterns, for which these corrections amount to

$$L_\tau(UL, \bar{U}L, QL, \bar{Q}L) \to c_\ell \begin{pmatrix} \delta\epsilon^4 & \delta\epsilon^4 & \epsilon^4 \\ \delta\epsilon^2 & \delta\epsilon^2 & \epsilon^2 \\ \delta\epsilon^0 & \delta\epsilon^0 & \epsilon^0 \end{pmatrix}, \quad L_\tau(DL, \bar{D}L) \to c_\ell \begin{pmatrix} \delta\epsilon^3 & \delta\epsilon^3 & \epsilon^3 \\ \delta\epsilon^2 & \delta\epsilon^2 & \epsilon^2 \\ \delta\epsilon^2 & \delta\epsilon^2 & \epsilon^2 \end{pmatrix}. \tag{6.9}$$

In the case of couplings to lepton singlets, the corrections stemming from the change to the mass basis are smaller due to the fact that the respective rotation matrix contains FN factors in addition to the parameter δ. Considering the τ isolation pattern as an example again, we find

$$R_\tau(UE, \bar{U}E, QE, \bar{Q}E) \to \begin{pmatrix} \delta\epsilon^8 & \delta\epsilon^6 & \epsilon^4 \\ \delta\epsilon^6 & \delta\epsilon^4 & \epsilon^2 \\ \delta\epsilon^4 & \delta\epsilon^2 & \epsilon^0 \end{pmatrix}, \quad R_\tau(DE, \bar{D}E) \to \begin{pmatrix} \delta\epsilon^7 & \delta\epsilon^5 & \epsilon^3 \\ \delta\epsilon^6 & \delta\epsilon^4 & \epsilon^2 \\ \delta\epsilon^6 & \delta\epsilon^4 & \epsilon^2 \end{pmatrix}. \tag{6.10}$$

Likewise, one can determine the corrections to the patterns that isolate two lepton generations. For the $R_{e\mu}$ pattern, which served as an example in the previous section, we obtain

$$R_{e\mu}(\bar{U}E) \to \begin{pmatrix} \kappa'\epsilon^0 & \kappa\epsilon^2 & \delta\epsilon^4(\kappa+\kappa') \\ \kappa'\epsilon^2 & \kappa\epsilon^0 & \delta\epsilon^2\kappa \\ \kappa'\epsilon^4 & \kappa\epsilon^2 & \delta\epsilon^4\kappa \end{pmatrix}. \tag{6.11}$$

Additional contributions to all entries of the flavor patterns arise directly from higher order flavon insertions. For L_ℓ – the flavor isolation patterns involving lepton doublets – the dominant corrections arise from replacing ϕ_ℓ with ϕ_ν and adding two insertions of either the A_4-triplet flavon ϕ_ν or the singlet flavons $\xi^{(\prime)}$ to compensate for the Z_3 charge. Hence, relative to the FN factors these corrections are of the orders c_ν^3/c_ℓ and $c_\nu\kappa^{(\prime)2}/c_\ell$, respectively, corresponding to the same order, δ, at which the lepton flavor rotations discussed before contribute.

The direct higher order contributions to the couplings involving lepton singlets require at least three flavon insertions, as, in contrast to the previous case, there is no flavon contribution at leading order that could be replaced by another one. Nevertheless, these corrections can in fact be larger than those originating from the flavor rotations, since the emerging FN factors do not result from the mixing matrix but are a direct consequence of the FN charges of the quarks and lepton singlets, which allows for cancellations. With $\delta' \sim \text{vev}^3$, we find

$$R_\tau(UE, \bar{Q}E) \to \begin{pmatrix} \delta'\epsilon^8 & \delta'\epsilon^6 & \epsilon^4 \\ \delta'\epsilon^6 & \delta'\epsilon^4 & \epsilon^2 \\ \delta'\epsilon^4 & \delta'\epsilon^2 & \epsilon^0 \end{pmatrix}, \quad R_\tau(\bar{U}E, QE) \to \begin{pmatrix} \delta'\epsilon^0 & \delta'\epsilon^2 & \epsilon^4 \\ \delta'\epsilon^2 & \delta'\epsilon^0 & \epsilon^2 \\ \delta'\epsilon^4 & \delta'\epsilon^2 & \epsilon^0 \end{pmatrix},$$
$$R_\tau(\bar{D}E) \to \begin{pmatrix} \delta'\epsilon & \delta'\epsilon & \epsilon^3 \\ \delta'\epsilon^2 & \delta'\epsilon^0 & \epsilon^2 \\ \delta'\epsilon^2 & \delta'\epsilon^0 & \epsilon^2 \end{pmatrix}. \tag{6.12}$$

For the patterns that isolate two lepton generation Z_3 invariance requires four flavon insertions, so that the direct higher order corrections read

$$R_{e\mu}(\bar{U}E, \bar{Q}E) \to \begin{pmatrix} \kappa'\epsilon^0 & \kappa\epsilon^2 & \delta''\epsilon^4 \\ \kappa'\epsilon^2 & \kappa\epsilon^0 & \delta''\epsilon^2 \\ \kappa'\epsilon^4 & \kappa\epsilon^2 & \delta''\epsilon^0 \end{pmatrix}, \tag{6.13}$$

where $\delta'' \sim \text{vev}^4$.

6.1.3. Quarks in Non-Trivial A_4 Representations

Assigning individual quark generations to a non-trivial singlet representation of A_4 allows for the construction of more complex patterns that lead to a richer phenomenology. For the sake of simplicity we only consider the case where one quark generation A_i transforms non-trivially. In order to preserve both $A_4 \times Z_3$ invariance and the structure of the SM Yukawa matrices the Z_3 and FN charges of the selected quark generation need to be adjusted as well. Invariance under A_4 then requires the insertion of one or two additional ξ' flavons if the selected quark generation transforms as $\mathbf{1''}$ or $\mathbf{1'}$, respectively. Since these flavons carry a non-zero Z_3 charge, the Z_3 charge of the quark generation must be adjusted accordingly. Furthermore, the additional vev suppression due to ξ' has to be compensated by reducing the FN charge of the affected quark generation. Assuming the vevs to be related as $\kappa' \sim \epsilon^n$ with an integer n, the two possible options can be summarized as

$$[A_i]_{A_4} \to \mathbf{1''}, \quad [A_i]_{Z_3} \to 1, \quad q(A_i) \to q(A_i) - n\,, \tag{6.14}$$

with one insertion, or

$$[A_i]_{A_4} \to \mathbf{1'}, \quad [A_i]_{Z_3} \to 2, \quad q(A_i) \to q(A_i) - 2n\,, \tag{6.15}$$

with two insertions, where $A \in \{\bar{Q}, U, D\}$ denotes a quark field of either the first or second generation, $i \in \{1, 2\}$.

This charge reassignment essentially causes a shift in the selection of the flavor pattern according to the rules of Table 6.1 which only affects the row corresponding to the quark generation A_i. If the original flavor pattern is given by the overall Z_3 charge $a \equiv [A\Delta B]_{Z_3}$ of the vertex and the A_4 representation $[\Delta]_{A_4}$ of the leptoquark, then the ith row, corresponding to the modified quark generation A_i, adheres to the pattern defined by

$$[A\Delta B]_{Z_3} = \begin{cases} (a+1) \bmod 3 & \text{for one insertion} \\ (a+2) \bmod 3 & \text{for two insertions} \end{cases}, \tag{6.16}$$

and the product of the representations of the quark and the leptoquark, i.e. $[A\Delta]_{A_4}$. Due to the modification of the FN charges the quark flavor rotations can have an impact on the patterns and need to be included explicitly.

As an example consider again the isolation patterns L_τ obtained for $[\Delta]_{A_4} = \mathbf{1}'$ and $[A\Delta B]_{Z_3} = 0$. If the second quark generation is put in the $\mathbf{1}''$ representation of A_4, the Z_3 charge of the vertex for this generation is shifted by one unit, according to (6.16), so that the second row follows the L_d pattern instead. Explicitly, for couplings involving the antiquark doublet, as it is the case for the leptoquarks V_1 and V_3, the modified pattern reads

$$\tilde{L}_\tau(\bar{Q}L) = \begin{pmatrix} 0 & 0 & c_\ell \epsilon^4 \\ c_\nu & c_\nu & c_\nu \\ 0 & 0 & c_\ell \end{pmatrix}, \tag{6.17}$$

where we assume $\kappa' \sim \epsilon^2$. The corrections resulting from the rotation to the mass basis amount to

$$\tilde{L}_\tau(\bar{Q}L) \to \begin{pmatrix} \epsilon^2 c_\nu & \epsilon^2 c_\nu & \epsilon^2 c_\nu \\ c_\nu & c_\nu & c_\nu \\ \epsilon^2 c_\nu + \delta c_\ell & \epsilon^2 c_\nu + \delta c_\ell & c_\ell \end{pmatrix}. \tag{6.18}$$

Note that the FN suppression of the first row is only of the order ϵ^2. Within our framework, this is an example of a pattern that yields the largest contributions to R_D and R_{D^*} with quark and lepton doublets involved.

Assigning the second generation up-type antiquark singlets to a non-trivial A_4 representation allows to create a similar pattern for the chirality-flipping coupling $Y_{\bar{U}L}$ that occurs in the S_2 leptoquark model. Including corrections due to the rotation to the mass basis, we find

$$\tilde{L}_\tau(\bar{U}L) \to \begin{pmatrix} \epsilon^2 \kappa c_\nu & \epsilon^2 \kappa c_\nu & \epsilon^2 \kappa c_\nu \\ \kappa c_\nu & \kappa c_\nu & \kappa c_\nu \\ \epsilon^2 \kappa c_\nu + \delta c_\ell & \epsilon^2 \kappa c_\nu + \delta c_\ell & c_\ell \end{pmatrix}. \tag{6.19}$$

Note that the charge reassignments (6.14) and (6.15) are reversed for the antiquark singlets so that the modified row follows the $L_{d'}$ pattern, which is subject to an additional vev suppression by κ.

In the case of $b \to s\mu^+\mu^-$ transitions, the muon isolation patterns $L_\mu(\bar{Q}L, QL)$ for couplings to the quark and lepton doublets are most relevant. Applying the same charge modifications to the second quark generation as before leads to the patterns

$$\tilde{L}_\mu(\bar{Q}L) = \begin{pmatrix} 0 & c_\ell\epsilon^4 & 0 \\ c_\nu & c_\nu & c_\nu \\ 0 & c_\ell\epsilon^0 & 0 \end{pmatrix}, \quad \tilde{L}_\mu(QL) = \begin{pmatrix} 0 & c_\ell\epsilon^4 & 0 \\ c_\nu\kappa & c_\nu\kappa & c_\nu\kappa \\ 0 & c_\ell\epsilon^0 & 0 \end{pmatrix}, \tag{6.20}$$

where two flavon insertions are necessary for the second pattern. Here, the flavor rotations yield the modifications

$$\begin{aligned} \tilde{L}_\mu(\bar{Q}L) &\to \begin{pmatrix} c_\nu\epsilon^2 & c_\nu\epsilon^2 & c_\nu\epsilon^2 \\ c_\nu & c_\ell\epsilon^2 + c_\nu & c_\nu \\ c_\ell\delta + c_\nu\epsilon^2 & c_\ell & c_\ell\delta + c_\nu\epsilon^2 \end{pmatrix}, \\ \tilde{L}_\mu(QL) &\to \begin{pmatrix} c_\nu\kappa\epsilon^2 & c_\ell\epsilon^4 + c_\nu\kappa\epsilon^2 & c_\nu\kappa\epsilon^2 \\ c_\nu\kappa & c_\ell\epsilon^2 + c_\nu\kappa & c_\nu\kappa \\ c_\ell\delta + c_\nu\kappa\epsilon^2 & c_\ell & c_\ell\delta + c_\nu\kappa\epsilon^2 \end{pmatrix}. \end{aligned} \tag{6.21}$$

6.2. Phenomenology

In order to reveal the full predictive power that is achieved by employing flavor symmetries to restrict the freedom of NP model, we will now explore the flavor phenomenology of several leptoquark scenarios using the coupling patterns derived in the previous section. We focus on the leptoquark scenarios that can potentially provide explanations for the B anomalies. Using data on kaon and charm decays as well as cLFV processes we constrain the vevs of the A_4-breaking flavons, thus following a data-driven approach that is grounded on a concrete theoretical foundation.

6.2.1. Impact of Flavorful Leptoquarks on $b \to c\ell\bar{\nu}$ Transitions

We begin by investigating leptoquark effects in the $b \to c\ell\bar{\nu}$ sector, where our main focus lies on different attempts to explain the anomalies in R_D and R_D^*. For each scenario we also work out predictions for the polarization fractions $P_\tau(D)$ and $P_\tau(D^*)$, for which more precise data is expected to be available in the future.

SM-like contributions The most favored explanation of the deviations in R_D and R_{D^*} is given by a flavor non-universal NP contribution to the SM-like operator $\mathcal{O}_{\mathrm{V}_1}$, which involves the quark and lepton doublets and hence offers a possible connection to the anomalies in $b \to s\ell^+\ell^-$. According to Table D.1, contributions to this operator can arise for the leptoquarks S_3, V_3, S_1 and V_1. For the leptoquarks S_3 and V_3 this is the only induced operator. In the case of V_1 the scalar operator $\mathcal{O}_{S_1}$ receives contributions as well, while the S_1 leptoquark additionally induces scalar and tensor operators, whose effects we discuss separately.

Generalizing the linearized expression (3.23) for $R_{D^{(*)}}$ from Section 3.3.2 to include light lepton flavors and expressing the Wilson coefficients in terms of leptoquark couplings according to Table D.1 yields

$$\begin{aligned}\hat{R}_{D^*} - 1 = \hat{R}_D - 1 &\simeq 2\,\mathrm{Re}\left(C^{\tau}_{\mathrm{V}_1} - C^{\ell}_{\mathrm{V}_1}\right) = 2\,n(\Delta)\,\mathrm{Re}\left(YY^*|_\tau - YY^*|_\ell\right)\frac{\sqrt{2}}{4G_{\mathrm{F}}V_{cb}M^2} \\ &\simeq 1.5\,n(\Delta)\,\mathrm{Re}\left(YY^*|_\tau - YY^*|_\ell\right)\left(\frac{\mathrm{TeV}}{M}\right)^2 ,\end{aligned} \tag{6.22}$$

where the Fierz factors for the different possible leptoquarks are given by

$$n(\Delta) = \begin{cases} -\frac{1}{2}, & \Delta = S_3 \\ +1, & \Delta = V_1 \\ -1, & \Delta = V_3 \end{cases} . \tag{6.23}$$

For the leptoquark V_1 the additional contributions to $\hat{R}_{D^*}$ stemming from $\mathcal{O}_{\mathrm{S}_1}$ are of the order of ten percent, but can be of order one for $\hat{R}_D$. Thus, we first discuss NP contributions to the SM-like operator $\mathcal{O}_{\mathrm{V}_1}$ alone and consider additional effects from chirality-flipping operators later on.

Following (6.22), the data on $R_{D^{(*)}}$ implies

$$\mathrm{Re}\left(YY^*|_\tau - YY^*|_\ell\right) \simeq \frac{0.20 \pm 0.05}{n(\Delta)}\left(\frac{M}{\mathrm{TeV}}\right)^2 . \tag{6.24}$$

for the leptoquark couplings. For these to remain perturbative it is necessary that $M \lesssim 3\,\mathrm{TeV}$. At the same time, collider searches impose lower bounds on leptoquark masses. In the context of $b \to c\ell\bar{\nu}$ transitions a relevant limit is $M > 685\,\mathrm{GeV}$ for scalar leptoquarks decaying to $t\tau$ final states [178]. For a viable explanation of $R_{D^{(*)}}$, this means that the leptoquark couplings cannot be too small, i.e. $\mathrm{Re}\left(YY^*|_\tau - YY^*|_\ell\right) > 0.07$ in this scenario. Similar limits can be obtained for the vector leptoquark V_1 where the final state includes a neutrino instead of a charged lepton [179]. Collider bounds on the masses of leptoquarks that predominantly couple to light leptons are generally stronger. In the case of scalar leptoquarks decaying exclusively into a muon (an electron) and a jet, current mass limits impose $M > 1160\,\mathrm{GeV}$ [180] ($M > 1755\,\mathrm{GeV}$ [181]), which yields $\mathrm{Re}\left(YY^*|_\tau - YY^*|_\ell\right) > 0.2$ (0.5) for the leptoquark couplings. Furthermore, current data

excludes vector leptoquarks with masses below 1200 GeV to 1720 GeV and 1150 GeV to 1660 GeV [182], assuming they decay entirely into a muon and a jet, or an electron and a jet, respectively.

Within the large class of flavor models in which the lepton doublets transform as a triplet under the flavor symmetry group, the maximal size predicted for the leptoquark couplings is

$$YY^*|_\tau - YY^*|_\ell \sim \text{vev}^2 \,. \tag{6.25}$$

In the $A_4 \times Z_3 \times U(1)_{\text{FN}}$ model considered here this can be achieved with the modified tau isolation pattern $\tilde{L}_\tau(\bar{Q}L)$ shown in (6.17), which evades the suppression due to the FN mechanism at the cost of the second quark generation transforming non-trivially under the flavor symmetry group. The suppression of the leptoquark couplings is then given by the product $c_\nu c_\ell$ of the vevs of the two triplet flavons. Here, the direct bound from $B \to K\nu\bar{\nu}$ applies for V_3 and implies $c_\nu c_\ell \lesssim 0.02(M/\text{TeV})$ (see Section 3.5.1). With less elaborate representation assignments the FN suppression of the quarks cannot be avoided, leading to even smaller couplings. This is the case for the unmodified tau isolation pattern $L_\tau(\bar{Q}L)$ from (6.9), which leads to

$$YY^*|_\tau - YY^*|_\ell \sim c_\ell^2 \epsilon^2 \lesssim 10^{-3} \,. \tag{6.26}$$

Thus, an explanation of the deviations in R_D and R_{D^*} is not viable in leptoquark scenarios that involve NP contributions to the SM-like operator $\mathcal{O}_{\text{V}_1}$ only, and where the couplings are governed by a flavor structure that falls into the same class as the AF $\times$ FN model studied here. Specifically, this excludes the leptoquarks S_3 and V_3 as explanations of the data within this scenario. Nevertheless, their impact on $\hat{R}_D$ and $\hat{R}_{D^*}$ is equally large and can reach the level of a few percent for the "maximal" flavor scenario (6.25), but only a few permille in the generic case (6.26). The polarization fractions $P_\tau(D^{(*)})$ remain unchanged for all NP scenarios that affect only $\mathcal{O}_{\text{V}_1}$.

Chirality-flipping contributions As a second option, we consider a scenario dominated by NP contributions to the scalar and tensor operators $\mathcal{O}_{\text{S}_2}$ and $\mathcal{O}_{\text{T}}$, respectively. These are only induced by the scalar leptoquarks S_1 and S_2. Due to the involved Fierz transformation of the lepton-quark currents the resulting Wilson coefficients are related as

$$C_{\text{S}_2} = \mp r C_{\text{T}} \,, \tag{6.27}$$

where $r = 4$ at the matching scale, which we assume to be close to the leptoquark mass. Throughout this section, the upper (lower) sign corresponds to S_1 (S_2). Since the scalar and tensor operators carry non-vanishing and distinct anomalous dimensions, as discussed in Section 3.3.1, this Fierz relation is modified by the RG evolution down to the hadronic

scale. Using the `CRunDec` package [183] we find

$$r = \begin{cases} 7.8, & M = 1\,\text{TeV} \\ 8.2, & M = 2\,\text{TeV} \\ 8.4, & M = 3\,\text{TeV} \end{cases} \tag{6.28}$$

at the b quark mass scale for leptoquark masses M in the TeV range. Following (3.17) and (3.18) linearized expressions for $\hat{R}_{D^{(*)}}$ in this scenario read

$$\begin{aligned} \hat{R}_D - 1 &\simeq \text{Re}\left(C^\tau_{\text{S}_2}\right)\left(\hat{A}^\tau_{\text{VS}} \mp \hat{A}^\tau_{\text{VT}}/r\right) - (\tau \to \ell) \\ &= \text{Re}\left(C^\tau_{\text{S}_2}\right)(1.73 \mp 0.09) - (\tau \to \ell) \\ &\simeq (-0.65 \pm 0.03)\,\text{Re}\left(YY^*|_\tau\right)\left(\frac{\text{TeV}}{M}\right)^2, \end{aligned} \tag{6.29}$$

and

$$\begin{aligned} \hat{R}_{D^*} - 1 &\simeq -\,\text{Re}\left(C^\tau_{\text{S}_2}\right)\left(\hat{B}^\tau_{\text{VS}} \pm \hat{B}^\tau_{\text{VT}}/r\right) - (\tau \to \ell) \\ &= \text{Re}\left(C^\tau_{\text{S}_2}\right)(-0.12 \pm 0.59) - (\tau \to \ell) \\ &\simeq (\mp 0.22 + 0.045)\,\text{Re}\left(YY^*|_\tau\right)\left(\frac{\text{TeV}}{M}\right)^2. \end{aligned} \tag{6.30}$$

The light lepton contributions can be neglected with respect to those involving the tau lepton due to the mass suppression present in chirality-flipping operators. It can be generally seen that $\hat{R}_D \neq \hat{R}_{D^*}$ and in particular for the S_2 leptoquark these observables acquire shifts in different directions.

In order to obtain a complete picture, we must go beyond the linear approximation and perform a fit based on the complete expressions from Section 3.3.1, allow for complex Wilson coefficients. Figure 6.1 shows the one sigma constraints imposed by $R_{D^{(*)}}$ on the real and imaginary parts of the Wilson coefficient $C^\tau_{\text{S}_2}$ and the respective combinations of leptoquark couplings. For S_1, contributions to the SM-like operator $\mathcal{O}_{\text{V}_1}$ are present as well. They are, however, strongly constrained by experimental data (3.50) on the branching ratio $B \to K\nu\bar{\nu}$. For the fit we employ the largest possible contribution to $\mathcal{O}_{\text{V}_1}$ that satisfies the conservative upper bound on $|C^{\nu_\tau\nu_\tau}_{\text{L}}|$ from (3.52) derived in Section 3.5.1. Applying this model-independent constraint to leptoquarks, we find

$$\left|Y^{b\nu_\tau}_{QL}\left(Y^{c\tau}_{QL}\right)^*\right| \lesssim 0.05\left(\frac{M}{\text{TeV}}\right)^2 \quad (\text{for } S_1)\,. \tag{6.31}$$

The resulting best fit points subsequently read

$$Y^{b\nu_\tau}_{QL}\,(Y^{c\tau}_{UE})^* = -0.4\left(\frac{M}{\text{TeV}}\right)^2 \quad (\text{for } S_1)\,, \tag{6.32}$$

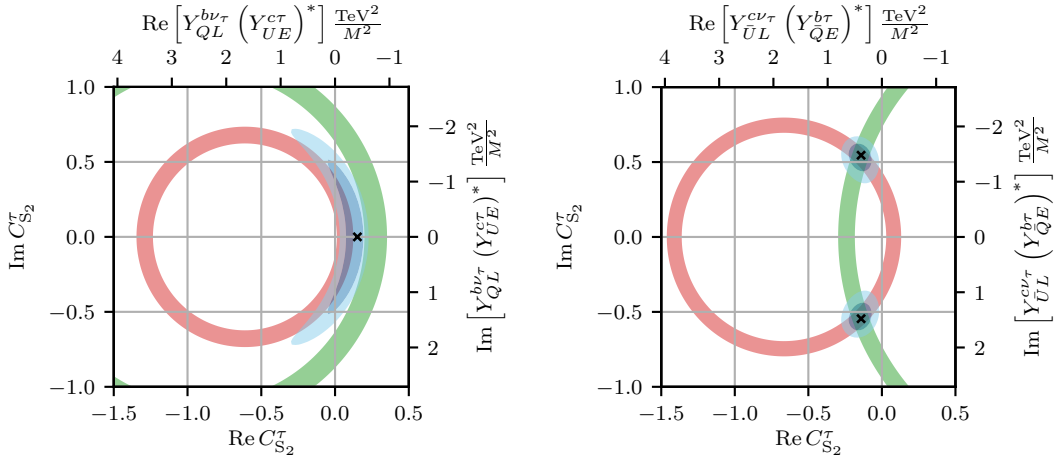

Figure 6.1.: Fits to the experimental data on $R_{D^{(*)}}$ for the leptoquark scenarios S_1 (left) and S_2 (right) in the complex plane of the Wilson coefficient $C_{S_2}^\tau$ and the leptoquark couplings $YY^*|_\tau$. For the S_1 leptoquark we allow Y_{QL} to saturate the limit (6.31). The red and green bands indicate the one sigma constraints from R_D and R_{D^*}, respectively. In the SM $C_{S_2}^\tau$ vanishes. The one and two sigma confidence intervals of the fit are shown in dark and light blue, respectively, and the best fit points are indicated by black crosses. This is an updated version of Figure 1 from [1] with the most recent data on $R_{D^{(*)}}$ from Table 3.1.

and

$$Y_{\bar{U}L}^{c\nu_\tau}\left(Y_{\bar{Q}E}^{b\tau}\right)^* = (0.4 \pm 1.4i)\left(\frac{M}{\text{TeV}}\right)^2 \quad (\text{for } S_2)\,. \tag{6.33}$$

Due to the $B \to K\nu\bar{\nu}$ bound the couplings must respect the hierarchy

$$\frac{Y_{QL}^{s\nu_\tau}}{Y_{UE}^{c\tau}} \simeq 0.13\,. \tag{6.34}$$

This is compatible with flavor model predictions thanks to the generic vev suppression of the couplings to lepton doublets, which is not present for interactions involving lepton singlets. In the particular case where the couplings adhere to the tau isolation patterns $L_\tau(QL)$ and $R_\tau(UE)$ this ratio is of the order c_ℓ. Generally, this means that the largest possible contributions to chirality-flipping operators are suppressed by a single vev as

$$YY^*|_\tau \sim \text{vev}\,. \tag{6.35}$$

This maximal case is realized for the scalar operator induced by the leptoquark V_1 with the patterns $L_\tau(\bar{Q}L)$ from (6.9) and $R_\tau(\bar{D}E)$, given by the maximum of (6.10) and (6.12), if we allow for quark FN-charges as in multi Higgs doublet models such that $R_\tau(\bar{D}E)_{33} \sim \epsilon^0$. We will come back to this particular model in the next section.

The largest effects within a scenario involving only chirality-flipping contributions are found for the S_2 leptoquark model where the couplings obey the patterns $\tilde{L}_\tau(\bar{U}L)$ from (6.19) and $R_\tau(\bar{Q}E)$, which is again given by the maximum of (6.10) and (6.12). Due to the additional vev suppression in $\tilde{L}_\tau(\bar{U}L)$ compared to $\tilde{L}_\tau(\bar{Q}L)$ the resulting contribution amounts to

$$YY^*|_\tau \sim \kappa c_\nu \,. \tag{6.36}$$

Constraints from μ-e conversion data impose $\kappa c_\nu \lesssim 0.02(M/\text{TeV})$ [122]. Bounds from the branching ratios of the rare charm decays $D \to \mu^+\mu^-$ and $D \to \pi\mu^+\mu^-$ are much weaker and read $\kappa^2 c_\nu^2 \epsilon^2 \lesssim 0.06(M/\text{TeV})$ [122].

In the generic case the FN suppression of the second quark generation leads to smaller chirality-flipping leptoquark contributions of the order

$$YY^*|_\tau \sim c_\ell \epsilon^2 \lesssim 10^{-2} \,, \tag{6.37}$$

which is realized with the patterns L_τ from (6.9) and R_τ from before.

Contributions to the chirality-flipping operator $\mathcal{O}_{S_1}$ are suppressed even stronger than in the generic case because V_2, the sole leptoquark that induces this operator, only couples to down-type quark singlets, which typically carry larger FN charges than their up-type counterparts. For the AF $\times$ FN model we find

$$YY^*|_\tau \sim c_\ell \epsilon^4 \,. \tag{6.38}$$

To summarize, effects in $\hat{R}_{D^{(*)}}$ stemming from chirality-flipping operators are largest in the S_2 leptoquark scenario, where they can reach up to a few percent in $\hat{R}_D$ and about ten percent in $\hat{R}_{D^*}$. However, in this case an enhancement of $\hat{R}_D$ implies a suppression of R_{D^*} and vice versa, so that the tension between the experimental data and the theory prediction cannot be relieved in both observables simultaneously.

For the τ-polarizations we find

$$\begin{aligned} \hat{P}_\tau(D) - 1 &\simeq \text{Re}(C_{S_2}^\tau) \left[(\hat{A}_{VS}^+ - \hat{A}_{VS}^- - \hat{A}_{VS}^\tau) \mp (\hat{A}_{VT}^+ - \hat{A}_{VT}^- - \hat{A}_{VT}^\tau)/r \right] \\ &\simeq \text{Re}(C_{S_2}^\tau)(3.50 \pm 0.18) \\ &\simeq (1.30 \pm 0.07)\, \text{Re}\,(YY^*|_\tau) \left(\frac{\text{TeV}}{M} \right)^2 , \end{aligned} \tag{6.39}$$

and

$$\begin{aligned} \hat{P}_\tau(D^*) - 1 &\simeq -\text{Re}(C_{S_2}^\tau) \left[(\hat{B}_{VS}^+ - \hat{B}_{VS}^- - \hat{B}_{VS}^\tau) \pm (\hat{B}_{V_1T}^+ - \hat{B}_{V_1T}^- - \hat{B}_{V_1T}^\tau)/r \right] \\ &\simeq -\text{Re}(C_{S_2}^\tau)(-0.36 \pm 0.19) \\ &\simeq (0.13 \mp 0.07)\, \text{Re}\,(YY^*|_\tau) \left(\frac{\text{TeV}}{M} \right)^2 , \end{aligned} \tag{6.40}$$

where again the upper and lower signs correspond to the S_1 and S_2 leptoquarks, respectively.

V_1 leptoquark As a final scenario we consider the leptoquark V_1, which contributes to the SM-like operator $\mathcal{O}_{\mathrm{V}_1}$ without being directly constrained by $B \to K\nu\bar{\nu}$, and also to the chirality-flipping operator $\mathcal{O}_{\mathrm{S}_1}$. For $\hat{R}_D$ and $\hat{R}_{D^*}$ we find

$$\begin{aligned}\hat{R}_D - 1 &\simeq 2\,\mathrm{Re}(C^\tau_{\mathrm{V}_1}) + \mathrm{Re}(C^\tau_{\mathrm{S}_1})\hat{A}^\tau_{\mathrm{VS}} - (\tau \to \ell) \\ &\simeq 1.5 c_\nu\,(c_\ell - 1.73)\left(\frac{\mathrm{TeV}}{M}\right)^2 \\ &\lesssim 0.03\left(\frac{\mathrm{TeV}}{M}\right),\end{aligned} \tag{6.41}$$

and

$$\begin{aligned}\hat{R}_{D^*} - 1 &\simeq 2\,\mathrm{Re}(C^\tau_{\mathrm{V}_1}) + \mathrm{Re}(C^\tau_{\mathrm{S}_1})\hat{B}^\tau_{\mathrm{VS}} - (\tau \to \ell) \\ &\simeq 1.5 c_\nu\,(c_\ell - 0.12)\left(\frac{\mathrm{TeV}}{M}\right)^2 \\ &\lesssim 0.02\,(c_\ell - 0.12)\left(\frac{\mathrm{TeV}}{M}\right).\end{aligned} \tag{6.42}$$

Here, the upper bounds stem from constraints on the vev c_ν. The strongest ones in this case arise from cLFV kaon decays $s \to de\mu$, which impose $c_\nu^2\epsilon^2 \lesssim 5 \times 10^{-6}(M/\mathrm{TeV})^2$ [127], or, $c_\nu \lesssim 0.01(M/\mathrm{TeV})$. Bounds from μ-e conversion are slightly weaker and read $\epsilon^4 c_\nu^2 \lesssim 7 \times 10^{-7}(M/\mathrm{TeV})$ [122], yielding, $c_\nu \lesssim 0.02(M/\mathrm{TeV})$. Although forbidden at tree-level, contributions to $B \to K\nu\bar{\nu}$ decays are still induced by RGE running between the matching scale $\mu \sim M$ and the electroweak scale [184]. Constraints due to this effect are, however, smaller than those from kaon decays and μ-e conversion.

The τ polarization is only affected by the chirality-flipping contribution. We obtain

$$\begin{aligned}\hat{P}_\tau(D) - 1 &\simeq \mathrm{Re}(C^\tau_{\mathrm{S}_1})(\hat{A}^+_{\mathrm{VS}} - \hat{A}^-_{\mathrm{VS}} - \hat{A}^\tau_{\mathrm{VS}}) \\ &\simeq 3.50\ \mathrm{Re}(C^\tau_{\mathrm{S}_1}) \lesssim 0.05\left(\frac{\mathrm{TeV}}{M}\right),\end{aligned} \tag{6.43}$$

and

$$\begin{aligned}\hat{P}_\tau(D^*) - 1 &\simeq \mathrm{Re}(C^\tau_{\mathrm{S}_1})(\hat{B}^+_{\mathrm{VS}} - \hat{B}^-_{\mathrm{VS}} - \hat{B}^\tau_{\mathrm{VS}}) \\ &\simeq -0.36\ \mathrm{Re}(C^\tau_{\mathrm{S}_1}) \lesssim 0.005\left(\frac{\mathrm{TeV}}{M}\right).\end{aligned} \tag{6.44}$$

Summary In Figure 6.2 we show the maximal predictions for $\hat{R}_{D^{(*)}} - 1$ that can be achieved with the leptoquarks V_1, V_3 and S_2 within flavor models. We omit the S_1 and S_3 scenarios, which yield only negligible contributions to the crucial flavor observables due to the strong suppression of their couplings, as given by (6.26). The colored regions of the plot correspond to the maximal effects emerging in the three different scenarios where we distinguish two cases: for the smaller, dark areas we assume that the a priori unknown

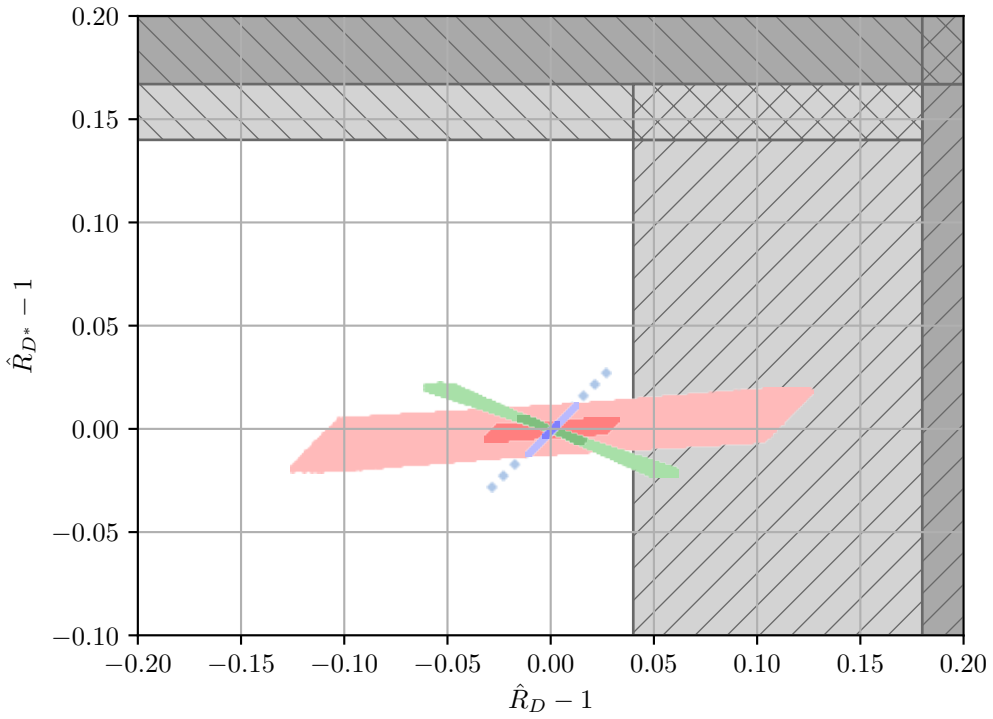

Figure 6.2.: Largest possible contributions to $\hat{R}_{D^{(*)}} - 1$ by the leptoquarks V_1 (red), V_3 (blue) and S_2 (green) with couplings dictated by flavor models. The dark and light areas correspond to variations of the unknown $\mathcal{O}(1)$ coefficients within the ranges of ± 1 and $\pm(1/\sqrt{2}; \sqrt{2})$, respectively. In the SM $\hat{R}_{D^{(*)}} - 1$ vanishes. Experimental data is shown in the form of dark and light one sigma bands that correspond to the averages including and excluding the 2019 Moriond data, respectively. The dashed extension of the blue region indicates the maximum reach in the V_3 scenario if only the direct bound from $B \to K\nu\bar{\nu}$ is used. Updated version of Figure 2 from [1].

$\mathcal{O}(1)$ factors have magnitude one, whereas for the larger, light areas these numbers can be as large as $\sqrt{2}$. In the second case this produces an effective enhancement of the product of couplings YY^* by a factor of four, where one factor of two arises directly and the second one emerges from the relaxation of the bounds from low energy processes. For contributions from V_1 and V_3, shown in red and blue, respectively, we employ data on kaon decays to constrain c_ν and require $c_\ell \lesssim 0.2$. The dashed extension of the blue region indicates the maximal reach of the effects induced by V_3 if only the direct bound on the product $c_\nu c_\ell$ from $B \to K\nu\bar{\nu}$ data is imposed. Depicted in green is the potential impact of S_3 where constraints from μ-e conversion on κc_ν are utilized. Lastly, we show the averages of the available experimental data on $\hat{R}_{D^{(*)}} - 1$ from 2016 and 2019 as light and dark grey bands, respectively. The normalized experimental values are calculated using the data from Table 3.1 and read

$$\hat{R}_D^{\text{exp, 2016}} = 1.35 \pm 0.17 \qquad \hat{R}_{D^*}^{\text{exp, 2016}} = 1.23 \pm 0.07 \tag{6.45}$$

and

$$\hat{R}_D^{\text{exp, 2019}} = 1.15 \pm 0.11 \qquad \hat{R}_{D^*}^{\text{exp, 2019}} = 1.19 \pm 0.05\,. \tag{6.46}$$

6.2.2. Impact of Flavorful Leptoquarks on $b \to s\ell\bar{\ell}$ Transitions

Let us now consider the effects of leptoquarks with couplings constrained by the AF $\times$ FN model on the FCNC transitions $b \to s\ell^+\ell^-$. Again, we concentrate on the flavor anomalies currently seen in data on R_K and R_{K^*}.

Benchmark Scenario As discussed in Section 3.4.3, we focus on the benchmark scenario (3.43) as a resolution to the $b \to s\ell^+\ell^-$ anomalies. The preferred Lorentz structure of left-handed quark and lepton currents is readily obtained within the leptoquark models V_1, V_3 and S_3, which all couple to quark and lepton doublets. In these cases the necessary Wilson coefficients are proportional to $Y_{QL}^{b\mu}\left(Y_{QL}^{s\mu}\right)^*$ or $Y_{\bar{Q}L}^{s\mu}\left(Y_{\bar{Q}L}^{b\mu}\right)^*$. With the exact relations given in Appendix D, we find that

$$Y_{QL}^{b\mu}\left(Y_{QL}^{s\mu}\right)^* \text{ or } Y_{\bar{Q}L}^{s\mu}\left(Y_{\bar{Q}L}^{b\mu}\right)^* \sim 10^{-3}\left(\frac{M}{\text{TeV}}\right)^2\,, \tag{6.47}$$

is required in order to explain the data.

This can be accommodated with the simple muon isolation pattern L_μ, as already discussed in [176], which imposes

$$Y_{QL}^{b\mu}\left(Y_{QL}^{s\mu}\right)^* \text{ or } Y_{\bar{Q}L}^{s\mu}\left(Y_{\bar{Q}L}^{b\mu}\right)^* \sim c_\ell^2\epsilon^2\,, \tag{6.48}$$

and thus requires $c_\ell \sim 0.2(M/\text{TeV})$. Therefore, typical values for the flavon vev indicate leptoquark masses of the order of a few TeV, which are well within the $B_s - \bar{B}_s$

mixing mass bound (4.3). The kaon decays $K \to \mu^+\mu^-$ receive leptoquark contributions of the order $c_\ell^2\epsilon^6$. Mass basis corrections (6.21) to the L_μ pattern induce μ-e conversion at the order $c_\ell^2\delta\epsilon^8$. In both cases present experimental bounds are not exceeded.

Using the modified patterns $\tilde{L}_\mu(QL, \bar{Q}L)$ from (6.21), which avoid the FN-suppression, results in

$$Y_{QL}^{b\mu}\left(Y_{QL}^{s\mu}\right)^* \sim c_\ell c_\nu \kappa\,, \quad Y_{\bar{Q}L}^{s\mu}\left(Y_{\bar{Q}L}^{b\mu}\right)^* \sim c_\ell c_\nu\,. \tag{6.49}$$

If the vevs that determine the values of the $Y^{s\mu}$ couplings saturate the upper limit allowed by current data on kaon decays, i.e. $c_\nu\kappa \sim 0.01(M/\text{TeV})$ for S_3 and $c_\nu \sim 0.01(M/\text{TeV})$ for $V_{1,3}$, the anomalies can again be explained with $c_\ell \sim 0.2(M/\text{TeV})$. Hence, upcoming experimental data on cLFV kaon decays and μ-e conversion is expected to show a signal if this scenario constitutes the origin of the deviations in R_K and R_{K^*}.

The benchmark scenario for the $b \to s\ell^+\ell^-$ anomalies can thus be realized with the S_3 and V_3 leptoquarks whose couplings are determined by the AF $\times$ FN model while the involved flavon vevs take typical values. For V_1 additional right-handed quark and lepton currents arise due to the singlet coupling $Y_{\bar{D}E}$. The charge assignments that give rise to the muon isolation pattern for the doublets necessarily induces the R_μ pattern for the singlet coupling, in which cancellations between the quark and lepton FN charges occur, as pointed out in Section 6.1.1. These cancellations lead to inverted flavor hierarchies which in turn can induce kaon decays at order ϵ, exceeding current experimental limits. However, this problem can be circumvented by flipping the signs of the lepton singlets' FN charges $q(E)$, as this only affects the flavor hierarchies in the leptoquark couplings but leaves the masses and mixing intact. In this case, kaon decays only arise at order ϵ^9, which is beyond any foreseeable experimental sensitivity. Thus, a flavorful V_1 constitutes a viable explanation for the $b \to s\ell^+\ell^-$ anomalies as well.

Furthermore, NP effects in $b \to s\ell^+\ell^-$ are induced by the V_3 model with couplings following the tau isolation pattern utilized to study contributions to $b \to c\ell\bar{\nu}$. However, these effects are negligible since they either stem from higher order corrections to the $L_\tau(\bar{Q}L)$ pattern, which are of the order $\delta^2 c_\ell^2\epsilon^2$, or they are strongly constrained by $b \to s\nu\bar{\nu}$ data and low energy physics, as it is the case for the modified tau isolation pattern $\tilde{L}_\tau(\bar{Q}L)$, where the largest contributions to $b \to s\ell^+\ell^-$ reach an order of $\delta c_\ell c_\nu + c_\nu^2\epsilon^2$. This means that in this scenario NP effects cannot be sizable in both $b \to s\ell^+\ell^-$ and $b \to s\nu\bar{\nu}$ transitions, let alone deliver simultaneous explanations of the $b \to s$ and $b \to c$ anomalies.

Right-Handed Quark Currents We will now briefly discuss the disfavored scenario with contributions to right-handed quark currents i.e. $C_9'^\mu = -C_{10}'^\mu$. According to Table 4.1, the necessary leptoquark couplings $Y_{\bar{D}L}$ and Y_{DL} occur in the models $\tilde{S}_2$ and V_2, respectively. As this scenario provides direct access to the FN charges $q(D)$ of the

down-type quark singlets, instead of using the fixed charges from (5.7) we keep them as free parameters here and employ the short form $q_i \equiv q(D_i)$.

An explanation of R_K then requires

$$Y^{b\mu}_{DL}\left(Y^{s\mu}_{DL}\right)^* \text{ or } Y^{s\mu}_{\bar{D}L}\left(Y^{b\mu}_{\bar{D}L}\right)^* \sim c_\ell^2 \epsilon^{q_3+q_2} \simeq 10^{-3}\left(\frac{M}{\text{TeV}}\right)^2 , \tag{6.50}$$

while data on $K \to \mu^+\mu^-$ [127] imposes the limit

$$Y^{s\mu}_{DL}\left(Y^{d\mu}_{DL}\right)^* \text{ or } Y^{s\mu}_{\bar{D}L}\left(Y^{d\mu}_{\bar{D}L}\right)^* \sim c_\ell^2 \epsilon^{q_2+q_1} \lesssim 1.3 \times 10^{-4} \text{ or } 2.6 \times 10^{-4}\left(\frac{M}{\text{TeV}}\right)^2 . \tag{6.51}$$

In order to satisfy both of these constraints the condition

$$\epsilon^{q_1-q_3} \lesssim 0.13 , \tag{6.52}$$

must be met, indicating

$$q_1 \geq q_3 + 2 , \tag{6.53}$$

for integer charges q_i. Lower bounds on the mass imply that the suppression of the couplings $Y^{b\mu}$ and $Y^{s\mu}$ cannot be too strong if (6.50) is to be fulfilled. Furthermore, we require the couplings to remain perturbative. Together, these two conditions require

$$0 \leq q_2 + q_3 \leq 3 . \tag{6.54}$$

This means that an explanation of R_K is not possible using our benchmark charge assignment $q(D) = (3, 2, 2)$ from (5.7). However, supersymmetric models or other multi-Higgs scenarios allow for FN charges of the form $q(D) = (q_3 + 1, q_3, q_3)$ with $0 \leq q_3 \leq 3$, which are viable if the mild tension with (6.52) can be tolerated.

Going one step further, if the FN charges of the up-type singlets and doublets are changed as well, we find the two possible solutions $q(Q) = q(U) = (3, 2, 0)$ and $q(D) = (2, 0, 0)$ or $q(D) = (3, 1, 1)$ [170]. The second option gives

$$Y^{b\mu}_{DL}\left(Y^{s\mu}_{DL}\right)^* \text{ or } Y^{s\mu}_{\bar{D}L}\left(Y^{b\mu}_{\bar{D}L}\right)^* \sim c_\ell^2 \epsilon^2 , \tag{6.55}$$

which carries the same suppression as in (6.48) from the benchmark scenario. Thus, we find a preference for typical flavon vevs and TeV-scale leptoquarks in this case as well. Contributions to μ-e conversion arise from mass basis rotations and are of the order of $\delta c_\ell^2 \epsilon^6$ – well below present experimental bounds. The $\tilde{S}_2$ leptoquark does not give rise to tree-level FCNCs in the charm sector.

6.2.3. cLFV Observables and Rare Charm and Kaon Decays

While contributions to cLFV processes only arise through mass basis corrections in the L_μ pattern, they are induced directly by the modified flavor structure of the $\tilde{L}_\mu$ pattern.

Process	Limit	LQs	Pattern
$\mathcal{B}(D \to \pi\nu\nu)$	3×10^{-10}	S_3, V_3	L_μ
$\mathcal{B}(D \to \pi e\mu)$	3×10^{-13}	V_3	L_μ
$\mathcal{B}(D \to e\mu)$	5×10^{-15}	V_3	$\tilde{L}_\mu$
$\mathcal{B}(D \to e\tau)$	7×10^{-17}	S_2	$\tilde{L}_\tau$
$\mathcal{B}(D \to \mu\mu)$	SM-like		
$\mathcal{B}(D \to \pi\mu\mu)$	SM-like		

Table 6.2.: Upper limit on branching ratios of rare and cLFV charm decays that can be reached with flavorful leptoquarks in the context of $R_{K^{(*)}}$. "SM-like" effects are indistinguishable from resonance contributions.

In relation to $b \to s\mu^+\mu^-$ transitions we find the ratios

$$b \to s\mu\mu \quad : \quad b \to s\mu(e,\tau) \quad : \quad b \to se\tau \quad \sim \quad 1 \quad : \quad \delta \quad : \quad \delta^2 \qquad (L_\mu)\,, \tag{6.56}$$

$$b \to s\mu\mu \quad : \quad b \to s\mu(e,\tau) \quad : \quad b \to se\tau \quad \sim \quad 1 \quad : \quad 1 \quad : \quad 1 \qquad (\tilde{L}_\mu)\,, \tag{6.57}$$

for the amplitudes of cLFV $b \to s\ell\ell'$ processes. Hence, the $\tilde{L}_\mu$ pattern yields sizable contributions to leptonic and semileptonic decays of B and B_s mesons. Following [176] we find the following estimates depending on R_K

$$\mathcal{B}(B \to K\mu^\pm e^\mp) \simeq 10^{-8} \left(\frac{1-R_K}{0.15}\right)^2, \tag{6.58}$$

$$\mathcal{B}(B \to K(e^\pm,\mu^\pm)\tau^\mp) \simeq 10^{-8} \left(\frac{1-R_K}{0.15}\right)^2, \tag{6.59}$$

$$\frac{\mathcal{B}(B_s \to \mu^+e^-)}{\mathcal{B}(B_s \to \mu^+\mu^-)_{\rm SM}} \simeq 4 \times 10^{-3} \left(\frac{1-R_K}{0.15}\right)^2, \tag{6.60}$$

$$\frac{\mathcal{B}(B_s \to \tau^+(e^-,\mu^-))}{\mathcal{B}(B_s \to \mu^+\mu^-)_{\rm SM}} \simeq 2 \left(\frac{1-R_K}{0.15}\right)^2. \tag{6.61}$$

Furthermore, cLFV signals induced by the triplet leptoquarks S_3 and V_3 can be large enough to be detected with upcoming data from the COMET [125] and Mu2e [124] experiments, which will improve current experimental limits by two to three orders of magnitude. For μ-e conversion in muonic gold we find $\frac{\sigma(\mu^-\mathrm{Au}\to e^-\mathrm{Au})}{\sigma(\mu^-\mathrm{Au}\to\mathrm{capture})} \lesssim 2 \times 10^{-13}$ (5×10^{-14}) for V_3 (S_3).

We follow [122] to discuss leptoquark effects in rare and cLFV charm decays. Table 6.2 shows the largest possible branching ratios that can be obtained within the flavorful leptoquark models addressing the B anomalies. The non-resonant SM predictions for the SM-like processes are $\mathcal{B}^{\rm SM}(D \to \mu^+\mu^-) \simeq 10^{-13}$ and $\mathcal{B}^{\rm SM}(D \to \pi\mu^+\mu^-) \simeq 10^{-12}$ [122]. Since explanations of $R_{K^{(*)}}$ strongly prefer couplings to left-handed quarks, all relevant leptoquark models involve couplings to the quark doublet, which means that the tight

constraints from kaon decays automatically lead to strongly suppressed leptoquark effects in the charm sector. Consequently, the predictions listed in Table 6.2 lie far below current experimental limits.

More generally, without a connection to the B anomalies, larger contributions to rare charm decays can be obtained from leptoquarks in flavor models. A promising scenario involves the skewed pattern $R_{e\mu}(\bar{U}E)$ for the $\tilde{V}_1$ leptoquark, where cancellations between the FN charges lead to potentially large effects in the charm sector. However, the strong constraint from μ-e conversion can only be avoided at the cost of suppressing the diagonal entries of the flavor coupling. Likewise, the $R_{e\mu}(UE)$ pattern, which can be realized within the S_1 leptoquark model, yields only very small effects of the order of $\delta^{(\prime)}\epsilon^{10}$. An evasion of the μ-e conversion constraints can be successfully achieved with the $R_{e\tau}(\bar{U}E)$ pattern applied to the coupling of the $\tilde{V}_1$ leptoquark. In this case $c \to ue\tau$ processes arise at the order of $\kappa\kappa'\epsilon^2 \lesssim 10^{-3}$, resulting in $\mathcal{B}(D \to e\tau) \lesssim 10^{-13}$.

Since the triplet leptoquarks S_3 and V_3 are most constrained by cLFV kaon decays, we predict large signals close to the experimental upper limit $\mathcal{B}(K_L \to e\mu) < 4.7 \times 10^{-12}$ [129]. For the S_2 leptoquark model in combination with the patterns $\tilde{L}_\tau(\bar{U}L)$ and $R_\tau(\bar{Q}E)$ we find only small contributions to rare kaon decays yielding $\mathcal{B}(K_L \to e\mu) \lesssim 4 \times 10^{-19}$ due to the constraints from μ-e conversion.

6.3. Summary and Conclusion

We have employed the AF $\times$ FN flavor model to derive patterns for leptoquark couplings. While the FN symmetry imposes a hierarchical structure on the rows of the coupling matrices, which relate to different quark generations, the discrete group A_4 allows to isolate couplings to a specific lepton generation based on the representation assigned to the leptoquark. Beyond that, modified patterns can be engineered which allow to evade experimental bounds and maximize NP effects in flavor observables. In general, we find that couplings to lepton singlets are larger than those involving doublets, resulting in more sizable contributions to chirality-flipping operators than to SM-like operators in the context of $R_{D^{(*)}}$.

Due to the strong constraints from $b \to s\nu\bar{\nu}$, rare kaon decays and μ-e conversion together with existing leptoquark mass bounds, an explanation of the anomalies in R_D and R_{D^*} is currently not possible within this framework. Predictions of the largest possible effects in $R_{D^{(*)}}$ and the τ polarizations $P_\tau(D^{(*)})$ are discussed in Section 6.2.1 and can be tested by upcoming data from the Belle II experiment with $50\,\text{ab}^{-1}$ [185].

However, an explanation of the R_K and R_{K^*} anomalies in the $b \to s\ell^+\ell^-$ sector arise naturally with the help of the muon isolation patterns $L_\mu(\bar{Q}L, QL)$ and $\tilde{L}_\mu(\bar{Q}L, QL)$ within the triplet leptoquark models S_3 and V_3. If the relative signs of the charged

lepton singlet and down-type quark singlet FN charges are adjusted in such a way that cancellations occur in $Y_{\bar{D}E}$, then the singlet vector leptoquark model V_1 provides a viable solution as well. While these options reproduce the benchmark scenario (3.43) compatible with global fits to $b \to s\mu^+\mu^-$ observables, it is also possible to explain R_K within the $\tilde{S}_2$ leptoquark model that gives rise to right-handed quark currents and thus predicts $R_K \neq R_{K^*}$.

A joint explanation of the $R_{D^{(*)}}$ and $R_{K^{(*)}}$ is not possible with flavorful leptoquarks as effects in R_D and in particular in R_{D^*} are strongly constrained by flavor processes. In order to obtain maximal contributions to $R_{D^{(*)}}$ and $R_{K^{(*)}}$, two types of flavorful leptoquarks in the TeV mass region are required.

Since we treat the flavon vevs as free parameters constrained by experimental data the results presented here apply to more general models than the particular AF $\times$ FN realization we consider.

Chapter 7.

Signatures of Flavorful Leptoquarks at Hadron Colliders

The strict bounds imposed by flavor symmetries on the couplings of leptoquarks that can explain the deviations in R_K and R_{K^*} highlight the $\mathcal{O}(1)$ TeV leptoquark mass region, which is accessible at future collider experiments. In this chapter, we study possible signatures of these leptoquarks focusing on single production, which provides an experimental handle on the flavor structure of the leptoquark couplings.

The results of this chapter are based on the findings of [2, 3].

7.1. The Leptoquarks S_3, V_1 and V_3

As discussed in Section 4.1, the only leptoquarks that can accommodate the $R_{K^{(*)}}$ data with couplings to quark and lepton doublets are the scalar triplet $S_3(\bar{\mathbf{3}}, \mathbf{3}, 1/3)$, the vector singlet $V_1(\mathbf{3}, \mathbf{1}, 2/3)$ and the vector triplet $V_3(\mathbf{3}, \mathbf{3}, 2/3)$. The kinetic terms and fermion interactions of these leptoquarks read

$$\begin{aligned}
\mathcal{L}_{S_3} &= \frac{1}{2}\,\mathrm{Tr}\left[(D_\mu S_3)^\dagger\, D^\mu S_3\right] + Y\,\bar{Q}^c i\sigma^2 \vec{\sigma} L\,\vec{S}_3 + \text{h.c.},\\
\mathcal{L}_{V_1} &= -\left(D^\mu V_1^\nu\,(D_\mu V_{1\nu})^\dagger - D^\mu V_1^\nu\,(D_\nu V_{1\mu})^\dagger\right) - i g_s \kappa V_1^{\dagger\mu} T^a V_1^\nu G^a_{\mu\nu}\\
&\quad + Y\,\bar{Q}\gamma_\mu L\, V_1^\mu + \text{h.c.},\\
\mathcal{L}_{V_3} &= -\left(D^\mu \vec{V}_3^\nu \cdot \left(D_\mu \vec{V}_{3\nu}\right)^\dagger - D^\mu \vec{V}_3^\nu \cdot \left(D_\nu \vec{V}_{3\mu}\right)^\dagger\right) - i g_s \kappa \vec{V}_3^{\dagger\mu} T^a \cdot \vec{V}_3^\nu G^a_{\mu\nu}\\
&\quad + Y\,\bar{Q}\gamma_\mu \vec{\sigma} L \cdot \vec{V}_3^\mu + \text{h.c.}
\end{aligned} \tag{7.1}$$

We neglect couplings that potentially induce proton decay or involve right-handed fermions and focus solely on the coupling to quark and lepton doublets, which we denote by Y. Since we only consider one leptoquark at a time we use the same symbol for the coupling throughout. Note that the interactions of different multiplet components are

related by $SU(2)_{\rm L}$. We use quark and lepton flavor indices, e.g. $Y_{q\ell}$, to refer to individual entries of the couplings in the mass basis. The couplings to up- and down-type quarks are related by

$$Y_{u_i\ell} = V^*_{ji} Y_{d_j\ell}\,, \tag{7.2}$$

where V is the CKM matrix.

The scalar and vector triplet can be decomposed in terms of their weak isospin components as

$$\vec{\sigma}\cdot\vec{S}_3 = \begin{pmatrix} S_3^{1/3} & \sqrt{2}S_3^{4/3} \\ \sqrt{2}S_3^{-2/3} & -S_3^{1/3} \end{pmatrix}\,, \tag{7.3}$$

and

$$\vec{\sigma}\cdot\vec{V}_3 = \begin{pmatrix} V_3^{2/3} & \sqrt{2}V_3^{-1/3} \\ \sqrt{2}V_3^{5/3} & -V_3^{2/3} \end{pmatrix}\,, \tag{7.4}$$

respectively. Here, fractional superscripts denote the electric charges of the isospin components. We assume that the masses of the individual components are approximately degenerate. Expanding the fermion interaction parts of the Lagrangians in terms of the weak isospin components gives

$$\begin{aligned}
\mathcal{L}_{S_3,\rm int} &= -Y\,\bar{d}^c_{\rm L}\,\nu_{\rm L}\,S_3^{1/3} - Y\,\bar{u}^c_{\rm L}\,e_{\rm L}\,S_3^{1/3} \\
&\quad + \sqrt{2}Y\,\bar{u}^c_{\rm L}\,\nu_{\rm L}\,S_3^{-2/3} - \sqrt{2}Y\,\bar{d}^c_{\rm L} e_{\rm L}\,S_3^{4/3} + \text{h.c.}, \\
\mathcal{L}_{V_1,\rm int} &= Y\,\bar{u}_{\rm L}\gamma^\mu\nu_{\rm L}V_{1,\mu}^{2/3} + Y\,\bar{d}_{\rm L}\gamma^\mu e_{\rm L}V_{1,\mu}^{2/3} + \text{h.c.}, \\
\mathcal{L}_{V_3,\rm int} &= Y\,\bar{u}_{\rm L}\gamma^\mu\nu_{\rm L}V_{3,\mu}^{2/3} - Y\,\bar{d}_{\rm L}\gamma^\mu e_{\rm L}V_{3,\mu}^{2/3} \\
&\quad + \sqrt{2}Y\,\bar{u}_{\rm L}\gamma^\mu e_{\rm L}\,V_{3\mu}^{5/3} + \sqrt{2}Y\,\bar{d}_{\rm L}\gamma^\mu\nu_{\rm L}\,V_{3,\mu}^{-1/3} + \text{h.c.}
\end{aligned} \tag{7.5}$$

Note that the diagonal components of V_3 have the same quantum numbers as V_1 and thus yield the same fermion interactions (up to a sign). The relevant leptoquarks in the context of $R_{K^{(*)}}$ are those which couple to down-type quarks and charged leptons, i.e. $S_3^{4/3}$, $V_1^{2/3}$ and $V_3^{2/3}$.

In order to study the collider phenomenology of these leptoquarks, we implement their Lagrangians in `Feynrules` [186] from which we obtain the `UFO` output [187] that can be used as an input to the `MadGraph` framework [188].

An explanation of the anomalies in the current data on R_K and R_{K^*} via leptoquarks requires

$$\frac{Y_{b\mu}Y^*_{s\mu} - Y_{be}Y^*_{se}}{M^2} \simeq \pm\frac{1}{(40\,\text{TeV})^2}\,, \tag{7.6}$$

where the upper (lower) sign applies in the case of the vector (scalar) leptoquarks. As a benchmark scenario we consider the simple pattern

$$Y_{\rm s} \sim Y_0 \begin{pmatrix} 0 & 0 & 0 \\ * & \epsilon^2 & * \\ * & 1 & * \end{pmatrix}\,, \tag{7.7}$$

which is motivated by the L_μ pattern discussed earlier. With the lepton flavor isolation patterns derived in the AF $\times$ FN model, couplings to first generation quarks are negligible, as they are FN-suppressed and additionally constrained by experimental data on μ–e conversion and rare kaon decays. For the sake of simplicity we set them to zero in the simple pattern (7.7). The entries marked with "$*$" are not necessary to explain $R_{K^{(*)}}$ but can potentially produce leptoquark signals with electrons or tau leptons in the final state and induce cLFV. In the previously discussed flavor models these entries only arise by means of higher order flavon insertions and are therefore strongly suppressed. We consider more general patterns and their phenomenology in Section 7.3.3. With this setup the $R_{K^{(*)}}$ data (7.6) points to $Y_0 \simeq M/8\,\text{TeV}$. If we allow $\mathcal{O}(1)$ factors between 1/3 and 3 the $R_{K^{(*)}}$ to be present in $Y_{s\mu}$, we find the range

$$M/14\,\text{TeV} \lesssim Y_0 \lesssim M/5\,\text{TeV}\,. \tag{7.8}$$

This interval is in accordance with existing experimental limits on Drell-Yan processes, which receive contributions from t-channel leptoquark exchange at tree-level. Explicitly, we find

$$C_{b_\text{L}L} = v^2 \frac{Y_0^2}{2M_{S_3}^2} \lesssim 2 \times 10^{-3} \tag{7.9}$$

in the basis of the Standard Model Effective Field Theory (SMEFT) Wilson coefficients. The experimental bounds on this coefficient are about one order of magnitude weaker for electrons as well as for muons [189]. Note that these limits still serve as a suitable approximation in the case of light leptoquarks for which the EFT approach does not apply [190].

7.2. Leptoquark Decay and Width

The partial decay widths of the leptoquark triplets S_3 and V_3 decaying to a lepton ℓ and a quark q, whose masses are negligible compared to the leptoquark mass, read

$$\Gamma(S_3 \to q\ell) = c\frac{|Y_{q\ell}|^2}{16\pi} M_{S_3}\,, \quad \text{and} \quad \Gamma(V_3 \to \bar{q}\ell) = c\frac{|Y_{q\ell}|^2}{24\pi} M_{V_3}\,, \tag{7.10}$$

respectively, with $c = 1$ for the diagonal multiplet components $S_3^{1/3}$ and $V_3^{2/3}$, and $c = 2$ for the off-diagonal components $S_3^{4/3}$ and $S_3^{-2/3}$ as well as $V_3^{-1/3}$ and $V_3^{5/3}$. For the singlet vector leptoquark $V_1^{2/3}$ the two-body decay width is the same as for the diagonal component $V_3^{2/3}$ of the triplet. If $Y_{q\ell}$ is the dominant coupling then the partial decay width Γ is a good approximation for the total width of the leptoquark. For large leptoquark masses a significant contribution to the total decay width can arise from inter-multiplet cascades such as $S_3^{-4/3} \to S_3^{-1/3} W^- \to b\nu W^-$.

In the case of the simple scenario (7.7), where the couplings to light quark generations are strongly suppressed, the leptoquark primarily decays to third generation quarks.

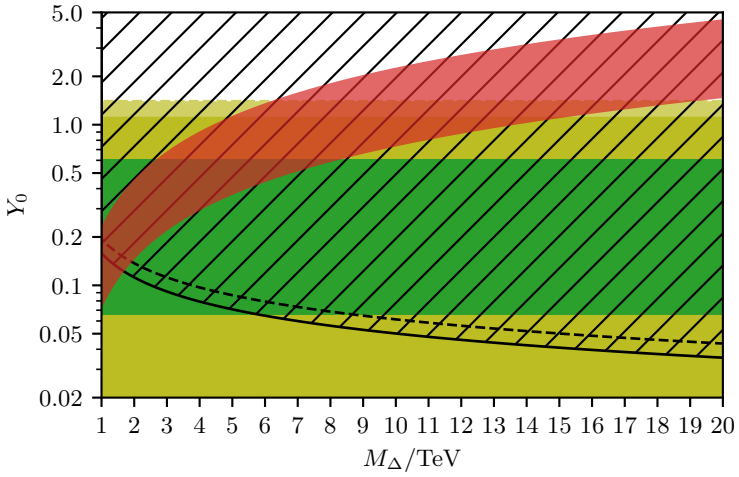

Figure 7.1.: Parameter space of the $S_3^{4/3}$ and $V_{1,3}^{2/3}$ leptoquark components within the simple scenario (7.7) with a dominant coupling to the third quark generation. The red band indicates the region relevant for $R_{K^{(*)}}$. Within the yellow area the narrow width approximation (NWA) holds. Inside the hatched region above the black curve the leptoquark does not hadronize. Dashed lines indicate the regions that apply for the vector leptoquarks. Flavor model predictions are shown in green. Updated version of Figure 1 from [2].

Figure 7.1 shows the relevant parameter space spanned by the leptoquark mass M_Δ and the dominant coupling $Y_0 \equiv Y_{b\mu}$ for the components $S_3^{4/3}$ and $V_{1,3}^{2/3}$, which couple to charged leptons and down-type quarks. The red region corresponds to the range (7.8) which allows for an explanation of $R_{K^{(*)}}$. Within the hatched area the leptoquark decays quickly enough so that it does not form QCD bound states, i.e. $\Gamma > \Lambda_{\text{QCD}}$. Indicated by the yellow band is the region where the couplings are small enough to employ the NWA for the production and decay of the leptoquark. We use the bound $\Gamma/M_{S_3} \lesssim 5\,\%$, which implies $Y_0 \lesssim 1.1\,(1.4)$ for scalar (vector) leptoquarks. The previously discussed flavor models require $Y_0 \sim \epsilon$ as indicated by the green band.

In this scenario the dominant decay modes of the leptoquarks that are capable of explaining the $R_{K^{(*)}}$ data are

$$\begin{aligned} S_3^{+2/3} &\to t\nu\,, \\ S_3^{-1/3} &\to b\nu,\ t\mu^-\,, \\ S_3^{-4/3} &\to b\mu^-\,, \end{aligned} \tag{7.11}$$

for the scalar triplet,

$$V_1^{+2/3} \to b\mu^+,\ t\nu \tag{7.12}$$

for the vector singlet, and

$$\begin{aligned} V_3^{-1/3} &\to b\nu\,, \\ V_3^{+2/3} &\to b\mu^+,\ t\nu, \\ V_3^{+5/3} &\to t\mu^+\,. \end{aligned} \tag{7.13}$$

for the vector triplet. At collider experiments, tagging the charge of the bottom quark in the final state would be very useful to determine the type and electric charge of the leptoquark, as for instance the processes $V_{1,3}^{-2/3} \to \bar{b}\mu^-$ and $S_3^{-4/3} \to b\mu^-$ both result in final states that contain a negatively charged lepton. Furthermore, note that due to the couplings to quark and lepton doublets, there are two possible final states with third generation quarks for the singlet and for the diagonal component of the triplet leptoquark. In particular, this yields $\mathcal{B}(S_3^{-1/3} \to b\nu) \simeq \mathcal{B}(S_3^{-1/3} \to t\ell^-) \simeq 1/2$ for the scalar, and $\mathcal{B}(V_{1,3}^{2/3} \to b\mu^+) \simeq \mathcal{B}(V_{1,3}^{2/3} \to t\nu) \simeq 1/2$ for the vectors.

7.3. Collider Phenomenology of Scalar Leptoquarks

7.3.1. Single Leptoquark Production: S_3

At hadron colliders single leptoquarks can be produced together with a lepton by means of quark–gluon fusion. The respective production cross section is sensitive to the flavor coupling $Y_{q\ell}$. Taking into account the decay of the leptoquark into a quark and a lepton then results in the characteristic collider signature consisting of a jet and two leptons. In the case of a dominant coupling to the third quark generation the leptoquarks that can potentially explain $R_{K^{(*)}}$ produce the signature $pp \to b\mu\mu$.

Figure 7.2 shows the leading order parton-level Feynman diagrams that induce the single and pair production of the S_3, V_1 and V_3 leptoquarks and their subsequent decay at hadron colliders. Due to the strong flavor hierarchies in (7.7), the hadronic production cross section is still dominated by the coupling to the third quark generation, despite the parton distribution function (PDF)-suppression of the bottom quark. To illustrate this, we show in Figure 7.4 the single leptoquark production cross sections for unit couplings to the d, s and b quarks in blue (dotted), brown (dash-dotted) and pink (dashed), respectively. The relative suppression of the bottom-induced production with respect to that caused by the s and d quarks amounts to factors of order one and 10^{-1} to 10^{-2}, respectively, which is much weaker than the suppression from the flavor pattern (7.7). For all single leptoquark production cross sections depicted in Figure 7.4 we add the contributions from the respective CP-conjugate final states. In the case of sea quark–gluon fusion this amounts to a factor of two in the limit of CP conservation. The contribution of the $\bar{d}$ quark in the initial state is included explicitly. Depicted as a red band is the CP-summed single production cross section of the S_3 leptoquark in association with a muon for the benchmark scenario (7.7). Additionally, we show the pair production cross section $\sigma(pp \to S_3^{-4/3} S_3^{+4/3})$ in green. The corresponding Feynman

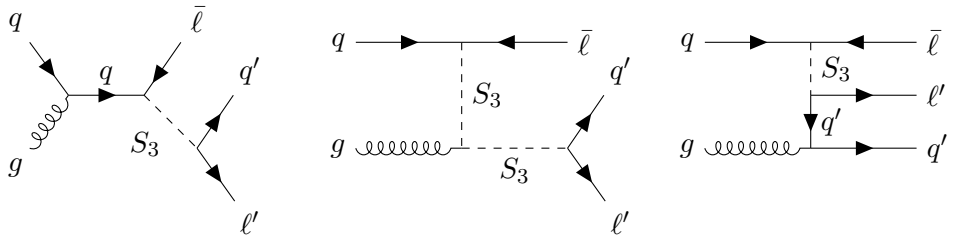

(a) Single production of the scalar leptoquark S_3.

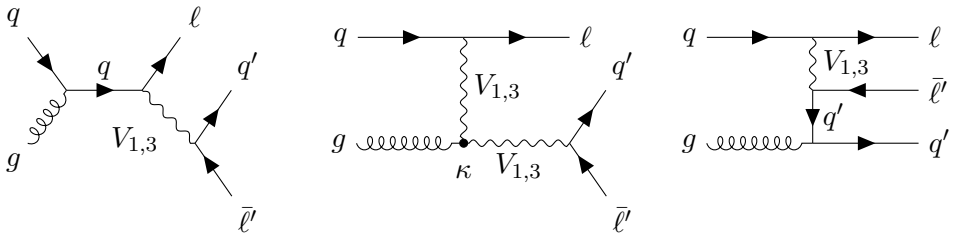

(b) Single production of the vector leptoquarks V_1 and V_3.

Figure 7.2.: Leading order Feynman diagrams of the scalar (a) and vector (b) leptoquark single production and decay at hadron colliders. The first two diagrams in each case yield resonant amplitudes, while the third one gives a non-resonant contribution whose effects can be suppressed by means of kinematic cuts (see text). For the vector leptoquark production (b) the final state lepton and antilepton are interchanged compared with the scalar case and an additional contribution to the leptoquark–gluon coupling proportional to κ arises in the second diagram.

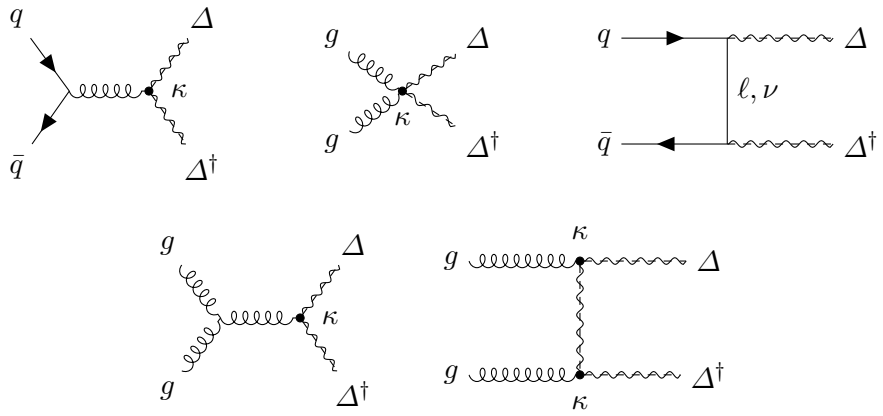

Figure 7.3.: Leading order Feynman diagrams of leptoquark pair production at hadron colliders. The process is dominated by the first two diagrams involving leptoquark–gluon couplings. For vector leptoquarks additional contributions proportional to κ arise for those diagrams. We use Δ to denote a generic scalar or vector leptoquark.

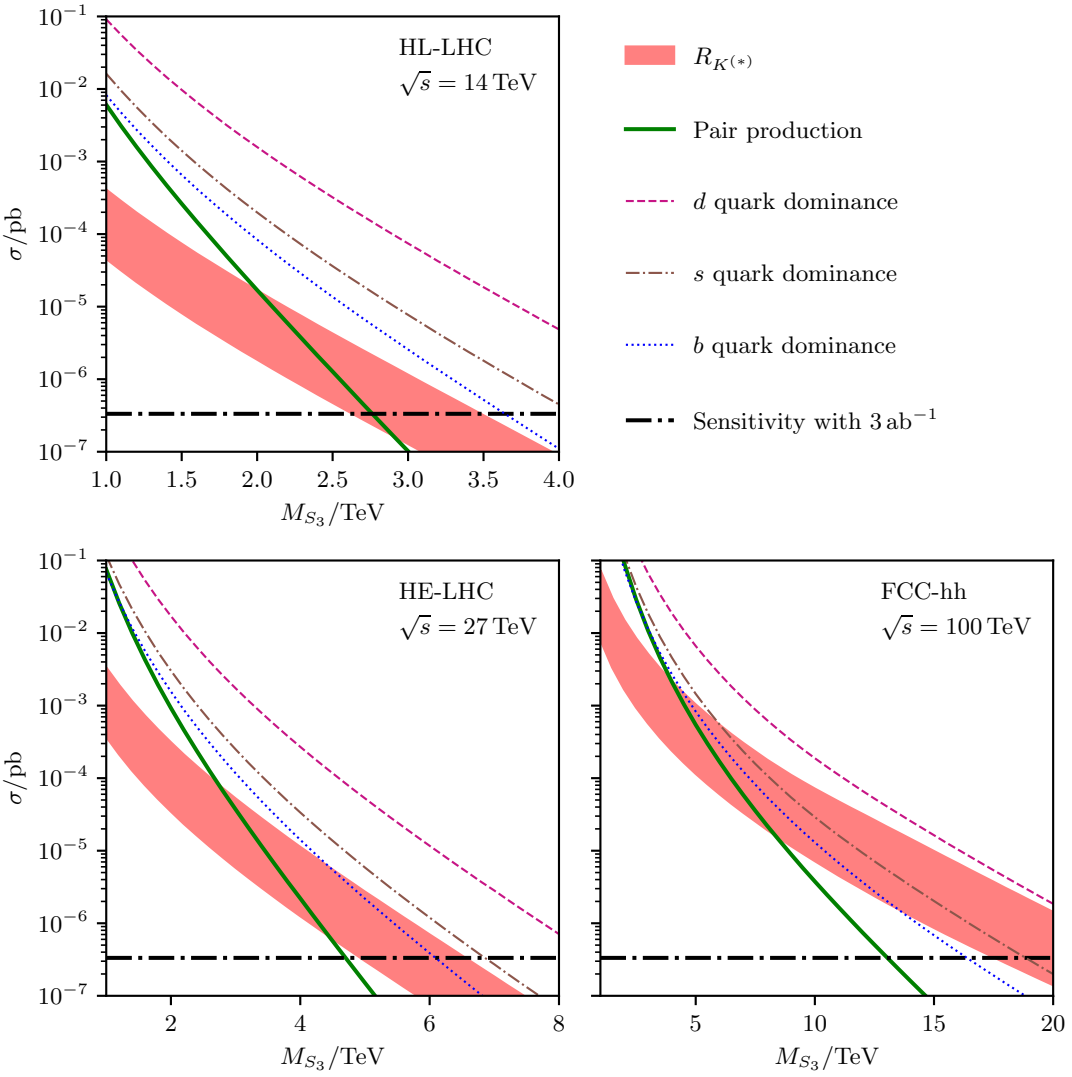

Figure 7.4.: Single leptoquark production cross section $\sigma(pp \to S_3^{-4/3}\mu^+ + S_3^{+4/3}\mu^-)$ as a function of the leptoquark mass M_{S_3} for the center of mass energies $\sqrt{s} = 14$, 27 and 100 TeV. The red band indicates the range of cross sections obtained in the simple scenario (7.7) with Y_0 chosen according to (7.8) which provides an explanation for $R_{K^{(*)}}$. As pink (dashed), brown (dash-dotted) and blue (dotted) lines we show the cross sections with only the coupling to the down, strange and bottom quark turned on and set to one, respectively. The green line shows the pair production cross section $\sigma(pp \to S_3^{-4/3}S_3^{+4/3})$. The smallest cross section that still allows for the production of a single event with an integrated luminosity of $3\,\text{ab}^{-1}$ is shown as a black line. Updated version of Figure 3 from [2].

diagrams are shown in Figure 7.3. With the flavor pattern relevant for $R_{K^{(*)}}$ the $S_3^{-4/3}$ leptoquark predominantly decays to $b\mu$ which means that pair production generates the signature $pp \to bb\mu\mu$. The final states $tt\mu\mu$, bbE_{miss}, $bt\mu E_{\text{miss}}$ and ttE_{miss} can be produced by pair production of the other components of the S_3 multiplet. Besides the results for a center of mass energy of $\sqrt{s} = 14\,\text{TeV}$, at which the LHC will operate in the following years, we also include projections for planned future experiments with center of mass energies of $\sqrt{s} = 27$ and $100\,\text{TeV}$ as proposed for the HE-LHC and the FCC-hh, respectively [191].

All numerical calculations discussed here are carried out at leading order in QCD using the `MadGraph` framework [188]. For the evaluation of the PDFs, which provide the largest source of uncertainty, we use `LHAPDF` [192]. We find that the PDF uncertainties of the single leptoquark production cross section associated with the $R_{K^{(*)}}$ data (red band in Figure 7.4) amount to $\mathcal{O}(10\,\%)$ for small leptoquark masses $M \simeq 1\,\text{TeV}$ and grow up to 35 % to 45 % for smaller cross sections of the order of $10^{-7}\,\text{pb}$. Further uncertainties stem from the factorization and renormalization scale and can reach up to 25 %. Both scales are assumed to equal half of the sum of the final state transverse masses. For the pair production cross section both scale and PDF uncertainties can rise up to $\mathcal{O}(40\,\%)$ in the high mass region where, the cross section drops to $\mathcal{O}(10^{-7})\,\text{pb}$. At small leptoquark masses $M \simeq 1\,\text{TeV}$ the PDF uncertainties remain as small as $\mathcal{O}(10\,\%)$, comparable to the case of single production. The scale uncertainties, however, stay approximately constant throughout the full leptoquark mass range.

Since leptoquark pair production is dominated by the leptoquark–gluon coupling, for small leptoquark masses the associated cross section is larger than the single leptoquark production cross section. For larger leptoquark masses the pair production cross section becomes increasingly phase space suppressed and eventually drops below the single production cross section. At higher center of mass energies of $\sqrt{s} = 27$ and $100\,\text{TeV}$ the mass reach for the pair production can be increased by factors of about two and five, respectively, compared with the reach at $\sqrt{s} = 14\,\text{TeV}$ and assuming the same luminosity of $3\,\text{ab}^{-1}$ in all cases. Increasing the center of mass energy has a moderately larger effect on the mass reach for the single leptoquark production. For $\sqrt{s} = 27\,(100)\,\text{TeV}$ naively a factor of two (seven) can be gained.

7.3.2. Top and Jet Final States

The $SU(2)_{\text{L}}$ multiplet structure of the S_3 leptoquark suggests to also consider single production processes with final states in which top quarks or jets instead of a bottom quark are produced alongside two leptons. This provides the opportunity to search for complimentary signatures at collider experiments.

As can be seen immediately from the interaction Lagrangian (7.5), the processes $gb \to \mu^+ S_3^{-4/3}(\to b\mu^-)$ and $gb \to \bar{\nu} S_3^{-1/3}(\to t\mu^-)$ are related and occur at the same order in

the flavor coupling. Note that for $S_3^{-1/3}$ an additional factor of 1/2 arises in the leading branching fractions, as it decays in equal parts to $b\nu$ and $t\ell^-$ within the hierarchical flavor scenario (7.7). From an experimental point of view $t\mu^-\bar{\nu}$ final states have the disadvantage over final states with two charged leptons that their SM background is larger, since $W^- \to \ell^-\bar{\nu}$ events cannot be removed as easily as $Z \to \ell^+\ell^-$ decays. However, flavor scenarios in which the coupling to second generation quarks is not suppressed can induce $gc \to \mu^+ S_3^{-1/3}(\to t\mu^-)$, leading to a $t\mu^+\mu^-$ signature. In the case of a democratic scenario where $Y_{b\mu} = Y_{s\mu}$ the branching ratio of the $t\mu^-$ channel reads $\mathcal{B}(S_3^{-1/3} \to t\mu^-) \simeq 1/4$. The $R_{K^{(*)}}$ data (7.8) then requires the leptoquark coupling Y_0 to be an order of magnitude smaller than in the hierarchical scenario. Consequently, with democratic couplings $pp \to t\mu^+\mu^-$ cross sections are about two orders of magnitude smaller compared to $pp \to b\mu^+\mu^-$, even though the initial state charm quark involved in the leptoquark production suffers from a much milder PDF suppression than the bottom quark.

As another variation of the simplified scenario (7.7) let us consider the case of inverted hierarchies, i.e. $Y_{s\mu} \gg Y_{b\mu}$. While this option is allowed by current experimental data, within the flavor models we consider here such a scenario is only possible for singlet leptons with the $R_\mu(QE)$ pattern if the FN charges of the quarks and leptons have opposite sign so that cancellations are possible. Considering $t\mu^+\mu^-$ final states this variant does not provide an improvement, since the branching fraction $\mathcal{B}(S_3^{-1/3} \to t\mu^-)$ suffers from suppression by $|Y_{b\mu}/Y_{s\mu}|^2$, where the product $Y_{b\mu}Y_{s\mu}^*$ is fixed by the data on $R_{K^{(*)}}$ (7.8). However, this scenario highlights $pp \to j\mu^+\mu^-$ signatures, which are strongly enhanced by the large coupling to second generation quarks and include the dominant decay channel of $S_3^{-1/3}$. Note that this signature receives contributions from the $S_3^{-4/3}$ component as well. Taking into account the upper limit $Y_{s\mu} \lesssim M/2\,\text{TeV}$, which stems from ATLAS measurements of high p_T tails in the dilepton invariant mass distribution of $pp \to \ell^+\ell^-$ processes [189], as well as the PDF enhancement that comes with second generation quark couplings, we find that the cross sections $\sigma(pp \to (j\mu^-)\mu^+ + (j\mu^+)\mu^-)$ can exceed the largest possible signals from processes linked to the $R_{K^{(*)}}$ data and dominated by third quark generation quarks by about one order of magnitude.

7.3.3. Flavor Benchmarks

So far we have only considered the simplified pattern from (7.7), which suffices to study collider signatures of flavorful leptoquarks that are strongly tied to the B anomalies. This pattern is inspired by the L_μ pattern introduced in Section 6.1.1 from which only small contributions to the entries that are not needed for an explanation of $R_{K^{(*)}}$ (marked with "$*$" in (7.7)) arise from higher order effects. However, as discussed in Section 6.1.3, it is possible to construct more general patterns within viable flavor symmetries that provide explanations for the flavor structure of the SM. One of these generalizations is the $\tilde{L}_\mu$ pattern (6.21), which weakens the hierarchy between the

	$b\mu$	be	$b\tau$	$j\mu$	je	$j\tau$
L_μ	1	δ^2	δ^2	λ^4	$\lambda^4\delta^2$	$\lambda^4\delta^2$
$\tilde{L}_\mu$	1	δ^2	δ^2	$(c_\nu\kappa/c_\ell)^2$	$(c_\nu\kappa/c_\ell)^2$	$(c_\nu\kappa/c_\ell)^2$
$Y_{\rm FD}$	1/2	$\kappa_e^2/2$	1/2	$\rho^2/2$	$\rho^2\kappa_e^2/2$	$\rho^2/2$

Table 7.1.: Parametric branching ratios of the leptoquark decay modes $S_3^{-4/3} \to b\ell$ and $S_3^{-4/3} \to j\ell$ for the flavor benchmark patterns L_μ, $\tilde{L}_\mu$ and $Y_{\rm FD}$.

second and third quark generation couplings and introduces sizable effects in the first and third lepton generations. In the most general approach, where all entries of the leptoquark flavor couplings are treated as free parameters that are constrained only by the $R_{K^{(*)}}$ data (7.8) and experimental upper bounds, it is currently not possible to determine the dominant collider signatures. Hence, we consider generalized benchmark flavor patterns that provide predictions for the entries marked with "$*$" in the simple pattern.

Besides the L_μ and $\tilde{L}_\mu$ patterns derived from flavor models, we employ the more general "flavor data" structure [176]

$$Y_{\rm FD} = Y_0 \begin{pmatrix} \rho_d\kappa_e & \rho_d & \rho_d\kappa_\tau \\ \rho\kappa_e & \rho & \rho\kappa_\tau \\ \kappa_e & 1 & \kappa_\tau \end{pmatrix} . \tag{7.14}$$

The hierarchy of the individual quark generations is parametrized by $\rho_d = Y_{d\ell}/Y_{b\ell}$ and $\rho = Y_{s\ell}/Y_{b\ell}$, while κ_e and κ_τ parametrize the column structure of the pattern with the second lepton generation as a reference point. Assuming $\kappa_\tau \simeq 1$ the phenomenologically viable range for these parameters is [176]

$$\rho_d \lesssim 0.02\,, \quad \kappa_e \lesssim 0.5\,, \quad 10^{-4} \lesssim \rho \lesssim 1\,, \quad \kappa_e/\rho \lesssim 0.5\,, \quad \rho_d/\rho \lesssim 1.6\,. \tag{7.15}$$

The limit on the ratio κ_e/ρ can be improved to about 0.2 by upcoming results from the MEG experiment [126].

In Table 7.1 we show the branching ratios for the leptoquark component $S_3^{-4/3}$ decaying to $b\ell$ and $j\ell$ final states, where $\ell = e, \mu, \tau$, for each of the flavor benchmark scenarios at leading order in the vevs c_ℓ, c_ν, κ and the flavor parameters ρ, ρ_d, k_e. These results can also be used to estimate the potential signal strength of leptoquark pair production. The branching ratios of the related $S_3^{-1/3}$ component are given by

$$\begin{aligned} &\mathcal{B}(S_3^{-1/3} \to t\ell)\,, \mathcal{B}(S_3^{-1/3} \to b\nu) \simeq \mathcal{B}(S_3^{-4/3} \to b\ell)/2 \\ &\mathcal{B}(S_3^{-1/3} \to j\ell)\,, \mathcal{B}(S_3^{-1/3} \to j\nu) \simeq \mathcal{B}(S_3^{-4/3} \to j\ell)/2\,. \end{aligned} \tag{7.16}$$

Note that for vector leptoquarks, which couple to $\bar{Q}L$ rather than QL, the $\tilde{L}_\mu$ pattern receives no suppression by κ, as can be seen in (6.21). Apart from that, the predictions

	$b\mu\mu$	$be\mu$	$b\tau\mu$	bee	$be\tau$	$b\tau\tau$
L_μ	c_ℓ^2	$c_\ell^2\delta^2$	$c_\ell^2\delta^2$	$c_\ell^2\delta^4$	$c_\ell^2\delta^4$	$c_\ell^2\delta^4$
$\tilde{L}_\mu$	c_ℓ^2	$c_\ell^2\delta^2$	$c_\ell^2\delta^2$	$c_\ell^2\delta^4$	$c_\ell^2\delta^4$	$c_\ell^2\delta^4$
$Y_{\rm FD}$	$\lambda_0^2/2$	$\lambda_0^2\kappa_e^2/2$	$\lambda_0^2/2$	$\lambda_0^2\kappa_e^4/2$	$\lambda_0^2\kappa_e^2/2$	$\lambda_0^2/2$

(a) $b\ell\ell'$ final states

	$j\mu\mu$	$je\mu$	$j\tau\mu$	jee	$je\tau$	$j\tau\tau$
L_μ	$c_\ell^2\lambda^4$	$c_\ell^2\delta^2\lambda^4$	$c_\ell^2\delta^2\lambda^4$	$c_\ell^2\delta^4\lambda^4$	$c_\ell^2\delta^4\lambda^4$	$c_\ell^2\delta^4\lambda^4$
$\tilde{L}_\mu$	$(c_\nu\kappa)^2$	$(c_\nu\kappa)^2$	$(c_\nu\kappa)^2$	$(c_\nu\kappa\delta)^2$	$(c_\nu\kappa\delta)^2$	$(c_\nu\kappa\delta)^2$
$Y_{\rm FD}$	$\lambda_0^2\rho^2/2$	$\lambda_0^2\rho^2\kappa_e^2/2$	$\lambda_0^2\rho^2/2$	$\lambda_0^2\rho^2\kappa_e^4/2$	$\lambda_0^2\rho^2\kappa_e^2/2$	$\lambda_0^2\rho^2/2$

(b) $j\ell\ell'$ final states

Table 7.2.: Parametric dependence of the single leptoquark induced cross sections $\sigma(pp \to b\ell\ell')$ and $\sigma(pp \to j\ell\ell')$ for the three flavor benchmark patterns.

for vector leptoquark branching ratios are analogous and are related as e.g. $\mathcal{B}(V_1 \to b\ell) \simeq \mathcal{B}(S_3^{-4/3} \to b\ell)/2$.

Table 7.2 shows the parametric single leptoquark production cross section for final states with bottom quarks (a) and jets (b) within the three flavor benchmark scenarios. For these estimates we employ the narrow width approximation

$$\sigma(pp \to S_3(\to q\ell)\ell) = \sigma(pp \to S_3\ell)\ \mathcal{B}(S_3 \to q\ell)\,. \tag{7.17}$$

While both the L_μ and the $\tilde{L}_\mu$ pattern yield the same hierarchies for final states involving bottom quarks, jet signals are enhanced with the $\tilde{L}_\mu$ pattern in which the FN suppression of the second quark generation is lifted. Dielectron signals are strongly suppressed for both flavor patterns. Predictions based on the third flavor benchmark pattern $Y_{\rm FD}$ depend on the size of the parameters k_e and ρ, which is restricted but not completely fixed by the currently available data, see (7.15). The two extreme cases are:

(i) Both k_e and ρ are of order one. In this case either the coupling Y_0 has to be small or the leptoquark mass has to be very large in order not to exceed experimental bounds. Both options lead to strongly suppressed $pp \to b\mu\mu$ signals that are too small to be detected at the LHC.

(ii) Both k_e and ρ are very small. This means that Y_0 can be large while leptoquark masses remain in the TeV range and that final states with jets or electrons are strongly suppressed.

In limit (ii) the collider phenomenology of the Y_{FD} benchmark pattern concerning modes with jets or electrons becomes similar to that of the L_μ and $\tilde{L}_\mu$ patterns. Stronger constraints on the parameter k_e can be obtained from studies of $b \to s e^+ e^-$ processes. As discussed in Section 3.4, a well suited set of observables with small theoretical uncertainties can be found in the angular distribution of $B \to K^*(\to K\pi) e^+ e^-$ decays [114].

If couplings to charged leptons other than the muon are large, leptoquark single production associated with the $R_{K^{(*)}}$ data is affected in two ways: On the one hand, the cross section $\sigma(pp \to S_3(\to b\mu)\mu)$ decreases due to the enlarged branching ratio of the leptoquark decay channel involving the other lepton(s). On the other hand, cLFV signatures such as $pp \to S_3(\to b\mu)\tau$ and $pp \to S_3(\to b\tau)\mu$ are induced in the case of a sizable coupling to tau leptons. Complementary searches for $B \to K^{(*)}\mu\tau$ decays can prove useful in this case.

The single leptoquark production signature $pp \to t\mu^+\mu^-$ is suppressed with respect to $pp \to b\mu\mu$ in all three flavor benchmark scenarios. This is due to the fact that the coupling to the charm quark, which is necessarily involved in the production of the $pp \to t\mu\mu$ signature, is suppressed in every pattern. For L_μ, $\tilde{L}_\mu$ and Y_{FD} the relative suppression is given by ϵ^4, $(c_\nu \kappa / c_\ell)^2$ and ρ^2, respectively. To leading order in the vevs and flavor parameters the cross sections $\sigma(pp \to t\mu\nu)$ and $\sigma(pp \to b\nu\nu)$ are as large as $\sigma(pp \to b\mu\mu)$ across all benchmarks.

7.4. Collider Phenomenology of Vector Leptoquarks

For the vector leptoquarks $V_1(\mathbf{3}, \mathbf{1}, 2/3)$, $V_3(\mathbf{3}, \mathbf{3}, 2/3)$ we follow a similar approach as for the scalar leptoquark discussed before. However, we focus on the simplified coupling pattern (7.7) and study variations thereof.

We work out bounds on the masses of vector leptoquarks using available search results for pair production of leptoquarks from ATLAS [193] (Section 7.4.3), and cross sections for future pp colliders in Section 7.4.4. We consider three setups corresponding to center of mass energies $\sqrt{s}$: 14 TeV (LHC run 3), 27 TeV (HE-LHC), and 100 TeV (FCC-hh) [191] with target integrated luminosities of $\mathcal{L} = 3\,\text{ab}^{-1}$, $15\,\text{ab}^{-1}$ and $20\,\text{ab}^{-1}$, respectively. In Section 7.4.5 we briefly discuss the resonant production mechanism, for which theoretical predictions have become possible recently. We analyze the mass reach of future pp colliders by extrapolating current limits on cross sections to higher center of mass energies and luminosities in Section 7.4.6.

7.4.1. Benchmark Flavor Patterns

In the following we consider three benchmark scenarios with coupling textures that couple the vector leptoquark predominantly to the second lepton generation.

Hierarchical scenario We start from the simplified, or "hierarchical" scenario (7.7) studied before, for which the unknown $\mathcal{O}(1)$ factors yield the range provided in (7.8).

Flipped scenario As a second scenario, we consider the inverted form of the previous texture, that is:

$$Y_{\bar{Q}L} \sim Y_0 \begin{pmatrix} 0 & 0 & 0 \\ * & 1 & * \\ * & \epsilon^2 & * \end{pmatrix} . \tag{7.18}$$

This yields the same effect in $b \to s\ell^+\ell^-$ transitions as the hierarchical pattern while enhancing the single production cross section due to the larger PDF of the strange quark. We obtain the same coupling range for Y_0 as in the hierarchical scenario given in (7.8).

Note that this pattern has a weaker foundation in flavor models and can potentially receive mixing induced contributions to the first quark generations at order ϵ if it is introduced in the interaction basis.

Democratic scenario Lastly, we consider a texture where the couplings to the second and third quark generation are of equal size:

$$Y_{\bar{Q}L} \sim Y_0 \begin{pmatrix} 0 & 0 & 0 \\ * & 1 & * \\ * & 1 & * \end{pmatrix} . \tag{7.19}$$

In this case the $R_{K^{(*)}}$ data (7.6) together with the unknown $\mathcal{O}(1)$ factors imply

$$M_V/70\,\text{TeV} \lesssim Y_0 \lesssim M_V/23\,\text{TeV} . \tag{7.20}$$

In each scenario there are four parameters, namely the leptoquark mass M_V, the parameter κ, and the dominant couplings $Y_{b\mu}$ and $Y_{s\mu}$. In order to determine all of these parameters, it suffices to measure the single or pair production cross section, the corresponding branching fractions and the resonance width including the reconstruction of the mass peak. Note that such an analysis requires b-tagging.

Allowing for significant entries "$*$" in the patterns (7.7), (7.18), (7.19) would open up further leptoquark decay modes and search channels, and reduce branching ratios in the signal channels studied here. Hence, negligible entries "$*$" correspond to the most favorable situation for an observation in the muon channel.

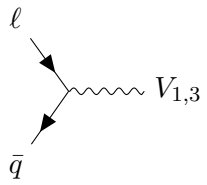

Figure 7.5.: Resonant leptoquark production.

7.4.2. Vector Leptoquark Production and Decay

We consider three dominant mechanisms of vector leptoquark production at pp colliders: pair production, single production in association with a lepton and resonant production induced by quark-lepton fusion, shown in Figures 7.3, 7.2b and 7.5, respectively.

The flavor scenarios (7.7), (7.18), (7.19) can be distinguished experimentally by different patterns of the final states in leptoquark two-body decays. For the hierarchical scenario (7.7) the dominant leptoquark decay modes are given in (7.12) and (7.13) for the singlet and triplet vector leptoquarks, respectively.

In the flipped scenario (7.18) the leading signatures involve charm and strange quarks

$$V_1^{+2/3} \to s\mu^+\,,\; c\bar{\nu}\,, \tag{7.21}$$

for the singlet and

$$\begin{aligned} V_3^{-1/3} &\to s\bar{\nu}\,, \\ V_3^{+2/3} &\to s\mu^+\,,\; c\bar{\nu}\,, \\ V_3^{+5/3} &\to c\mu^+\,, \end{aligned} \tag{7.22}$$

for the triplet.

In the democratic scenario (7.19) all of the aforementioned modes arise and final states with both light and heavy quarks are relevant. Note that the unknown $\mathcal{O}(1)$ factors can strongly impact the relative size of the possible final state branching ratios as $\mathcal{B} \sim |Y_{\bar{Q}\ell}|^2$. Approximate branching ratios for the benchmark patterns (7.7), (7.18), (7.19) are given in Table 7.3.

In Figure 7.6 we show the pair- and single production cross sections as functions of κ for the example of a vector leptoquark with mass $M_{V_1} = 3\,\text{TeV}$ at the HL-LHC with a center of mass energy of $\sqrt{s} = 14\,\text{TeV}$. The cross sections exhibit minima for κ in the vicinity of 0 or -1, see also [194]. Within the mass range suitable for a 14 TeV collider, the shape of these curves only mildly depends on the leptoquark mass.

	$b\mu^+$	$t\bar{\nu}$	$s\mu^+$	$c\bar{\nu}$
hierarchical	1/2	1/2	0	0
flipped	0	0	1/2	1/2
democratic	1/4	1/4	1/4	1/4

(a) V_1 and triplet component $V_3^{2/3}$.

	$b\bar{\nu}$ $(t\mu^+)$	$s\bar{\nu}$ $(c\mu^+)$
hierarchical	1	0
flipped	0	1
democratic	1/2	1/2

(b) $V_3^{-1/3}$ $(V_3^{+5/3})$.

Table 7.3.: Branching fractions of the V_1 and V_3 leptoquarks in the benchmark scenarios from Section 7.4.1.

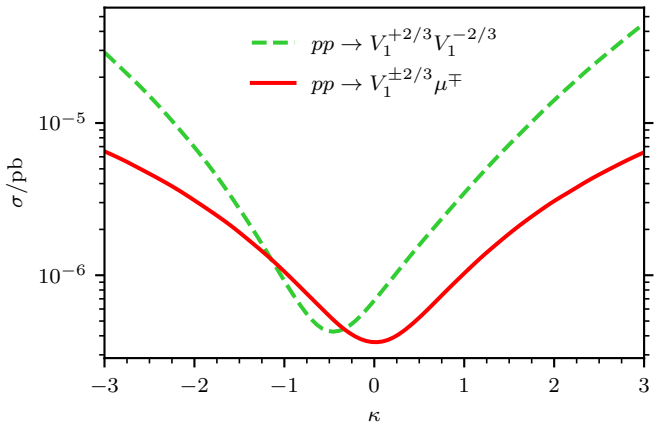

Figure 7.6.: κ-dependence (7.1) of the single- (red, solid) and pair production cross section (green, dashed) for V_1. We fix $\sqrt{s} = 14\,\text{TeV}$ and $M_{V_1} = 3\,\text{TeV}$. For the single production cross section we employ the hierarchical scenario. Analogous results are obtained for other choices of the parameters and flavor benchmarks.

7.4.3. Current Vector Leptoquark Mass Bounds

Leptoquark-based explanations of the B anomalies motivated a recent search for pair produced scalar leptoquarks with $139\,\text{fb}^{-1}$ of data from 13 TeV pp collisions at the ATLAS experiment [195]. This search imposes lower mass bounds of 1470 GeV (1480 GeV) on scalar leptoquarks that predominantly decay to a top quark and an electron (muon). Such final states appear in decays of the scalar (vector) $SU(2)_L$ triplet leptoquark S_3 (V_3). Previously derived collider bounds on vector leptoquarks from pair production searches are $M_{V_1} > 1.3\,\text{TeV}$ for dominant decays to τb, and $M_{V_1} > 1.7\,\text{TeV}$ in the μb channel [196], in the case of $\kappa = 1$.

We evaluate the current lower mass bounds on the V_1 leptoquark by reinterpreting limits imposed on the pair production cross sections of scalar leptoquarks by the ATLAS search [193], which uses data collected in the 13 TeV LHC run with a luminosity of $\mathcal{L} = 139\,\text{fb}^{-1}$. For the hierarchical scenario we use the limits obtained in the $(b\mu, b\mu)$-channel while for the flipped scenario we use the $(q\mu, q\mu)$-channel. The role of q in the latter channel is played in our model by the strange quark. In order to obtain the V_1 mass limits we compare the theoretical cross sections for V_1 pair production and subsequent decay into the corresponding final state channels to the ATLAS data as shown in Figure 7.7 (left). The resulting bounds are the same for the hierarchical and flipped scenarios, as the experimental limits for the cross sections to $(b\mu, b\mu)$- and $(s\mu, s\mu)$ final states nearly coincide in the region of large leptoquark masses. We find mass limits of $(1.7 \pm 0.1)\,\text{TeV}$ and $(2.0 \pm 0.1)\,\text{TeV}$ for $\kappa = 0$ and $\kappa = 1$, respectively, in this case. For the democratic scenario we employ the experimental results for the $(b\mu, b\mu)$ channel as they provide stricter bounds in the relevant mass range than the $(q\mu, q\mu)$ channel. We find slightly weaker limits of $(1.5 \pm 0.1)\,\text{TeV}$ and $(1.8 \pm 0.1)\,\text{TeV}$ for $\kappa = 0$ and $\kappa = 1$, respectively, owing to the smaller branching ratios of the $b\mu$ and $s\mu$ final states, shown in Table 7.3.

In the hierarchical scenario the mass limits imposed by the ATLAS data on V_1 also apply for the triplet V_3 because only the diagonal component $V_3^{2/3}$, whose quantum numbers are the same as those of V_1, gives a relevant contribution. Due to additional contributions to $(c\mu, c\mu)$ final states from the $V_3^{\pm 5/3}$ components with $\mathcal{B}(V_3^{5/3} \to c\mu^+) \sim 1$, we find stronger limits in the case of the flipped scenario. For $\kappa = 0$ and $\kappa = 1$ we find the mass limits $(2.0 \pm 0.1)\,\text{TeV}$ and $(2.3 \pm 0.1)\,\text{TeV}$, respectively. The $(c\mu, c\mu)$ channel also provides the strongest bound for the democratic scenario, where we find the limits $(1.7 \pm 0.1)\,\text{TeV}$ and $(2.0 \pm 0.1)\,\text{TeV}$.

In Figure 7.7 (right) we show the κ dependence of the mass bounds for the V_1 leptoquark in the hierarchical and flipped scenarios. The weakest bounds on the V_1 mass are obtained for $\kappa = -0.3$, where the pair production cross section reaches its minimum (see also Figure 7.6). In the hierarchical and flipped scenarios we find $M_{V_1} > 1.6\,\text{TeV}$ for this value of κ. However, the lowest mass bound is reached in the democratic scenario, where the

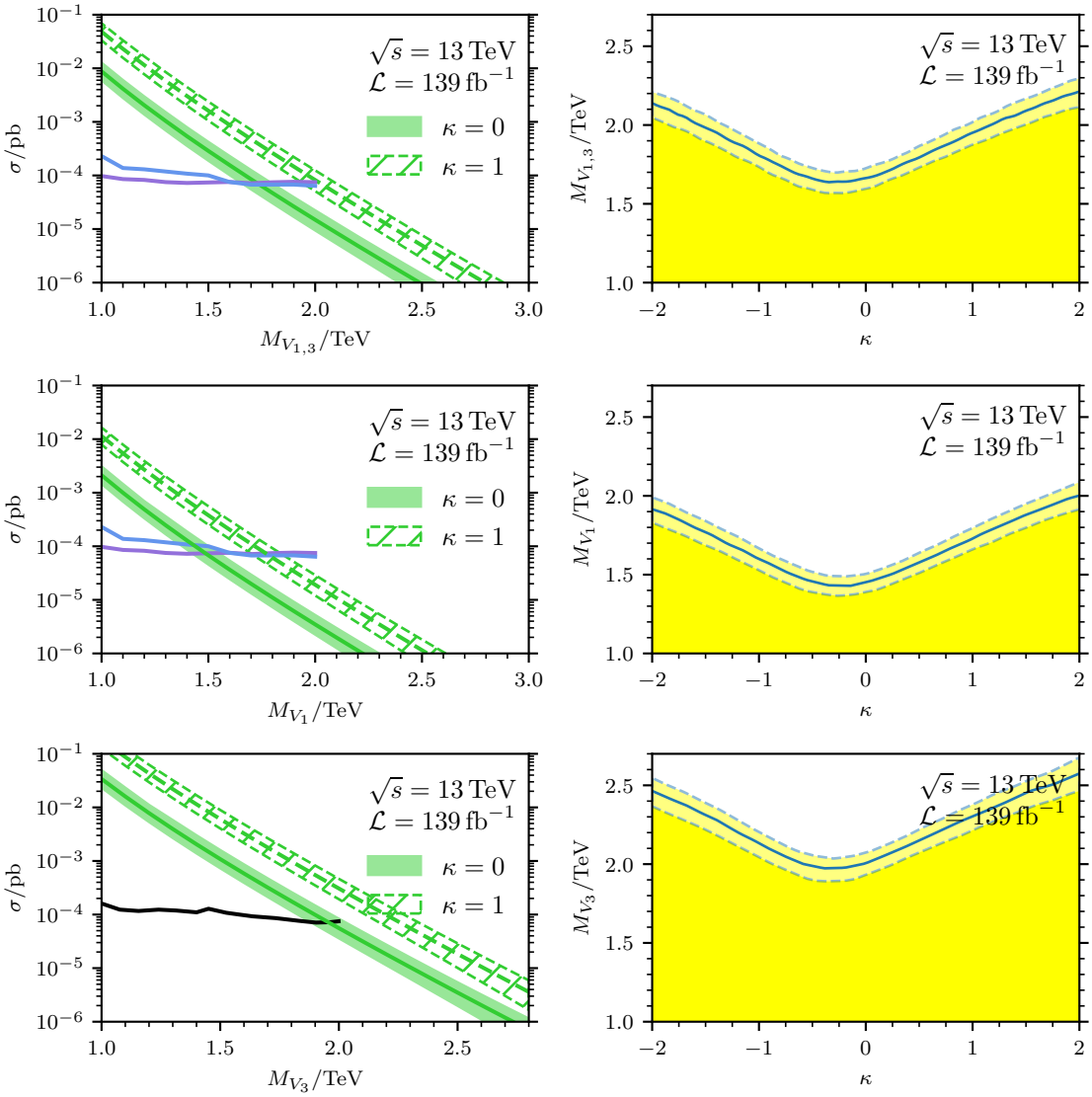

Figure 7.7.: Sensitivity and mass bounds from reinterpretation of a current ATLAS search [193]. Top row: V_1 in the hierarchical and flipped flavor scenarios, which equals V_3 in the hierarchical and democratic flavor scenarios. Middle row: V_1 in the democratic scenario, and bottom row: V_3 in the flipped scenario. Left: Sensitivity to V_1, V_3-pair production, assuming dominant decays to μb, μq and μc in purple, blue and black, respectively; q denotes quarks lighter than the charm quark. The green bands indicate the theory prediction including the pdf- and scale uncertainties, for $\kappa = 0$ (solid) and $\kappa = 1$ (dashed). Right: Mass bounds for the leptoquarks V_1, V_3 as a function of κ. The boundary of the excluded region is represented by the band whose width results from the pdf- and scale uncertainties.

ATLAS data imposes $M_{V_1} > 1.4\,\text{TeV}$. The corresponding weakest bound on the V_3 mass arises in the hierarchical scenario and reads $M_{V_3} > 1.6\,\text{TeV}$.

7.4.4. Single and pair production cross sections

We evaluate the leading order cross sections for the single production of V_1 in association with a muon, represented by the first two diagrams in Figure 7.2b, as functions of the leptoquark mass. We neglect non-resonant contributions as shown in the third diagram, assuming that they can be removed by appropriate kinematic cuts. The results are shown in the form of solid (hatched) red bands for $\kappa = 0$ ($\kappa = 1$) in Figures 7.8 and 7.9 for V_1 and V_3, respectively. The band widths correspond to the ranges given in (7.8) and (7.20), which stem from the unknown $\mathcal{O}(1)$ factors. Likewise, the solid and hatched green bands display the leading order pair production cross sections including subsequent resonant decay.

Pair production is predominantly induced by QCD interactions and is hence essentially independent of the flavor structure of the leptoquark couplings. As an exception to this, the contribution stemming from the third diagram in Figure 7.3 can become sizable for large leptoquark masses within the flipped scenario, as can be seen in the last plot of the second row in Figure 7.8. This is due to the fact that the $R_{K^{(*)}}$ constraint drives $Y_{s\mu}$ to large values close to the limit of perturbativity.

The magnitude of the single production cross section induced by $qg \to V_1^{2/3}\ell$ at parton level is directly proportional to the square of the magnitude of the corresponding flavor coupling $Y_{\bar{Q}\ell}$. Assuming the narrow width approximation, we multiply the corresponding production cross sections by the corresponding branching fractions given in Table 7.3. Since there are no available single production searches involving b quarks in the final state, we add the contributions involving jets and b quarks which amounts to the branching fraction 1/2 for each of the three flavor scenarios.

7.4.5. Resonant production

Recent advances in the determination of the lepton PDFs [197] have opened up the possibility to study resonant leptoquark production from quark–lepton fusion in pp collisions [198], as depicted in Figure 7.5. Next-to-leading-order QCD and QED corrections to the resonant production of scalar leptoquarks have recently become available [199].

In order to estimate the resonant V_1 production cross section in our flavor benchmark scenarios (7.7), (7.18) and (7.19), we employ the `LUXlep-NNPDF31_nlo_as_0118_luxqed` [197] PDF set. Numerical results for a $\sqrt{s} = 14\,\text{TeV}$ pp collider are shown in Figure 7.5. Due to the much smaller phase space suppression, the resonant cross section is larger than those of pair and single production.

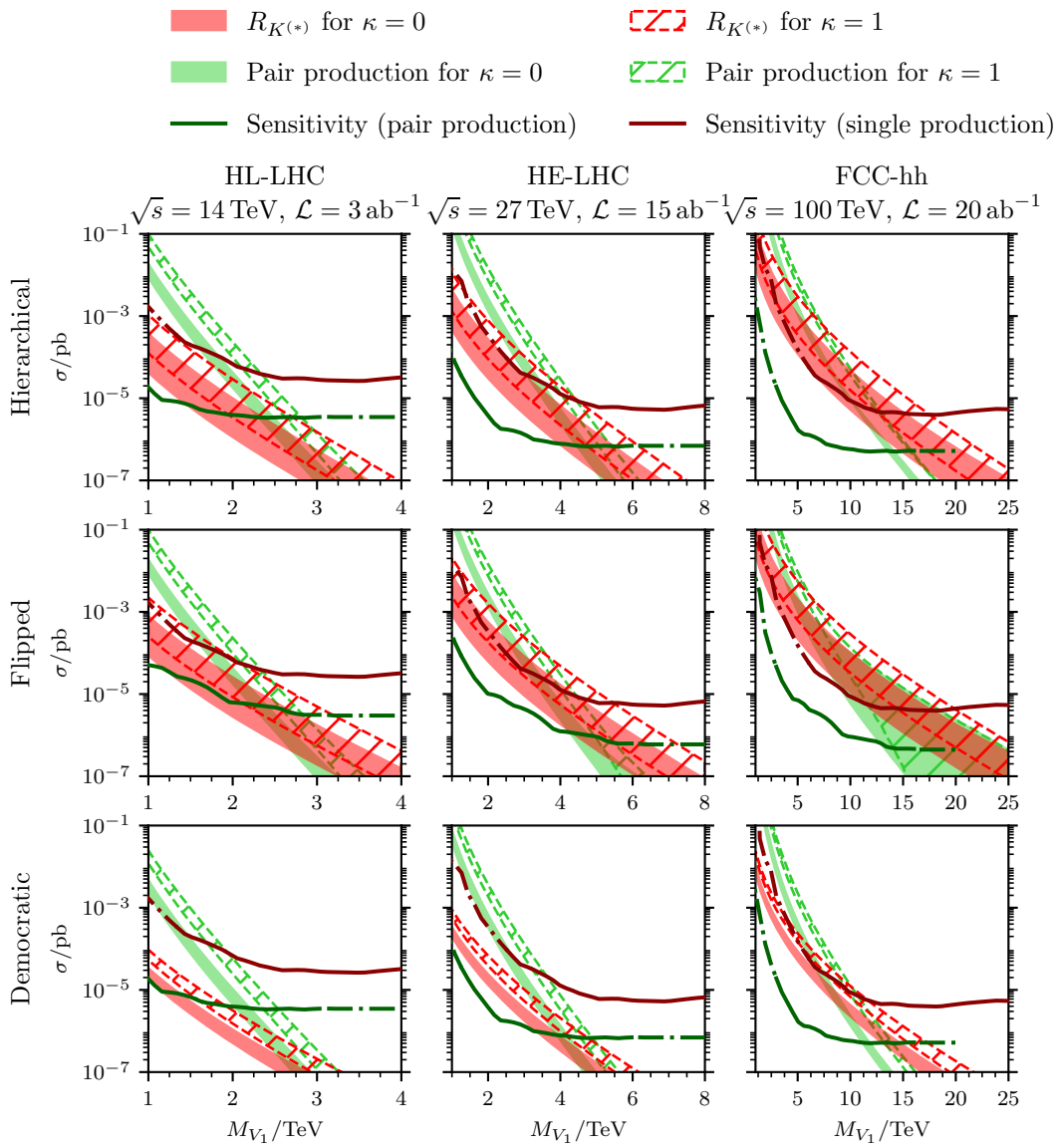

Figure 7.8.: V_1-leptoquark production in pp-collisions in the flavor scenarios introduced in Section 7.4.1 (rows) for different future collider experiments (columns). Red bands: Single production cross section for $\sigma(pp \to V_1^{\pm 2/3}(\to \mu^{\pm} b)\mu^{\mp}) + \sigma(pp \to V_1^{\pm 2/3}(\to \mu^{\pm} j)\mu^{\mp})$, derived from the $R_{K^{(*)}}$-band in (7.8) for hierarchical and flipped scenarios, and (7.20) for the democratic scenario. Light green: pair production with final states $(b\mu, b\mu)$ for the hierarchical and democratic scenarios and $(q\mu, q\mu)$ for the flipped scenario. The error bands for pair production are evaluated by combining the PDF-, and scale uncertainties. Results for $\kappa = 1$ are shown in a dashed/hatched form together with the solid curves for $\kappa = 0$. The solid dark red and the dark green curves depict the projected experimental sensitivity for single and pair production, respectively. See Section 7.4.6 for details.

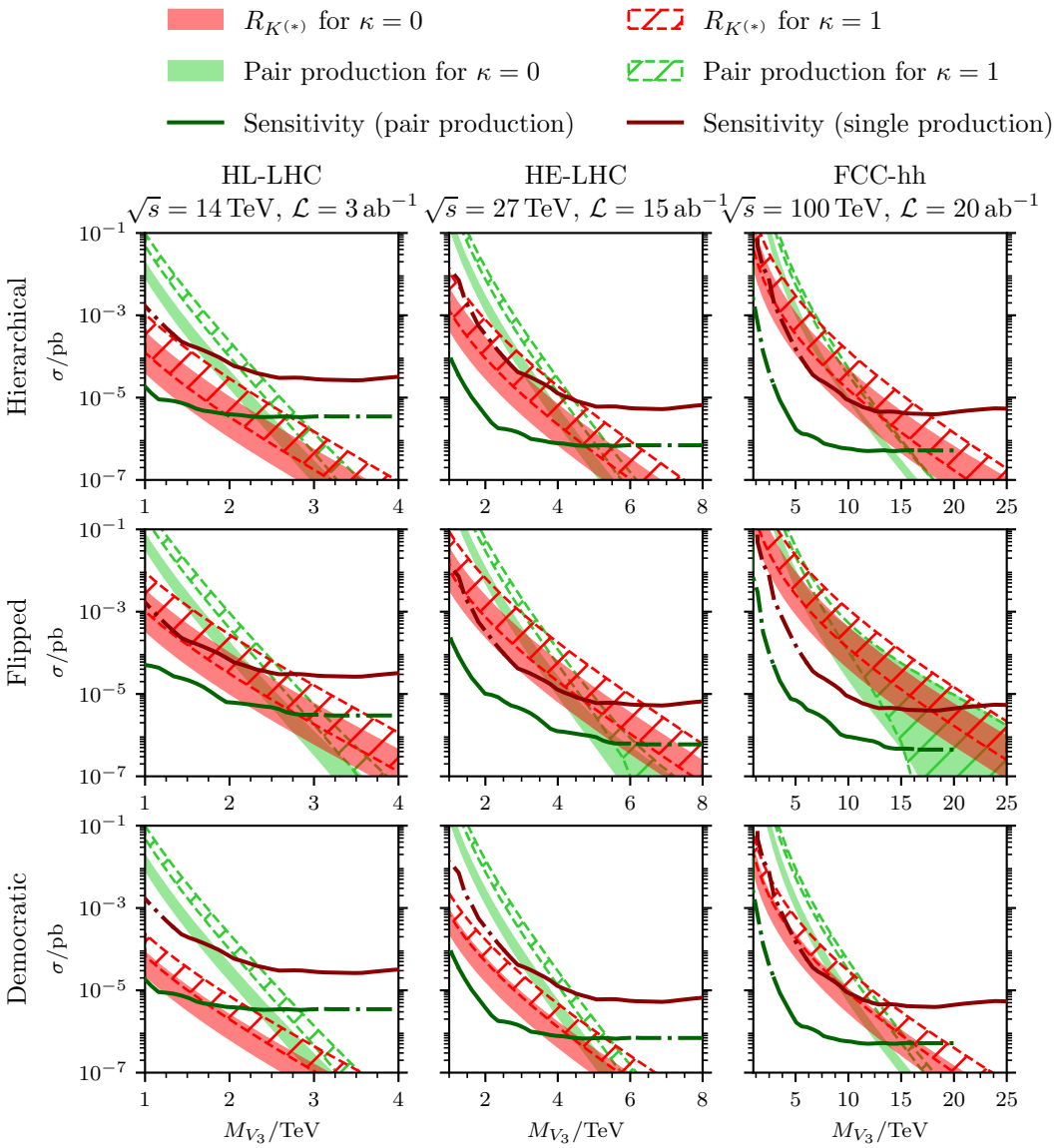

Figure 7.9.: V_3-leptoquark production in pp-collisions in the flavor scenarios introduced in Section 7.4.1 (rows) for different future collider experiments (columns). Red bands: Single production cross section for $\sigma(pp \to \mu^+\mu^- j)$ induced by the triplet V_3, derived from the $R_{K^{(*)}}$-band in (7.8) for hierarchical and flipped scenarios, and (7.20) for the democratic scenario. Light green: pair production with final states $(b\mu, b\mu)$ for the hierarchical and democratic scenarios and $(c\mu, c\mu)$ for the flipped scenario. The error bands for pair production are evaluated by combining the PDF-, and scale uncertainties, see Figure 7.8 and Section 7.4.6 for details.

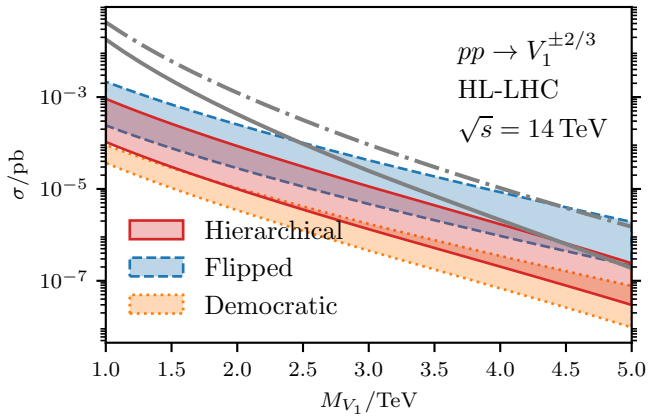

Figure 7.10.: Resonant leptoquark production cross section from lepton-quark fusion for the flavor scenarios (7.7), (7.18), (7.19) at the HL-LHC. The solid (dash-dotted) grey line indicates the resonant cross section with only the $b\mu$ ($s\mu$) coupling set to one.

In Figure 7.11 we compare the cross sections of the resonant and single production for V_1 masses up to $\sim 10\,\text{TeV}$. In the regions of the M_{V_1}–$\sqrt{s}$ plane to the right of the thick blue lines the resulting resonant cross section is larger than the one for single production. Currently, the lepton PDF uncertainties are too large to allow for extrapolations to larger center of mass energies.

7.4.6. Sensitivity Projections for Future Colliders

In order to estimate the mass reach of the future colliders for the flavor benchmark scenarios, we extrapolate existing bounds from single- and pair production using the limit extrapolation method following [200, 201]. The method assumes that the exclusion limits are determined by the numbers of background events and involves the appropriate re-scaling of the background processes with the corresponding parton luminosity functions, see [200, 201] for more details. We expect the method to be less suitable for the case of leptoquarks than for the case of s-channel resonances, for which it was initially used [200], however, it should provide a correct estimate of the order of magnitude for the collider limits on the corresponding cross sections.

As the starting point for our approximation of the future sensitivity projections for single production searches, we employ the limits obtained by the CMS collaboration at a center of mass energy of $\sqrt{s} = 8\,\text{TeV}$ and with an integrated luminosity of $\mathcal{L} = 19.6\,\text{fb}^{-1}$ [181]. In our extrapolations, we assume that the b quark in the final state is not tagged but rather counted as a light jet and thus contributes to the $j\mu\mu$ final states considered in the CMS search. We emphasize that b-tagging is necessary to distinguish between our

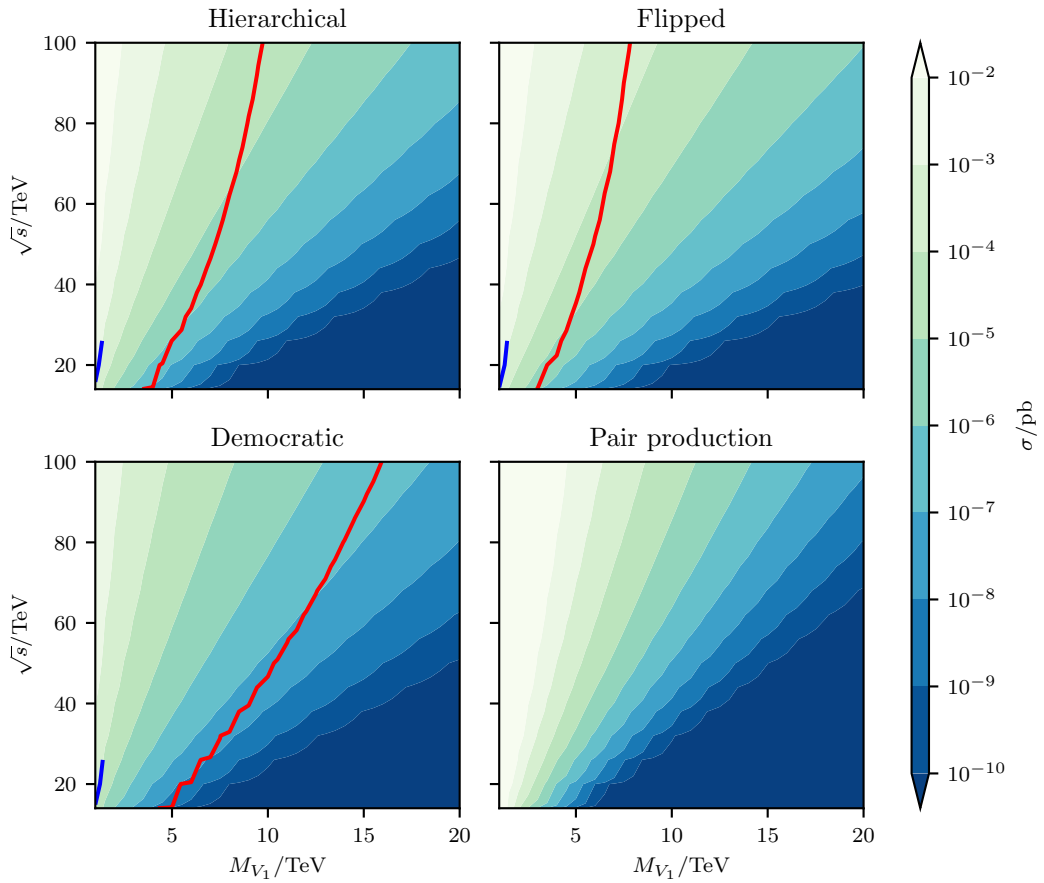

Figure 7.11.: Single leptoquark production cross section for V_1 depending on the center of mass energy $\sqrt{s}$, and the leptoquark mass M_{V_1}. For each scenario we use the central value of the allowed ranges from (7.8), (7.20). In the regions to the right of the red lines the single leptoquark production cross section is larger than the pair production cross section. In the regions to the right of the blue lines (up to $M_{V_1} \sim 10\,\text{TeV}$) the resonant leptoquark production cross section is larger than the single production one, see text. In the plot to the lower right we show in addition the pair production cross section $\sigma(pp \to V_1^{+2/3} V_1^{-2/3})$. All plots are for $\kappa = 0$.

Collider	$\sqrt{s}$/TeV	$\mathcal{L}$ /ab^{-1}	hierarchical	flipped	democratic	pair
Mass reach for $\kappa = 0$						
HL-LHC	14	3	—	(2.3)	—	2 (3)
HE-LHC	27	15	2.7	4.4 (5.6)	—	5 (5)
FCC-hh	100	20	15.1	17.7 (20.5)	(10.7)	13 (15)
Mass reach for $\kappa = 1$						
HL-LHC	14	3	—	2.1 (2.8)	—	3 (3)
HE-LHC	27	15	4.5	5.5 (6.4)	—	5 (6)
FCC-hh	100	20	17.5	19.9 (22.7)	11.7 (14.0)	15 (18)

Table 7.4.: Mass reach in TeV for vector leptoquark single production in the hierarchical, flipped and democratic scenarios from Section 7.4.1 and pair production, at different future colliders for $\kappa = 0$ and $\kappa = 1$. For single production we provide the mass reaches corresponding to the upper limit of the cross section band resulting from (7.8) and (7.20). In the flipped and democratic scenarios as well as for pair production we show the increased mass reaches for V_3 in parentheses, for the hierarchical scenario the V_1,V_3 reaches are the same, see text for details.

flavor benchmark textures and can potentially yield stronger limits in the hierarchical and democratic scenarios.

For the extrapolations of the limits on the pair production cross sections we use results from the ATLAS collaboration performed at 13 TeV with $\mathcal{L} = 139\,\text{fb}^{-1}$ [193]. We further employ the leading order PDF sets provided by the MSTW collaboration [202] and use the `NNPDF23_lo_as_0130_qed` PDF set [203] as a cross check. As mentioned previously in Section 7.4.3, for the hierarchical and democratic scenarios we consider the $(b\mu, b\mu)$-channel, while the $(q\mu, q\mu)$-channel is used in the case of the flipped scenario, where q corresponds to the strange quark. We compare the extrapolations of the sensitivity limits for the single and pair production cross sections with their respective theoretical predictions for the V_1 leptoquark in Figure 7.8. The results for V_3 are depicted in Figure 7.9.

In Table 7.4 we list the possible mass reaches at future colliders for the V_1 leptoquark in each of the three flavor benchmark scenarios for both single and pair production. Additionally, we provide the reach for V_3 in parentheses if it differs from the V_1 result.

The cross sections of V_3 are larger than the ones of V_1 in the flipped and democratic scenario, due to the contributions from the additional components in the $SU(2)_L$ triplet. In the hierarchical flavor scenario the dominant contribution stems from b quarks and

involves only the $V_3^{2/3}$ component, which makes the cross section equal to that of the singlet.

We estimate the single production cross section of V_3 with a $pp \to j\mu\mu$ signature in the flipped and democratic scenarios using $\sigma(pp \to V_3^{2/3}\mu^-) = \sigma(pp \to V_1^{2/3}\mu^-)$ and including the contribution from $cg \to V_3^{5/3}(\to j\mu^+)\mu^-$. In case of the flipped scenario we find

$$\begin{aligned}\sigma_{V_3}^{\text{Flipped}}(pp \to j\mu\mu) = 2\big[&\sigma(sg \to V_3^{2/3}\mu^-)\mathcal{B}(V_3^{2/3} \to s\mu^+) \\ &+ \sigma(cg \to V_3^{5/3}\mu^-)\mathcal{B}(V_3^{5/3} \to c\mu^+)\big]\,,\end{aligned} \tag{7.23}$$

where the factor of 2 stem from adding the CP-conjugate of the process. Assuming that the PDFs for the strange and charm quarks are roughly the same, i.e. $\sigma(sg \to V_3^{2/3}\mu^-) \simeq (\sqrt{2})^2\,\sigma(cg \to V_3^{5/3}\mu^-)$, where the $(\sqrt{2})^2$ is an isospin factor. Using the branching ratios given in Table 7.3, we find $\sigma_{V_3}^{\text{Flipped}}(pp \to j\mu\mu) \simeq 5\,\sigma_{V_1}^{\text{Flipped}}(pp \to j\mu\mu)$. An explicit numerical evaluation shows that the ratio $\sigma_{V_3}^{\text{Flipped}}(pp \to j\mu\mu)/\sigma_{V_1}^{\text{Flipped}}(pp \to j\mu\mu)$ decreases with larger leptoquark masses, and lies within the range between 4 and 2.5 for values of $\sqrt{s}$ and M_V relevant for this study.

For the democratic scenario we find

$$\begin{aligned}\sigma_{V_3}^{\text{Democratic}}(pp \to j\mu\mu) = 2\big[&\sigma(bg \to V_3^{2/3}\mu^-)\mathcal{B}(V_3^{2/3} \to (b,s)\mu^+) \\ &+ \sigma(sg \to V_3^{2/3}\mu^-)\mathcal{B}(V_3^{2/3} \to (b,s)\mu^+) \\ &+ \sigma(cg \to V_3^{5/3}\mu^-)\mathcal{B}(V_3^{5/3} \to c\mu^+)\big]\,.\end{aligned} \tag{7.24}$$

Assuming $\sigma(sg \to V_3^{2/3}\mu^-) = 4\,\sigma(bg \to V_3^{2/3}\mu^-)$ results in $\sigma_{V_3}^{\text{Democratic}}(pp \to j\mu\mu) \simeq 2.5\,\sigma_{V_1}^{\text{Democratic}}(pp \to j\mu\mu)$, while a numerical evaluation shows that the ratio drops from 2.5 to about 1.5 throughout the relevant mass range. Numerical results from explicit evaluations of $\sigma(cg \to V_3^{5/3}\mu^-)$ are included in Fig. 7.9.

In Figure 7.12 we compare the expectations for the single production cross sections for the flavor scenarios and different future collider experiments; the values span up to two orders of magnitude. An observation of a single production signal with a cross section that is much larger than those shown here would point to a leptoquark that is unrelated to the $R_{K^{(*)}}$ anomalies.

The comparison of the single and pair production cross sections in Figure 7.11 shows that pair production is instrumental for the discovery or exclusion of vector leptoquarks in the mass region of a few TeV. Leptoquark single production cross sections exceed corresponding pair production cross sections for large leptoquark masses in the parameter regions to the right of the solid red lines.

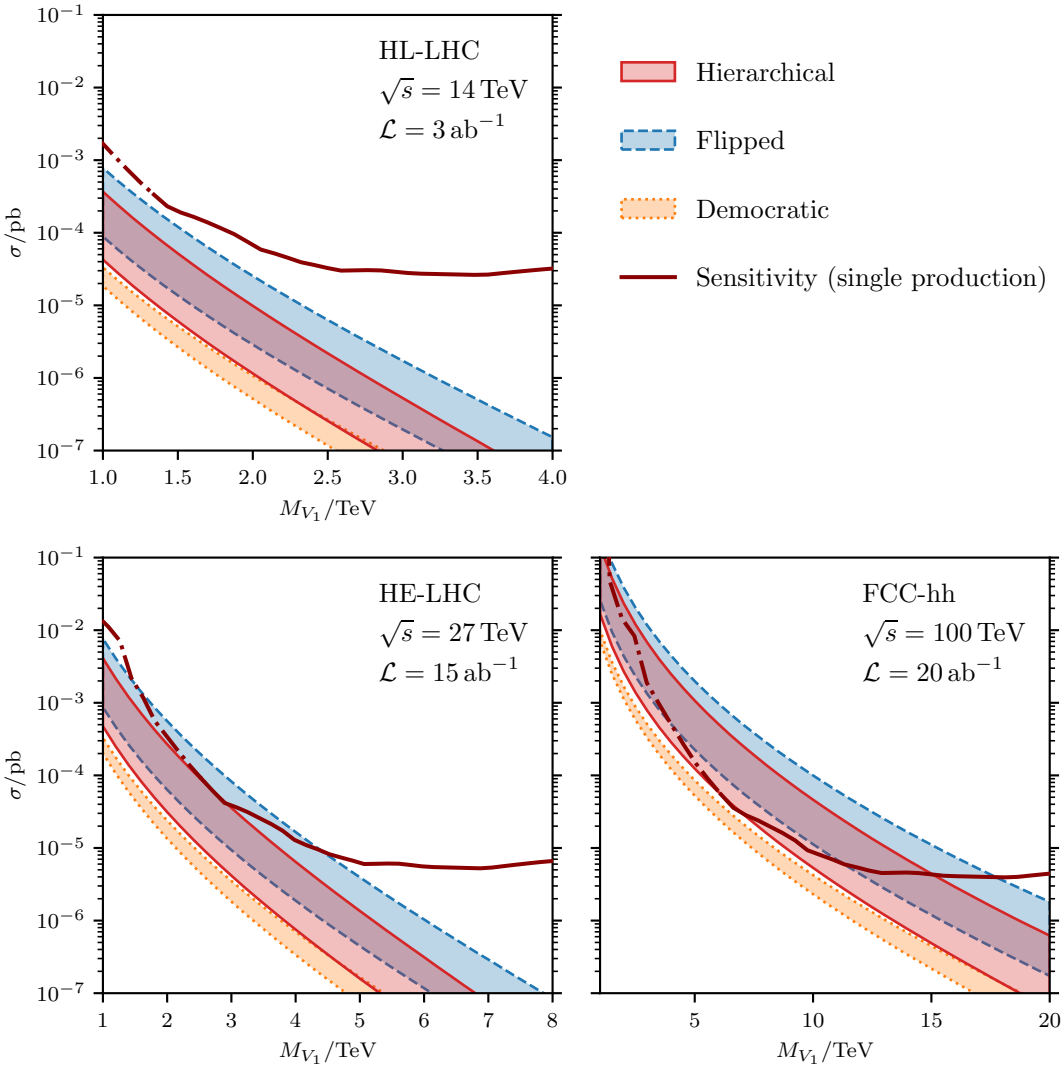

Figure 7.12.: Comparison of the single leptoquark production cross sections $\sigma(pp \to V_1^{\pm 2/3}\mu^{\mp})$ for the benchmarks (7.7), (7.18), (7.19) at different future colliders, for $\kappa = 0$.

7.5. Summary and Conclusion

Flavorful leptoquark explanations of the deviations in R_K and R_{K^*} can be realized with the scalar triplet S_3, the vector singlet V_1, or the vector triplet V_3, and suggest masses of a few TeV, which can be probed at hadron colliders. Here, we have focused on leptoquark single production, which is sensitive to the leptoquark coupling to fermions and the associated flavor structure. In a flavor model context, the B anomalies highlight $pp \to \Delta\mu \to b\mu\mu$ as a prime channel. Together with the missing energy modes $pp \to \Delta\nu \to b\nu\nu$ and $pp \to \Delta\nu \to t\mu\nu$, these processes yield the dominant cross sections. Experimental studies of the latter modes can potentially provide additional information on the flavor structure of the leptoquark coupling and also serve as a cross check with pair production searches or indirect probes such as Drell-Yan processes and semileptonic rare B decays. A crucial flavor model prediction is the strong hierarchy among quark flavors, which causes $j\ell\ell$ signatures to be heavily suppressed with respect to $b\ell\ell$. Experimental results indicating an inverted hierarchy $Y_{s\ell} \gg Y_{b\ell}$ would hence hint at an origin of flavor beyond symmetries. We have explored variations of the hierarchical flavor pattern in more detail for the vector leptoquarks V_1 and V_3 and considered signatures including second generation quarks. The results obtained for vector leptoquarks with the modified flavor patterns also apply to the scalar leptoquark S_3 on a qualitative level. Numerical predictions are shown in Figures 7.4, 7.8, 7.9 and 7.11.

Furthermore, we have considered leptoquark pair production, which has a larger cross section than single production in the low leptoquark mass region, as can be seen in the aforementioned Figures as well. Hence, we encourage searches for pair production signatures of leptoquarks decaying into a bottom quark and a lepton, or a top quark and a lepton (7.11)-(7.13). By reinterpreting a recent ATLAS search for pair-produced scalar leptoquarks, we have obtained new mass limits for the vector leptoquarks V_1 and V_3. The weakest limits are $M_{V_1} > 1.4\,\text{TeV}$ and $M_{V_3} > 1.6\,\text{TeV}$ for $\kappa = -0.3$. For different values of κ, including the Yang-Mills ($\kappa = 1$) and minimal coupling ($\kappa = 0$) cases the limits are stronger – see Figure 7.7.

We find that data from the LHC alone is not sufficient to probe the full parameter space of flavorful leptoquarks, but rather a future hadron collider with larger center of mass energy and luminosity is required. In particular, we estimate that the future collider scenarios HL-LHC, HE-LHC and FCC-hh are sensitive to V_1 leptoquark signatures up to masses of 3 TeV, 5.5 TeV and 19.9 TeV, respectively, for the case of $\kappa = 1$. Similar estimates hold for single production signatures of V_3 in the hierarchical scenario, but are generically larger otherwise.

The "flavor data" benchmark (7.14) can be improved by upcoming data on rare B decays from LHCb and Belle II. Relevant processes are the electronic modes $b \to see$, and cLFV decays $b \to se\mu$ and those including tau leptons. Furthermore, dedicated studies of angular observables in $B \to K^*ee$ decays, analogously to $B \to K^*\mu\mu$ [99, 114] as well as searches for cLFV transitions such as $B \to K^{(*)}e(\mu,\tau)$ and $B \to K^{(*)}\mu\tau$ at the

order of 10^{-8} and below, and $B_s \to e\mu$ at $\mathcal{O}(10^{-11})$ are needed in order to constrain the leptoquark coupling matrix. For an exhaustive study of the flavor structure of the leptoquark couplings, tagging the flavor of the bottom quark is necessary. This would also allow to determine the charge of the leptoquark and to distinguish between different leptoquark representations.

Recent progress in the field of leptonic PDFs has facilitated studies concerning resonant leptoquark production from lepton-quark fusion at hadron colliders. This provides another flavor-sensitive production mechanism besides leptoquark single production, as shown in Figure 7.10. An in-depth study regarding (future-)collider sensitivities is, however, beyond the scope of this thesis.

Chapter 8.

Summary and Conclusion

In this thesis we have investigated theory implications of anomalies currently present in the experimental data on theoretically clean observables in rare B decays. The deviations in the ratios $R_{K^{(*)}}$ and $R_{D^{(*)}}$ hint at a violation of LFU – an essential feature of the SM. In Chapter 3, we have seen that these observables are constructed in such a way that theoretical uncertainties stemming from non-perturbative QCD contributions are strongly suppressed. We have then reviewed the current status of these anomalies in a data-driven and model-independent EFT approach and isolated several possible NP scenarios. While the discrepancy in $R_{D^{(*)}}$ has diminished over time and there is no preferred NP scenario, the situation is quite different for $R_{K^{(*)}}$: since the 2014 LHCb result on R_K, showing a deviation of $2.6\,\sigma$ from the SM prediction, the tension has grown to 3.1σ with the latest data published this year. Furthermore, if current data on R_{K^*} is taken into account, the combined result deviates from unity by more than four sigma. Remarkably, the favored NP solution $C_{\mathrm{LL}}^{\mathrm{NP}} \simeq -1$ is also strongly supported by global fits to other $b \to s\mu^+\mu^-$ observables.

In Chapter 4, we have considered different UV completions of the potential BSM scenarios and put a special focus on leptoquark models, which provide a unique perspective on quark and lepton flavor. To fully exploit this perspective we have then employed flavor models that can successfully explain the masses and mixing of the SM fermions to impose theoretically motivated constraints on the leptoquark couplings. The FN and AF flavor symmetries discussed in Chapter 5 have allowed us to construct flavor patterns for the leptoquark couplings. In Chapter 6, we have then classified the possible flavor patterns and studied the effects of higher order corrections and mass basis rotations. We have identified simple patterns that can isolate single lepton generations and present quark hierarchies that are stable under mass basis rotations. Additionally, we have studied modified patterns that partially evade the strong quark hierarchies and maximize NP effects, but in turn introduce sizable cLFV effects. In order to explore the phenomenology of the flavor patterns, we have used experimental data on $b \to s\nu\bar{\nu}$, rare kaon and charm decays and cLFV processes to constrain the flavor parameters in a data-driven manner. Due to these strong constraints in combination with current leptoquark mass bounds, obtained from

direct searches, we have found that an explanation of R_D and R_{D^*} is presently not possible within this setup. The maximal effects of flavorful leptoquarks in $R_{D^{(*)}}$ are summarized in Figure 6.2. On the other hand, the deviations in R_K and R_{K^*} can be accounted for with the S_3, V_1 and V_3 leptoquarks in combination with the muon isolation patterns that naturally emerge from the AF $\times$ FN flavor model.

Another consequence of the flavor structure imposed on the couplings of leptoquarks is that the mass range which allows for an explanation of R_K and R_{K^*} is lowered from $\sim 30\,\text{TeV}$, in the case of $\mathcal{O}(1)$ couplings, down to a few TeV. This makes flavorful leptoquarks accessible at current and future collider experiments. Potential signatures have been worked out in Chapter 7 using the `MadGraph` framework. We have put an emphasis on the single production mechanism, as it provides direct access to the leptoquark couplings and their flavor structure. We identify $pp \to b\mu^+\mu^-$ as the central channel, while we also expect sizable contributions to $pp \to b\nu\bar{\nu}$ and $pp \to t\mu^-\bar{\nu}$. For low leptoquark masses, pair production dominates over single production and accentuates final states consisting of two quarks and two leptons such as $b\bar{b}\mu^+\mu^-$ – see Figures 7.4, 7.8, 7.9 and 7.11. Alternative flavor scenarios and variations beyond the simple hierarchical pattern can be probed with searches for $pp \to j\ell^+\ell^-$ signatures.

We find that the LHC only allows to access a small part of the parameter space, thus a future hadron collider with increased center of mass energy and luminosity is needed to explore flavorful leptoquarks as a solution to the B anomalies in detail. For the future collider scenarios HL-LHC, HE-LHC and FCC-hh, we estimate sensitivities to V_1 leptoquark signatures up to masses of $3\,\text{TeV}$, $5.5\,\text{TeV}$ and $19.9\,\text{TeV}$, respectively, for the case of $\kappa = 1$, with comparable projections for single production signatures of V_3.

We conclude that flavorful leptoquarks provide viable solutions to the long-standing and continually growing discrepancies seen in R_K and R_{K^*}. Furthermore, they can be probed at future hadron colliders and have the potential to help decipher the flavor puzzles in and beyond the SM.

Appendix A.

Notation and Conventions

Throughout this thesis we use the conventions described in this appendix.

The metric tensor reads

$$\eta_{\mu\nu} = \mathrm{diag}(+1, -1, -1, -1)\,. \tag{A.1}$$

The Levi–Civita symbol is normalized as

$$\varepsilon^{0123} = +1\,. \tag{A.2}$$

The Pauli matrices read

$$\sigma^0 = \begin{pmatrix} 1 & 0 \\ 0 & 1 \end{pmatrix}, \quad \sigma^1 = \begin{pmatrix} 0 & 1 \\ 1 & 0 \end{pmatrix}, \quad \sigma^2 = \begin{pmatrix} 0 & -i \\ i & 0 \end{pmatrix}, \quad \sigma^3 = \begin{pmatrix} 1 & 0 \\ 0 & -1 \end{pmatrix}. \tag{A.3}$$

The Dirac matrices obey

$$\gamma^\mu\gamma^\nu + \gamma^\nu\gamma^\mu = 2\eta^{\mu\nu}\mathbb{1}_{4\times4} \tag{A.4}$$

and are given in the chiral basis as

$$\gamma^\mu = \begin{pmatrix} 0 & \sigma^\mu \\ \bar{\sigma}^\mu & 0 \end{pmatrix}, \tag{A.5}$$

where $\bar{\sigma}^\mu \equiv (\mathbb{1}_{2\times2}, -\sigma^i)^T$. Furthermore, we define

$$\gamma^5 \equiv i\gamma^0\gamma^1\gamma^2\gamma^3\gamma^4\,. \tag{A.6}$$

We employ four-component Dirac spinors, generically denoted by ψ.

We follow the charge conjugation conventions of [204], i.e.

$$\psi^c \equiv C\bar{\psi}^T \equiv D\psi^*, \tag{A.7}$$

where $C = i\gamma^0\gamma^2$ and $D = -i\gamma^2$ holds numerically.

The order of charge conjugations, projectors and Dirac conjugation is defined by

$$\begin{aligned}
\psi_{\mathrm{L}} &= P_{\mathrm{L}}\psi = \frac{1-\gamma_5}{2}\psi\,, \\
\bar{\psi}_{\mathrm{L}} &\equiv \overline{\psi_{\mathrm{L}}} = \bar{\psi}P_{\mathrm{R}}\,, \\
\psi^c_{\mathrm{L}} &\equiv (\psi_{\mathrm{L}})^c = (\psi^c)_{\mathrm{R}} = P_{\mathrm{R}}\psi^c\,, \\
\bar{\psi}^c_{\mathrm{L}} &\equiv \overline{\psi^c_{\mathrm{L}}} = \overline{(\psi_{\mathrm{L}})^c} = \overline{(\psi^c)_{\mathrm{R}}} = \overline{\psi^c}P_{\mathrm{L}}\,.
\end{aligned} \tag{A.8}$$

The standard parametrization of the fermion mixing matrices reads

$$\begin{aligned}
U &= \begin{pmatrix} 1 & 0 & 0 \\ 0 & c_{23} & s_{23} \\ 0 & -s_{23} & c_{23} \end{pmatrix} \begin{pmatrix} c_{13} & 0 & s_{13}e^{-i\delta} \\ 0 & 1 & 0 \\ -s_{13}e^{i\delta} & 0 & c_{13} \end{pmatrix} \begin{pmatrix} c_{12} & s_{12} & 0 \\ -s_{12} & c_{12} & 0 \\ 0 & 0 & 1 \end{pmatrix} \\
&= \begin{pmatrix} c_{12}c_{13} & s_{12}c_{13} & s_{13}e^{-i\delta} \\ -s_{12}c_{23} - c_{12}s_{23}s_{13}e^{i\delta} & c_{12}c_{23} - s_{12}s_{23}s_{13}e^{i\delta} & s_{23}c_{13} \\ s_{12}s_{23} - c_{12}c_{23}s_{13}e^{i\delta} & -c_{12}s_{23} - s_{12}c_{23}s_{13}e^{i\delta} & c_{23}c_{23} \end{pmatrix}.
\end{aligned} \tag{A.9}$$

The Kallén function is defined as

$$\lambda(x,y,z) \equiv x^2 + y^2 + z^2 - 2xy - 2yz - 2xz\,. \tag{A.10}$$

Appendix B.

Numerical Constants

For all numerical calculations performed in this thesis, we use the input parameters compiled in Table B.1.

Quantity	Symbol	Value		Unit	Reference
Fermi constant	G_F	1.166 378 7(6)	$\times 10^{-5}$	GeV^{-2}	PDG [23]
Fine structure constant	$\alpha_e(m_b)$	1/133			
CKM elements	$\lvert V_{cb}\rvert$	0.0411(13)			PDG [205]
	$\lvert V_{tb}\rvert$	0.999 146(50)			PDG [205]
	$\lvert V_{ts}\rvert$	0.0404(12)			PDG [205]
Meson masses	m_{D^+}	1.869 61(9)		GeV	PDG [23]
	m_{D^0}	1.864 84(5)		GeV	PDG [23]
	$m_{D^{*+}}$	2.010 27(5)		GeV	PDG [23]
	$m_{D^{*0}}$	2.006 97(8)		GeV	PDG [23]
	m_{K^+}	0.493 677(16)		GeV	PDG [23]
	m_{K^0}	0.497 614(24)		GeV	PDG [23]
	$m_{K^{*+}}$	0.891 66(26)		GeV	PDG [23]
	$m_{K^{*0}}$	0.8955(8)		GeV	PDG [23]
	m_{B^+}	5.279 29(15)		GeV	PDG [23]
	m_{B^0}	5.279 61(16)		GeV	PDG [23]
Meson lifetimes	τ_{B^+}	1.638(4)	$\times 10^{-12}$	s	PDG [23]
	τ_{B^0}	1.520(4)	$\times 10^{-12}$	s	PDG [23]
Quark and lepton masses	m_s	0.095(5)		GeV	PDG [205]
	m_c	1.275(25)		GeV	PDG [205]
	$m_b^{\overline{\text{MS}}}$	4.18(3)		GeV	PDG [205]
	m_t^{pole}	1.73(1)	$\times 10^{2}$	GeV	PDG [205]
	m_e	0.510 998 928	$\times 10^{-3}$	GeV	PDG [205]
	m_μ	0.105 658 371 5		GeV	PDG [205]
	m_τ	1.776 86(12)		GeV	PDG [205]

Table B.1.: Numerical values of the input parameters used in this thesis.

Appendix C.

Numerical Evaluation of $\bar{B} \to D^{(*)}\ell\bar{\nu}$ Observables

In this appendix we provide details on the numerical evaluation of the observables discussed in Section 3.3.1, following [1].

The q^2-dependent coefficient functions $A_i(q^2)$ and $B_i(q^2)$ that occur in the expressions for the differential branching ratios of the decays $\bar{B} \to D\ell\bar{\nu}$ (3.17) and $\bar{B} \to D^*\ell\bar{\nu}$ (3.18), respectively, read

$$A_{\mathrm{S}}(q^2) = \frac{3}{2} N(q^2) H_S^{s2}(q^2)\,, \tag{C.1}$$

$$A_{\mathrm{T}}(q^2) = 8N(q^2)\left(1 + \frac{2m_\ell^2}{q^2}\right) H_T^{s2}(q^2)\,, \tag{C.2}$$

$$A_{\mathrm{VS}}(q^2) = 3N(q^2)\frac{m_\ell}{\sqrt{q^2}} H_S^s(q^2) H_{V,t}^s(q^2)\,, \tag{C.3}$$

$$A_{\mathrm{VT}}(q^2) = -12N(q^2)\frac{m_\ell}{\sqrt{q^2}} H_T^s(q^2) H_{V,0}^s(q^2)\,, \tag{C.4}$$

and

$$\begin{aligned} B_{\mathrm{V_1V_2}}(q^2) = N(q^2)\Bigg[&\left(1 + \frac{m_\ell^2}{2q^2}\right)\left(H_{V,0}^2(q^2) + 2H_{V,+}(q^2)H_{V,-}(q^2)\right) \\ &+ \frac{3}{2}\frac{m_\ell^2}{q^2} H_{V,t}^2(q^2)\Bigg]\,, \end{aligned} \tag{C.5}$$

$$B_{\mathrm{S}}(q^2) = \frac{3}{2} N(q^2) H_S^2(q^2)\,, \tag{C.6}$$

$$B_{\mathrm{T}}(q^2) = 8N(q^2)\left(1 + \frac{2m_\ell^2}{q^2}\right)\left(H_{T,+}^2(q^2) + H_{T,-}^2(q^2) + H_{T,0}^2(q^2)\right)\,, \tag{C.7}$$

$$B_{\mathrm{VS}}(q^2) = 3N(q^2)\frac{m_\ell}{\sqrt{q^2}} H_S(q^2) H_{V,t}(q^2)\,, \tag{C.8}$$

ℓ	$\hat{A}_{\mathrm{S}}^{\ell}$	$\hat{A}_{\mathrm{T}}^{\ell}$	$\hat{A}_{\mathrm{VS}}^{\ell}$	$\hat{A}_{\mathrm{VT}}^{\ell}$
e	1.45 ± 0.16	0.38 ± 0.20	0.00 ± 0.00	0.00 ± 0.00
μ	1.45 ± 0.16	0.36 ± 0.17	0.17 ± 0.02	0.13 ± 0.09
τ	1.36 ± 0.15	0.35 ± 0.13	1.73 ± 0.19	0.69 ± 0.15

Table C.1.: The normalized $\bar{B} \to D\ell\nu$ coefficients $\hat{A}_i^{\ell} = A_i^{\ell}/\mathcal{B}^{\mathrm{SM}}$.

ℓ	$\hat{B}_{\mathrm{V_1V_2}}^{\ell}$	$\hat{B}_{\mathrm{S}}^{\ell}$	$\hat{B}_{\mathrm{T}}^{\ell}$	$\hat{B}_{\mathrm{VS}}^{\ell}$	$\hat{B}_{\mathrm{V_1T}}^{\ell}$	$\hat{B}_{\mathrm{V_2T}}^{\ell}$
e	-1.72 ± 0.13	0.06 ± 0.01	12.98 ± 0.98	0.00 ± 0.00	0.00 ± 0.00	0.00 ± 0.00
μ	-1.72 ± 0.13	0.06 ± 0.01	12.98 ± 0.98	0.02 ± 0.00	-0.43 ± 0.03	0.70 ± 0.05
τ	-1.78 ± 0.13	0.04 ± 0.01	13.35 ± 1.00	0.12 ± 0.01	-4.58 ± 0.34	6.14 ± 0.45

Table C.2.: The normalized $\bar{B} \to D^*\ell\nu$ coefficients $\hat{B}_i^{\ell} = B_i^{\ell}/\mathcal{B}^{\mathrm{SM}}$.

$$\begin{aligned} B_{\mathrm{V_1T}}(q^2) = -12N(q^2)\frac{m_\ell}{\sqrt{q^2}}\Big(&H_{T,0}(q^2)H_{V,0}(q^2) \\ &+ H_{T,+}(q^2)H_{V,+}(q^2) - H_{T,-}(q^2)H_{V,-}(q^2)\Big)\,, \end{aligned} \tag{C.9}$$

$$\begin{aligned} B_{\mathrm{V_2T}}(q^2) = 12N(q^2)\frac{m_\ell}{\sqrt{q^2}}\Big(&H_{T,0}(q^2)H_{V,0}(q^2) \\ &+ H_{T,+}(q^2)H_{V,-}(q^2) - H_{T,+}(q^2)H_{V,-}(q^2)\Big)\,. \end{aligned} \tag{C.10}$$

Here, $N(q^2)$ denotes the normalization factor from (3.20). The hadronic matrix elements $H_i(q^2)$ can be found in [35]. We employ the lattice form factors [43] for $\bar{B} \to D$ and rely on the HQET form factors from [35] for $B \to D^*$. In Tables C.1 and C.2 we provide numerical results for the $A_i(q^2)$ and $B_i(q^2)$ integrated over the full kinematic range, summed over the lepton polarizations and normalized to the SM branching fractions. For the latter we find

$$\begin{aligned} \mathcal{B}^{\mathrm{SM}}(\bar{B}^0 \to D^+\tau\nu) &= (6.66 \pm 0.67) \times 10^{-3}\,, \\ \mathcal{B}^{\mathrm{SM}}(\bar{B}^0 \to D^+(e,\mu)\nu) &= (2.23 \pm 0.24) \times 10^{-2}\,, \end{aligned} \tag{C.11}$$

and

$$\begin{aligned} \mathcal{B}^{\mathrm{SM}}(\bar{B}^0 \to D^{+*}\tau\nu) &= (1.35 \pm 0.10) \times 10^{-2}\,, \\ \mathcal{B}^{\mathrm{SM}}(\bar{B}^0 \to D^{+*}(e,\mu)\nu) &= (5.34 \pm 0.40) \times 10^{-2}\,. \end{aligned} \tag{C.12}$$

In order to estimate the uncertainties, we draw 10^5 random samples of the form factor parameters provided in the respective references and calculate the coefficients A_i and B_i for each sample. The mean and standard deviation of the resulting distributions are then considered as the central value and uncertainty. We assume that the form factor parameters are normally distributed and incorperate all correlations provided by [35, 43].

k	$\hat{A}_{\mathrm{S}}^{k}$	$\hat{A}_{\mathrm{T}}^{k}$	$\hat{A}_{\mathrm{VS}}^{k}$	$\hat{A}_{\mathrm{VT}}^{k}$
$+$	4.12 ± 0.45	0.56 ± 0.20	5.23 ± 0.57	0.70 ± 0.15
$-$	-	0.50 ± 0.19	-	1.39 ± 0.30

Table C.3.: The normalized $\bar{B} \to D\tau\nu$ coefficients $\hat{A}_i^k = A_i^k / \left(\mathcal{B}_{k=+}^{\mathrm{SM}} - \mathcal{B}_{k=-}^{\mathrm{SM}}\right)$ for a given polarization k of the τ lepton.

k	$\hat{B}_{\mathrm{V_1V_2}}^{k}$	$\hat{B}_{\mathrm{S}}^{k}$	$\hat{B}_{\mathrm{T}}^{k}$	$\hat{B}_{\mathrm{VS}}^{k}$	$\hat{B}_{\mathrm{V_1T}}^{k}$	$\hat{B}_{\mathrm{V_2T}}^{k}$
$+$	0.62 ± 0.06	0.04 ± 0.00	-14.15 ± 1.06	-0.24 ± 0.03	3.08 ± 0.23	-4.12 ± 0.30
$-$	1.26 ± 0.10	-	-12.72 ± 0.95	-	6.15 ± 0.46	-8.24 ± 0.61

Table C.4.: The normalized $\bar{B} \to D^*\tau\nu$ coefficients $\hat{B}_i^k = B_i^k / \left(\mathcal{B}_{k=+}^{\mathrm{SM}} - \mathcal{B}_{k=-}^{\mathrm{SM}}\right)$ for a given polarization k of the τ lepton.

Additionally, we provide the coefficients for given τ-polarizations in Tables C.3 and C.4, where we normalize to the difference $\mathcal{B}_{k=+}^{\mathrm{SM}} - \mathcal{B}_{k=-}^{\mathrm{SM}}$ of the SM values of the polarized branching fractions. For the latter we obtain

$$\begin{aligned} \mathcal{B}_{k=+}^{\mathrm{SM}}(\bar{B}^0 \to D^+\tau\nu) &= (4.43 \pm 0.47) \times 10^{-3}\,, \\ \mathcal{B}_{k=-}^{\mathrm{SM}}(\bar{B}^0 \to D^+\tau\nu) &= (2.22 \pm 0.22) \times 10^{-3}\,, \end{aligned} \tag{C.13}$$

and

$$\begin{aligned} \mathcal{B}_{k=+}^{\mathrm{SM}}(\bar{B}^0 \to D^{+*}\tau\nu) &= (3.40 \pm 0.27) \times 10^{-3}\,, \\ \mathcal{B}_{k=-}^{\mathrm{SM}}(\bar{B}^0 \to D^{+*}\tau\nu) &= (1.01 \pm 0.07) \times 10^{-2}\,. \end{aligned} \tag{C.14}$$

Scalar operators do not contribute to the case where $k = -$.

Appendix D.

LQ Contributions to Wilson Coefficients of the Weak Hamiltonian

By comparing the effective vertices listed in the Tables 4.2 and 4.3 with the effective Hamiltonians that govern the flavor transitions $b \to c\ell\bar{\nu}$ (see (3.14), (3.15)), $b \to s\ell^+\ell^-$ (see (3.25), (3.26)) and $c \to u\ell^+\ell^-$ (see [122]), we obtain the Wilson coefficients compiled in the Tables below. In order to avoid clutter, we define the rescaled coefficients

$$\tilde{C} \equiv \frac{4G_{\rm F}}{\sqrt{2}} V_{cb} M^2 C \tag{D.1}$$

for $b \to c\ell\bar{\nu}$,

$$\tilde{C} \equiv \frac{4G_{\rm F}}{\sqrt{2}} V_{tb} V_{ts}^* \frac{\alpha}{4\pi} M^2 C \tag{D.2}$$

for $b \to s\ell^+\ell^-$ and $b \to s\nu\bar{\nu}$, as well as

$$\tilde{\mathcal{C}} \equiv \frac{4G_{\rm F}}{\sqrt{2}} \frac{\alpha}{4\pi} M^2 \mathcal{C} \tag{D.3}$$

for $c \to u\ell^+\ell^-$ and $c \to u\nu\bar{\nu}$, where M denotes the leptoquark mass.

	$\tilde{C}_{V_1}$	$\tilde{C}_{S_1}$	$\tilde{C}_{S_2}$	$\tilde{C}_T$
S_1	$\frac{1}{2}Y^{b\nu}_{QL}\left(Y^{c\ell}_{QL}\right)^*$	-	$-\frac{1}{2}Y^{b\nu}_{QL}\left(Y^{c\ell}_{UE}\right)^*$	$\frac{1}{8}Y^{b\nu}_{QL}\left(Y^{c\ell}_{UE}\right)^*$
S_2	-	-	$-\frac{1}{2}Y^{c\nu}_{\bar{U}L}\left(Y^{b\ell}_{\bar{Q}E}\right)^*$	$-\frac{1}{8}Y^{c\nu}_{\bar{U}L}\left(Y^{b\ell}_{\bar{Q}E}\right)^*$
S_3	$-\frac{1}{2}Y^{b\nu}_{QL}\left(Y^{c\ell}_{QL}\right)^*$	-	-	-
V_1	$Y^{c\nu}_{\bar{Q}L}\left(Y^{b\ell}_{\bar{Q}L}\right)^*$	$-2Y^{c\nu}_{\bar{Q}L}\left(Y^{b\ell}_{\bar{D}E}\right)^*$	-	-
V_2	-	$-2Y^{b\nu}_{DL}\left(Y^{c\ell}_{QE}\right)^*$	-	-
V_3	$-Y^{c\nu}_{\bar{Q}L}\left(Y^{b\ell}_{\bar{Q}L}\right)^*$	-	-	-

Table D.1.: Contributions from leptoquarks to $b \to c\ell\bar{\nu}$ transitions at matching scale.

	$\tilde{C}_{\mathrm{L}}$	$\tilde{C}_{\mathrm{R}}$	$\tilde{\mathcal{C}}_{\mathrm{L}}$	$\tilde{\mathcal{C}}_{\mathrm{R}}$
S_1	$\frac{1}{2}Y^{b\ell}_{QL}\left(Y^{s\ell'}_{QL}\right)^*$	-	-	-
S_2	-	-	-	$-\frac{1}{2}Y^{u\ell}_{\bar{U}L}\left(Y^{c\ell'}_{\bar{U}L}\right)^*$
$\tilde{S}_2$	-	$-\frac{1}{2}Y^{s\ell}_{\bar{D}L}\left(Y^{b\ell'}_{\bar{D}L}\right)^*$	-	-
S_3	$\frac{1}{2}Y^{b\ell}_{QL}\left(Y^{s\ell'}_{QL}\right)^*$	-	$Y^{c\ell}_{QL}\left(Y^{u\ell'}_{QL}\right)^*$	-
V_1	-	-	$-Y^{u\ell}_{\bar{Q}L}\left(Y^{c\ell'}_{\bar{Q}L}\right)^*$	-
V_2	-	$Y^{b\ell}_{DL}\left(Y^{s\ell'}_{DL}\right)^*$	-	-
$\tilde{V}_2$	-	-	-	$Y^{c\ell}_{UL}\left(Y^{u\ell'}_{UL}\right)^*$
V_3	$-2Y^{s\ell}_{\bar{Q}L}\left(Y^{b\ell'}_{\bar{Q}L}\right)^*$	-	$-Y^{u\ell}_{\bar{Q}L}\left(Y^{c\ell'}_{\bar{Q}L}\right)^*$	-

Table D.2.: Contributions from leptoquarks to $b \to s\nu\bar{\nu}$ and $c \to u\nu\bar{\nu}$ transitions at matching scale.

	$\tilde{C}_9$	$\tilde{C}_{10}$	$\tilde{C}'_9$	$\tilde{C}'_{10}$
$\tilde{S}_1$	-	-	$\frac{1}{4}Y^{b\ell}_{DE}\left(Y^{s\ell'}_{DE}\right)^*$	$+\tilde{C}'_9$
S_2	$-\frac{1}{4}Y^{s\ell}_{\bar{Q}E}\left(Y^{b\ell'}_{\bar{Q}E}\right)^*$	$+\tilde{C}_9$	-	-
$\tilde{S}_2$	-	-	$-\frac{1}{4}Y^{s\ell}_{\bar{D}L}\left(Y^{b\ell'}_{\bar{D}L}\right)^*$	$-\tilde{C}'_9$
S_3	$\frac{1}{2}Y^{b\ell}_{QL}\left(Y^{s\ell'}_{QL}\right)^*$	$-\tilde{C}_9$	-	-
V_1	$-\frac{1}{2}Y^{s\ell}_{\bar{Q}L}\left(Y^{b\ell'}_{\bar{Q}L}\right)^*$	$-\tilde{C}_9$	$-\frac{1}{2}Y^{s\ell}_{\bar{D}E}\left(Y^{b\ell'}_{\bar{D}E}\right)^*$	$+\tilde{C}'_9$
V_2	-	-	$\frac{1}{2}Y^{b\ell}_{DL}\left(Y^{s\ell'}_{DL}\right)^*$	$-\tilde{C}'_9$
V_3	$-\frac{1}{2}Y^{s\ell}_{\bar{Q}L}\left(Y^{b\ell'}_{\bar{Q}L}\right)^*$	$-\tilde{C}_9$	-	-

Table D.3.: Contributions from leptoquarks to $b \to s\ell^+\ell^-$ transitions at matching scale (vectors).

	$\tilde{C}_{\mathrm{S}}$	$\tilde{C}_{\mathrm{P}}$	$\tilde{C}'_{\mathrm{S}}$	$\tilde{C}'_{\mathrm{P}}$
V_1	$Y^{s\ell}_{\bar{Q}L}\left(Y^{b\ell'}_{\bar{D}E}\right)^*$	$+\tilde{C}_{\mathrm{S}}$	$Y^{s\ell}_{\bar{D}E}\left(Y^{b\ell'}_{\bar{Q}L}\right)^*$	$+\tilde{C}'_{\mathrm{S}}$
V_2	$Y^{b\ell}_{DL}\left(Y^{s\ell'}_{QE}\right)^*$	$-\tilde{C}_{\mathrm{S}}$	$Y^{b\ell}_{QE}\left(Y^{s\ell'}_{DL}\right)^*$	$+\tilde{C}'_{\mathrm{S}}$

Table D.4.: Contributions from leptoquarks to $b \to s\ell^+\ell^-$ transitions at matching scale (scalars).

	$\tilde{\mathcal{C}}_9$	$\tilde{\mathcal{C}}_{10}$	$\tilde{\mathcal{C}}'_9$	$\tilde{\mathcal{C}}'_{10}$
S_1	$\frac{1}{4}Y^{c\ell}_{QL}\left(Y^{u\ell'}_{QL}\right)^*$	$-\tilde{\mathcal{C}}_9$	$\frac{1}{4}Y^{c\ell}_{UE}\left(Y^{u\ell'}_{UE}\right)^*$	$+\tilde{\mathcal{C}}'_9$
S_2	$-\frac{1}{4}Y^{u\ell}_{\bar{Q}E}\left(Y^{c\ell'}_{\bar{Q}E}\right)^*$	$+\tilde{\mathcal{C}}_9$	$-\frac{1}{4}Y^{u\ell}_{\bar{U}L}\left(Y^{c\ell'}_{\bar{U}L}\right)^*$	$-\tilde{\mathcal{C}}'_9$
S_3	$\frac{1}{4}Y^{c\ell}_{QL}\left(Y^{u\ell'}_{QL}\right)^*$	$-\tilde{\mathcal{C}}_9$	-	-
$\tilde{V}_1$	-	-	$-\frac{1}{2}Y^{u\ell}_{\bar{U}E}\left(Y^{c\ell'}_{\bar{U}E}\right)^*$	$+\tilde{\mathcal{C}}'_9$
V_2	$\frac{1}{2}Y^{c\ell}_{QE}\left(Y^{u\ell'}_{QE}\right)^*$	$+\tilde{\mathcal{C}}_9$	-	-
$\tilde{V}_2$	-	-	$\frac{1}{2}Y^{c\ell}_{UL}\left(Y^{u\ell'}_{UL}\right)^*$	$-\tilde{\mathcal{C}}'_9$
V_3	$-Y^{u\ell}_{\bar{Q}L}\left(Y^{c\ell'}_{\bar{Q}L}\right)^*$	$-\tilde{\mathcal{C}}_9$	-	-

Table D.5.: Contributions from leptoquarks to $c \to u\ell^+\ell^-$ transitions at matching scale (vectors).

	$\tilde{\mathcal{C}}_{\mathrm{S}}$	$\tilde{\mathcal{C}}_{\mathrm{P}}$	$\tilde{\mathcal{C}}'_{\mathrm{S}}$	$\tilde{\mathcal{C}}'_{\mathrm{P}}$	$\tilde{\mathcal{C}}_{\mathrm{T}_1}$	$\tilde{\mathcal{C}}_{\mathrm{T}_2}$
S_1	$-\frac{1}{4}Y^{c\ell}_{UE}\left(Y^{u\ell'}_{QL}\right)^*$	$+\tilde{\mathcal{C}}_{\mathrm{S}}$	$-\frac{1}{4}Y^{c\ell}_{QL}\left(Y^{u\ell'}_{UE}\right)^*$	$-\tilde{\mathcal{C}}'_{\mathrm{S}}$	$\frac{1}{8}Y^{c\ell}_{UE}\left(Y^{u\ell'}_{QL}\right)^*$	$\frac{1}{8}Y^{c\ell}_{QL}\left(Y^{u\ell'}_{UE}\right)^*$
S_2	$\frac{1}{4}Y^{u\ell}_{\bar{Q}E}\left(Y^{c\ell'}_{\bar{U}L}\right)^*$	$+\tilde{\mathcal{C}}_{\mathrm{S}}$	$\frac{1}{4}Y^{u\ell}_{\bar{U}L}\left(Y^{c\ell'}_{\bar{Q}E}\right)^*$	$-\tilde{\mathcal{C}}'_{\mathrm{S}}$	$\frac{1}{8}Y^{u\ell}_{\bar{U}L}\left(Y^{c\ell'}_{\bar{Q}E}\right)^*$	$\frac{1}{8}Y^{u\ell}_{\bar{Q}E}\left(Y^{c\ell'}_{\bar{U}L}\right)^*$

Table D.6.: Contributions from leptoquarks to $c \to u\ell\ell$ transitions at matching scale (scalars and tensors).

Acronyms

AF Altarelli–Feruglio. 52, 53, 105

AMM anomalous magnetic moment. 1

BSM beyond the Standard Model. 1–3, 9, 12, 13, 42, 105

CKM Cabbibo–Kobayashi–Maskawa. 6, 7, 18, 58, 78, 109

cLFV charged lepton flavor violation. 8, 37, 38, 42, 57, 62, 68, 71–74, 79, 88, 102, 105

EFT effective field theory. 2, 9, 11–13, 16, 18, 24, 35, 39, 46, 50, 79, 105

EW electroweak. 3–7, 11–13

FCCC flavor-changing charged current. 1, 6, 17

FCNC flavor-changing neutral current. 1, 6–9, 24, 36, 40, 42, 45, 70, 72

FN Froggatt–Nielsen. 50–53, 56, 58–61, 64, 66, 67, 71, 72, 74, 79, 85, 87, 105

GIM Glashow–Iliopoulos–Maiani. 6, 8, 24

GUT Grand Unified Theory. 40, 45

HFLAV Heavy Flavor Averaging Group. 19, 21, 37

HQET Heavy Quark Effective Theory. 16, 18, 112

LCSR Light Cone Sum Rules. 16, 29

LFU lepton flavor universality. 1, 31, 105

LFUV lepton flavor universality violation. 31, 56

LHC Large Hadron Collider. 1, 84, 87

LQCD Lattice Quantum Chromodynamics. 16

MFV minimal flavor violation. 9, 42

NP new physics. 2, 9, 11, 12, 17–19, 21, 22, 24, 26, 28, 30, 31, 33–35, 38, 39, 42, 47, 62–64, 71, 74, 105

NWA narrow width approximation. 80

OPE Operator Product Expansion. 12, 14

PDF parton distribution function. 81, 84, 85, 89, 94–97, 99, 100, 103

PMNS Pontecorvo–Maki–Nakagawa–Sakata. 8, 58

QCD Quantum Chromodynamics. 3, 4, 7, 9, 11, 13, 14, 16, 28, 29, 31, 37, 80, 84, 105

QED Quantum Electrodynamics. 3, 24, 26, 31

QFT quantum field theory. 3, 16

RG renormalization group. 13, 64

RGE renormalization group equation. 13, 68

SM Standard Model. 1, 3–10, 12, 16–21, 23, 24, 26, 28–33, 35–37, 40, 42–47, 49, 50, 56, 60, 63–66, 68, 69, 73, 74, 85, 105, 106, 112, 113

SMEFT Standard Model Effective Field Theory. 79

TBM tribimaximal. 8, 52, 53

UV ultraviolet. 12, 39, 45, 50, 51, 53, 105

vev vacuum expectation value. 5, 6, 50–53, 56–60, 62, 64, 66–68, 70–72, 75, 86, 88

Bibliography

[1] G. Hiller, D. Loose, and K. Schönwald.
"Leptoquark Flavor Patterns & B Decay Anomalies".
In: *JHEP* 12 (2016), p. 027. DOI: 10.1007/JHEP12(2016)027.
arXiv: 1609.08895 [hep-ph].

[2] G. Hiller, D. Loose, and I. Nišandžić. "Flavorful leptoquarks at hadron colliders".
In: *Phys. Rev.* D97.7 (2018), p. 075004. DOI: 10.1103/PhysRevD.97.075004.
arXiv: 1801.09399 [hep-ph].

[3] G. Hiller, D. Loose, and I. Nišandžić.
"Flavorful leptoquarks at the LHC and beyond: spin 1".
In: *JHEP* 06 (2021), p. 080. DOI: 10.1007/JHEP06(2021)080.
arXiv: 2103.12724 [hep-ph].

[4] G. Aad et al. "Observation of a new particle in the search for the Standard Model Higgs boson with the ATLAS detector at the LHC".
In: *Phys. Lett.* B716 (2012), pp. 1–29. DOI: 10.1016/j.physletb.2012.08.020.
arXiv: 1207.7214 [hep-ex].

[5] S. Chatrchyan et al. "Observation of a New Boson at a Mass of 125 GeV with the CMS Experiment at the LHC". In: *Phys. Lett.* B716 (2012), pp. 30–61.
DOI: 10.1016/j.physletb.2012.08.021. arXiv: 1207.7235 [hep-ex].

[6] R. Aaij et al. "Test of lepton universality using $B^+ \to K^+\ell^+\ell^-$ decays".
In: *Phys. Rev. Lett.* 113 (2014), p. 151601.
DOI: 10.1103/PhysRevLett.113.151601. arXiv: 1406.6482 [hep-ex].

[7] R. Aaij et al. "Search for lepton-universality violation in $B^+ \to K^+\ell^+\ell^-$ decays".
In: *Phys. Rev. Lett.* 122.19 (2019), p. 191801.
DOI: 10.1103/PhysRevLett.122.191801. arXiv: 1903.09252 [hep-ex].

[8] R. Aaij et al. "Test of lepton universality in beauty-quark decays". In: (2021).
arXiv: 2103.11769 [hep-ex].

[9] F. Beaujean, C. Bobeth, and D. van Dyk.
"Comprehensive Bayesian analysis of rare (semi)leptonic and radiative B decays".
In: *Eur. Phys. J.* C74 (2014). [Erratum: Eur. Phys. J.C74,3179(2014)], p. 2897.
DOI: 10.1140/epjc/s10052-014-2897-0,10.1140/epjc/s10052-014-3179-6.
arXiv: 1310.2478 [hep-ph].

[10] B. Capdevila et al.
"Patterns of New Physics in $b \to s\ell^+\ell^-$ transitions in the light of recent data".
In: *JHEP* 01 (2018), p. 093. DOI: 10.1007/JHEP01(2018)093.
arXiv: 1704.05340 [hep-ph].

[11] J. Aebischer et al. "B-decay discrepancies after Moriond 2019".
In: *Eur. Phys. J.* C80.3 (2020), p. 252.
DOI: 10.1140/epjc/s10052-020-7817-x. arXiv: 1903.10434 [hep-ph].

[12] Y. S. Amhis et al.
"Averages of b-hadron, c-hadron, and τ-lepton properties as of 2018".
In: *Eur. Phys. J.* C81.3 (2021), p. 226. DOI: 10.1140/epjc/s10052-020-8156-7.
arXiv: 1909.12524 [hep-ex].

[13] T. Aoyama et al.
"The anomalous magnetic moment of the muon in the Standard Model".
In: *Phys. Rept.* 887 (2020), pp. 1–166. DOI: 10.1016/j.physrep.2020.07.006.
arXiv: 2006.04822 [hep-ph].

[14] H. Davoudiasl and W. J. Marciano. "Tale of two anomalies".
In: *Phys. Rev.* D98.7 (2018), p. 075011. DOI: 10.1103/PhysRevD.98.075011.
arXiv: 1806.10252 [hep-ph].

[15] M. D. Schwartz. *Quantum Field Theory and the Standard Model*.
Cambridge University Press, 2014. ISBN: 1107034736, 9781107034730. URL: http://www.cambridge.org/us/academic/subjects/physics/theoretical-physics-and-mathematical-physics/quantum-field-theory-and-standard-model.

[16] M. E. Peskin and D. V. Schroeder. *An Introduction to quantum field theory*.
Reading, USA: Addison-Wesley, 1995. ISBN: 9780201503975, 0201503972.
URL: http://www.slac.stanford.edu/~mpeskin/QFT.html.

[17] S. Weinberg. *The Quantum theory of fields. Vol. 1: Foundations*.
Cambridge University Press, 2005. ISBN: 9780521670531, 9780511252044.

[18] S. Weinberg. *The quantum theory of fields. Vol. 2: Modern applications*.
Cambridge University Press, 2013.
ISBN: 9781139632478, 9780521670548, 9780521550024.

[19] J. Goldstone, A. Salam, and S. Weinberg. "Broken Symmetries".
In: *Phys. Rev.* 127 (1962), pp. 965–970. DOI: 10.1103/PhysRev.127.965.

[20] Y. Grossman and P. Tanedo. "Just a Taste: Lectures on Flavor Physics".
In: *Proceedings, Theoretical Advanced Study Institute in Elementary Particle Physics : Anticipating the Next Discoveries in Particle Physics (TASI 2016): Boulder, CO, USA, June 6-July 1, 2016*. 2018, pp. 109–295.
DOI: 10.1142/9789813233348_0004. arXiv: 1711.03624 [hep-ph].

[21] B. Grinstein. "Lectures on Flavor Physics and CP Violation".
In: *Proceedings, 8th CERN-Latin-American School of High-Energy Physics (CLASHEP2015): Ibarra, Ecuador, March 05-17, 2015*. 2016, pp. 43–84.
DOI: 10.5170/CERN-2016-005.43. arXiv: 1701.06916 [hep-ph].

[22] P. A. Zyla et al. "Review of Particle Physics".
In: *PTEP* 2020.8 (2020), p. 083C01. DOI: 10.1093/ptep/ptaa104.

[23] C. Patrignani et al. "Review of Particle Physics".
In: *Chin. Phys.* C40.10 (2016), p. 100001.
DOI: 10.1088/1674-1137/40/10/100001.

[24] Y. Nir. "Probing new physics with flavor physics (and probing flavor physics with new physics)". In: *Prospects in Theoretical Physics (PiTP) summer program on The Standard Model and Beyond IAS, Princeton, NJ, June 16-27, 2007*. 2007.
arXiv: 0708.1872 [hep-ph].

[25] P. F. Harrison, D. H. Perkins, and W. G. Scott.
"Tri-bimaximal mixing and the neutrino oscillation data".
In: *Phys. Lett.* B530 (2002), p. 167. DOI: 10.1016/S0370-2693(02)01336-9.
arXiv: hep-ph/0202074 [hep-ph].

[26] M. Lindner, T. Ohlsson, and G. Seidl.
"Seesaw mechanisms for Dirac and Majorana neutrino masses".
In: *Phys. Rev.* D65 (2002), p. 053014. DOI: 10.1103/PhysRevD.65.053014.
arXiv: hep-ph/0109264 [hep-ph].

[27] R. S. Chivukula and H. Georgi. "Composite Technicolor Standard Model".
In: *Phys. Lett.* B188 (1987), pp. 99–104. DOI: 10.1016/0370-2693(87)90713-1.

[28] G. D'Ambrosio, G. F. Giudice, G. Isidori, and A. Strumia.
"Minimal flavor violation: An Effective field theory approach".
In: *Nucl. Phys.* B645 (2002), pp. 155–187.
DOI: 10.1016/S0550-3213(02)00836-2. arXiv: hep-ph/0207036 [hep-ph].

[29] V. Cirigliano, B. Grinstein, G. Isidori, and M. B. Wise.
"Minimal flavor violation in the lepton sector".
In: *Nucl. Phys.* B728 (2005), pp. 121–134.
DOI: 10.1016/j.nuclphysb.2005.08.037. arXiv: hep-ph/0507001 [hep-ph].

[30] T. Mannel. "Effective Field Theories in Flavor Physics".
In: *Springer Tracts Mod. Phys.* 203 (2004), pp. 1–175. DOI: 10.1007/b62268.

[31] T. Appelquist and J. Carazzone. "Infrared Singularities and Massive Fields".
In: *Phys. Rev.* D11 (1975), p. 2856. DOI: 10.1103/PhysRevD.11.2856.

[32] A. J. Buras. "Weak Hamiltonian, CP violation and rare decays".
In: *Probing the standard model of particle interactions. Proceedings, Summer School in Theoretical Physics, NATO Advanced Study Institute, 68th session, Les Houches, France, July 28-September 5, 1997. Pt. 1, 2*. 1998, pp. 281–539.
arXiv: hep-ph/9806471 [hep-ph].

[33] J. Ellis. "TikZ-Feynman: Feynman diagrams with TikZ".
In: *Comput. Phys. Commun.* 210 (2017), pp. 103–123.
DOI: 10.1016/j.cpc.2016.08.019. arXiv: 1601.05437 [hep-ph].

[34] M. Wirbel, B. Stech, and M. Bauer.
"Exclusive Semileptonic Decays of Heavy Mesons".
In: *Z. Phys.* C29 (1985), p. 637. DOI: 10.1007/BF01560299.

[35] Y. Sakaki, M. Tanaka, A. Tayduganov, and R. Watanabe.
"Testing leptoquark models in $\bar{B} \to D^{(*)}\tau\bar{\nu}$".
In: *Phys. Rev.* D88.9 (2013), p. 094012. DOI: 10.1103/PhysRevD.88.094012.
arXiv: 1309.0301 [hep-ph].

[36] N. Isgur and M. B. Wise.
"Weak Decays of Heavy Mesons in the Static Quark Approximation".
In: *Phys. Lett.* B232 (1989), pp. 113–117.
DOI: 10.1016/0370-2693(89)90566-2.

[37] T. Mannel, W. Roberts, and Z. Ryzak.
"A Derivation of the heavy quark effective Lagrangian from QCD".
In: *Nucl. Phys.* B368 (1992), pp. 204–217.
DOI: 10.1016/0550-3213(92)90204-O.

[38] M. Neubert. "Heavy quark symmetry". In: *Phys. Rept.* 245 (1994), pp. 259–396.
DOI: 10.1016/0370-1573(94)90091-4. arXiv: hep-ph/9306320 [hep-ph].

[39] K. G. Wilson. "Quark Confinement."
In: *Conf. Proc.* C7406241 (1974), pp. 125–147.

[40] A. Bharucha, D. M. Straub, and R. Zwicky.
"$B \to V\ell^+\ell^-$ in the Standard Model from light-cone sum rules".
In: *JHEP* 08 (2016), p. 098. DOI: 10.1007/JHEP08(2016)098.
arXiv: 1503.05534 [hep-ph].

[41] J. Aebischer, M. Fael, C. Greub, and J. Virto.
"B physics Beyond the Standard Model at One Loop: Complete Renormalization Group Evolution below the Electroweak Scale". In: *JHEP* 09 (2017), p. 158.
DOI: 10.1007/JHEP09(2017)158. arXiv: 1704.06639 [hep-ph].

[42] I. Caprini, L. Lellouch, and M. Neubert. "Dispersive bounds on the shape of anti-B —> D(*) lepton anti-neutrino form-factors".
In: *Nucl. Phys.* B530 (1998), pp. 153–181.
DOI: 10.1016/S0550-3213(98)00350-2. arXiv: hep-ph/9712417 [hep-ph].

[43] H. Na et al. "$B \to Dl\nu$ form factors at nonzero recoil and extraction of $|V_{cb}|$".
In: *Phys. Rev.* D92.5 (2015). [Erratum: Phys. Rev.D93,no.11,119906(2016)], p. 054510.
DOI: 10.1103/PhysRevD.93.119906,10.1103/PhysRevD.92.054510.
arXiv: 1505.03925 [hep-lat].

[44] J. P. Lees et al. "Measurement of an Excess of $\bar{B} \to D^{(*)}\tau^-\bar{\nu}_\tau$ Decays and Implications for Charged Higgs Bosons". In: *Phys. Rev.* D88.7 (2013), p. 072012. DOI: 10.1103/PhysRevD.88.072012. arXiv: 1303.0571 [hep-ex].

[45] R. Glattauer et al. "Measurement of the decay $B \to D\ell\nu_\ell$ in fully reconstructed events and determination of the Cabibbo-Kobayashi-Maskawa matrix element $|V_{cb}|$". In: *Phys. Rev.* D93.3 (2016), p. 032006. DOI: 10.1103/PhysRevD.93.032006. arXiv: 1510.03657 [hep-ex].

[46] A. Abdesselam et al. "Precise determination of the CKM matrix element $|V_{cb}|$ with $\bar{B}^0 \to D^{*+}\ell^-\bar{\nu}_\ell$ decays with hadronic tagging at Belle". In: (2017). arXiv: 1702.01521 [hep-ex].

[47] C. Murgui, A. Peñuelas, M. Jung, and A. Pich. "Global fit to $b \to c\tau\nu$ transitions". In: *JHEP* 09 (2019), p. 103. DOI: 10.1007/JHEP09(2019)103. arXiv: 1904.09311 [hep-ph].

[48] W. Altmannshofer et al. "The Belle II Physics Book". In: *PTEP* 2019.12 (2019). Ed. by E. Kou and P. Urquijo. [erratum: PTEP2020,no.2,029201(2020)], p. 123C01. DOI: 10.1093/ptep/ptz106,10.1093/ptep/ptaa008. arXiv: 1808.10567 [hep-ex].

[49] R. Aaij et al. "Measurement of the ratio of branching fractions $\mathcal{B}(B_c^+ \to J/\psi\tau^+\nu_\tau)/\mathcal{B}(B_c^+ \to J/\psi\mu^+\nu_\mu)$". In: *Phys. Rev. Lett.* 120.12 (2018), p. 121801. DOI: 10.1103/PhysRevLett.120.121801. arXiv: 1711.05623 [hep-ex].

[50] A. Y. Anisimov, I. M. Narodetsky, C. Semay, and B. Silvestre-Brac. "The B_c meson lifetime in the light front constituent quark model". In: *Phys. Lett.* B452 (1999), pp. 129–136. DOI: 10.1016/S0370-2693(99)00273-7. arXiv: hep-ph/9812514 [hep-ph].

[51] V. V. Kiselev. "Exclusive decays and lifetime of B_c meson in QCD sum rules". In: (2002). arXiv: hep-ph/0211021 [hep-ph].

[52] M. A. Ivanov, J. G. Korner, and P. Santorelli. "Exclusive semileptonic and nonleptonic decays of the B_c meson". In: *Phys. Rev.* D73 (2006), p. 054024. DOI: 10.1103/PhysRevD.73.054024. arXiv: hep-ph/0602050 [hep-ph].

[53] E. Hernandez, J. Nieves, and J. M. Verde-Velasco. "Study of exclusive semileptonic and non-leptonic decays of B_c - in a nonrelativistic quark model". In: *Phys. Rev.* D74 (2006), p. 074008. DOI: 10.1103/PhysRevD.74.074008. arXiv: hep-ph/0607150 [hep-ph].

[54] T. Huang and F. Zuo.
"Semileptonic B_c decays and charmonium distribution amplitude".
In: *Eur. Phys. J.* C51 (2007), pp. 833–839.
DOI: 10.1140/epjc/s10052-007-0333-4. arXiv: hep-ph/0702147 [HEP-PH].

[55] W. Wang, Y.-L. Shen, and C.-D. Lu.
"Covariant Light-Front Approach for B(c) transition form factors".
In: *Phys. Rev.* D79 (2009), p. 054012. DOI: 10.1103/PhysRevD.79.054012.
arXiv: 0811.3748 [hep-ph].

[56] W.-F. Wang, Y.-Y. Fan, and Z.-J. Xiao.
"Semileptonic decays $B_c \to (\eta_c, J/\Psi) l\nu$ in the perturbative QCD approach".
In: *Chin. Phys.* C37 (2013), p. 093102.
DOI: 10.1088/1674-1137/37/9/093102. arXiv: 1212.5903 [hep-ph].

[57] A. Issadykov and M. A. Ivanov. "The decays $B_c \to J/\psi + \bar{\ell}\nu_\ell$ and
$B_c \to J/\psi + \pi(K)$ in covariant confined quark model".
In: *Phys. Lett.* B783 (2018), pp. 178–182. DOI: 10.1016/j.physletb.2018.06.056.
arXiv: 1804.00472 [hep-ph].

[58] D. Leljak, B. Melic, and M. Patra.
"On lepton flavour universality in semileptonic $B_c \to \eta_c, J/\psi$ decays".
In: *JHEP* 05 (2019), p. 094. DOI: 10.1007/JHEP05(2019)094.
arXiv: 1901.08368 [hep-ph].

[59] K. Azizi, Y. Sarac, and H. Sundu.
"Lepton flavor universality violation in semileptonic tree level weak transitions".
In: *Phys. Rev.* D99.11 (2019), p. 113004. DOI: 10.1103/PhysRevD.99.113004.
arXiv: 1904.08267 [hep-ph].

[60] X.-Q. Hu, S.-P. Jin, and Z.-J. Xiao.
"Semileptonic decays $B_c \to (\eta_c, J/\psi) l\bar{\nu}_l$ in the "PQCD + Lattice" approach".
In: *Chin. Phys.* C44.2 (2020), p. 023104.
DOI: 10.1088/1674-1137/44/2/023104. arXiv: 1904.07530 [hep-ph].

[61] D. Marangotto. "Angular and CP-Violation Analyses of $\bar{B} \to D^{*+} l^- \bar{\nu}_l$ Decays at
Hadron Collider Experiments".
In: *Adv. High Energy Phys.* 2019 (2019), p. 5274609.
DOI: 10.1155/2019/5274609. arXiv: 1812.08144 [hep-ex].

[62] B. Aubert et al. "A Measurement of the branching fractions of exclusive
$\bar{B} \to D^{(*)}(\pi)\ell^-\bar{\nu}(\ell^+$ decays in events with a fully reconstructed B meson".
In: *Phys. Rev. Lett.* 100 (2008), p. 151802.
DOI: 10.1103/PhysRevLett.100.151802. arXiv: 0712.3503 [hep-ex].

[63] J. P. Lees et al. "Evidence for an excess of $\bar{B} \to D^{(*)}\tau^-\bar{\nu}_\tau$ decays".
In: *Phys. Rev. Lett.* 109 (2012), p. 101802.
DOI: 10.1103/PhysRevLett.109.101802. arXiv: 1205.5442 [hep-ex].

[64] M. Huschle et al. "Measurement of the branching ratio of $\bar{B} \to D^{(*)}\tau^-\bar{\nu}_\tau$ relative to $\bar{B} \to D^{(*)}\ell^-\bar{\nu}_\ell$ decays with hadronic tagging at Belle".
In: *Phys. Rev.* D92.7 (2015), p. 072014. DOI: 10.1103/PhysRevD.92.072014.
arXiv: 1507.03233 [hep-ex].

[65] A. Abdesselam et al.
"Measurement of $\mathcal{R}(D)$ and $\mathcal{R}(D^*)$ with a semileptonic tagging method".
In: (2019). arXiv: 1904.08794 [hep-ex].

[66] R. Aaij et al. "Measurement of the ratio of branching fractions $\mathcal{B}(\bar{B}^0 \to D^{*+}\tau^-\bar{\nu}_\tau)/\mathcal{B}(\bar{B}^0 \to D^{*+}\mu^-\bar{\nu}_\mu)$". In: *Phys. Rev. Lett.* 115.11 (2015). [Erratum: Phys. Rev. Lett.115,no.15,159901(2015)], p. 111803.
DOI: 10.1103/PhysRevLett.115.159901,10.1103/PhysRevLett.115.111803.
arXiv: 1506.08614 [hep-ex].

[67] Y. Sato et al. "Measurement of the branching ratio of $\bar{B}^0 \to D^{*+}\tau^-\bar{\nu}_\tau$ relative to $\bar{B}^0 \to D^{*+}\ell^-\bar{\nu}_\ell$ decays with a semileptonic tagging method".
In: *Phys. Rev.* D94.7 (2016), p. 072007. DOI: 10.1103/PhysRevD.94.072007.
arXiv: 1607.07923 [hep-ex].

[68] S. Hirose et al. "Measurement of the τ lepton polarization and $R(D^*)$ in the decay $\bar{B} \to D^*\tau^-\bar{\nu}_\tau$". In: *Phys. Rev. Lett.* 118.21 (2017), p. 211801.
DOI: 10.1103/PhysRevLett.118.211801. arXiv: 1612.00529 [hep-ex].

[69] R. Aaij et al. "Test of Lepton Flavor Universality by the measurement of the $B^0 \to D^{*-}\tau^+\nu_\tau$ branching fraction using three-prong τ decays".
In: *Phys. Rev.* D97.7 (2018), p. 072013. DOI: 10.1103/PhysRevD.97.072013.
arXiv: 1711.02505 [hep-ex].

[70] J. A. Bailey et al.
"$B \to D\ell\nu$ form factors at nonzero recoil and $|V_{cb}|$ from 2+1-flavor lattice QCD".
In: *Phys. Rev.* D92.3 (2015), p. 034506. DOI: 10.1103/PhysRevD.92.034506.
arXiv: 1503.07237 [hep-lat].

[71] S. Aoki et al. "Review of lattice results concerning low-energy particle physics".
In: *Eur. Phys. J.* C77.2 (2017), p. 112. DOI: 10.1140/epjc/s10052-016-4509-7.
arXiv: 1607.00299 [hep-lat].

[72] D. Bigi and P. Gambino. "Revisiting $B \to D\ell\nu$".
In: *Phys. Rev.* D94.9 (2016), p. 094008. DOI: 10.1103/PhysRevD.94.094008.
arXiv: 1606.08030 [hep-ph].

[73] S. Fajfer, J. F. Kamenik, and I. Nisandzic.
"On the $B \to D^*\tau\bar{\nu}_\tau$ Sensitivity to New Physics".
In: *Phys. Rev.* D85 (2012), p. 094025. DOI: 10.1103/PhysRevD.85.094025.
arXiv: 1203.2654 [hep-ph].

[74] F. U. Bernlochner, Z. Ligeti, M. Papucci, and D. J. Robinson. "Combined analysis of semileptonic B decays to D and D^*: $R(D^{(*)})$, $|V_{cb}|$, and new physics". In: *Phys. Rev.* D95.11 (2017). [erratum: Phys. Rev.D97,no.5,059902(2018)], p. 115008. DOI: 10.1103/PhysRevD.95.115008,10.1103/PhysRevD.97.059902. arXiv: 1703.05330 [hep-ph].

[75] D. Bigi, P. Gambino, and S. Schacht. "$R(D^*)$, $|V_{cb}|$, and the Heavy Quark Symmetry relations between form factors". In: *JHEP* 11 (2017), p. 061. DOI: 10.1007/JHEP11(2017)061. arXiv: 1707.09509 [hep-ph].

[76] S. Jaiswal, S. Nandi, and S. K. Patra. "Extraction of $|V_{cb}|$ from $B \to D^{(*)}\ell\nu_\ell$ and the Standard Model predictions of $R(D^{(*)})$". In: *JHEP* 12 (2017), p. 060. DOI: 10.1007/JHEP12(2017)060. arXiv: 1707.09977 [hep-ph].

[77] M. Beneke, T. Feldmann, and D. Seidel. "Systematic approach to exclusive $B \to Vl^+l^-$, $V\gamma$ decays". In: *Nucl. Phys.* B612 (2001), pp. 25–58. DOI: 10.1016/S0550-3213(01)00366-2. arXiv: hep-ph/0106067 [hep-ph].

[78] K. G. Chetyrkin, M. Misiak, and M. Munz. "Weak radiative B meson decay beyond leading logarithms". In: *Phys. Lett.* B400 (1997). [Erratum: Phys. Lett.B425,414(1998)], pp. 206–219. DOI: 10.1016/S0370-2693(97)00324-9. arXiv: hep-ph/9612313 [hep-ph].

[79] C. Bobeth, T. Ewerth, F. Kruger, and J. Urban. "Analysis of neutral Higgs boson contributions to the decays $\bar{B}_s \to \ell^+\ell^-$ and $\bar{B} \to K\ell^+\ell^-$". In: *Phys. Rev.* D64 (2001), p. 074014. DOI: 10.1103/PhysRevD.64.074014. arXiv: hep-ph/0104284 [hep-ph].

[80] C. Bouchard et al. "Rare decay $B \to K\ell^+\ell^-$ form factors from lattice QCD". In: *Phys. Rev.* D88.5 (2013). [Erratum: Phys. Rev.D88,no.7,079901(2013)], p. 054509. DOI: 10.1103/PhysRevD.88.079901,10.1103/PhysRevD.88.054509. arXiv: 1306.2384 [hep-lat].

[81] C. Bobeth, G. Hiller, and G. Piranishvili. "Angular distributions of $\bar{B} \to \bar{K}\ell^+\ell^-$ decays". In: *JHEP* 12 (2007), p. 040. DOI: 10.1088/1126-6708/2007/12/040. arXiv: 0709.4174 [hep-ph].

[82] C. Bobeth, G. Hiller, and D. van Dyk. "General analysis of $\bar{B} \to \bar{K}^{(*)}\ell^+\ell^-$ decays at low recoil". In: *Phys. Rev.* D87.3 (2013). [Phys. Rev.D87,034016(2013)], p. 034016. DOI: 10.1103/PhysRevD.87.034016. arXiv: 1212.2321 [hep-ph].

[83] P. Ball and R. Zwicky.
"$B_{d,s} \to \rho, \omega, K^*, \phi$ decay form-factors from light-cone sum rules revisited".
In: *Phys. Rev.* D71 (2005), p. 014029. DOI: 10.1103/PhysRevD.71.014029.
arXiv: hep-ph/0412079 [hep-ph].

[84] T. Blake, T. Gershon, and G. Hiller. "Rare b hadron decays at the LHC".
In: *Ann. Rev. Nucl. Part. Sci.* 65 (2015), pp. 113–143.
DOI: 10.1146/annurev-nucl-102014-022231. arXiv: 1501.03309 [hep-ex].

[85] A. Ghinculov, T. Hurth, G. Isidori, and Y. P. Yao.
"New NNLL results on the decay B —> X(s) l+ l-".
In: *Eur. Phys. J.* C33 (2004), S288–S290.
DOI: 10.1140/epjcd/s2003-03-206-2. arXiv: hep-ph/0310187 [hep-ph].

[86] R. Aaij et al. "Differential branching fraction and angular analysis of the decay $B^0 \to K^{*0}\mu^+\mu^-$". In: *JHEP* 08 (2013), p. 131.
DOI: 10.1007/JHEP08(2013)131. arXiv: 1304.6325 [hep-ex].

[87] R. Aaij et al. "Differential branching fractions and isospin asymmetries of $B \to K^{(*)}\mu^+\mu^-$ decays". In: *JHEP* 06 (2014), p. 133.
DOI: 10.1007/JHEP06(2014)133. arXiv: 1403.8044 [hep-ex].

[88] R. Aaij et al.
"Angular analysis and differential branching fraction of the decay $B_s^0 \to \phi\mu^+\mu^-$".
In: *JHEP* 09 (2015), p. 179. DOI: 10.1007/JHEP09(2015)179.
arXiv: 1506.08777 [hep-ex].

[89] R. Aaij et al.
"Differential branching fraction and angular analysis of $\Lambda_b^0 \to \Lambda\mu^+\mu^-$ decays".
In: *JHEP* 06 (2015). [Erratum: JHEP09,145(2018)], p. 115.
DOI: 10.1007/JHEP09(2018)145,10.1007/JHEP06(2015)115.
arXiv: 1503.07138 [hep-ex].

[90] W. Altmannshofer and D. M. Straub.
"New physics in $b \to s$ transitions after LHC run 1".
In: *Eur. Phys. J.* C75.8 (2015), p. 382. DOI: 10.1140/epjc/s10052-015-3602-7.
arXiv: 1411.3161 [hep-ph].

[91] W. Detmold, C. .-J. D. Lin, S. Meinel, and M. Wingate.
"$\Lambda_b \to \Lambda\ell^+\ell^-$ form factors and differential branching fraction from lattice QCD".
In: *Phys. Rev.* D87.7 (2013), p. 074502. DOI: 10.1103/PhysRevD.87.074502.
arXiv: 1212.4827 [hep-lat].

[92] W. Altmannshofer et al. "Symmetries and Asymmetries of $B \to K^*\mu^+\mu^-$ Decays in the Standard Model and Beyond". In: *JHEP* 01 (2009), p. 019.
DOI: 10.1088/1126-6708/2009/01/019. arXiv: 0811.1214 [hep-ph].

[93] F. Kruger and J. Matias. "Probing new physics via the transverse amplitudes of $B^0 \to K^{*0}(\to K^-\pi^+)l^+l^-$ at large recoil". In: *Phys. Rev.* D71 (2005), p. 094009.
DOI: 10.1103/PhysRevD.71.094009. arXiv: hep-ph/0502060 [hep-ph].

[94] C. Bobeth, G. Hiller, and D. van Dyk.
"The Benefits of $\bar{B} -> \bar{K}^* l^+ l^-$ Decays at Low Recoil".
In: *JHEP* 07 (2010), p. 098. DOI: 10.1007/JHEP07(2010)098.
arXiv: 1006.5013 [hep-ph].

[95] D. Becirevic and E. Schneider. "On transverse asymmetries in B –> K* l+l-".
In: *Nucl. Phys.* B854 (2012), pp. 321–339.
DOI: 10.1016/j.nuclphysb.2011.09.004. arXiv: 1106.3283 [hep-ph].

[96] J. Matias, F. Mescia, M. Ramon, and J. Virto.
"Complete Anatomy of $\bar{B}_d -> \bar{K}^{*0}(-> K\pi) l^+ l^-$ and its angular distribution".
In: *JHEP* 04 (2012), p. 104. DOI: 10.1007/JHEP04(2012)104.
arXiv: 1202.4266 [hep-ph].

[97] S. Descotes-Genon, J. Matias, M. Ramon, and J. Virto. "Implications from clean observables for the binned analysis of $B -> K * \mu^+ \mu^-$ at large recoil".
In: *JHEP* 01 (2013), p. 048. DOI: 10.1007/JHEP01(2013)048.
arXiv: 1207.2753 [hep-ph].

[98] R. Aaij et al. "Angular analysis of the $B^0 \to K^{*0} \mu^+ \mu^-$ decay using 3 fb^{-1} of integrated luminosity". In: *JHEP* 02 (2016), p. 104.
DOI: 10.1007/JHEP02(2016)104. arXiv: 1512.04442 [hep-ex].

[99] S. Wehle et al. "Lepton-Flavor-Dependent Angular Analysis of $B \to K^* \ell^+ \ell^-$".
In: *Phys. Rev. Lett.* 118.11 (2017), p. 111801.
DOI: 10.1103/PhysRevLett.118.111801. arXiv: 1612.05014 [hep-ex].

[100] M. Aaboud et al. "Angular analysis of $B_d^0 \to K^* \mu^+ \mu^-$ decays in *pp* collisions at $\sqrt{s} = 8$ TeV with the ATLAS detector". In: *JHEP* 10 (2018), p. 047.
DOI: 10.1007/JHEP10(2018)047. arXiv: 1805.04000 [hep-ex].

[101] A. M. Sirunyan et al. "Measurement of angular parameters from the decay $\text{B}^0 \to \text{K}^{*0} \mu^+ \mu^-$ in proton-proton collisions at $\sqrt{s} = 8$ TeV".
In: *Phys. Lett.* B781 (2018), pp. 517–541. DOI: 10.1016/j.physletb.2018.04.030.
arXiv: 1710.02846 [hep-ex].

[102] S. Descotes-Genon, L. Hofer, J. Matias, and J. Virto. "On the impact of power corrections in the prediction of $B \to K^* \mu^+ \mu^-$ observables".
In: *JHEP* 12 (2014), p. 125. DOI: 10.1007/JHEP12(2014)125.
arXiv: 1407.8526 [hep-ph].

[103] E. Graverini. "Flavour anomalies: a review".
In: *J. Phys. Conf. Ser.* 1137.1 (2019), p. 012025.
DOI: 10.1088/1742-6596/1137/1/012025. arXiv: 1807.11373 [hep-ex].

[104] A. Khodjamirian, T. Mannel, A. A. Pivovarov, and Y. .-M. Wang.
"Charm-loop effect in $B \to K^{(*)} \ell^+ \ell^-$ and $B \to K^* \gamma$".
In: *JHEP* 09 (2010), p. 089. DOI: 10.1007/JHEP09(2010)089.
arXiv: 1006.4945 [hep-ph].

[105] B. Capdevila et al.
"$B \to K^*(\to K\pi)\ell^+\ell^-$ theory and the global picture: What's next?"
In: *PoS* LHCP2016 (2016), p. 073. DOI: 10.22323/1.276.0073.
arXiv: 1609.01355 [hep-ph].

[106] T. Blake et al. "Round table: Flavour anomalies in $b \to s\ell^+\ell^-$ processes".
In: *EPJ Web Conf.* 137 (2017), p. 01001. DOI: 10.1051/epjconf/201713701001.
arXiv: 1703.10005 [hep-ph].

[107] G. Hiller and F. Kruger. "More model-independent analysis of $b \to s$ processes".
In: *Phys. Rev.* D69 (2004), p. 074020. DOI: 10.1103/PhysRevD.69.074020.
arXiv: hep-ph/0310219 [hep-ph].

[108] M. Bordone, G. Isidori, and A. Pattori.
"On the Standard Model predictions for R_K and R_{K^*}".
In: *Eur. Phys. J.* C76.8 (2016), p. 440. DOI: 10.1140/epjc/s10052-016-4274-7.
arXiv: 1605.07633 [hep-ph].

[109] R. Aaij et al. "Test of lepton universality with $B^0 \to K^{*0}\ell^+\ell^-$ decays".
In: *JHEP* 08 (2017), p. 055. DOI: 10.1007/JHEP08(2017)055.
arXiv: 1705.05802 [hep-ex].

[110] A. Abdesselam et al.
"Test of Lepton-Flavor Universality in $B \to K^*\ell^+\ell^-$ Decays at Belle".
In: *Phys. Rev. Lett.* 126.16 (2021), p. 161801.
DOI: 10.1103/PhysRevLett.126.161801. arXiv: 1904.02440 [hep-ex].

[111] J. P. Lees et al. "Measurement of Branching Fractions and Rate Asymmetries in the Rare Decays $B \to K^{(*)}l^+l^-$". In: *Phys. Rev.* D86 (2012), p. 032012.
DOI: 10.1103/PhysRevD.86.032012. arXiv: 1204.3933 [hep-ex].

[112] J. .-T. Wei et al. "Measurement of the Differential Branching Fraction and Forward-Backword Asymmetry for $B \to K^{(*)}\ell^+\ell^-$".
In: *Phys. Rev. Lett.* 103 (2009), p. 171801.
DOI: 10.1103/PhysRevLett.103.171801. arXiv: 0904.0770 [hep-ex].

[113] G. Hiller and I. Nisandzic. "R_K and R_{K^*} beyond the standard model".
In: *Phys. Rev.* D96.3 (2017), p. 035003. DOI: 10.1103/PhysRevD.96.035003.
arXiv: 1704.05444 [hep-ph].

[114] G. Hiller and M. Schmaltz. "Diagnosing lepton-nonuniversality in $b \to s\ell\ell$".
In: *JHEP* 02 (2015), p. 055. DOI: 10.1007/JHEP02(2015)055.
arXiv: 1411.4773 [hep-ph].

[115] A. J. Buras, J. Girrbach-Noe, C. Niehoff, and D. M. Straub.
"$B \to K^{(*)}\nu\overline{\nu}$ decays in the Standard Model and beyond".
In: *JHEP* 02 (2015), p. 184. DOI: 10.1007/JHEP02(2015)184.
arXiv: 1409.4557 [hep-ph].

[116] J. Brod, M. Gorbahn, and E. Stamou.
"Two-Loop Electroweak Corrections for the $K \to \pi\nu\bar{\nu}$ Decays".
In: *Phys. Rev.* D83 (2011), p. 034030. DOI: 10.1103/PhysRevD.83.034030.
arXiv: 1009.0947 [hep-ph].

[117] J. P. Lees et al. "Search for $B \to K^{(*)}\nu\overline{\nu}$ and invisible quarkonium decays".
In: *Phys. Rev.* D87.11 (2013), p. 112005. DOI: 10.1103/PhysRevD.87.112005.
arXiv: 1303.7465 [hep-ex].

[118] J. H. Christenson, J. W. Cronin, V. L. Fitch, and R. Turlay.
"Evidence for the 2π Decay of the K_2^0 Meson".
In: *Phys. Rev. Lett.* 13 (1964), pp. 138–140. DOI: 10.1103/PhysRevLett.13.138.

[119] M. K. Gaillard, B. W. Lee, and J. L. Rosner. "Search for Charm".
In: *Rev. Mod. Phys.* 47 (1975), pp. 277–310.
DOI: 10.1103/RevModPhys.47.277.

[120] A. Lenz et al. "Anatomy of New Physics in $B - \bar{B}$ mixing".
In: *Phys. Rev.* D83 (2011), p. 036004. DOI: 10.1103/PhysRevD.83.036004.
arXiv: 1008.1593 [hep-ph].

[121] L. Di Luzio, M. Kirk, A. Lenz, and T. Rauh.
"ΔM_s theory precision confronts flavour anomalies". In: *JHEP* 12 (2019), p. 009.
DOI: 10.1007/JHEP12(2019)009. arXiv: 1909.11087 [hep-ph].

[122] S. de Boer and G. Hiller.
"Flavor and new physics opportunities with rare charm decays into leptons".
In: *Phys. Rev.* D93.7 (2016), p. 074001. DOI: 10.1103/PhysRevD.93.074001.
arXiv: 1510.00311 [hep-ph].

[123] R. Kitano, M. Koike, and Y. Okada. "Detailed calculation of lepton flavor violating muon electron conversion rate for various nuclei".
In: *Phys. Rev.* D66 (2002). [Erratum: Phys. Rev.D76,059902(2007)], p. 096002.
DOI: 10.1103/PhysRevD.76.059902,10.1103/PhysRevD.66.096002.
arXiv: hep-ph/0203110 [hep-ph].

[124] L. Bartoszek et al. "Mu2e Technical Design Report". In: (2014).
DOI: 10.2172/1172555. arXiv: 1501.05241 [physics.ins-det].

[125] Y. G. Cui et al. "Conceptual design report for experimental search for lepton flavor violating mu- - e- conversion at sensitivity of 10**(-16) with a slow-extracted bunched proton beam (COMET)". In: (2009).

[126] A. M. Baldini et al. "MEG Upgrade Proposal". In: (2013).
arXiv: 1301.7225 [physics.ins-det].

[127] M. Carpentier and S. Davidson.
"Constraints on two-lepton, two quark operators".
In: *Eur. Phys. J.* C70 (2010), pp. 1071–1090.
DOI: 10.1140/epjc/s10052-010-1482-4. arXiv: 1008.0280 [hep-ph].

[128] S. Davidson, D. C. Bailey, and B. A. Campbell.
"Model independent constraints on leptoquarks from rare processes".
In: *Z. Phys.* C61 (1994), pp. 613–644. DOI: 10.1007/BF01552629.
arXiv: hep-ph/9309310 [hep-ph].

[129] D. Ambrose et al. "New limit on muon and electron lepton number violation from K0(L) —> mu+- e-+ decay".
In: *Phys. Rev. Lett.* 81 (1998), pp. 5734–5737.
DOI: 10.1103/PhysRevLett.81.5734. arXiv: hep-ex/9811038 [hep-ex].

[130] W. Buchmuller, R. Ruckl, and D. Wyler.
"Leptoquarks in Lepton - Quark Collisions".
In: *Phys. Lett.* B191 (1987). [Erratum: Phys. Lett.B448,320(1999)], pp. 442–448.
DOI: 10.1016/S0370-2693(99)00014-3,10.1016/0370-2693(87)90637-X.

[131] H. Georgi and S. L. Glashow. "Unity of All Elementary Particle Forces".
In: *Phys. Rev. Lett.* 32 (1974), pp. 438–441.
DOI: 10.1103/PhysRevLett.32.438.

[132] J. C. Pati and A. Salam. "Lepton Number as the Fourth Color".
In: *Phys. Rev.* D10 (1974). [Erratum: Phys. Rev.D11,703(1975)], pp. 275–289.
DOI: 10.1103/PhysRevD.10.275,10.1103/PhysRevD.11.703.2.

[133] G. Bhattacharyya, D. Choudhury, and K. Sridhar.
"R-parity violating SUSY or leptoquarks: Virtual effects in dilepton production".
In: *Phys. Lett.* B349 (1995), pp. 118–124.
DOI: 10.1016/0370-2693(95)00238-G. arXiv: hep-ph/9412259 [hep-ph].

[134] D. B. Kaplan. "Flavor at SSC energies: A New mechanism for dynamically generated fermion masses". In: *Nucl. Phys.* B365 (1991), pp. 259–278.
DOI: 10.1016/S0550-3213(05)80021-5.

[135] I. Dorsner, S. Fajfer, and N. Kosnik.
"Heavy and light scalar leptoquarks in proton decay".
In: *Phys. Rev.* D86 (2012), p. 015013. DOI: 10.1103/PhysRevD.86.015013.
arXiv: 1204.0674 [hep-ph].

[136] G. Hiller and M. Schmaltz.
"R_K and future $b \to s\ell\ell$ physics beyond the standard model opportunities".
In: *Phys. Rev.* D90 (2014), p. 054014. DOI: 10.1103/PhysRevD.90.054014.
arXiv: 1408.1627 [hep-ph].

[137] S. Biswas, D. Chowdhury, S. Han, and S. J. Lee. "Explaining the lepton non-universality at the LHCb and CMS within a unified framework".
In: *JHEP* 02 (2015), p. 142. DOI: 10.1007/JHEP02(2015)142.
arXiv: 1409.0882 [hep-ph].

[138] B. Gripaios, M. Nardecchia, and S. A. Renner.
"Composite leptoquarks and anomalies in B-meson decays".
In: *JHEP* 05 (2015), p. 006. DOI: 10.1007/JHEP05(2015)006.
arXiv: 1412.1791 [hep-ph].

[139] S. Sahoo and R. Mohanta. "Scalar leptoquarks and the rare B meson decays".
In: *Phys. Rev.* D91.9 (2015), p. 094019. DOI: 10.1103/PhysRevD.91.094019.
arXiv: 1501.05193 [hep-ph].

[140] R. Alonso, B. Grinstein, and J. Martin Camalich.
"Lepton universality violation and lepton flavor conservation in B-meson decays".
In: *JHEP* 10 (2015), p. 184. DOI: 10.1007/JHEP10(2015)184.
arXiv: 1505.05164 [hep-ph].

[141] S. Fajfer, J. F. Kamenik, I. Nisandzic, and J. Zupan.
"Implications of Lepton Flavor Universality Violations in B Decays".
In: *Phys. Rev. Lett.* 109 (2012), p. 161801.
DOI: 10.1103/PhysRevLett.109.161801. arXiv: 1206.1872 [hep-ph].

[142] B. Bhattacharya, A. Datta, D. London, and S. Shivashankara.
"Simultaneous Explanation of the R_K and $R(D^{(*)})$ Puzzles".
In: *Phys. Lett.* B742 (2015), pp. 370–374. DOI: 10.1016/j.physletb.2015.02.011.
arXiv: 1412.7164 [hep-ph].

[143] L. Calibbi, A. Crivellin, and T. Ota. "Effective Field Theory Approach to $b \to s\ell\ell^{(\prime)}$, $B \to K^{(*)}\nu\overline{\nu}$ and $B \to D^{(*)}\tau\nu$ with Third Generation Couplings".
In: *Phys. Rev. Lett.* 115 (2015), p. 181801.
DOI: 10.1103/PhysRevLett.115.181801. arXiv: 1506.02661 [hep-ph].

[144] B. Bhattacharya et al.
"Simultaneous Explanation of the R_K and $R_{D^{(*)}}$ Puzzles: a Model Analysis".
In: *JHEP* 01 (2017), p. 015. DOI: 10.1007/JHEP01(2017)015.
arXiv: 1609.09078 [hep-ph].

[145] D. Buttazzo, A. Greljo, G. Isidori, and D. Marzocca.
"B-physics anomalies: a guide to combined explanations".
In: *JHEP* 11 (2017), p. 044. DOI: 10.1007/JHEP11(2017)044.
arXiv: 1706.07808 [hep-ph].

[146] L. Di Luzio, A. Greljo, and M. Nardecchia.
"Gauge leptoquark as the origin of B-physics anomalies".
In: *Phys. Rev.* D96.11 (2017), p. 115011. DOI: 10.1103/PhysRevD.96.115011.
arXiv: 1708.08450 [hep-ph].

[147] R. Barbieri and A. Tesi. "B-decay anomalies in Pati-Salam SU(4)".
In: *Eur. Phys. J.* C78.3 (2018), p. 193. DOI: 10.1140/epjc/s10052-018-5680-9.
arXiv: 1712.06844 [hep-ph].

[148] M. Blanke and A. Crivellin. "B Meson Anomalies in a Pati-Salam Model within the Randall-Sundrum Background". In: *Phys. Rev. Lett.* 121.1 (2018), p. 011801. DOI: 10.1103/PhysRevLett.121.011801. arXiv: 1801.07256 [hep-ph].

[149] J. Kumar, D. London, and R. Watanabe. "Combined Explanations of the $b \to s\mu^+\mu^-$ and $b \to c\tau^-\bar{\nu}$ Anomalies: a General Model Analysis". In: *Phys. Rev.* D99.1 (2019), p. 015007. DOI: 10.1103/PhysRevD.99.015007. arXiv: 1806.07403 [hep-ph].

[150] B. Fornal, S. A. Gadam, and B. Grinstein. "Left-Right SU(4) Vector Leptoquark Model for Flavor Anomalies". In: *Phys. Rev.* D99.5 (2019), p. 055025. DOI: 10.1103/PhysRevD.99.055025. arXiv: 1812.01603 [hep-ph].

[151] M. Davier, A. Hoecker, B. Malaescu, and Z. Zhang. "Reevaluation of the Hadronic Contributions to the Muon g-2 and to alpha(MZ)". In: *Eur. Phys. J.* C71 (2011). [Erratum: Eur. Phys. J.C72,1874(2012)], p. 1515. DOI: 10.1140/epjc/s10052-012-1874-8,10.1140/epjc/s10052-010-1515-z. arXiv: 1010.4180 [hep-ph].

[152] M. Bauer and M. Neubert. "Minimal Leptoquark Explanation for the $R_{D^{(*)}}$, R_K , and $(g-2)_\mu$ Anomalies". In: *Phys. Rev. Lett.* 116.14 (2016), p. 141802. DOI: 10.1103/PhysRevLett.116.141802. arXiv: 1511.01900 [hep-ph].

[153] O. Popov and G. A. White. "One Leptoquark to unify them? Neutrino masses and unification in the light of $(g-2)_\mu$, $R_{D^{(*)}}$ and R_K anomalies". In: *Nucl. Phys.* B923 (2017), pp. 324–338. DOI: 10.1016/j.nuclphysb.2017.08.007. arXiv: 1611.04566 [hep-ph].

[154] C.-H. Chen, T. Nomura, and H. Okada. "Excesses of muon $g-2$, $R_{D^{(*)}}$, and R_K in a leptoquark model". In: *Phys. Lett.* B774 (2017), pp. 456–464. DOI: 10.1016/j.physletb.2017.10.005. arXiv: 1703.03251 [hep-ph].

[155] A. Leike. "The Phenomenology of extra neutral gauge bosons". In: *Phys. Rept.* 317 (1999), pp. 143–250. DOI: 10.1016/S0370-1573(98)00133-1. arXiv: hep-ph/9805494 [hep-ph].

[156] R. Gauld, F. Goertz, and U. Haisch. "On minimal Z' explanations of the $B \to K^*\mu^+\mu^-$ anomaly". In: *Phys. Rev.* D89 (2014), p. 015005. DOI: 10.1103/PhysRevD.89.015005. arXiv: 1308.1959 [hep-ph].

[157] R. Gauld, F. Goertz, and U. Haisch. "An explicit Z'-boson explanation of the $B \to K^*\mu^+\mu^-$ anomaly". In: *JHEP* 01 (2014), p. 069. DOI: 10.1007/JHEP01(2014)069. arXiv: 1310.1082 [hep-ph].

[158] A. Crivellin et al. "Lepton-flavour violating B decays in generic Z' models". In: *Phys. Rev.* D92.5 (2015), p. 054013. DOI: 10.1103/PhysRevD.92.054013. arXiv: 1504.07928 [hep-ph].

[159] D. Aristizabal Sierra, F. Staub, and A. Vicente. "Shedding light on the $b \to s$ anomalies with a dark sector". In: *Phys. Rev.* D92.1 (2015), p. 015001. DOI: 10.1103/PhysRevD.92.015001. arXiv: 1503.06077 [hep-ph].

[160] A. Celis, W.-Z. Feng, and M. Vollmann. "Dirac dark matter and $b \to s\ell^+\ell^-$ with U(1) gauge symmetry". In: *Phys. Rev.* D95.3 (2017), p. 035018. DOI: 10.1103/PhysRevD.95.035018. arXiv: 1608.03894 [hep-ph].

[161] W. Altmannshofer, S. Gori, S. Profumo, and F. S. Queiroz. "Explaining dark matter and B decay anomalies with an $L_\mu - L_\tau$ model". In: *JHEP* 12 (2016), p. 106. DOI: 10.1007/JHEP12(2016)106. arXiv: 1609.04026 [hep-ph].

[162] J. M. Cline, J. M. Cornell, D. London, and R. Watanabe. "Hidden sector explanation of B-decay and cosmic ray anomalies". In: *Phys. Rev.* D95.9 (2017), p. 095015. DOI: 10.1103/PhysRevD.95.095015. arXiv: 1702.00395 [hep-ph].

[163] A. Falkowski, S. F. King, E. Perdomo, and M. Pierre. "Flavourful Z' portal for vector-like neutrino Dark Matter and $R_{K^{(*)}}$". In: *JHEP* 08 (2018), p. 061. DOI: 10.1007/JHEP08(2018)061. arXiv: 1803.04430 [hep-ph].

[164] F. Sala and D. M. Straub. "A New Light Particle in B Decays?" In: *Phys. Lett.* B774 (2017), pp. 205–209. DOI: 10.1016/j.physletb.2017.09.072. arXiv: 1704.06188 [hep-ph].

[165] F. Bishara, U. Haisch, and P. F. Monni. "Regarding light resonance interpretations of the B decay anomalies". In: *Phys. Rev.* D96.5 (2017), p. 055002. DOI: 10.1103/PhysRevD.96.055002. arXiv: 1705.03465 [hep-ph].

[166] A. Datta, J. Kumar, J. Liao, and D. Marfatia. "New light mediators for the R_K and R_{K^*} puzzles". In: *Phys. Rev.* D97.11 (2018), p. 115038. DOI: 10.1103/PhysRevD.97.115038. arXiv: 1705.08423 [hep-ph].

[167] B. Aubert et al. "Direct CP, Lepton Flavor and Isospin Asymmetries in the Decays $B \to K^{(*)}\ell^+\ell^-$". In: *Phys. Rev. Lett.* 102 (2009), p. 091803. DOI: 10.1103/PhysRevLett.102.091803. arXiv: 0807.4119 [hep-ex].

[168] I. Adachi et al. "Measurement of the Differential Branching Fraction and Forward-Backward Asymmetry for B —> K(*)l+l-". In: (2008). arXiv: 0810.0335 [hep-ex].

[169] C. D. Froggatt and H. B. Nielsen.
"Hierarchy of Quark Masses, Cabibbo Angles and CP Violation".
In: *Nucl. Phys.* B147 (1979), pp. 277–298.
DOI: 10.1016/0550-3213(79)90316-X.

[170] P. H. Chankowski, K. Kowalska, S. Lavignac, and S. Pokorski.
"Update on fermion mass models with an anomalous horizontal U(1) symmetry".
In: *Phys. Rev.* D71 (2005), p. 055004. DOI: 10.1103/PhysRevD.71.055004.
arXiv: hep-ph/0501071 [hep-ph].

[171] E. Ma and G. Rajasekaran.
"Softly broken A(4) symmetry for nearly degenerate neutrino masses".
In: *Phys. Rev.* D64 (2001), p. 113012. DOI: 10.1103/PhysRevD.64.113012.
arXiv: hep-ph/0106291 [hep-ph].

[172] G. Altarelli and F. Feruglio.
"Tri-bimaximal neutrino mixing from discrete symmetry in extra dimensions".
In: *Nucl. Phys.* B720 (2005), pp. 64–88.
DOI: 10.1016/j.nuclphysb.2005.05.005. arXiv: hep-ph/0504165 [hep-ph].

[173] G. Altarelli and F. Feruglio.
"Tri-bimaximal neutrino mixing, A(4) and the modular symmetry".
In: *Nucl. Phys.* B741 (2006), pp. 215–235.
DOI: 10.1016/j.nuclphysb.2006.02.015. arXiv: hep-ph/0512103 [hep-ph].

[174] G. Altarelli and F. Feruglio.
"Discrete Flavor Symmetries and Models of Neutrino Mixing".
In: *Rev. Mod. Phys.* 82 (2010), pp. 2701–2729.
DOI: 10.1103/RevModPhys.82.2701. arXiv: 1002.0211 [hep-ph].

[175] I. de Medeiros Varzielas and D. Pidt.
"UV completions of flavour models and large θ_{13}". In: *JHEP* 03 (2013), p. 065.
DOI: 10.1007/JHEP03(2013)065. arXiv: 1211.5370 [hep-ph].

[176] I. de Medeiros Varzielas and G. Hiller.
"Clues for flavor from rare lepton and quark decays".
In: *JHEP* 06 (2015), p. 072. DOI: 10.1007/JHEP06(2015)072.
arXiv: 1503.01084 [hep-ph].

[177] Y. Nir and G. Raz. "Quark squark alignment revisited".
In: *Phys. Rev.* D66 (2002), p. 035007. DOI: 10.1103/PhysRevD.66.035007.
arXiv: hep-ph/0206064 [hep-ph].

[178] V. Khachatryan et al. "Search for Third-Generation Scalar Leptoquarks in the tτ Channel in Proton-Proton Collisions at $\sqrt{s} = 8$ TeV".
In: *JHEP* 07 (2015). [Erratum: JHEP11,056(2016)], p. 042.
DOI: 10.1007/JHEP11(2016)056,10.1007/JHEP07(2015)042.
arXiv: 1503.09049 [hep-ex].

[179] M. Freytsis, Z. Ligeti, and J. T. Ruderman. "Flavor models for $\bar{B} \to D^{(*)}\tau\bar{\nu}$". In: *Phys. Rev.* D92.5 (2015), p. 054018. DOI: 10.1103/PhysRevD.92.054018. arXiv: 1506.08896 [hep-ph].

[180] M. Aaboud et al. "Search for scalar leptoquarks in pp collisions at $\sqrt{s} = 13$ TeV with the ATLAS experiment". In: *New J. Phys.* 18.9 (2016), p. 093016. DOI: 10.1088/1367-2630/18/9/093016. arXiv: 1605.06035 [hep-ex].

[181] V. Khachatryan et al. "Search for single production of scalar leptoquarks in proton-proton collisions at $\sqrt{s} = 8\ TeV$". In: *Phys. Rev.* D93.3 (2016). [Erratum: Phys. Rev.D95,no.3,039906(2017)], p. 032005. DOI: 10.1103/PhysRevD.95.039906,10.1103/PhysRevD.93.032005. arXiv: 1509.03750 [hep-ex].

[182] V. Khachatryan et al. "Search for pair production of first and second generation leptoquarks in proton-proton collisions at $\sqrt{s} = 8$ TeV". In: *Phys. Rev.* D93.3 (2016), p. 032004. DOI: 10.1103/PhysRevD.93.032004. arXiv: 1509.03744 [hep-ex].

[183] B. Schmidt and M. Steinhauser. "CRunDec: a C++ package for running and decoupling of the strong coupling and quark masses". In: *Comput. Phys. Commun.* 183 (2012), pp. 1845–1848. DOI: 10.1016/j.cpc.2012.03.023. arXiv: 1201.6149 [hep-ph].

[184] F. Feruglio, P. Paradisi, and A. Pattori. "Revisiting Lepton Flavor Universality in B Decays". In: *Phys. Rev. Lett.* 118.1 (2017), p. 011801. DOI: 10.1103/PhysRevLett.118.011801. arXiv: 1606.00524 [hep-ph].

[185] T. Aushev et al. "Physics at Super B Factory". In: (2010). arXiv: 1002.5012 [hep-ex].

[186] A. Alloul et al. "FeynRules 2.0 - A complete toolbox for tree-level phenomenology". In: *Comput. Phys. Commun.* 185 (2014), pp. 2250–2300. DOI: 10.1016/j.cpc.2014.04.012. arXiv: 1310.1921 [hep-ph].

[187] C. Degrande et al. "UFO - The Universal FeynRules Output". In: *Comput. Phys. Commun.* 183 (2012), pp. 1201–1214. DOI: 10.1016/j.cpc.2012.01.022. arXiv: 1108.2040 [hep-ph].

[188] J. Alwall et al. "The automated computation of tree-level and next-to-leading order differential cross sections, and their matching to parton shower simulations". In: *JHEP* 07 (2014), p. 079. DOI: 10.1007/JHEP07(2014)079. arXiv: 1405.0301 [hep-ph].

[189] A. Greljo and D. Marzocca. "High-p_T dilepton tails and flavor physics". In: *Eur. Phys. J.* C77.8 (2017), p. 548. DOI: 10.1140/epjc/s10052-017-5119-8. arXiv: 1704.09015 [hep-ph].

[190] A. Bessaa and S. Davidson. "Constraints on t -channel leptoquark exchange from LHC contact interaction searches". In: *Eur. Phys. J.* C75.2 (2015), p. 97. DOI: 10.1140/epjc/s10052-015-3313-0. arXiv: 1409.2372 [hep-ph].

[191] F. Zimmermann. "HE-LHC Overview, Parameters and Challenges". In: *ICFA Beam Dyn. Newslett.* 72 (2017), pp. 138–141.

[192] A. Buckley et al. "LHAPDF6: parton density access in the LHC precision era". In: *Eur. Phys. J.* C75 (2015), p. 132. DOI: 10.1140/epjc/s10052-015-3318-8. arXiv: 1412.7420 [hep-ph].

[193] G. Aad et al. "Search for pairs of scalar leptoquarks decaying into quarks and electrons or muons in $\sqrt{s} = 13$ TeV pp collisions with the ATLAS detector". In: *JHEP* 10 (2020), p. 112. DOI: 10.1007/JHEP10(2020)112. arXiv: 2006.05872 [hep-ex].

[194] T. G. Rizzo. "Searches for scalar and vector leptoquarks at future hadron colliders". In: *eConf* C960625 (1996), NEW151. arXiv: hep-ph/9609267 [hep-ph].

[195] G. Aad et al. "Search for pair production of scalar leptoquarks decaying into first- or second-generation leptons and top quarks in proton-proton collisions at $\sqrt{s} = 13$ TeV with the ATLAS detector". In: *Eur. Phys. J.* C81.4 (2021), p. 313. DOI: 10.1140/epjc/s10052-021-09009-8. arXiv: 2010.02098 [hep-ex].

[196] B. Diaz, M. Schmaltz, and Y.-M. Zhong. "The leptoquark Hunter's guide: Pair production". In: *JHEP* 10 (2017), p. 097. DOI: 10.1007/JHEP10(2017)097. arXiv: 1706.05033 [hep-ph].

[197] L. Buonocore, P. Nason, F. Tramontano, and G. Zanderighi. "Leptons in the proton". In: *JHEP* 08.08 (2020), p. 019. DOI: 10.1007/JHEP08(2020)019. arXiv: 2005.06477 [hep-ph].

[198] L. Buonocore et al. "Lepton-Quark Collisions at the Large Hadron Collider". In: *Phys. Rev. Lett.* 125.23 (2020), p. 231804. DOI: 10.1103/PhysRevLett.125.231804. arXiv: 2005.06475 [hep-ph].

[199] A. Greljo and N. Selimovic. "Lepton-Quark Fusion at Hadron Colliders, precisely". In: *JHEP* 03 (2021), p. 279. DOI: 10.1007/JHEP03(2021)279. arXiv: 2012.02092 [hep-ph].

[200] A. Thamm, R. Torre, and A. Wulzer. "Future tests of Higgs compositeness: direct vs indirect". In: *JHEP* 07 (2015), p. 100. DOI: 10.1007/JHEP07(2015)100. arXiv: 1502.01701 [hep-ph].

[201] B. C. Allanach, B. Gripaios, and T. You. "The case for future hadron colliders from $B \to K^{(*)}\mu^+\mu^-$ decays". In: *JHEP* 03 (2018), p. 021. DOI: 10.1007/JHEP03(2018)021. arXiv: 1710.06363 [hep-ph].

[202] A. D. Martin, W. J. Stirling, R. S. Thorne, and G. Watt.
"Parton distributions for the LHC". In: *Eur. Phys. J.* C63 (2009), pp. 189–285.
DOI: 10.1140/epjc/s10052-009-1072-5. arXiv: 0901.0002 [hep-ph].

[203] R. D. Ball et al. "Parton distributions with QED corrections".
In: *Nucl. Phys.* B877 (2013), pp. 290–320.
DOI: 10.1016/j.nuclphysb.2013.10.010. arXiv: 1308.0598 [hep-ph].

[204] H. K. Dreiner, H. E. Haber, and S. P. Martin. "Two-component spinor techniques and Feynman rules for quantum field theory and supersymmetry".
In: *Phys. Rept.* 494 (2010), pp. 1–196. DOI: 10.1016/j.physrep.2010.05.002.
arXiv: 0812.1594 [hep-ph].

[205] J. Beringer et al. "Review of Particle Physics (RPP)".
In: *Phys. Rev.* D86 (2012), p. 010001. DOI: 10.1103/PhysRevD.86.010001.

Eidesstattliche Versicherung

Ich versichere hiermit an Eides statt, dass ich die vorliegende Abschlussarbeit mit dem Titel “Flavorful New Physics Models in the Light of the B Decay Anomalies” selbstständig und ohne unzulässige fremde Hilfe erbracht habe. Ich habe keine anderen als die angegebenen Quellen und Hilfsmittel benutzt, sowie wörtliche und sinngemäße Zitate kenntlich gemacht.

Die Arbeit hat in gleicher oder ähnlicher Form noch keiner Prüfungsbehörde vorgelegen.

Rom, 10.8.21 D. Loose

Ort, Datum Unterschrift

Belehrung

Wer vorsätzlich gegen eine die Täuschung über Prüfungsleistungen betreffende Regelung einer Hochschulprüfungsordnung verstößt, handelt ordnungswidrig. Die Ordnungswidrigkeit kann mit einer Geldbuße von bis zu 50 000 € geahndet werden. Zuständige Verwaltungsbehörde für die Verfolgung und Ahndung von Ordnungswidrigkeiten ist der Kanzler/die Kanzlerin der Technischen Universität Dortmund. Im Falle eines mehrfachen oder sonstigen schwerwiegenden Täuschungsversuches kann der Prüfling zudem exmatrikuliert werden (§ 63 Abs. 5 Hochschulgesetz –HG–).

Die Abgabe einer falschen Versicherung an Eides statt wird mit Freiheitsstrafe bis zu 3 Jahren oder mit Geldstrafe bestraft.

Die Technische Universität Dortmund wird ggf. elektronische Vergleichswerkzeuge (wie z. B. die Software “turnitin”) zur Überprüfung von Ordnungswidrigkeiten in Prüfungsverfahren nutzen.

Die oben stehende Belehrung habe ich zur Kenntnis genommen.

Rom, 10.8.21 D. Loose

Ort, Datum Unterschrift